Figure 3.7: Frequency Spectra of Pulse and Pulse Train....83
Figure 3.8: Energy Detectors....84
Figure 3.9: Combination and Threshold Block....85
Figure 3.10: Equivalent Series Resistance of LC Tank Circuit....87
Figure 3.11: Impulse Response of a Filter Circuit....88
Figure 3.12: Filter Responses with Short (τ < PRI) RC Time Constants....89
Figure 3.13: Filter Responses with Long (τ > PRI) RC Time Constants....90
Figure 3.14: Pulse Sense Block with Squaring Circuit at LNA Inputs....92
Figure 3.15: Filter Responses with Long (τ > PRI) RC Time Constants and a Squaring Circuit....93
Figure 3.16: Cumulative Probability Distribution....96
Figure 3.17: Analytical P_d versus P_{fa} for AWGN....100
Figure 3.18: Simulated P_d versus P_{fa} AWGN....101
Figure 3.19: P_d versus P_{fa} for CM1 and CM4....101
Figure 3.20: P_d versus P_{fa} with Additional Sensing Time, CM4, SNR = 12 dB....102
Figure 3.21: P_d versus P_{fa} with Strong Narrowband Interferer, CM1, SNR = 15dB....104
Figure 3.22: P_d versus P_{fa} with Jitter and Multiple Transmissions, CM1, E_b/N_0 = 12 dB....106
Figure 3.23: P_d versus P_{fa} for longer PRI, CM4. Also with PPM modulation....106
Figure 3.24: Performance Comparison of Circuit-Level Implementation, Analytical Expression, and System-Level Implementation for Short Time Constant....107
Figure 3.25: Performance Comparison of Circuit-Level Implementation, Analytical Expression, and System-Level Implementation for Long Time Constant....108
Figure 4.1: Multichannel MAC operation....114
Figure 4.2: Probability of at Least X Nodes Transmitting Simultaneously Compared to the Probability of any of the Pulses Overlapping....117
Figure 4.3: Overall Probability of Collision for Different Offered Loads....117
Figure 4.4: I-UWB Receiver with Multiuser Timing Recovery....119
Figure 4.5: Interference from Overlapping Transmissions....122
Figure 4.6: Normalized Throughput for Multi-user Receivers in Multichannel PSMA and ALOHA....124
Figure 4.7: Normalized Throughput for Different PRIs in Multichannel PSMA and ALOHA....125
Figure 4.8: Energy Efficiency for PSMA and ALOHA with Multi-user Receivers....126
Figure 4.9: Energy Efficiency for PSMA and ALOHA at Different PRIs....127
Figure 4.10: Normalized Delay for PSMA and TDMA....128
Figure 5.1: Types of Duplexing....133
Figure 5.2: Full Duplex System Architectures for Ad Hoc Radios....138
Figure 5.3: Handshaking Overhead in CSMA/CA and BSMA....139
Figure 5.4: Overlap Effect....143
Figure 5.5: P_D versus P_{FA} for Busy Signals with Interference....152
Figure 5.6: Calculated P_D versus P_{FA} Busy Signal with Overlap in AWGN Channel....154
Figure 5.7: P_D versus P_{FA} for Orthogonal Busy Signals with Interference and Overlap....156
Figure 5.8: P_D versus P_{FA} for Multiple Busy Signals....158
Figure 5.9: Busy Signal Noise for Different Levels of Interference....159

INTEL-1010
U.S. Patent 9,265,043

Figure 5.10: Busy Signal Noise for Different Spreading Factors 160
Figure 5.11: Busy Signal Noise for Different Pulse Shapes.....161
Figure 5.12: Busy Signal Noise for Different Busy Signal Protocols.....162
Figure 5.13: Busy Signal Noise with Equalization Scheme 163
Figure 5.14: Throughput for PSMA, PSMA/CA, ALOHA, BSMA, and TDMA. 166
Figure 5.15: Energy efficiency for PSMA, PSMA/CA, ALOHA, BSMA, and TDMA. 167
Figure 6.1: Proposed Approach for Resource Allocation.....172
Figure 6.2: Block Diagram of Adaptive I-UWB System 174
Figure 6.3: BER versus E_b/N_0 at a Data Rate of 25 Mbps.....180
Figure 6.4: Maximum Data Rate versus E_b/N_0 181
Figure 6.5: Energy per Bit for Various QoS Requirements 182
Figure 6.6: BER of Adaptive versus Non-Adaptive System 184
Figure 6.7: Data Rate Maximization of Adaptive versus Non-Adaptive System.....185
Figure 6.8: Energy of Adaptive versus Non-Adaptive System 186
Figure 6.9: Cost of Adaptive versus Non-Adaptive System.....188

INTEL-1010
U.S. Patent 9,265,043

Chapter 1: Introduction

Ongoing developments in wireless technology and embedded systems have spawned extensive research in ad hoc and sensor networks [1]-[3]. Such networks enable applications such as inventory tracking, radio frequency identification (RFID) tags, home networking, or structural integrity monitoring. These applications must manage a large number of low-power, low-cost nodes with no infrastructure. Nodes rely on limited energy resources such as a battery, and the useful lifetime of the network depends on each node's ability to conserve energy. Because these networks may contain several thousand nodes or more, low node cost is essential to contain the overall network cost.

Since the Federal Communications Commission's historic allocation of spectrum for ultra wideband (UWB) on February 14 of 2002, UWB radio communication has attracted an enormous amount of interest from scientific, commercial, and military sectors [4]-[29]. In fact, the upcoming IEEE 802.15.4a standard intends to use UWB as the physical layer for ad hoc and sensor networks [78],[130],[131]. Compared to narrowband systems, UWB has several advantages for deployment in ad hoc and sensor networks. First, the low radiated power is at least an order magnitude less than narrowband radios [77],[79],[97],[98]. This leads to advantages such as low probability of detection and intercept, reuse of existing spectrum, minimal impact to existing users, and energy efficient transmitters [47],[58],[68],[93]. Next, the wide bandwidth enables an extremely high data rate, which can be traded for longer range or more robust operation [94]-[96]. The wide instantaneous bandwidth also enables fine time resolution for use in radar, imaging, and ranging. Due to these and many other desirable properties, UWB is an attractive radio technology for ad hoc and sensor networks [30],[31].

Two different UWB communications systems – impulse-based UWB (I-UWB) systems [4]-[23] and multi-carrier UWB (MC-UWB) systems [24]-[29] – have been pursued recently. For ad hoc and sensor networks, I-UWB has several advantages over multi-carrier systems including robustness to harmful multipath fading effects, sub-

INTEL-1010
U.S. Patent 9,265,043

centimeter ranging ability, and low-cost, low-power hardware. Resilience to fading permits placement of UWB systems in areas inhospitable to narrowband systems, such as inside metal ship hulls. The ranging capability allows nodes to accurately (under a centimeter) discern location, which is an important building block for many applications and network protocols [32],[33]. Finally, the carrierless nature of I-UWB results in simple, low power transceiver circuitry, which does not require intermediate mixers and oscillators. Hence, I-UWB systems are more suitable than MC-UWB systems for large ad hoc and sensor networks.

A narrowband radio modulates data onto a carrier signal to occupy a narrow frequency band of a few KHz to a few MHz, and the signal is continuous in time. The unique signaling of I-UWB represents the dual of narrowband signaling. A sharp pulse may occupy several GHz of spectrum, but it only lasts for a few hundred picoseconds during a pulse repetition interval (PRI) that lasts from nanoseconds to microseconds.

In wireless networks, the medium access control (MAC) protocol performs the important function of preventing multiple nodes from interfering with each other. Current MAC protocols for I-UWB target small wireless personal area networks (WPANs) and cellular networks. The most popular methods of medium access for I-UWB include time division multiple access (TDMA), time hopping, frequency hopping, or direct sequence UWB (DS-UWB) [34]-[69]. In these protocols, a central controller prevents collisions by assigning concurrently transmitting nodes to different time slots or code channels. A centralized approach is a good strategy for a small network with heavy traffic and strict Quality of Service (QoS) requirements. However, in larger ad hoc and sensor networks, the central coordination increases complexity and overhead, and it also leads to a central point of failure. While applicable to WPAN and cellular applications, the above MAC protocols are impractical for ad hoc and sensor networks.

Instead of the above MAC protocols, large ad hoc and sensor networks implement distributed MAC protocols, which generally realize random access and require a method to detect medium activity [70]-[80]. A simple example of such a protocol is carrier sense multiple access (CSMA). The protocol allows any node to transmit data providing that it first detects an idle medium. If the medium is busy, then

INTEL-1010
U.S. Patent 9,265,043

the node must delay its transmission until after the current transmission ends. Each individual node makes it own decision to transmit with no central guidance, so the MAC is distributed. Further, the access is considered random since there is no strict order to the access. I-UWB presents difficulties in detecting medium activity, so large ad hoc and sensor networks have thus far been unable to realize the benefits of I-UWB.

Thus, this paper investigates MAC protocols for I-UWB in ad hoc and sensor networks. Specifically, it endeavors to answer the following questions:

1) How does the unique signaling of I-UWB affect the MAC layer of ad hoc and sensor networks?
2) How can we overcome the challenges of applying I-UWB to ad hoc and sensor networks?
3) How can we exploit the unique signaling of I-UWB to benefit ad hoc and sensor networks?

As an end result, this paper intends to arrive at MAC protocols custom tailored to both I-UWB and to ad hoc and sensor networks.

Chapter 2 answers the first question. The chapter starts with the basics of I-UWB, including signaling, channel model, and transceiver architectures. Next, it presents some ad hoc and sensor network applications that benefit from an I-UWB radio. Finally, it examines MAC protocols with an emphasis on the specific requirements of I-UWB and ad hoc and sensor networks.

Chapter 3 answers the second question. The low duty cycle and low power of I-UWB create difficulties in implementing a distributed MAC protocol because there is no good method to detect medium activity. Nodes are unsynchronized with each other, so it becomes a significant challenge to search for a narrow, low-power pulse within a large time window. Existing methods are either inaccurate or require a prohibitive amount of time or hardware complexity. Thus, Chapter 3 proposes a new method to detect I-UWB activity. It is termed *pulse sense*, as it is analogous to carrier sense in narrowband systems. The key idea of pulse sense is to examine the spectral power components of the received signal, which are always present, to avoid searching for

INTEL-1010
U.S. Patent 9,265,043

narrow I-UWB pulses in the time domain. Pulse sense detects medium activity reliably, quickly, and efficiently. Pulse sense enables distributed, random medium access for I-UWB, and in turn, offers the advantages of I-UWB to ad hoc and sensor networks.

Chapters 4, 5, and 6 each provide an answer to the third question. First, Chapter 4 builds on pulse sense to create a distributed multichannel MAC protocol for I-UWB. A traditional multichannel MAC subdivides the channel into time slots or code channels, and each sub-channel's data rate is a fraction of the full channel data rate. Multichannel protocols increase network throughput because the multiple channels decrease the probability of collisions [81]. However, multichannel protocols require more complex multichannel receivers or central timing control. In addition, the reduced sub-channel bandwidth increases delay at low offered load. The unique signaling of I-UWB allows a multichannel MAC that requires neither centralized control nor modifications to an I-UWB receiver. The proposed MAC significantly improves throughput over traditional multichannel protocols without incurring the delay penalty. A multi-user I-UWB receiver, which can receive several time-interleaved transmissions concurrently, further improves performance with moderate hardware complexity.

Chapter 5 also builds on pulse sense and suggests using the unique signaling of I-UWB for a busy signal MAC. A busy signal MAC provides superior performance to current wireless MAC protocols because nodes can assess the status of ongoing transmissions [82]-[86]. Whereas narrowband systems require two transceivers to implement a busy signal MAC, the proposed I-UWB system requires only a single transceiver to save cost, power, and circuit complexity. The single transceiver leverages the inherently low duty cycle of an I-UWB pulse train to detect collisions and corrupted packets through transmission of a busy signal. Because I-UWB systems dissipate far less power transmitting than receiving, the transmission of a busy signal has insignificant impact on the power dissipated in a transaction. The proposed busy signal MAC permits random, distributed medium access with no central point of failure, so it is appropriate for any large ad hoc or sensor network.

Next, because the I-UWB Physical Layer and MAC Layer affect the network and application layers, Chapter 6 introduces a cross-level optimization scheme. The scheme varies parameters in the MAC protocol and in the I-UWB radio to meet various

INTEL-1010
U.S. Patent 9,265,043

application level QoS constraints – e.g., packet error rate (PER), data rate, or energy dissipation – as environmental conditions change. Environmental conditions vary depending on node mobility, transmitter-receiver distance, interference level, and channel conditions. QoS constraints change depending on the type of data. For example, control data may require the lowest possible BER [87]; video or real time data may require the highest possible data rate [88]; and sensor data may require energy efficiency to save battery power [89]. Typical communications systems are built to meet all such QoS constraints even under the worst environmental conditions. However, a communications system operates in the worst conditions infrequently, so it wastes valuable resources as a result. I-UWB can implement a unique adaptive modulation scheme with simple hardware. Adapting the modulation scheme for various environmental conditions and QoS criteria improves overall BER, energy efficiency, and data rate.

Finally, Chapter 7 concludes the paper.

INTEL-1010
U.S. Patent 9,265,043

Chapter 2: Preliminaries

Figure 2.1 displays the International Organization for Standardization (ISO) Open System Interconnect (OSI) model for networking. The model compartmentalizes networking tasks into a seven-layer hierarchy, and nearly all networking products, protocols, and standards parallel the model [90]. The top layer is the Application Layer, and it can include such familiar applications as File Transfer Protocol (FTP) or Hyper Text Transfer Protocol (HTTP). Applications pass data to the Presentation Layer, which provides a common syntax for the communicating applications. Next, the Session Layer maintains synchronization between the two users. Then, the Transport Layer hides the underlying network from the upper layers and provides a reliable end-to-end connection. The Network Layer routes the data from the Transport Layer and controls congestion. The Data Link Layer hides the characteristics of the physical medium from the upper layers and also provides medium access control. The bottom layer, the Physical Layer, provides a point-to-point connection between communicating nodes.

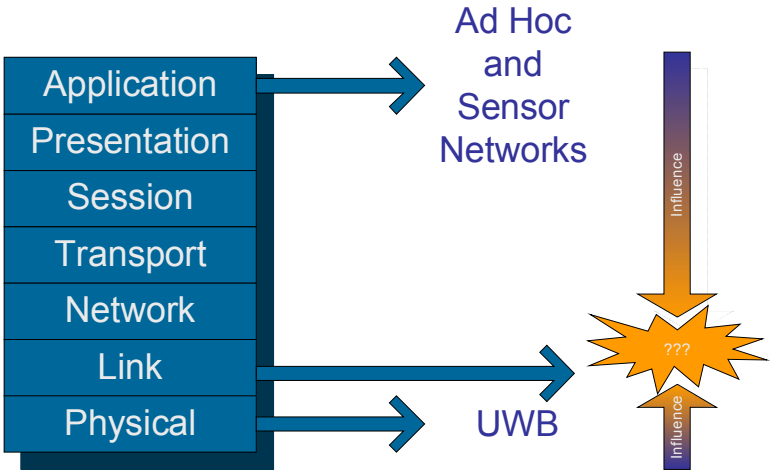

Figure 2.1: ISO Networking Layers

INTEL-1010
U.S. Patent 9,265,043

The unique nature of the I-UWB Physical Layer directly impacts both the Link Layer and the Application Layer, whereas the other layers are indirectly unaffected. Section 2.1 begins this chapter with the basics of I-UWB, including signaling, channel model, and transceiver architectures. Next, Section 2.2 presents some ad hoc and sensor network applications that are enabled by I-UWB. Section 2.3 discusses previous MAC protocols for ad hoc and sensor networks and also for I-UWB. Finally, Section 2.4 emphasizes the specific requirements applying a MAC protocol to I-UWB and to ad hoc and sensor networks.

2.1 UWB

2.1.1 Background

The origins of I-UWB follow those of wireless communication itself [200]. In the late 1800s, the Marconi Spark Gap Emitter created the first wireless transmission from an impulsive spark. The technology of the time did not allow more than one transmitter-receiver pair within range of each other. Therefore, regulatory bodies, such as the Federal FCC divided the spectrum into narrow bands and licensed these bands to users. The narrowband regulatory structure relegated UWB to military and experimental systems until recently. Advances in VLSI technology and digital signal processing solve many of the problems that could not be addressed with earlier technology. The FCC freed spectrum for low power UWB transmissions in 2002, and this sparked immediate and immense interest from both academic and commercial entities.

2.1.1.1 Definition

In general, A UWB signal has a bandwidth much greater than the minimum bandwidth (B_{min}) required to achieve a data rate R, normally $B_{min} \geq \frac{1}{2} \cdot R$. Figure 2.2 compares the power spectral density of a UWB signal with that of a narrowband and

INTEL-1010
U.S. Patent 9,265,043

wideband signals. UWB devices efficiently use scarce spectrum because they may occupy bandwidth and coexist with existing narrowband systems. The low power spectral density of UWB avoids interference to the underlying narrowband signals.

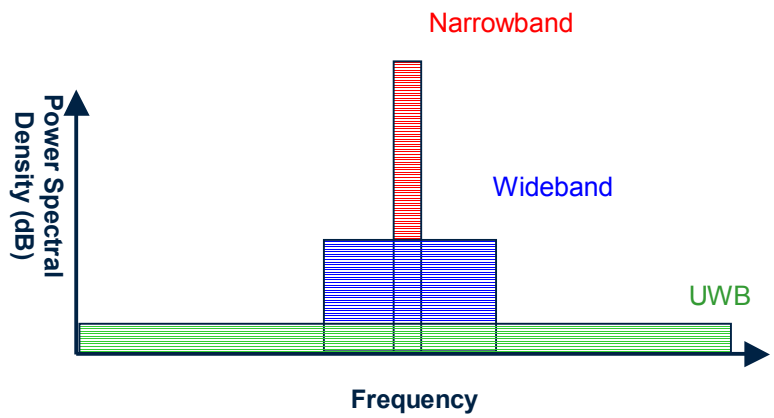

Figure 2.2: Power Spectral Density of UWB, Narrowband, and Wideband

In the United States, the FCC released its first report and order for power emissions from UWB devices on February 14, 2002 [91]. On December 8, 2003, a formal rule change to Section 15 Title 47 of the United States Code of Federal Regulations allowed intentional, low power radiation from UWB devices [92]. The FCC limits the operating bands for a UWB device according to its application. The rules allow for both unlicensed communications applications and licensed applications such as health monitoring, ground penetrating radar (GPR), and through-walls sensing. The spectral limits on UWB consider the effect of an ultra wide bandwidth intruding into the sensitive communications bands located below 2 GHz. Such existing bands include TV, radio, PCS, public safety, and GPS bands. The FCC prohibits UWB communications in toys, aircraft, ships, or satellites.

The FCC defines bandwidth and spectral limits for UWB devices, but it does not specify a signal type, e.g. I-UWB or MC-UWB. The FCC identifies two types of UWB bandwidths: absolute bandwidth or fractional bandwidth, which are defined by the 10 dB cutoff bandwidths in Figure 2.3. The absolute bandwidth is the difference between the 10 dB high cutoff frequency and the 10 dB low cutoff frequency (f_h - f_l). The fractional bandwidth is defined as 2*(f_h - f_l)/(f_h + f_l), and the center frequency is

INTEL-1010
U.S. Patent 9,265,043

defined as $f_c = (f_h - f_l)/2$. In Figure 2.3, the frequency of maximum radiation f_m is the same as f_c, but it need not be. Given these definitions, the FCC classifies a device as UWB if either

(1) The transmitted signal has a fractional bandwidth greater than $0.20*f_c$, or

(2) The transmitted signal has an absolute bandwidth greater than 500 MHz [92].

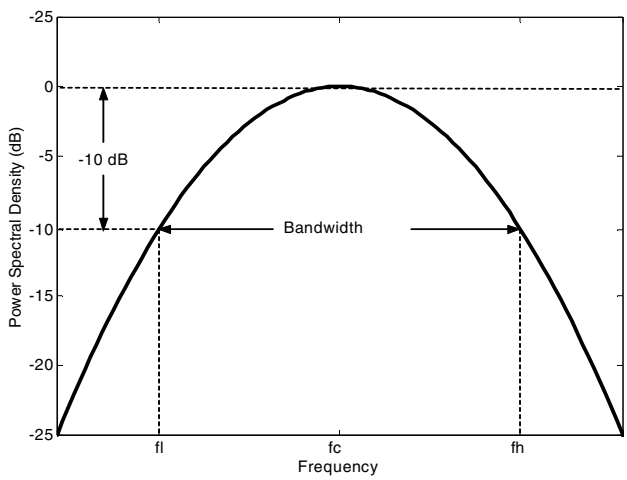

Figure 2.3: FCC UWB Definition

The FCC regulations cover three classes of devices: imaging systems, vehicular radar systems, and communications and measurement systems. This paper deals only with communications devices, so we briefly review their characteristics and EIRP (equivalent isotropically radiated power) limits. The EIRP is equivalent to the signal power level given to the antenna multiplied by the antenna gain. Note that the EIRP can be converted to the field strength at 3 m in dBμV/m by adding 95.2 to the EIRP in dBm. The radiation limits are based on interference studies of devices likely to be victims of UWB interference.

Communications systems received license-free spectrum allocation, so anyone anywhere in the United States may use a certified device for communications purposes.

INTEL-1010
U.S. Patent 9,265,043

The FCC classifies communications devices as either indoor or outdoor devices. Indoor devices should be inoperable when not indoors, e.g. a device could operate on AC power only. Outdoor devices must be handheld devices and must not be supported by an outdoor UWB infrastructure. Further, outdoor devices must stop transmitting when no response is received from a receiver within a ten second period. These systems operate in the band from 3100 MHz to 10600 MHz. Figure 2.4 and Table 2.1 show the average EIRP limits for both indoor and outdoor communications and measurement systems. In addition to the average power limits in Figure 2.4, a communications system must also limit its average EIRP to -85.3 dBm/kHz in the frequency bands 1164-1240 MHz and 1559-1610 MHz.

Table 2.1: Average EIRP Limits for Communications Systems

Frequency (MHz)	**Maximum EIRP (dBm) Indoor Devices**	**Maximum EIRP (dBm) Hand-Held Devices**
0-960	-41.3	-41.3
960-1610	-75.3	-75.3
1610-1990	-53.3	-63.3
1990-3100	-51.3	-61.3
3100-10600	-41.3	-41.3
Above 10600	-51.3	-61.3

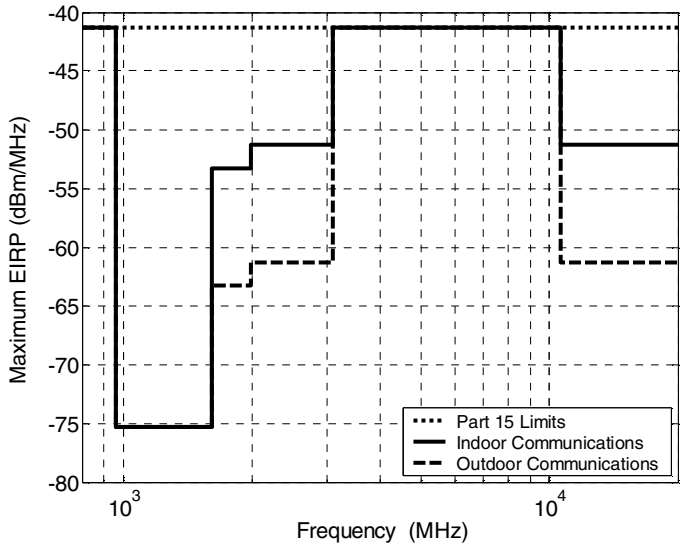

Figure 2.4: Average EIRP Limits for Communications and Measurement Systems

INTEL-1010
U.S. Patent 9,265,043

2.1.1.2 Advantages

Compared to narrowband systems, UWB has several advantages. Because of the combination of wide bandwidth and low power, UWB signals have a low probability of detection and intercept [93]. Additionally, the wide bandwidth gives UWB excellent immunity to interference from narrowband systems and from multipath effects [44],[47],[58],[68]. Another significant advantage of UWB is its high data rate [23],[94],[95]. Figure 2.5 shows that a high data rate is more easily achieved by increasing bandwidth than by increasing SNR. This is a consequence of Shannon's channel capacity theorem, which states that channel capacity increases linearly with bandwidth, but increases only with the $\log_2$ of the SNR. In Figure 2.5, theoretical data rates of over 500 Mbps are achieved easily in by a UWB system in a low-SNR environment, but such data rates are nearly impossible for the narrowband systems in the figure.

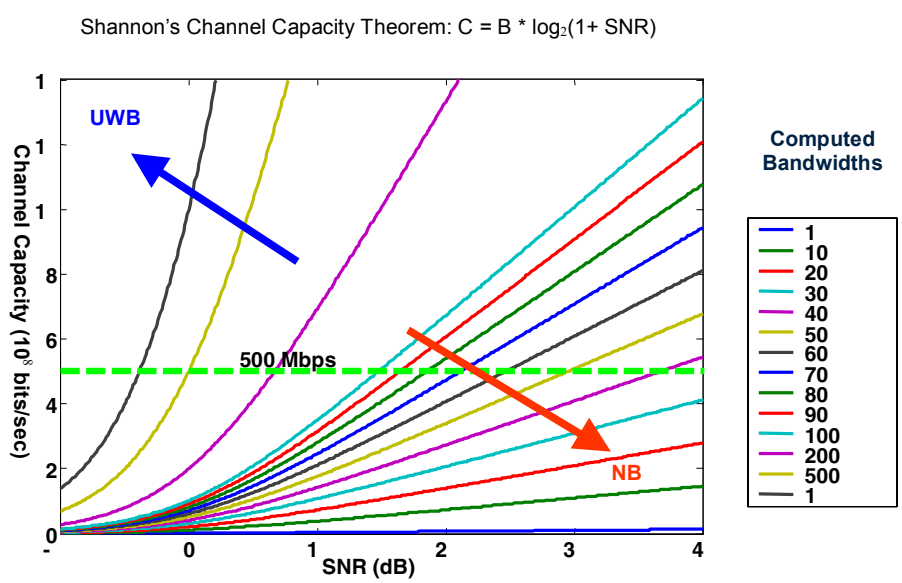

Figure 2.5: Channel Capacity of UWB versus Narrowband

INTEL-1010
U.S. Patent 9,265,043

UWB also offers a high degree of flexibility. The high data rate can be traded for longer range or more robust operation. Figure 2.6 shows the flexibility of UWB in trading range for data rate.

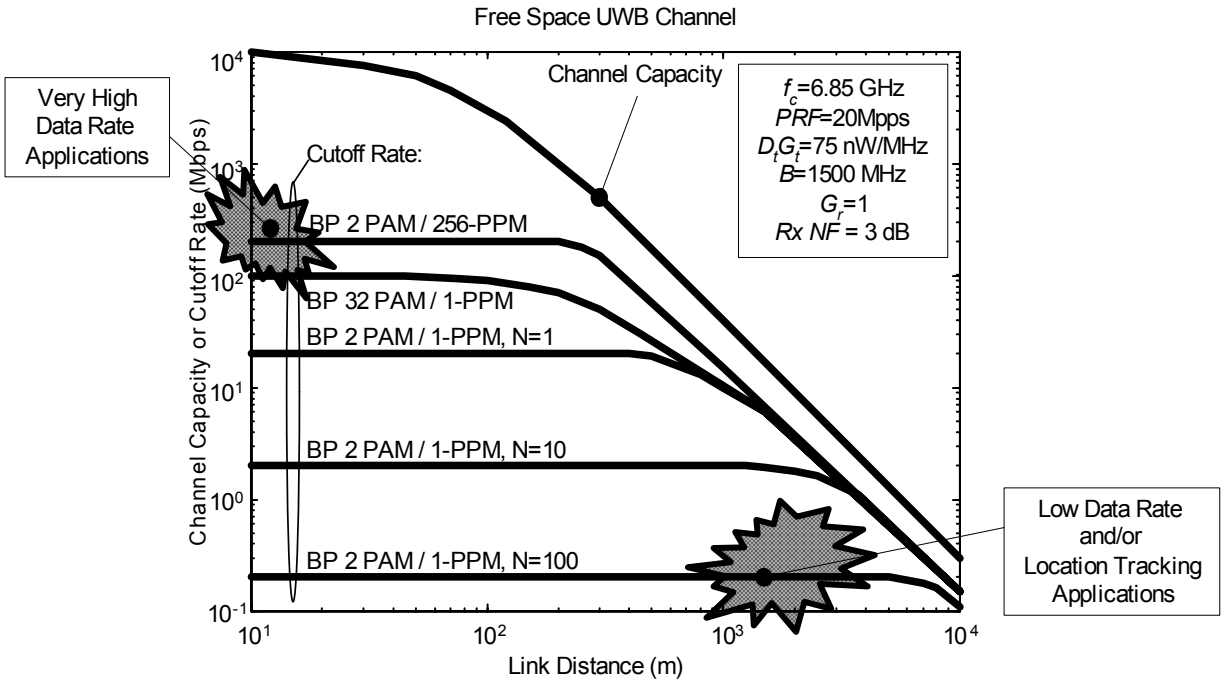

Figure 2.6: Ability of UWB to Trade Distance for Data Rate [96]

Furthermore, UWB permits coexistence with both narrowband systems and other UWB systems. FCC regulations limit UWB devices to low average power in order to minimize interference with narrowband systems. Thus, UWB provides a method to reuse large amounts of existing spectrum without disturbing existing users, and it should be available worldwide in the near future. UWB is unique in that its radiated power is inherently ultra low as mandated by the FCC maximum of 560 µW, which is at least an order of magnitude less than the radiated power of traditional narrowband systems [77],[79],[97],[98]

In addition, I-UWB is relatively immune to multipath induced fading effects in both indoor and outdoor environments. The wide instantaneous bandwidth increases the number of resolvable multipaths and results in robustness to harmful multipath effects [95],[99]. For an application such as maritime asset tracking, the multipath

INTEL-1010
U.S. Patent 9,265,043

environment may be particularly harsh with several layers of densely packed containers stacked inside a ship's metal hold. With an appropriate receiver, a UWB system may harvest energy from the resolvable multipath signals to improve data rate or BER. The wide instantaneous bandwidth also enables fine time resolution for use in radar, imaging, and ranging.

Finally, the carrierless nature of I-UWB gives it potential for simple circuit implementations without intermediate oscillators and mixers [100]-[102]. UWB devices may have a nearly all-digital implementation in CMOS with minimal analog RF electronics [103],[104]. This simple architecture can translate to low power dissipation and low cost, which opens a variety of possible mobile applications.

2.1.1.3 Signaling

Two forms of UWB signaling have been pursued recently. They vary mostly in the method used to fill the ultra wideband spectrum because the FCC does not mandate any particular method. At one extreme, a sharp impulse fills the band as in I-UWB; and at the other extreme, many simultaneous narrowband tones fill the band as in MC-UWB. Many solutions exist in between these extremes - a single band may be divided or notched into a few narrower bands; or, alternatively, several narrow bands may combine to fill increasingly larger spectrums. The solutions may or may not utilize a carrier frequency. Figure 2.7 shows that many options between MC-UWB and I-UWB are also possible, including the two leading proposals for UWB WPAN standardization, direct sequence UWB (DS-UWB) and Multi-Band Orthogonal Frequency Division Multiplexing (MB-OFDM) [21],[29]. Due to the advantages of I-UWB for ad hoc and sensor networks, this section describes I-UWB signaling.

INTEL-1010
U.S. Patent 9,265,043

Figure 2.7: Solution Space for UWB Signaling

Traditional narrowband radio systems modulate data onto a carrier signal to occupy a narrow frequency band of a few KHz to a few MHz, but the signal is continuous in time. The unique signaling of I-UWB represents the dual of narrowband signaling. A narrow pulse may occupy several GHz of spectrum, but it may last only a few hundred picoseconds. The pulse is repeated at a pulse repetition interval (PRI) that lasts from nanoseconds to microseconds, so the transmitted signal takes the form

$$s(t) = \sum_{i=-\infty}^{\infty} A_i(t)\, p(t - iT_f) \quad (2.1) \quad ,$$

where $A_i(t)$ is the amplitude of the pulse, equal to $\pm\sqrt{E_P}$ with E_p the energy of a pulse, $p(t)$ is the received pulse shape with normalized energy, and T_f is the PRI. The PRI is generally much larger then the pulse width, i.e. an I-UWB pulse train has a small duty cycle (<< 1). The low duty cycle results in the low power spectral density mandated by the FCC. The inverse of the PRI is the pulse repetition frequency (PRF).

Common pulse shapes for UWB communications are derived from the Gaussian pulse [105]-[107]. The Gaussian pulse itself has a DC center frequency, which makes it undesirable for radio communications. However, its derivatives have decreasing bandwidth and increasing center frequency. Figure 2.8 shows the Gaussian pulse, its first derivative (a Gaussian monopulse), and its second derivative (a Gaussian doublet) in both the time and frequency domains.

INTEL-1010
U.S. Patent 9,265,043

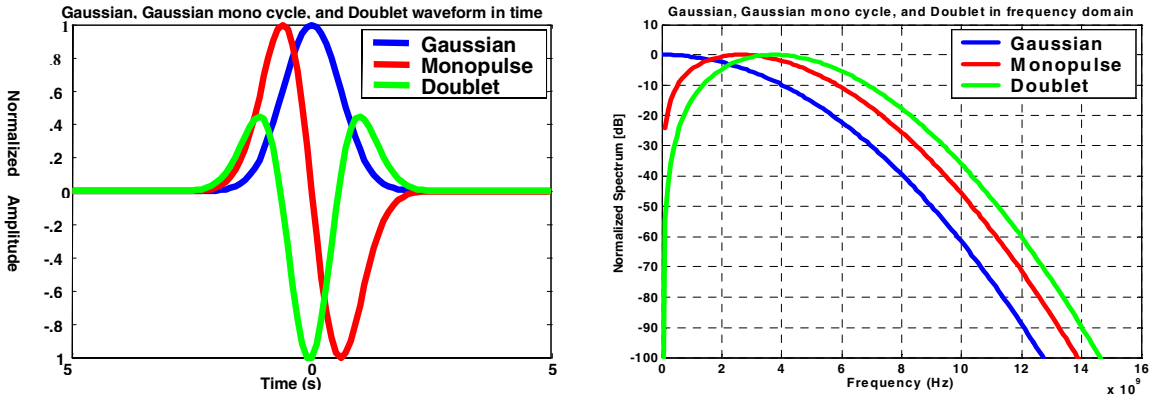

Figure 2.8: Gaussian Pulses Useful for UWB [105]

Equation (2.2) describes a Gaussian pulse in terms of the pulse width t_n. The center frequency is zero (DC offset), and μ is the center point in time of the Gaussian pulse.

$$p(t) = \frac{1}{\sqrt{2\pi\sigma^2}} e^{\frac{(t-\mu)^2}{2\sigma^2}} \quad (2.2)$$

Equation (2.3) describes a Gaussian monocycle doublet in terms of the pulse width t_n and center frequency.

$$p(t) = \left(\frac{32k^6}{\pi}\right)^{\frac{1}{4}} te^{-(kt)^2} \quad (2.3)$$

Equation (2.4) describes a Gaussian doublet in term of t_n, which is the time difference between the minimum and maximum signal values. For the Gaussian doublet, we can adjust the pulse width (= $4*t_n$), center frequency (= $0.8/t_n$), and bandwidth (= $1.2/t_n$) by adjusting t_n in (2.4).

INTEL-1010
U.S. Patent 9,265,043

$$p(t) = \left(1 - 4\pi\left(\frac{t}{t_n}\right)^2\right) \cdot \exp\left(-2\pi\left(\frac{t}{t_n}\right)^2\right) \quad (2.4)$$

Because of effects from the antenna and the channel, a transmitted Gaussian monopulse can appear at the receiver as a Gaussian doublet. Hence, simulations often use various pulse shapes depending on whether the perspective is the receiver's or the transmitter's. In general, a received UWB signal is modeled as

$$r(t) = s(t) * h(t) + n(t) \quad (2.5) \quad ,$$

where *h(t)* is the channel impulse response and *n(t)* is Additive White Gaussian Noise (AWGN) with power $\sigma^2 = 1 / SNR$, where *SNR* is the average signal-to-noise ratio.

Most practical systems will use some form of pulse shaping to control the spectral occupation of each pulse to conform to regulatory limits. Figure 2.9 shows a bandpass filter shaping a Gaussian monocycle to meet the FCC mask.

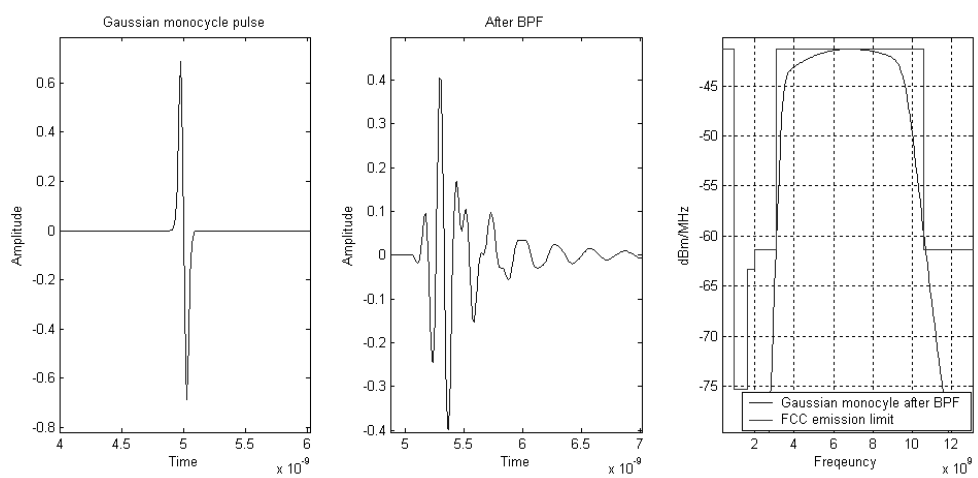

Figure 2.9: Filtering of a Gaussian Monocycle to Meet FCC Limits

INTEL-1010
U.S. Patent 9,265,043

Another method of meeting the FCC mask is to modulate the Gaussian pulse on to a sinusoidal pulse with center frequency f_c as in (2.6).

$$\mathrm{p(t)} = \left(\frac{8k}{\pi}\right)^{\frac{1}{4}} \frac{1}{\sqrt{1+e^{\frac{2\pi^2 f_c^2}{k}}}} e^{kt^2} \cos\left(2\pi f_c^2 t\right) \quad (2.6)$$

To transmit information, the pulse train of (2.1) must be modulated according to the data. This paper considers two popular modulation schemes for I-UWB: orthogonal pulse position modulation (PPM), which results in the same constellation as frequency shift keying (FSK) in narrowband systems; and antipodal amplitude modulation, which results in the same signal constellation as binary phase shift keying (BPSK) in narrowband systems. Figure 2.10 shows the signal constellations of antipodal amplitude modulation (BPSK) and binary PPM (FSK).

INTEL-1010
U.S. Patent 9,265,043

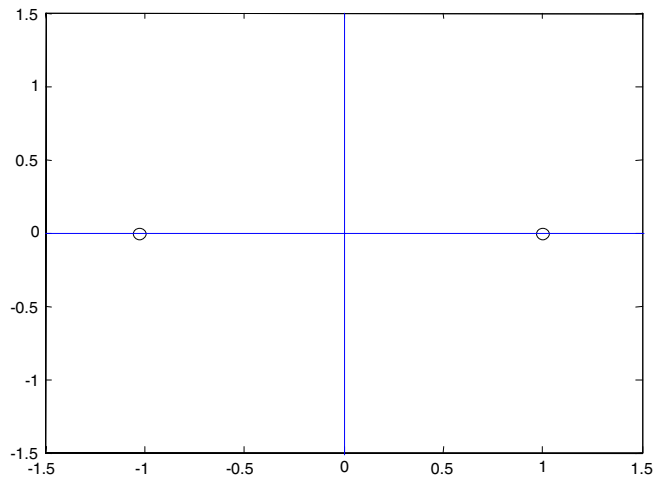

(a) Antipodal Amplitude Modulation (BPSK)

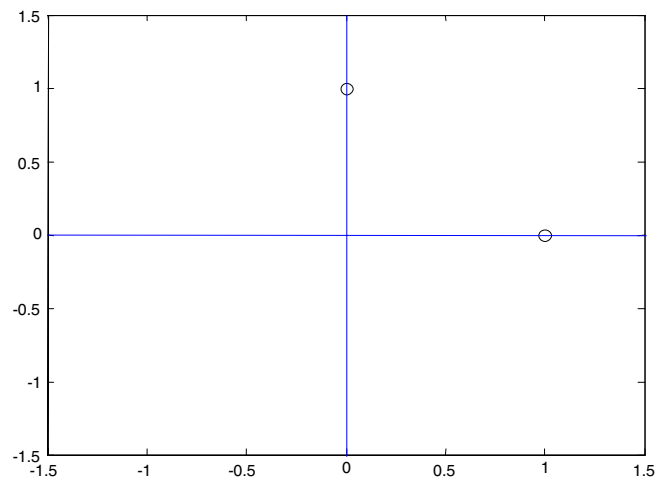

(b) Binary PPM (FSK)

Figure 2.10: Constellation Diagram Representation of Modulation Schemes for I-UWB

For BPSK, the pulse train of (2.1) becomes

$$s(t)=\sum_{i=-\infty}^{\infty} A_i(t)\, p\left(t-iT_f\right) \quad (2.7) \quad ,$$

INTEL-1010
U.S. Patent 9,265,043

where $A_i = d_i(t)$ is the amplitude of the ith pulse modulated by data bit $d_i(t) \in [-1,1]$. For PPM, the pulse train of (2.1) becomes

$$s(t) = \sum_{i=-\infty}^{\infty} Ap\left(t - iT_f - \delta d_i(t)\right) \quad (2.8) \quad ,$$

where $d_i(t)$ shifts the pulse in time by some multiple of δ, which should be larger than the pulse width to assure an orthogonal signal set. Note that for PPM, a single pulse can represent multiple bits or chips. If there are m time slots, then the signal may represent $\log_2 m$ chips or bits. It is possible for δ to be less than the pulse width and still obtain an orthogonal signal set, but this imposes impractical timing requirements on transceivers [107],[108].

Figure 2.11 shows the time domain representation of BPSK, binary PPM, and 4-ary PPM modulation. The guard time T_g is the time between the end of the current pulse and the beginning of the next pulse. The symbol time T_s is the time between the beginning and end of a symbol. Part (a) shows BPSK, in which the polarity of the pulse determines the data. Part (b) shows the binary case of PPM. The two pulses are offset in non-overlapping positions in time. The position of the pulse relative to the reference point (shown as a dotted line) determines the data. A pulse sent before the reference point represents a data value of '0', whereas a pulse sent after the reference point represents a data value of '1'. Part (c) shows the 4-ary extension of PPM, which has four different orthogonal pulse positions. Higher order m-ary extensions of PPM require m different non-overlapping pulse positions.

In PPM, the signals are non-overlapping in time, so they are orthogonal to each other. Note that m-ary PPM requires m orthogonal signals, which decreases the guard time. PPM behaves similarly to FSK for narrowband systems. As m increases, the performance should improve as the distance between the orthogonal symbols stays constant.

INTEL-1010
U.S. Patent 9,265,043

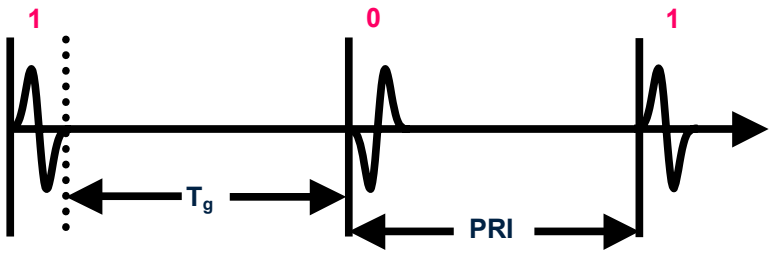

(a) BPSK

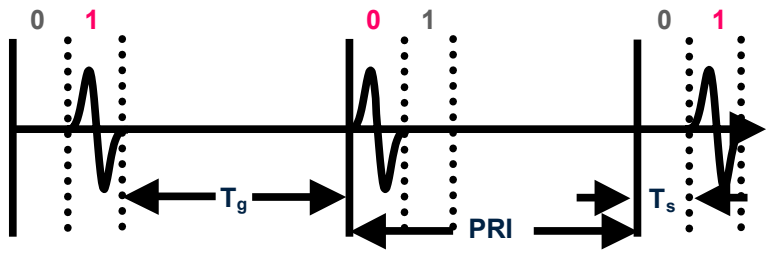

(b) Binary PPM

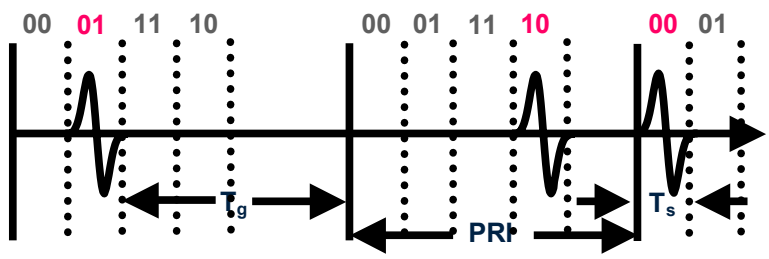

(c) 4-ary PPM

Figure 2.11: Time Domain Representation of Modulation Schemes for I-UWB

2.1.1.4 Channel Model

As a UWB signal propagates, it is distorted by reflections, shadowing, and fading. These effects are accounted for in the channel model. The UWB channel is usually modeled as a Finite Impulse Response (FIR) filter as

INTEL-1010
U.S. Patent 9,265,043

$$h(t) = \sum_{i=1}^{N_p} \beta_i \delta(t - \tau_i) \quad (2.9) \quad ,$$

where β_i is the amplitude and polarity of the ith path, τ_i is the delay of the ith path, $\delta(t)$ is an impulse function and N_p is the number of paths. Figure 2.12 shows the filter structure.

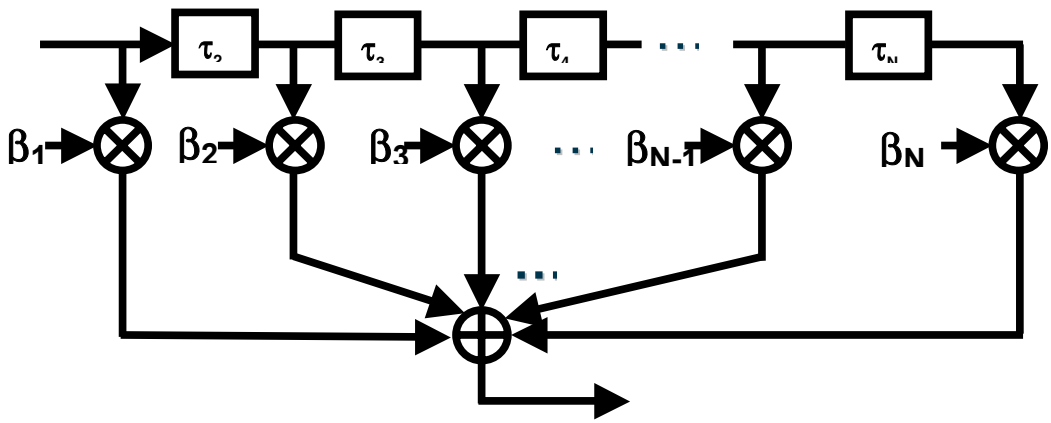

Figure 2.12: Filter Structure for Modeling UWB Channel Response

Most channel models give these parameters random values whose statistics are obtained from observation. This paper uses simulations based two different channel models: the Cassioli model and the Intel model [109],[110]. The Cassioli model was implemented in Agilent's Advanced Design System (ADS), and the Intel model was modeled in Matlab.

Cassioli et al. have proposed an indoor channel model specifically for UWB [109]. The measurements are taken at 14 different indoor locations every 2 ns starting at the first multipath arrival and continuing for 300 ns of excess delay. This results in 150 measurement bins of duration 2 ns. The 14 different receiver locations each contain a grid of 49 closely-spaced measurement points. The 14 locations measure the large-scale effects and the grid of 49 points measures small-scale effects.

In the Cassioli model, the boxes in Figure 2.12 labeled τ represent a delay of 2 ns, which is the time resolution of the measurements. Each β_i represents the energy

INTEL-1010
U.S. Patent 9,265,043

gain realized during a 2 ns period. Each β_i is a stochastic variable with a gamma distribution. The mean of each gamma distribution decays exponentially from β_1 to β_N. The decay constant and the ratio of β_1 to β_0 are both lognormal random variables with constant mean and variance. The total energy (or sum of β_0 to β_N) is a lognormal random variable with a constant variance and a mean determined by transmitter-receiver distance.

The procedure for determining the channel model is as follows. First, calculate overall energy received at a location, β_{TOT}, which is a lognormal random variable. Assuming a reference power of 0 dB, the mean of β_{TOT}, β_{μ}, is a function of distance, d.

$$\beta\mu = \begin{cases} -20.4\log_{10}(d) & d \le 11m \\ 56 - 74\log_{10}(d) & d > 11m \end{cases} \qquad (2.10)$$

Next, the power ratio, $r=G_1/G_0$, is a lognormal random variable that describes the energy ratio of the second 2 ns bin to the first 2 ns bin. Then, the decay constant, ε, is another lognormal random variable that describes the exponential decay rate of the subsequent 2 ns bins. The large-scale channel model is characterized by these three random variables with the lognormal distributions of Table 2.2.

Table 2.2: Lognormal Distributions of Channel Parameters

Parameter	Mean (dB)	Variance (dB)
$G_{TOT.}$	$G\mu$	4.3
R	16.1	1.27
ε	-4	3

Next, determine the small-scale parameters. The average energy gain of each 2 ns delay bin, $G_{k\ avg}$, is computed from the large-scale parameters and then modified according to a gamma distribution to produce the final G_k. Table 2.3 lists the

INTEL-1010
U.S. Patent 9,265,043

parameters of the gamma distribution. The parameter τ_k is the time at the *k*th bin ($\tau_k = k * 2$ ns).

Table 2.3: Distributions of Small-Scale Channel Parameters

Parameter	Distribution	Mean	Variance	α	β
$\beta_{k.}$	Gamma	$\beta_{k\ avg}$	$\beta_{k\ avg} * \beta_{k\ avg} / m$	m	$\beta_{k\ avg} / m$
M	Truncated Gaussian	$3.5 - \tau_k / 73$	$1.84 - \tau_k / 160$	N/A	N/A

The above procedure completely determines the channel because the energy gains between bins are uncorrelated. This is because the wide bandwidth and fine resolution of UWB usually causes discrete multipath components to fall within the 2 ns interval of the delay resolution. This means that the UWB system need not consider distortion due to frequency selective channels or to multipaths spread over adjacent delay bins.

Figure 2.13 shows an exemplary impulse response of the Cassioli channel at a transmitter-receiver distance of 10 m. The top graph shows large-scale parameters only, while the bottom graph includes small-scale parameters.

INTEL-1010
U.S. Patent 9,265,043

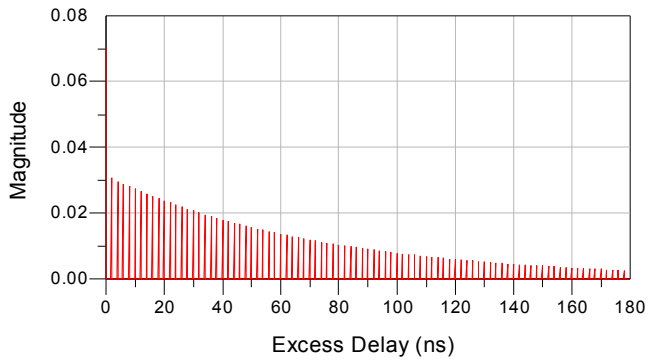

(a) Average Response

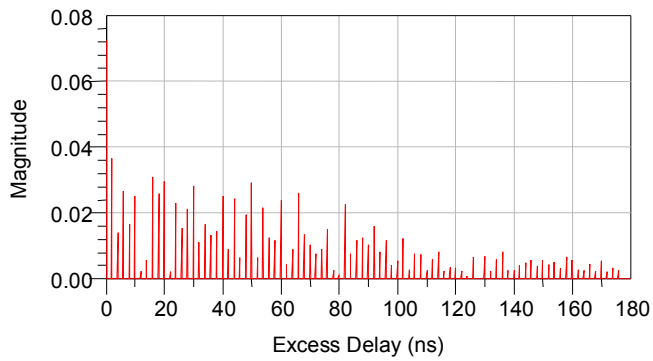

(b) Exemplary Response

Figure 2.13: Impulse Responses of Cassioli Channel

Figure 2.13 shows that the multipath significantly disperses the energy of a UWB signal over many possible paths. However, due to the short duration of I-UWB pulses these paths may separated from each other and fully resolvable. An appropriate receiver can capture the energy from most of the paths and add it coherently to cancel most of the effects of the channel.

Note that the first delay bin (at excess delay 0) contains significantly more energy than the subsequent delay bins, which follow an exponential decay starting at the second delay bin. The first multipath arrives at the LOS delay time and receives the gain associated with the first delay bin. For NLOS conditions, it is unlikely that that the first multipath contains the largest amount of energy. On average, 11% of total energy

INTEL-1010
U.S. Patent 9,265,043

arrives with the strongest multipath, 57% arrives after 30 ns, and 92% arrives within 100 ns. Since the channel model will vary due to small-scale variations, we use the average of many simulations with different multipath model realizations to obtain average performance trends.

Figure 2.14 shows a histogram of the RMS delay spread of the Cassioli model. The RMS delay spread shows the dispersion of the symbol energy over the excess delay time. The RMS delay spread is useful for investigating the maximum data rate of an unequalized channel. Multipaths from a previous pulse can corrupt the current pulse. So unequalized transceivers should wait until most of the energy disperses before sending the next pulse. Figure 2.14 shows that most of the symbol energy has dissipated after approximately 70 ns of excess delay.

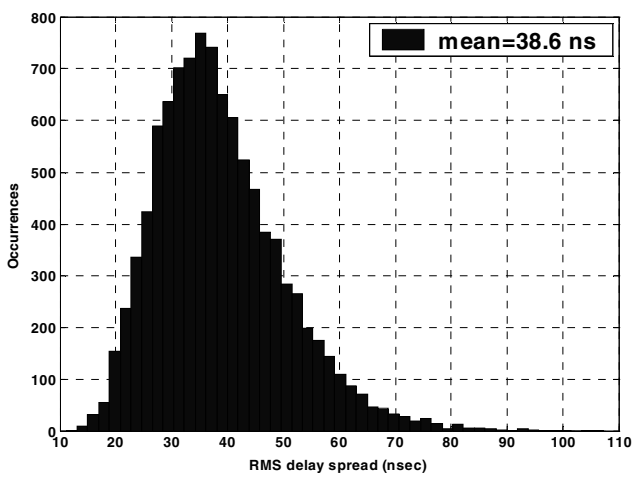

Figure 2.14: RMS Delay Spread of the Channel

To get another perspective on the effects of the UWB channel, we compare the simulated constellation diagram of binary PPM with the theoretical constellation diagram. Figure 2.15 compares the constellation diagrams of binary PPM under two conditions. The top row shows constellations that are corrupted by AWGN only. The bottom row shows constellations that are corrupted by both multipath effects and AWGN. The E_b/N_0 ratio increases from left to right. For low E_b/N_0 (= 0dB), both cases show significant corruption of the received signals. The system under AWGN performs

INTEL-1010
U.S. Patent 9,265,043

better that system with multipath effects because the received signal energy is not dispersed over the multiple paths. As the E_b/N_0 ratio increases to 12 dB, the AWGN channel exhibits less effect than the multipath channel on the signals. Under the AWGN channel, the signal energy dominates the noise and the constellation points are more clustered around the baseline points of Figure 2.10 (b). The constellation points under the multipath channel still overlap each other, and the contribution of ISI from the multipaths causes significant performance degradation. When E_b/N_0 is very high (20 dB), the multipath interference is finally insignificant enough to show some separation between the two baseline signals, but the effects from the multipath channel still dominate those from noise alone.

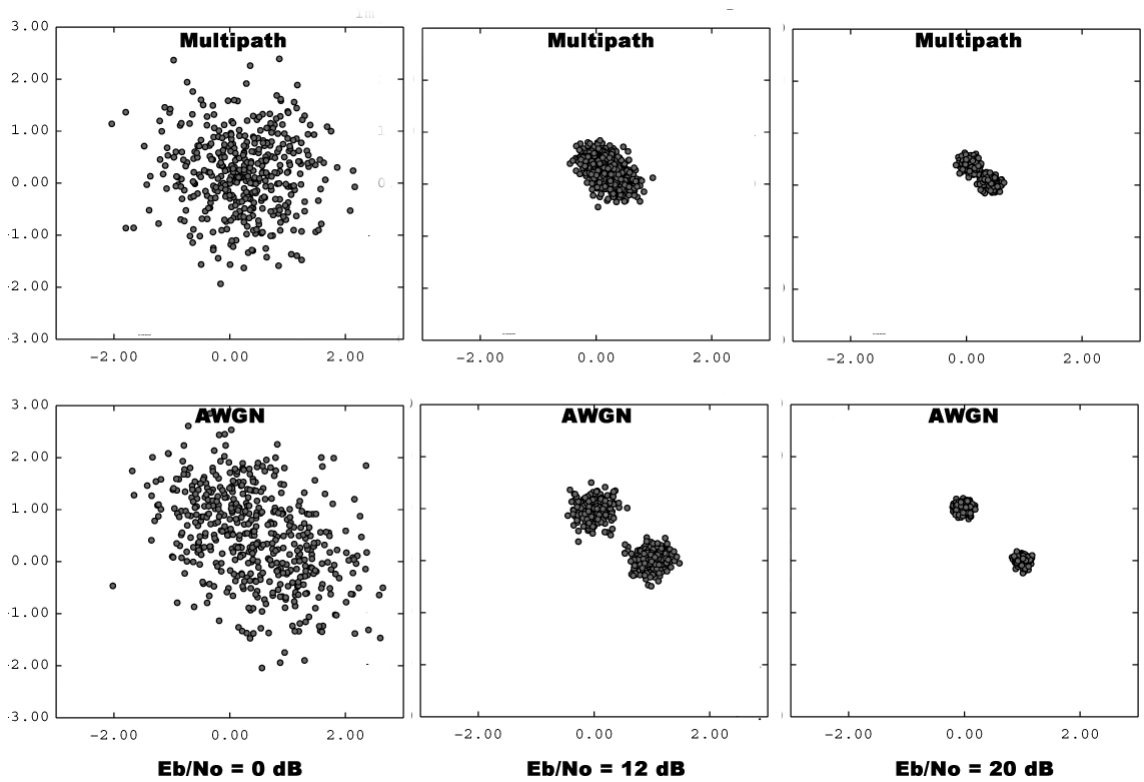

Figure 2.15: Constellation Diagrams with Multipath Effects and AWGN

The Intel channel model is similar to the Cassioli channel model, and it is used in the IEEE 802.15.3a working group to characterize multipath effects for UWB radios in WPANs. It is based on [109] and is derived from the Saleh-Valenzuela model [201].

INTEL-1010
U.S. Patent 9,265,043

Each multipath belongs to a cluster, which is a group of multipaths that arrive close together in time. The arrival times of each cluster and each multipath within a cluster are exponentially distributed random variables conditioned upon the previous arrival time. Each cluster, as well as each multipath within a cluster, undergoes independent fading. However, a lognormal distribution – rather than the Rayleigh distribution of the Saleh-Valenzuela model – describes the magnitudes of the multipath gains.

The channel model divides the possible channel conditions according to four scenarios:

- CM1: line-of-sight (LOS) at distances of 0-4 m;
- CM2: non-LOS (NLOS) at distances of 0-4 m;
- CM3: NLOS at distances of 6-10m; and
- CM4: extreme NLOS.

Table 2.4 shows the corresponding parameters for each of these channel conditions.

INTEL-1010
U.S. Patent 9,265,043

Table 2.4: Channel Model Parameters [109]

Target Channel Characteristics[5]	CM 1[1]	CM 2[2]	CM 3[3]	CM 4[4]
Mean excess delay (nsec) (τ_m)	5.05	10.38	14.18	
RMS delay (nsec) (τ_{rms})	5.28	8.03	14.28	25
NP_{10dB}			35	
NP (85%)	24	36.1	61.54	
Model Parameters				
Λ - cluster arrival rate (1/nsec)	0.0233	0.4	0.0667	0.0667
λ - ray arrival rate (1/nsec)	2.5	0.5	2.1	2.1
Γ- cluster decay factor	7.1	5.5	14.00	24.00
γ- ray decay factor	4.3	6.7	7.9	12
σ_1 cluster fading s.d. (dB)	3.3941	3.3941	3.3941	3.3941
σ_2 ray fading s.d. (dB)	3.3941	3.3941	3.3941	3.3941
σ_x total shadowing s.d. (dB)	3	3	3	3
Model Characteristics[5]				
Mean excess delay (nsec) (τ_m)	5.0	9.9	15.9	30.1
RMS delay (nsec) (τ_{rms})	5	8	15	25
NP_{10dB}	12.5	15.3	24.9	41.2
NP (85%)	20.8	33.9	64.7	123.3
Channel energy mean (dB)	-0.4	-0.5	0.0	0.3
Channel energy std (dB)	2.9	3.1	3.1	2.7

[1] LOS (0-4m). Channel measurements reported in [202].
[2] NLOS (0-4m). Channel measurements reported in [202].
[3] NLOS (4-10m). Channel measurements reported in [202],[203].
[4] Extreme NLOS. 25 nsec RMS delay spread.
[5] These characteristics are based upon a 167 psec sampling time.

For evaluation purposes, there are 100 pre-computed channel realizations for each of the four classes. In each class, the power levels are normalized for an average gain of 0 dB with a standard deviation of 3 dB. The pre-computed channel realizations statistically model typical impulse responses of the UWB channel. Each impulse in a channel realization corresponds to a multipath component and is described with a magnitude, an arrival time, and a polarity.

INTEL-1010
U.S. Patent 9,265,043

2.1.2 Impact of I-UWB Signaling

2.1.2.1 Spectral Lines

The pulse train of I-UWB leads to some unintended side-effects in the frequency domain, as a pulse train has different characteristics than a single pulse. Figure 2.16 shows the spectrum of a pulse train compared to that of a single pulse. The right figure is a close view of the left. The red line shows the spectrum of one pulse, while the blue line shows the spectrum of a pulse train. The spectral lines of the pulse train are maximum for integer multiples of pulse repetition frequency (PRF). The amplitude of the spectral lines relative to the average power increases with increasing PRF [91].

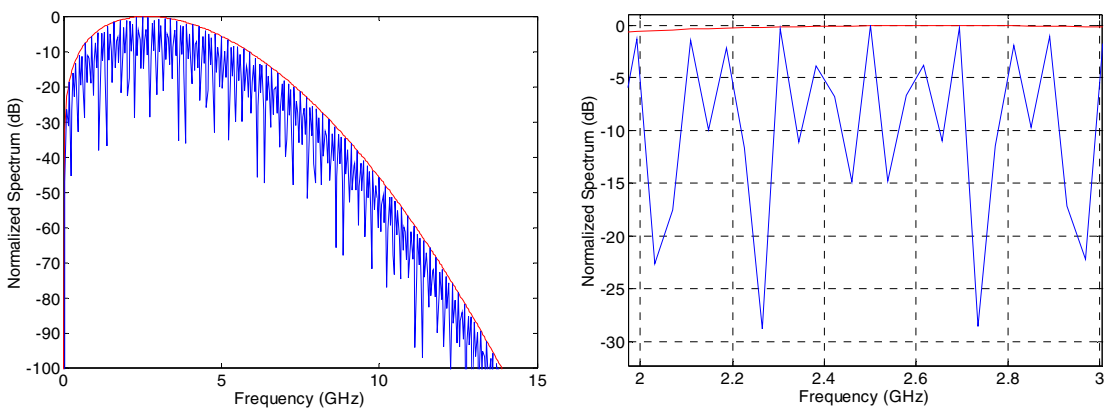

Figure 2.16: Frequency Spectra of Pulse and Pulse Train

The spectral lines appear at integer multiples of the PRF. This is explained by examining the power spectral density (PSD) of a UWB signal, which can be obtained as the Fourier Transform of the autocorrelation. For any linear modulation, such as BPSK, pulse amplitude modulation (PAM), or on-off keying (OOK), with a wide sense stationary sequence of information, the PSD can expressed as [204]

INTEL-1010
U.S. Patent 9,265,043

$$\Phi_{ss}(f) = \frac{\sigma_i^2}{T_f}\left|P(f)\right|^2 + \frac{\mu_i^2}{T_f^2}\sum_{m=-\infty}^{\infty}\left|P\left(\frac{m}{T_f}\right)\right|^2 \delta\left(f - \frac{m}{T_f}\right) \quad (2.11) \quad ,$$

where δ is the impulse function, μ_i is the mean of the information sequence, and σ_i^2 is the variance of the information sequence. The first term of (2.11) represents the continuous spectrum, and the second term represents the discrete frequency components spaced every $1/T_f$ in the spectrum. If we let

$$X(f) = \frac{1}{T_f}\left|P(f)\right|^2 \quad (2.12) \quad \text{and}$$

$$Y(f) = \frac{1}{T_f^2}\sum_{m=-\infty}^{\infty}\left|P\left(\frac{m}{T_f}\right)\right|^2 \delta\left(f - \frac{m}{T_f}\right) \quad (2.13) \quad ,$$

then the continuous Φ_{ss}^c and discrete Φ_{ss}^d parts of the spectrum can be expressed as

$$\Phi_{ss}^c = \sigma_i^2 X(f) \quad (2.14) \quad \text{and}$$

$$\Phi_{ss}^d = \mu_i^2 Y(f) \quad (2.15) \quad .$$

Thus, the in the limiting cases, the entire spectrum can be continuous if $\mu_i = 0$; or the entire spectrum can be discrete if $\sigma_i^2 = 0$, i.e. a train of uniform pulses. In either case, the total spectral energy must remain the same, so we can set the two limiting cases equal to each other as

INTEL-1010
U.S. Patent 9,265,043

$$\frac{1}{T_f}|P(f)|^2 = \frac{1}{T_f^2}\sum_{m=-\infty}^{\infty}\left|P\left(\frac{m}{T_f}\right)\right|^2 \delta\left(f-\frac{m}{T_f}\right) \quad \text{or}$$

$$|P(f)|^2 = \frac{1}{T_f}\sum_{m=-\infty}^{\infty}\left|P\left(\frac{m}{T_f}\right)\right|^2 \delta\left(f-\frac{m}{T_f}\right) \qquad (2.16) \quad .$$

The discrete spectrum contains the same amount of energy as the continuous spectrum, but the energy is placed at discrete frequencies spaced apart by $1/T_f$, or the pulse repetition frequency (PRF). Systems with higher PRF incur fewer spectral lines but with greater amplitude. These systems must reduce their average power to prevent the spectral lines from exceeding FCC limits. A similar analysis can be performed for PPM modulation. Since the modulation is nonlinear, the PSD is given as [205]

$$\Phi_{ss}(f) = \frac{1}{T_f}|P(f)|^2\left\{1-|\Phi_{ii}(fT_p)|^2\right\} + \frac{1}{T_f^2}\sum_{m=-\infty}^{\infty}\left|P\left(\frac{m}{T_f}\right)\right|^2\left|\Phi_{ii}\left(\frac{mT_p}{T_f}\right)\right|^2 \delta\left(f-\frac{m}{T_f}\right) \qquad (2.17) \quad ,$$

where

$$\Phi_{ii}(f) = \sum_{k=0}^{N_s-1} p_k e^{j(2\pi fk)} \qquad (2.18)$$

for a PPM scheme with $N_s - 1$ pulse positions. Thus, the spectral lines further complicate signal detection and acquisition for systems with high PRF.

For systems with lower PRF, the FCC limits the peak power of a single pulse (as opposed to average power over many PRIs) to prevent overloading nearby victim receivers. Figure 2.17 shows the peak to average power of a UWB pulse train as seen by a victim receiver with 1 MHz bandwidth [91]. When the UWB system has a PRF less than 11 MHz, the peak interference power will not exceed the average interference power (including spectral lines). However, at frequencies lower than 11 MHz, the peak

INTEL-1010
U.S. Patent 9,265,043

power exceeds the average power. Although the lower PRI reduces the spectral lines, the system must limit its output power to comply with FCC peak limits. Thus, FCC peak power limits further complicate signal detection and acquisition for signals with low PRF.

Regardless of the PRF, signal detection and acquisition is encumbered.

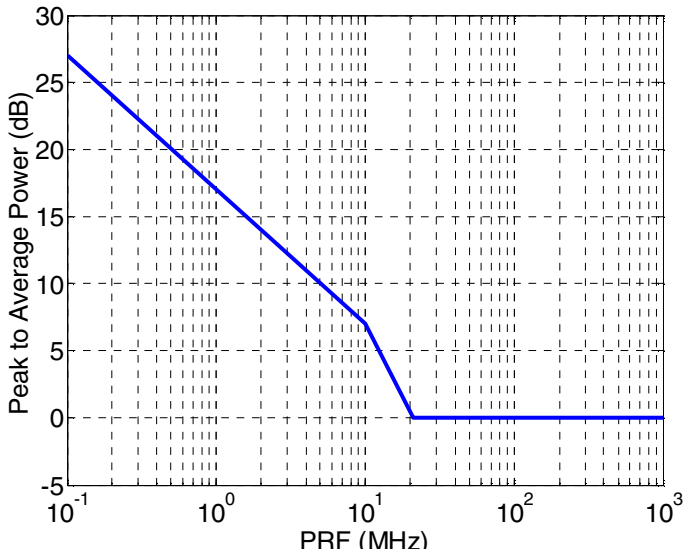

Figure 2.17: Peak-to-Average PSD of Spectral Lines as PRF Increases

2.1.2.2 Detection and Acquisition

The narrow pulses, low radiated power, harsh channel conditions, and strict FCC power limits combine to I-UWB signal detection and acquisition difficult. Narrowband systems normally detect activity by looking for energy in a certain frequency band. However, I-UWB does not have a carrier, and the narrow, low power pulses are difficult to detect over a long PRI.

Narrowband receivers perform a sliding correlation to acquire a signal. However, a sliding correlation is not practical for an I-UWB system. For a pulse repetition interval (PRI) of 10 ns and a pulse width of 160 ps, a sliding correlator requires a time step of about 80 ps for coarse acquisition [94]. For E_b/N_o = 5 dB, a time

INTEL-1010
U.S. Patent 9,265,043

window of 11 pulses provide a false alarm probability of 10^{-5}. Therefore, to guarantee detection, the receiver must listen to the channel for at least (10 ns / 0.08 ns) * 11 pulses = 1,375 symbols. Multipath spreading complicates sliding correlation by spreading the signal power over a longer period of time. There are many resolvable paths, but the power in each path is severely attenuated. Consider a channel with four strong, detectable multipaths equally spaced within the PRI window (the spacing that results in fastest average detection time). In this channel, the circuit only has to discover one of the four strong multipaths to reduce the search window by a factor of four; however, each signal is attenuated by a factor of ten or more, so there is still a net increase in detection time.

Figure 2.18 shows an I-UWB (T1) signal in Additive White Gaussian Noise (AWGN) (T2) with a relatively good signal to noise ratio of 10 dB. The I-UWB signal is also dispersed through the multipath channel, and the PRI is 100 ns. The top figure shows the signal and the noise as seen by a receiver. It requires the separation of the signal from the noise, as in the bottom figure, to even see the I-UWB signal with the human eye

INTEL-1010
U.S. Patent 9,265,043

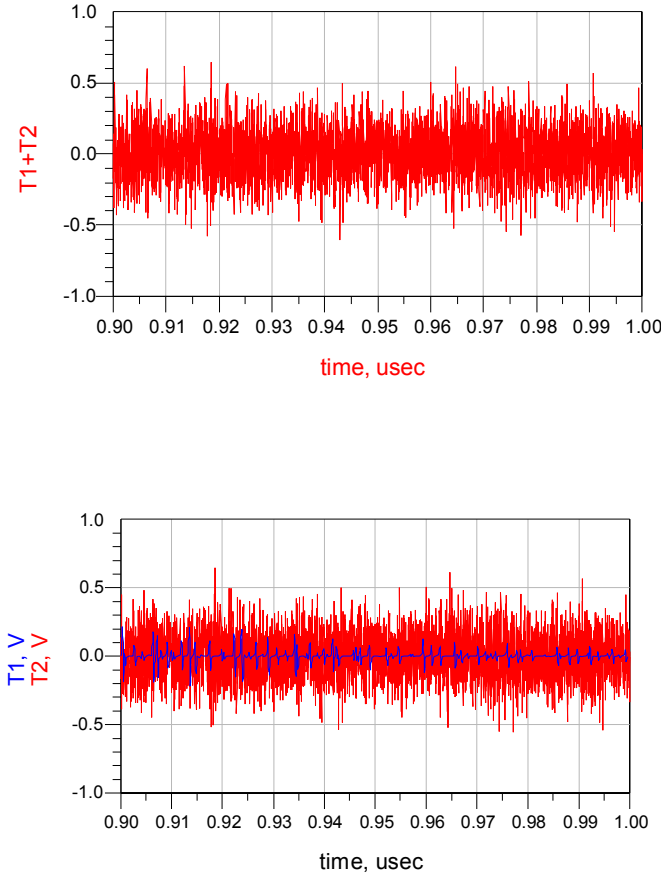

Figure 2.18: I-UWB signal (T1) in AWGN (T2)

2.1.3 Transceiver Architectures

This section reviews prior work on an I-UWB receiver and transmitter for the proposed system. The transmitter has been laid out in 0.18 µm CMOS [102], and the receiver components have been fabricated in 0.18 µm CMOS and tested [100],[101],[103],[104]. We choose CMOS implementation because its low power and low cost are suitable for ad hoc and sensor network applications. This work builds upon these basic communications components, but it is not limited to adopting these specific components and instead may use others [111]-[116].

INTEL-1010
U.S. Patent 9,265,043

2.1.3.1 Low Power Transmitter

The transmitter is based on the energy efficient pulse generator in Figure 2.19 [102], which can generate various pulse shapes and data rates through a programmable control block. Depending on the desired data rate and pulse shape, the control block adjusts the control voltages C_1, C_2, … C_n to control the direction of current flow and output voltage. The bandpass filter (BPF) limits the output to the FCC mandated -41.3 dBm/MHz over its bandwidth from 3.1 GHz to 10.6 GHz. For BPSK, the pulse shape also determines the modulation. Digital timing control determines the PRI provides the modulation for PPM. The total power from the circuitry is less than 10 μW, and the FCC limits the radiated power to 560 μW.

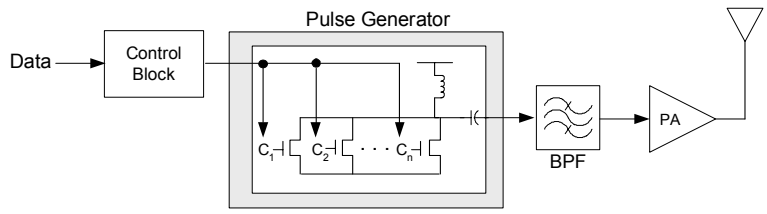

Figure 2.19: Low Power I-UWB Transmitter

2.1.3.2 Receiver

The receiver presents more demanding implementation constraints, especially in sampling the received signal for digital processing. One solution is a frequency domain receiver [100],[101]. Digital signal processing theory explains the advantages of sampling an I-UWB signal in the frequency domain. A signal may be represented in either the frequency domain or the time domain, and communications systems normally reconstruct a signal from discrete samples in time. I-UWB signals can occupy between 500 MHz and 7.5 GHz of bandwidth, and the resulting minimum sampling rate is at least twice that bandwidth. Analog to digital converters (ADCs) operating between 1 GHz and 15 GHz push the limits of existing CMOS technology and dissipate enormous power. Therefore, existing I-UWB receivers process the received signal with analog

INTEL-1010
U.S. Patent 9,265,043

correlators in SiGe technology, which is more expensive and consumes more power than CMOS. Thus, a CMOS implementation is more advantageous for ad hoc and sensor networks.

Frequency domain sampling supports CMOS ADC implementation by relaxing the sampling rate, decreasing circuit complexity, and reducing power dissipation. Instead of reconstructing the signal from discrete samples in time, spectral samples (each containing a frequency, a phase, and a magnitude) represent each received symbol. The receiver captures harmonic spectral components of a signal that falls within a time window longer than the pulse width and shorter than the pulse repetition interval (PRI). The spectral components captured during the time window describe the received signal as Fourier series coefficients. Because the time window extends beyond the desired length of the received signal, any discontinuous points at the window boundaries can be safely discarded.

Figure 2.20 shows the architecture of the receiver. At the front end, a low-noise amplifier (LNA) feeds typical narrowband resonator filters realizing the second order transfer function $1/(s^2+(k\omega_0)^2)$. A filter captures an in-band spectral component of the received signal at frequency f_i, where $f_i = kF_0$ for an integer k. The fundamental frequency F_0 is determined by an observation period T_p such that $F_0=1/T_p$. The length of the observation window also determines the number of ADCs. In Figure 2.20, the receiver set the time window to 1 ns to capture an I-UWB pulse with a 7 GHz bandwidth (3.1 ~ 10.1 GHz) and 100 ns PRI. The resulting fundamental frequency is the inverse of the time window (1 GHz), and the harmonic frequencies are multiples of the fundamental frequency. Two second-order filters extract the complex valued spectral components. Thus, in Figure 2.20, the receiver requires fourteen filters and ADCs to sample seven real and seven imaginary coefficients at 4 GHz, 5 GHz, …, 10 GHz.

Next, the ADC captures spectral samples at the pulse repetition rate, which is much lower than the Nyquist over-sampling rate to save power as well as circuit complexity. The sampling rate depends only on the PRI, and it is 10 MSps (1/PRI). Within a time window, each set of spectral samples represents a portion of the received signal as a continuous waveform.

INTEL-1010
U.S. Patent 9,265,043

For efficient operation, the receiver may perform signal processing on the spectral samples, or if necessary, a zero-padded *n*-point Inverse Fourier Transform (IFT) reconstructs the signal in the time domain with *n* samples. The narrow pulses of I-UWB result in many resolvable multipaths. A conventional narrowband receiver harvests and constructively combines multipath energy with a rake receiver. One rake finger processes each multipath, so the number of fingers fixes the number of harvested multipaths and the performance. However, each rake finger increases circuit complexity, power dissipation, and storage requirements. In contrast, when harvesting multipath energy in the frequency domain, the circuit complexity is independent of the number of multipaths within the time window. Spectral samples represent all multipath energy within the time window without tracking and de-skewing individual multipaths.

During channel estimation, the multipath energy harvester identifies multipaths by multiplying the received signal with a sliding template of a pulse in the frequency domain. In the time domain, the multiplication result is a correlation function that characterizes the channel impulse response with the arrival time of all multipaths that exceed a threshold. The impulse response yields a multipath template, which is converted to the frequency domain.

During operation, the receiver multiplies the spectral samples by the multipath template. The simple multiplication operation results in simpler hardware than a correlation operation. Further, a single set of coefficients represents multipath energy, so the frequency domain energy harvester does not require the additional fingers, samples, and processing speed of a rake receiver.

The clock recovery circuit tracks the optimal point for correlation within a PRI under time variant and frequency selective channel conditions. It is based on a basic PLL architecture with two modifications. First, to handle time-variant channel conditions, the reference ($\Re(\omega_k)$ in Figure 2.20) is updated according to channel conditions. In this process, the newly sampled signal is compensated for its phase error and fed into a noise reduction filter. Second, to handle the frequency selective channel, the circuit considers variations of signal-to-noise ratio (SNR) over the entire frequency band. The circuit tracks the reference phase with highest SNR among spectral components.

INTEL-1010
U.S. Patent 9,265,043

As shown in Figure 2.20, the structure of the clock recovery circuit is similar to a time domain clock recovery circuit, but the basic difference is that the proposed circuit detects phase error from a sampled spectral component. This results from the time shift property of Fourier transform, which states that the amount of time shift is represented as a phase rotation in the frequency domain.

$$\Im\{f(t-t_0)\} = e^{-\omega t_0} F(\omega) \quad (2.19)$$

Thus, k^{th} harmonic spectral component of the received signal, $\Re(\omega_k, t_0)$, with time shift t_0, appears as

$$\Re(\omega_k, t_0) = e^{-\omega_k t_0} \Re(\omega_k) \quad (2.20) \quad ,$$

where $\omega_k = k\omega_0$ with fundamental frequency ω_0, and $\Re(\omega_k)$ is the kth harmonic spectral component of the received signal under perfect synchronization.

From (2.20), a simple conjugate multiplication can detect phase error due to time shift as

$$\Re(\omega_k, t_0)\Re(\omega_k)' = e^{-\omega_k t_0} \Re(\omega_k)\Re(\omega_k)' = |\Re(\omega_k)|^2 e^{-\omega_k t_0} \quad (2.21) \quad .$$

Practical operation requires a narrow range of controlling phase, which allows a linear approximation of (2.21) as

$$|\Re(\omega_k)|^2 e^{-\omega_k t_0} = |\Re(\omega_k)|^2 (\cos\omega_k t_0 - j\sin\omega_k t_0) \approx |\Re(\omega_k)|^2 (1 - j\omega_k t_0) \quad (2.22) \quad .$$

INTEL-1010
U.S. Patent 9,265,043

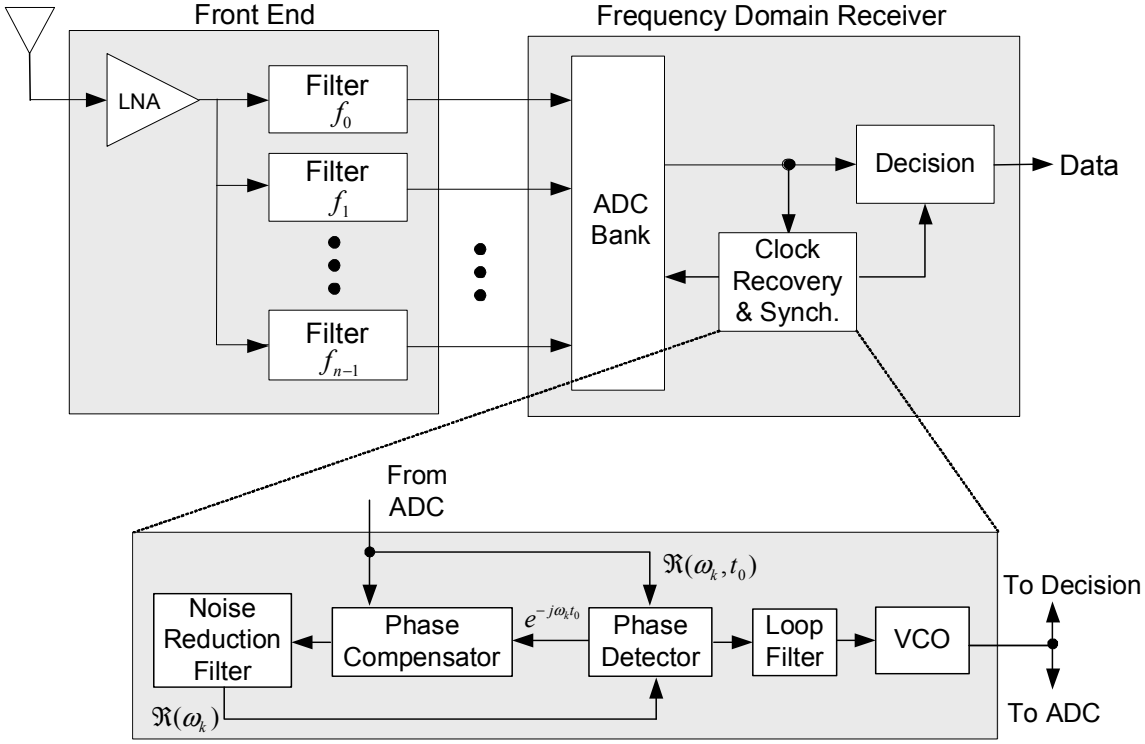

Figure 2.20: Frequency Domain UWB Receiver with Timing Recovery.

The transceiver supports data rates from 1 Kbps to 1 Gbps, and it can achieve a bit error rate (BER) of approximately 2×10^{-4} for a link distance of 10 meters in extreme non line-of-sight channel conditions at a data rate of 100 Mbps [101]. Lowering the data rate can increase link distance or improve the BER. The transmitter dissipates less than 600 μW of power, which is significantly less than the 200 mW from the receiver. The receiver can equalize channel conditions and inter-symbol interference.

2.2 Applications

Before the FCC allocated spectrum for UWB devices in their First Report and Order on February 14, 2002, most UWB research was relegated to small, proprietary systems addressing military communications and radar. After the report and order, UWB has generated tremendous interest, and many new ideas for applications have come from both industry and academia. The radar capability and flexibility in data rate

INTEL-1010
U.S. Patent 9,265,043

and link distance open the possibility of many new applications not suitable for narrowband systems. Table 2.5 presents examples in three major UWB application spaces: radar, communications, and location-aware communications.

Table 2.5: Application Spaces for UWB

Application Space	**Example Application**	**Type of Network**
Radar	Medical imaging	None
Communications	Wireless USB; WPANs	WPAN
Location-aware Communications	Asset tracking; Structural Integrity Monitoring	Ad hoc, Sensor

2.2.1 Radar

With a low duty cycle and wide bandwidth, UWB is naturally suitable to radar applications, which were among the first applications studied for UWB [117]. As the bandwidth of a pulse increases, it provides finer resolution of radar images for improved target identification. UWB also provides low probability of intercept and detection because the wide bandwidth to information ratio results in low energy across the spectrum. Because a UWB system may use the same transceiver for both radar and communications purposes, UWB provides one low-cost interface that is both a sensor and a communications system.

When radar systems utilize a UWB signal, the wide bandwidth and short pulse duration identifies more target information, improves range accuracy, improves resilience to passive scatterers (clutter), mitigates destructive multipath effects from ground reflection, and enables a narrow antenna beam pattern [93]. The wideband pulses carry more information about the target, such as shape or material. Further, the pulse may have a low center frequency to penetrate solid structures. Finally, narrow pulses eliminate the ambiguity between polarity reversal and time delay found in a continuous wave narrowband signal, thus reducing clutter from magnetic reflectors.

INTEL-1010
U.S. Patent 9,265,043

In traditional radar systems, resolution is proportional to wavelength. For impulse radar, the resolution of a target approximately depends on its bandwidth (or pulse width) as

$$\Delta R = \frac{c\tau}{2} \quad (2.23) \quad ,$$

where ΔR is the target resolution (m), c is the speed of light (m/s), and τ is the pulse width (sec). Thus, a Gaussian monocycle with a bandwidth of 7.5 GHz (~100 ps time duration) could achieve a resolution of $\Delta R = (3\times10^{8}\ \text{m/s} \cdot 100\times10^{-12}\ \text{s})/2 = 0.015$ m without extended signal processing. A single pulse is unlikely to both meet FCC regulations with regards to out-of-band emissions and have a 7.5 GHz bandwidth, so the actual resolution will be slightly larger. With added signal processing, the resolution can be improved close to the Cramer-Rao lower bound [118].

Because of its high-resolution radar capability, UWB has been proposed for many novel radar applications, such as vehicular radar to enhance driver safety and comfort [119]. UWB radar can provide proximity sensing around the exterior of a car to detect any objects within range of the vehicle. Initially, applications will notify the driver of hazards. For example, a vehicular radar system would alert the driver through audio or visual output when it detects potential collisions at the side, front, or rear of the vehicle. Such a system may aid the driver by "seeing" blind spots while changing lanes, reversing, or parking. In later stages of development, multiple UWB sensors can be networked with other vehicular systems and provide autonomous control of tasks such as parking, cruise control, transmission control, braking, airbags, safety belts, or suspension tuning. Because of its communication capability, UWB may even be applicable for complete control of autonomous vehicles on smart, networked roadways.

UWB vehicular radar has been allocated spectrum from 22 GHz to 29 GHz with the stipulation that the center frequency and the highest radiation level must be above 24.075 GHz. A further restriction is placed on the direction of radiation, which must attenuate energy above 38 degrees to the horizontal plane by 25 dB with respect to Part

INTEL-1010
U.S. Patent 9,265,043

15 limits. This requirement is scheduled to grow stricter year-by-year as more vehicular radar devices are included as standard equipment on commercial vehicles.

Another high-resolution radar application is Ground Penetrating Radar (GPR), which detects objects buried underground [120]. The crowded infrastructure of cities places a crisscrossed web of water pipes, electrical lines, communications links, and other obstacles underground. Heavy construction equipment can damage these structures and even cause injury or loss of life. GPR provides precise location information for such obstacles, and it does not rely on records, which can be incomplete, inaccurate, inaccessible, or missing. Another valuable use of GPR is to detect abandoned land mines and unexploded ordinance [121].

GPR operates mostly in the low frequency band below 960 MHz because these frequencies penetrate substances such as soil and sand better than higher frequencies. The operation of GPR is restricted to construction, law enforcement, fire and rescue, commercial mining, and scientific research. GPR is not seen as a severe source of interference to other devices since the device is positioned close to the ground and signal energy is directed into the ground.

Through-walls imaging is based on the same principle as GPR, however, signal energy is now directed horizontally. Therefore, through-walls imaging has considerable potential to interfere with existing systems, and the FCC restricts it to the public safety sector for use by firefighters and law enforcement officials. Law enforcement is particularly interested in using through-walls imaging to look through the double hulls of boats for hidden compartments and concealed contraband. The military also has significant interest in through-walls imaging for urban warfare situations. UWB can provide resolution fine enough to identify the presence of humans through walls, and it can even detect the small involuntary motions of respiration or heartbeats.

Finally, UWB offers promise for medical imaging for health care professionals to look inside the body of a human or animal [122]. For example, UWB can detect movements of the heart, lungs, vocal cords, vessels, bowels, chest, bladder, or a fetus. Since UWB radar can resolve images with safe levels of radiation, it can be used even in sensitive patients, such as mothers in the final stages of pregnancy. UWB has a significant advantage over induced field devices such as magnetic resonance imaging

INTEL-1010
U.S. Patent 9,265,043

(MRI), which confines the patient to a small space. With the radiated field of UWB, the patient can be anywhere, and the imaging device moves while the patient remains in a comfortable position. Since UWB radar may function a few meters from the target, it can provide remote monitoring of patients through blankets and clothing. An initial medical application of UWB radar is early detection of breast cancer with space-time processing of UWB signals through an antenna array [123].

2.2.2 Communications

More recently, the high-speed communications capability of UWB has been exploited for wireless personal area networks (WPANs) such IEEE 802.15.3a, which provides a high data rate physical layer (PHY) for personal area multimedia networking.

Because of potential interference to and from narrowband devices, early UWB research was primarily for military communications applications. Most research was performed quietly before the FCC opened the spectrum for UWB in February of 2002. Thus, many military systems developed prior to 2002 provided long-range communication capability with power levels that exceed current regulations [41]. Examples include aircraft-to-aircraft communications, augmentation of graphic display plans (GDP) for instrument landing in inclement weather, communication and control for unmanned aerial vehicles, sensors for monitoring aerospace structures, and secure location and RF identification systems for soldiers in urban combat situations [41].

More recent applications focus on wireless personal area networks (WPANs), which connect a limited number of devices in a small coverage area (within 10 m). Current UWB radios for WPANs must meet the FCC power limits, and hence, they radiate much less power than earlier systems. Taking full advantage of the high data rate of UWB, the IEEE 802.15.3a standard endeavors to define medium access and physical layers with the highest data rate possible for WPAN applications. UWB promises to deliver extremely high data rates (up to Gbps range) for multimedia applications and quick download times for large data files. To support these applications, the UWB physical layer for IEEE 802.15.3a offers data rates of 110 Mbps

INTEL-1010
U.S. Patent 9,265,043

at 10 meters, 200 Mbps at 4 meters, and, optionally, 480 Mbps or higher at a shorter distance. Such data rates allow high-quality multimedia services and comfortable download times (seconds as opposed to minutes) for large media files [124].

Currently, the most common application for UWB WPAN communications is cable replacement for high-speed devices. Cabling is a bulky and aesthetically displeasing means of connecting devices, and it also tethers devices together to limit device mobility. XtremeSpectrum Inc.[1] proposed cable replacement for home networking [125], and Intel Corporation proposed cable replacement for office environments [126]. In fact, there are proposals for wireless Universal Serial Bus (USB) and wireless IEEE 1394 for consumer electronic (CE) devices [127]. These standards would connect peripherals such as digital video players, projectors, MP3 players, portable disk drives, camcorders, high-resolution digital cameras, PDAs, printers, scanners, web cams, home theaters, CD players, keyboards, or mice [128]. UWB could even provide a standard interface for wireless docking of laptops [126] or wireless inter-chip connections.

Because cables are inconvenient in clothing, another cable replacement proposal enables wearable peripherals for health, entertainment, military, or medical purposes [129]. UWB could clean up the awkward clutter of cables within a wearable computer system.

Time Domain Corporation has noted that environments for the proposed applications would likely be shared among multiple families or multiple businesses within a single building or confined space. Additionally, a large number of devices may be networked, so most of these applications require a standard that exploits the spatial reuse property of UWB. Operation of UWB communications in such an environment requires high aggregate data rate, low cost, low power, and small size; so performance can be measured as [125]

$$P = \frac{SpatialCapacity}{Power \cdot Cost \cdot Size}\left(\frac{bps/m^2}{W \cdot \$ \cdot m^3}\right) \quad (2.24) \quad ,$$

[1] Motorola bought Xtreme Spectrum in November 2003. Xtreme Spectrum made these proposals before then.

INTEL-1010
U.S. Patent 9,265,043

where P is the performance metric, *SpatialCapacity* is in bits/second per square meter of coverage, *Power* is in Watts, *Cost* is the cost of the device, and *Size* is the amount of physical space the device occupies, in cubic meters.

2.2.3 Location/Communication/Low Power

I-UWB offers a unique blend of radar and communication applications known as *Location Aware Communications* [96],[130]-[138]. The Cramer-Rao Lower Bound (CRLB) provides a limit on the accuracy of the delay estimate (which reduces to the ranging accuracy), that increases with the bandwidth and the signal-to-noise ratio (SNR) of the received signal [139]. Even at low SNR, I-UWB can resolve distances with sub-centimeter accuracy using simple signal processing. When nodes share distance estimates, they can cooperatively calculate location information, which is an important feature for many sensor network applications and network protocols [32],[33]. Because I-UWB RF circuitry is shared for communications and ranging purposes, I-UWB may provide low-cost, high-resolution ranging; and unlike GPS, I-UWB's location capabilities can function in indoor environments.

As an example of the potential for location aware communications, the upcoming IEEE 802.15.4a standard will take advantage of a UWB physical layer that emphasizes low data rate, low power, robustness to fading, flexible link distance, and precision ranging. The goal of the standard is to provide simple, pervasive, and seamless wireless connectivity among devices. Although this prospective standard is still in the initial stages of development, it has generated tremendous interest and is expected to move rapidly to publish a standard in early 2006. Suggested applications spaces include sensors, controllers, and logistical devices. The following applications are based on the response to the IEEE 802.15.4a Call for Applications [130],[131].

With the improved robustness, larger communication range, and precision ranging ability, the standard targets such applications as building and home automation, automated meter reading, industrial, safety, personnel monitoring, security, inventory control, process control and logistic applications. The standards committee notes that there will be broad demand for such applications in the near future.

INTEL-1010
U.S. Patent 9,265,043

Many parties desire to use UWB to provide communications devices that can locate people. Aetherwire & Location, Inc. and the city of Chicago propose a location aware communication device for firefighters [131]. In a burning building, heavy smoke and darkness impair both audio and visual communications. With a UWB communications system, firefighters may monitor environmental conditions, communicate with each other, and locate injured personnel. Aetherwire proposes a similar application for soldiers to positively and quickly identify friendly soldiers to reduce accidental deaths and injuries [131]. Harris Corporation stipulates that military communications should adopt a modulation scheme with low probability of detection and intercept for stealth communications [132]. Samsung and Staccato Communications have proposed smart home applications that manage almost all aspects of the home including doors, keys, TV, radio, or computers [131]. The system would be aware of individual users and their preferences. As individuals move throughout the smart home, a tracking system could automatically adjust room temperatures and activate entertainment devices to a particular television channel or website. General Atomics offers proximity sensors that provide security for cars, computers, or homes, which automatically lock and unlock as the owner travels in and out of range [131]. LB & J consulting suggests that UWB could be used to track students and personnel in school buildings [131]. In schools, the tracking system could control access to school buildings, conduct instant roll call, produce reports to analyze incident patterns, monitor school bus transportation, and engage parents in student supervision. Ubisense Ltd. proposes to increase productivity in office environments by locating key personnel [131]. Privacy and security concerns, however, would have to be addressed before such systems would be implemented.

Location aware communications capability can also be used to manage assets. UWB expedites the inventory control process because the network can automatically scan individual containers and report status information without physical examination of the container's contents. Further, UWB performs well in a densely packed environment such as stacked pallets in trucks or stacked containers in ships. Aetherwire has suggested precision asset location and autonomous manifesting applications for the Department of Defense, which is the largest U.S. transporter of goods [131]. Inforange

offers a similar suggested application for tracking packages during shipment to reduce the amount of lost and misrouted packages [131]. They propose a transmit-only device to save power in the tags. General Atomics extends this idea to tracking for inventory control in warehouses and retail shops [131]. A similar technology could be used as small discrete security tags for high valued items such as leather jackets in retail stores [131]. Both Ubisense and MSSI have suggested tracking life-saving equipment in hospitals, as it is not always possible to locate equipment quickly in an emergency [133].

Tracking mobile objects is another application that uses UWB's radar capability. One idea is a UWB network that provides a protective security "bubble" around a geographic area. The radar capability of UWB would detect intruders and track their motion. In a networked environment, this could provide accurate tracking over a large geographic area. In outer space, UWB could automatically track an astronaut outside of a spacecraft or track the position of two spacecraft that are docking. Time Derivative and Q-Track suggest unique applications for professional sports to track balls, athletes, or racecars [131]. On farms and wildlife sanctuaries, a tracking system could automatically track the movement of cattle or wildlife.

In the proposed applications for IEEE 802.15.4a, several companies mention sensor networks, which stand to derive huge benefits from the low power and location aware properties of UWB [1],[134]. Position location capability aids in network configuration and provides a service for the networking and application layers. Aetherwire notes the demand for sensor networks to monitor industrial automation and control [131]. They cite the high cost ($10 to $25 per foot) of wiring for pipe sensors, which typically exceeds the cost of the sensors. Mobile nodes may take advantage of UWB's location capability to organize and perform tactical maneuvers [135]. Staccato and Aetherwire suggest UWB for heating, ventilation, and air conditioning (HVAC) control for home and office environments [131]. Extending this idea, Echelon Corporation proposes to add UWB radios to water and gas meters to report readings directly to the consumer and also to the utility company through power lines [136]. Another possibility is monitoring a human for early warning of seizures or heart beat monitoring [137]. ST Microeletronics notes that the location aware capability allows

INTEL-1010
U.S. Patent 9,265,043

such networks to configure themselves (so that they become ad-hoc networks) circumventing installation by a technician [131]. Samsung and CUNY want to augment the Global Positioning System (GPS), which is not usually receivable indoors, to enable location assisted routing of network data. UWB is an excellent low power physical layer for sensor networks [131]. The extremely low duty cycle of UWB allows sensors to conserve energy and operate for many years without maintenance. Because of its robust operation in harsh multipath environments and penetration capability, UWB also supports sensor networks in warehouse and cargo hull environments and even embedded in solid structures to provide a real-time non-invasive report on structural integrity.

2.2.4 Ad Hoc and Sensor Networks

Many of the above location aware communications applications also qualify as ad hoc or sensor networks. Most current research into ad hoc and sensor networks concentrates on the Network Layer and above. However, the unique properties of I-UWB affect the MAC and Physical Layer of ad hoc and sensor networks as well. This section discusses some major characteristics of ad hoc and sensor networks and their relationship to these bottom layers of the OSI model.

Ad hoc networks include any network without existing infrastructure, so the network is responsible for self-configuration. This concept is especially useful considering the recent proliferation of wireless communications – a network can be anywhere, and the nodes within that network can be mobile. Wireless ad hoc networks are useful in emergency situations, military applications, and other situations where there is no existing network infrastructure. Generally, this entails multi-hop routing at the Network Layer and also possibly some QoS guarantees. Nodes may be peers to one another, i.e. any node may transmit to any other node; or there may be a hierarchy. Such networks may be large – on the order of thousands of nodes or more – so protocols should scale to a large number of nodes.

INTEL-1010
U.S. Patent 9,265,043

Sensor networks are a type of ad hoc network with unique characteristics. They consist of a few (for structural integrity monitoring) to thousands to millions (for environmental monitoring) of sensors randomly deployed in an area of interest. The sensors monitor physical phenomenon. Typical sensors require only limited sensing and processing capabilities because wireless communication allows them to coordinate among themselves. In this case, the whole is much greater than the sum of the parts.

The unique characteristics of sensor networks place special constraints on the design of all layers in the OSI model. At the Application Layer, data are often correlated in space and time because they represent physical measurements. Therefore, data compression and aggregation are often useful. Additionally, sensor data is usually not required frequently, and it often consists of only a few bytes of data. Therefore, throughput can be sacrificed to meet the other constraints. Note that a high data rate is still advantageous for saving power: a faster data rate means that radios transmit and receive data faster, and hence are awake for a shorter period of time. Further, a faster data rate means there is less probability of collision at a given offered load. At the Routing Layer, the data flow from the sensor nodes to one or a few sinks instead of peer-to-peer, so routing can be simplified. However, the routing protocol should not favor certain sensors over others, causing them to drain their battery before the others and possibly disconnecting the network. At the Link Layer, the data may also be correlated in time, thus leading to collisions from multiple nodes reporting a similar event. Further, energy efficiency is a huge priority not addressed in the OSI model. Because devices may be in inhospitable areas such as industrial monitoring or war zones, the nodes should last for a long period of time with limited energy resources such as a battery or energy scavenging hardware. The energy constraints also constrain protocols and algorithms to be as simple as possible to reduce processing overhead.

From the above, power consumption, cost, and QoS are important design considerations for any layer of ad hoc and sensor networks, including the MAC and Physical Layer. The MAC protocol and the radio play a crucial role in determining both fairness and the amount of energy spent on a successful transmission [70]. The radio dictates the energy efficiency and hardware complexity of the physical layer, and

INTEL-1010
U.S. Patent 9,265,043

the MAC layer implements the collision avoidance strategy and also shapes the fairness of the network.

2.3 MAC Protocols

In any broadcast network, the medium access control (MAC) protocol performs the important function of controlling each node's access to the channel to prevent collisions. A common analogy is the protocol used by a group of people attempting to talk in a room. In such a situation, people usually abide by rules such as

- Don't talk while someone else is talking. If two conversations occur concurrently, then both parties' words may be unintelligible.
- Listen before speaking. This prevents most concurrent conversations.
- If the intended listener does not understand the message, he requests the speaker to repeat the message.

For the speakers, the conversations are transmitted via sound waves through the air. For data networks, the messages may be transmitted via electromagnetic signals through the air or through wires. The same types of rules that apply to people in a room can also apply to data networks that share a common medium. In a data network, the MAC protocol is simply a set of rules that every node should follow.

MAC protocols for data networks are usually characterized according to throughput and delay. Throughput refers to the total amount of information that source nodes successfully transfer to destination nodes. Delay refers to the average amount of time that information waits before it successfully arrives at the destination.

INTEL-1010
U.S. Patent 9,265,043

2.3.1 General

2.3.1.1 Wired Protocols

By far, the most common MAC protocol for wired networks is carrier sense multiple access with collision detect (CSMA/CD) [90]. It is a distributed protocol, so there is no central node to coordinate transmissions. The basic operation of CSMA/CD is as follows. When a node has data to transmit, it first senses the state of the medium. If the medium is idle, the node is free to transmit. If the medium is busy, the node waits a short time period until after the medium becomes free. The short time period provides a chance to finish any transmissions that belong to the current transaction. After a node transmits its data, there is the possibility that another station has also transmitted data simultaneously. Therefore, the node also listens to the medium while transmitting to determine if the data matches its expected transmission. If the data does not match, the node knows there has been a collision, so it stops transmitting and tries again after a random backoff period. The random backoff period lowers the probability of the two competing nodes retransmitting simultaneously. CSMA/CD performs well because a node knows the status of its transmission during the transmission. Thus, nodes may terminate a corrupted packet immediately instead wasting bandwidth with an unsuccessful transmission.

2.3.1.2 Wireless Protocols

The wireless medium is fundamentally different from wired medium. First, not every node is within range of each other. In a wired network, every node attached to the wire can hear every other node attached to the wire, so each node has a similar picture of the network. However, when radio signals propagate, they lose power according to the inverse of x^n, where x is the distance and n ranges between 2 and 4 [140]. The received power decreases rapidly with distance, so each node has a different picture of the network. Second, radio nodes cannot simultaneously receive and transmit. The radiated power is many orders of magnitude greater than any incoming radiation, so

INTEL-1010
U.S. Patent 9,265,043

any incoming signal in the same band would be undetectable. To simultaneously transmit and receive, a transceiver must listen in one frequency bands while transmitting in a second band. This is known as full duplexing, and it rarely implemented in practice because of the hardware expense, the additional power dissipation, the spectral inefficiency, and the reduced data rate. Half duplexing – or receiving and transmitting at different times – is much more common.

Because of the characteristics of the wireless medium, wireless MAC protocols may need to address the hidden terminal problem illustrated in Figure 2.21 [86]. The dotted circles represent the radio ranges of nodes A, B, and C. Node B is within range of both A and C. Due to rapid degradation in signal strength, nodes C and A are out of each other's range. The channel is initially clear, so node A transmits to node B. Some time after node A starts transmitting, node C decides to transmit to node B. Node C is out of range of node A, so it cannot hear node A's transmission to node B. Further, due to Node B's half duplex radio, it cannot inform Node C that it is currently receiving a packet. Node C thinks the channel is clear, so node C transmits and there is a collision at node B, which corrupts the data from both A and C.

The wireless medium also leads to exposed nodes. In this case, consider an ongoing transmission from Node B to Node A. If Node C has a packet to transmit to Node D, it will wait until Node B finishes. This is not necessary, since Node C's transmission will not interfere with reception at Node A. The exposed node problem results in a waste of bandwidth from inefficient spatial multiplexing.

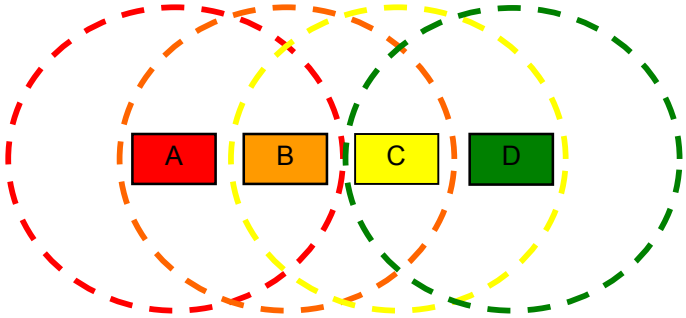

Figure 2.21: Hidden and Exposed Terminal Problem

INTEL-1010
U.S. Patent 9,265,043

Due to the hidden terminal problem, only the destination node is in a position to identify if there has been a collision. Further, the transmitting nodes may not know of a collision until after their unsuccessful packets have wasted bandwidth and transmit power. Wireless MAC protocols are primarily built to solve the hidden node problem. Figure 2.22 shows the design space for wireless MAC protocols, and this section briefly reviews the characteristics of each type of protocol.

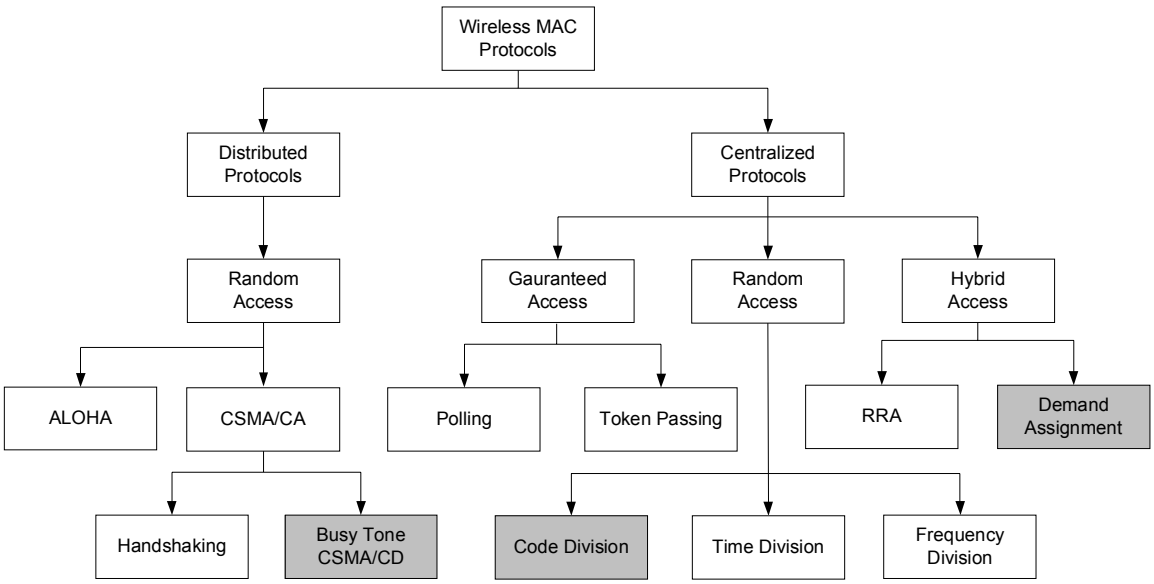

Figure 2.22: Wireless MAC Protocols

Centralized protocols are generally suitable for small networks that place a higher priority on performance than on power consumption or on hardware complexity. Because they collect information about the state of the network, centralized protocols offer high throughput, low delay, and firm QoS guarantees. They avoid hidden and exposed nodes because the centralized control guarantees that only one transaction occurs at a time. Some examples of centralized protocols include Bluetooth and IEEE 802.15.3a, which are designed to support multimedia devices and low latency computer peripherals. QoS is the most important priority, and as a result, such networks are typically limited to ten or fewer devices to reduce overhead and to maintain the serviceability of the network. Centralized protocols may further be divided into guaranteed access, random access, and hybrid access protocols.

INTEL-1010
U.S. Patent 9,265,043

The guaranteed access protocols give each node a regular opportunity to be the sole transmitter. Token passing protocols implement guaranteed access by passing around a special "token" packet (through a central controller), and the owner of the token is the only node allowed to transmit. Polling is similar, but a central node directly queries each node, possibly in a round robin fashion [141]-[143]. Both token passing and polling protocols require a central controller to prevent token loss, and the constant querying incurs a large transmission overhead when the network is idle.

The centralized random access protocols partition the channel into mutually orthogonal sub-channels according to codes, frequencies, time slots, or a combination of these. The data rate of each channel is a fraction of the full channel data rate. A base station has a special transceiver with the ability to receive and transmit on every channel. In idle sense multiple access (ISMA), a central node broadcasts a signal when the medium is busy [144],[145]. Performance is similar to CSMA/CD [146]. In code division protocols, all traffic flows through the base station, which translates codes between users. For example, in randomly addressed polling (RAP), the central node notifies all the nodes of a free channel; each node responds on a different code channel; and the central node picks a winner at random [147]-[149]. Frequency division operates similarly to code division, but the central node requires additional RF circuitry and signal processing.

Finally hybrid centralized protocols combine random access and guaranteed access to improve performance. These protocols generally consist of three phases: request, scheduling, and data transmission. Nodes first request a reservation with a random access, contention-based protocol such as ALOHA. The controller either schedules or denies the reservations that it receives. Any node with a confirmed reservation then has guaranteed access, usually in the form of a a time slot. The scheduling algorithm determines if the protocol is random reservation access (RRA) or demand assignment. RRA protocols provide QoS guarantees for data and voice [150]-[154]. Demand assignment protocols are derived from ATM networks, and they differentiate between classes of data. The controller provides different classes of service depending on a strict hierarchy [155]-[157].

INTEL-1010
U.S. Patent 9,265,043

If centralized protocols were applied to large ad hoc or sensor networks, the centralized control traffic would significantly increase the amount of overhead bits, thus wasting bandwidth, consuming excessive energy, and reducing the useful network lifetime. Consider a network that detects intruders. Most of the time, there will be nothing to report, and so the control traffic adds nothing but overhead. While idle, nodes should instead conserve energy to extend the lifetime of the network. Additionally, in a network of thousands of nodes, the centralized control does not scale well. The amount of control traffic would be unwieldy and the scheduling algorithms too complex. The central controller also needs to be within range of all nodes in the network. Finally, because nodes may not be easily serviceable (e.g. battlefields or industrial monitoring) a central failure would render useless thousands of deployed nodes.

Distributed protocols offer no firm guarantees on latency, throughput, or fairness. However, they are far less complex, and they scale to large ad hoc and sensor networks. Further, distributed protocols avoid the centralized control and overhead of centralized protocols.

The most basic MAC protocol is the ALOHA protocol. A node may transmit at will. If the transmission is successful, the target node responds with an acknowledgment (ACK). Otherwise, the source node waits a random period of time and tries again. The protocol performs well for light traffic but poorly under heavy traffic. An improvement over ALOHA is carrier sense multiple access (CSMA). It operates similarly to ALOHA, but it requires a node to listen to the medium before transmitting. If the medium is busy, the node defers its transmission until the medium is free.

Carrier sense is more generally known as clear channel assessment (CCA), which provides two important services. One role is to detect an incoming packet and the other is to ensure that the channel is free before transmitting. In narrowband systems, carrier sense performs the CCA function by detecting in-band energy. Wired systems detect voltage transitions. I-UWB systems currently have no quick, reliable, and efficient method to perform CCA.

INTEL-1010
U.S. Patent 9,265,043

In wireless networks, distributed MAC protocols may also address collisions, particularly from hidden terminals. To prevent collisions from hidden terminals, the destination node must give feedback to its neighbors because it is the only node that can definitively report a collision. The destination node informs its neighbors through a feedback channel in time, frequency, or code.

The CSMA/CD protocol manages collisions through a form of code duplexing. The receiver checks the received signal against its transmitted data, and a mismatched signal encodes two simultaneous transmissions. The advantage of such duplexing is that the source node immediately knows of a collision and does not waste energy transmitting a corrupted packet. The disadvantage is that it requires full duplexing in the same frequency band, and so it only works for wires networks, which uses different pins to separate the received signal from the transmitted signal. Therefore, wireless networks emulate CSMA/CD through other methods of duplexing.

Busy tone multiple access (BTMA) manages collisions through frequency duplexing, and it is a distributed form of ISMA. BTMA differs from ISMA in that BTMA does not require a central node to track and report the state of the medium. Nodes involved in a transaction share this responsibility. During a transmission, the target node (and possibly other neighbors of the source node) emits a busy tone to prevent neighbors of the target from interfering [82]-[86]. The out-of-band busy tone is frequency duplexed with the data transmission. BTMA maintains the immediate feedback of CSMA/CD, and it works in the wireless channel. The disadvantage of BTMA is that it requires two frequency bands. Therefore, all nodes require radio front-ends, and the protocol is less efficient in hardware, spectral efficiency, and power.

To reduce cost and power, wireless ad hoc and sensor networks usually manage collisions through time-duplexing [71]-[81]. An example is carrier sense multiple access with collision avoidance (CSMA/CA), and it is illustrated in Figure 2.23 (a) for the hidden terminal topology of Figure 2.21. The collision avoidance is implemented with small request-to-send (RTS) and clear-to-send packets (CTS). With an RTS/CTS exchange, node A first sends a short RTS to node B that contains the size of the upcoming data packet form node A. Node B replies with a CTS that echoes the size of the packet. All nodes within range of node B (including C) hear this CTS and know to

INTEL-1010
U.S. Patent 9,265,043

refrain from transmitting for the duration of the transaction from node A to node B. This handshaking implements a sort of virtual carrier sense, as all nodes within range of the source and destination know the duration of the upcoming channel activity. The ACK packet informs the source of a successful transmission. If the source does not receive an ACK, it retransmits its data.

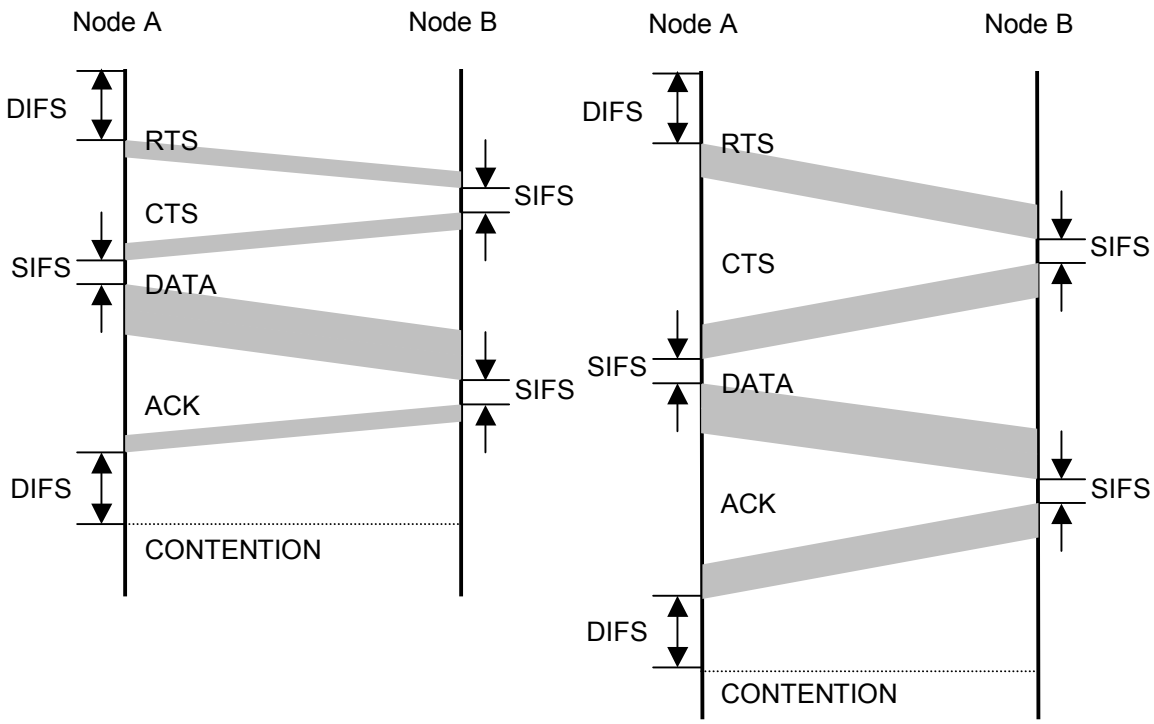

(a) Short Preamble for Narrowband (b) Long Preamble for UWB

Figure 2.23: CMSA/CA with RTS/CTS Data Exchange

In summary, centralized protocols perform well for smaller networks at the cost of hardware and control overhead. Distributed protocols perform relatively worse, but they are moderate in hardware complexity and scale to larger networks. The next sections discuss wireless MAC protocols implemented specifically for ad hoc and sensor networks and also MAC protocols implemented specifically for I-UWB.

INTEL-1010
U.S. Patent 9,265,043

2.3.2 Ad Hoc and Sensor Networks

Ad hoc and sensor networks generally adopt a distributed MAC protocol to scale to the large size. Further, there is no central point of failure and no central synchronization. The simpler protocols save power and overhead, and sensor data can tolerate the lack of strict QoS guarantees.

Collision avoidance protocols are widely used for wireless ad hoc networks, and such protocols have their roots in MACA, MACAW, and floor acquisition multiple access (FAMA) [71],[73]-[75]. With the right parameters, they can guarantee collision-free transfer of data. The basic structure of the RTS-CTS-DATA-ACK exchange also forms the foundation for medium access in the distributed foundation wireless MAC (DFWMAC) of the popular IEEE 802.11 standard [75]-[77].

Because of their collaborative operation, unique data flow, and more limited resources, sensor networks impose additional constraints on MAC protocols. For a tree topology, in which branch nodes report events to their parents and eventually to the base, hidden node problems exist on every other layer. An RTS/CTS exchange adds excessive overhead considering the small packet sizes. Further, neighboring nodes may sense a common phenomenon and their simultaneous transmissions may collide.

Researchers at UC Berkeley start with CSMA as the basic MAC protocol, and they custom tailor the protocol for sensor networks [70]. A reduced carrier sensing period as compared to 802.11 saves receiver power. Instead of performing handshaking to avoid collisions, the UC Berkeley protocol controls collisions by adaptively controlling its injected traffic according to the amount of through traffic. This eliminates the overhead energy of sending RTS and CTS packets. The network leverages the tree topology to eliminate ACKs; instead of an ACK, each node knows of a successful transmission when its parent node passes the message on to the grandparent [79]. Because nodes often transmit in a correlated manner, the MAC protocol injects a random pre-transmit delay before any transmission [80]. Finally, data aggregation effectively transmits many small packets with the overhead of just one packet. Such modifications to the basic CSMA MAC support sensor network traffic and achieve high energy efficiency per successfully transmitted bit [79].

INTEL-1010
U.S. Patent 9,265,043

The IEEE 802.15.4 standard defines a MAC protocol and a narrowband Physical Layer for large ad hoc and sensor networks [78],[158]. The upcoming IEEE 802.15.4a protocol will include a UWB Physical Layer to extend the capabilities of IEEE 802.15.4 to include precision ranging, extended link distances, and robust operation [131]. The protocol is ideal for low power networks because it provides a low power mode that cycles devices through sleep and awake modes.

IEEE 802.15.4 also adopts carrier sense multiple access (CSMA) as its base MAC protocol. The 802.15.4 MAC requires the following methods of CCA [78]:

(1) Detect in-band energy above threshold
(2) Detect 802.15.4-like modulation & spreading
(3) Detect 802.15.4-like modulation & spreading above threshold

The narrowband radios of 802.15.4 perform method (1) reliably, quickly, and efficiently by detecting energy in a certain frequency band. The remaining methods require acquisition and synchronization with the signal. All three methods are difficult in I-UWB systems. Because of this difficulty, the IEEE 802.15.4 MAC layer does not yet apply to UWB, and a partial aim of this thesis is to address the above challenges.

2.3.3 I-UWB

The above MAC protocols for ad hoc and sensor networks encounter difficulties with I-UWB radios. The low probability of detecting and intercepting a UWB signal now becomes a liability when implementing a MAC protocol for ad hoc and sensor networks.

Consider a handshaking protocol. For the narrowband system in Figure 2.24, the RTS and CTS packets are relatively short compared to the data packet, so the control packets contribute modest overhead. The control packets and the link layer preambles (which include acquisition overhead) are short. For example, in IEEE 802.11, the preamble length for the DSSS radio interface is 144 bits long, and the RTS

INTEL-1010
U.S. Patent 9,265,043

and CTS packets are 320 – 352 bits long. The data packets may be up to 4096 bytes long. In I-UWB, the long acquisition time creates significant overhead for the RTS and CTS packets. For current I-UWB receivers, the preamble is on the order of 1000 bits [28],[21],[94]. Thus, the length of the handshaking packets significantly increases as compared to a narrowband system. Figure 2.24 shows the overhead graphically. Simply amortizing the cost of the control packets over the length of a longer data packet cannot resolve this problem because large data packets incur more bit errors. Although CSMA/CA helps narrowband ad hoc networks, I-UWB incurs severe performance degradation due to the increased control packet overhead [159].

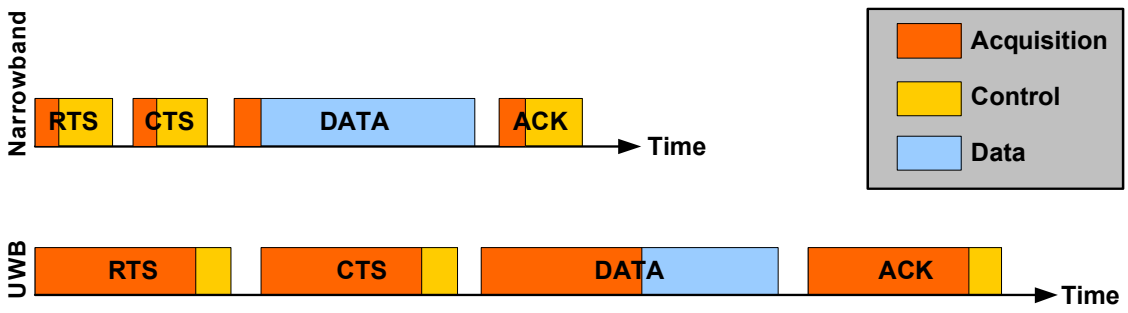

Figure 2.24: Handshaking Overhead in UWB and Narrowband Systems

Furthermore, in I-UWB, the narrow pulses and low radiated power make CCA difficult. Currently there is no reliable, quick, and efficient method for CCA for I-UWB as in narrowband systems. Because I-UWB systems cannot simply detect energy in a certain frequency band, they instead provide CCA with the synchronization and acquisition functions of the receiver. The synchronization and acquisition are performed during the preamble, and the 1000 symbol latency results in useless channel information and poor performance [160].

Figure 2.25 and Figure 2.26 show through simulation that long CCA and acquisition times degrade throughput. Both figures consider a simple linear network of three nodes A-B-C. In Figure 2.25, all nodes are within range of each other, and nodes A and C both transmit to B with a 1 Mbps data rate. The time between packets is determined by a Poisson distribution with a mean time between packets given by (offered load / 2). As the CCA takes a longer amount of time, the throughput

INTEL-1010
U.S. Patent 9,265,043

diminishes at all offered loads. With no coding, the systems transmit 1 Mpps, so a reasonable CCA time for I-UWB is between 800 µs and 1600 µs (800 to 1600 symbols). At these long CCA times, the throughput is reduced by 50% or more as compared to the ideal case. Further, the network is unstable, i.e. the throughput decreases with increasing offered load.

The results in Figure 2.26 consider the same node configuration as Figure 2.25 with the exception that nodes A and C are outside of one another's radio range, so they are hidden from one another. Figure 2.26 shows that the handshaking with CSMA/CA is much more efficient than CSMA for a topology with hidden nodes. However, as the acquisition time increases, the throughput decreases. The decrease is mainly due to the added acquisition overhead from the RTS and CTS packets. Note that the CSMA/CA protocol is much more stable than CSMA due to the virtual carrier sense provided by the handshaking packets. However performance for I-UWB is still severely degraded for acquisition (CCA) times of between 800 µs and 1600 µs.

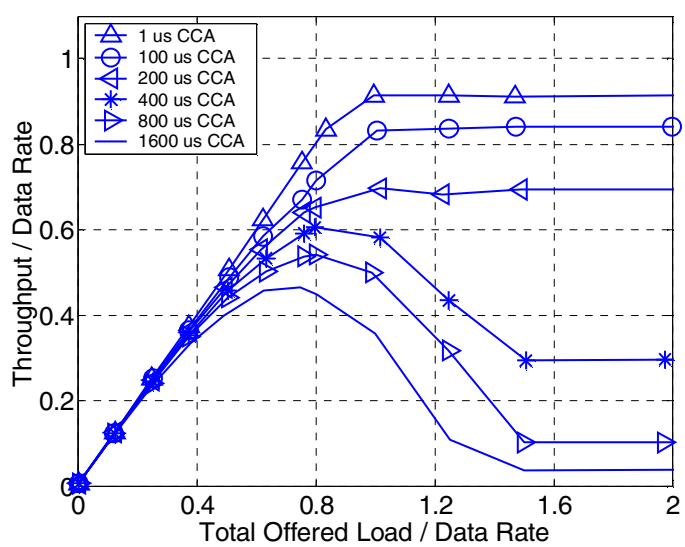

Figure 2.25: Throughput for CSMA as CCA Time Increases. All Nodes Are Within Radio Range.

INTEL-1010
U.S. Patent 9,265,043

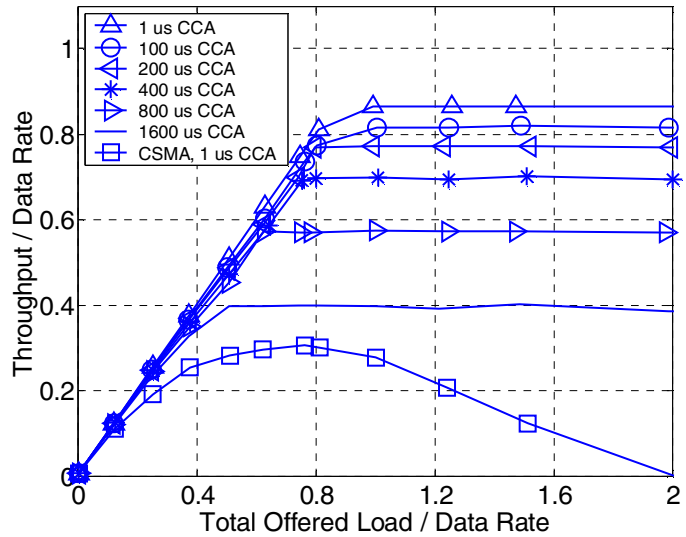

Figure 2.26: Throughput for CSMA/CA as CCA Time Increases. The Transmitting Nodes Are Hidden w.r.t. to One Another.

Due to the problems with implementing a distributed MAC protocol for I-UWB, current MAC protocols target small wireless personal area networks (WPANs) and cellular networks. These centralized protocols do not require handshaking packets or CCA capability to prevent collisions [34]-[69]. Instead, a central controller assigns concurrently transmitting nodes to different time slots or code channels. For a network of I-UWB systems, the received signal at a node with K neighbors is given by

$$r(t) = \sum_{i=1}^{K} s^{(k)}(t) * h^{(k)}(t) + n(t) \quad (2.25) \quad ,$$

where $h^{(k)}(t)$ is the channel impulse response between the kth user and the receiver, K is the number of neighbors, and $n(t)$ is AWGN.

The next two sections review the most popular methods of implementing MAC protocols for I-UWB. IEEE 802.15.3/3a is a centralized hybrid protocol, where nodes compete for time slots, and it is proposed for WPANs. Code division MAC protocols are also very popular for UWB networks with a cellular topology.

2.3.3.1 IEEE 802.15.3/3a

The IEEE 802.15.3a standard [95] is currently under development, and it is based on the narrowband IEEE 802.15.3 standard [55],[56]. The IEEE 802.15.3 MAC protocol was designed with foresight for an I-UWB Physical Layer.

Although commonly called a TDMA protocol, IEEE 802.15.3/3a is, more strictly, a hybrid protocol according to Figure 2.22. This is because nodes contend for a time slot with random access using slotted ALOHA (in 802.15.3a) or CSMA/CA (in 802.15.3), and then a central controller assigns available time slots for data transmissions. The centralized approach provides QoS guarantees for applications with heavy traffic such as video data. Due to the overhead of the control traffic and the limited number of slots, the IEEE 802.15.3/3a MAC is a good strategy for small networks (typically ten devices or less) [55]. The TDMA approach for data transmissions prevents collisions of data packets that would otherwise result from hidden terminals and simultaneous transmissions. This is because the central controller permits only one node in a piconet to transmit at a time. The central controller notifies nodes of the nodes and timing involved in upcoming transmissions, so nodes may disable their radios during time slots in which they are inactive. This is a good strategy for I-UWB because an I-UWB device may dissipate more power receiving than transmitting [95]. The data signal model for the system is equivalent to that of (2.25), since only one node may transmit data at one time.

The IEEE 802.15.3/3a protocol operates in a small group of nodes called a piconet. A piconet coordinator (PNC) node assumes the responsibility of assigning guaranteed time slots (GTS) to each requesting node. A data transmission sequence within a piconet follows the structure of a superframe as shown in Figure 2.27.

INTEL-1010
U.S. Patent 9,265,043

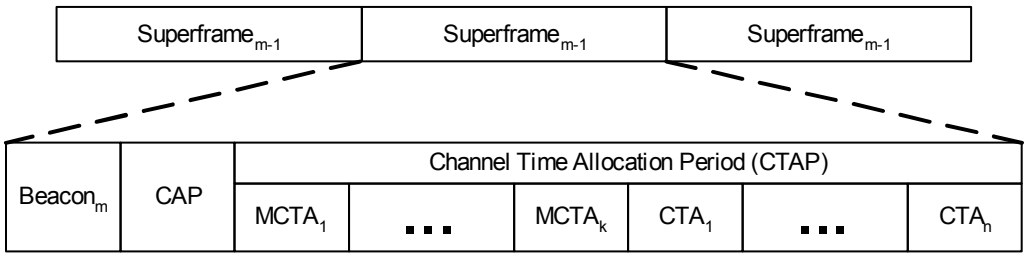

CAP: Contention Access Period
MCTA: Management Channel Time Allocation
CTA: Channel Time Allocation

Figure 2.27: Superframe Structure for IEEE 802.15.3/3a

The first part of the superframe is the beacon, which transmits control information from a PNC. This information may include the number and timing of available GTS slots. Next, the contention access period (CAP) provides nodes a chance to send short data packets, channel requests, and other commands. During the CAP, nodes access the medium using slotted ALOHA. Finally, there is a contention free period, where each node may send data during a reserved time slot in which no other node is allowed to transmit. The timing and number of slots may shift from superframe to superframe. The PNC guarantees QoS by admitting or denying new traffic depending on the available bandwidth.

IEEE 802.15.3/3a is targeted for small WPANs, and it is not suited to managing traffic in large ad hoc and sensor networks. IEEE 802.15.3/3a requires that all nodes have the capability of coordinating a piconet. This eliminates the central point of failure, but it greatly increases node cost and complexity. Further, power consumption is of secondary concern for IEEE 802.15.3/3a because the user can easily replace the batteries of a home device. In low data rate applications, the overhead from the beacon and CAP periods significantly increases the number of transmitted bits and thus reduces the useful lifetime of the network. The contention free period eliminates collisions from hidden terminals, but it prevents spatial multiplexing within a piconet. Finally, multihop transmission becomes especially difficult in the context of IEEE 802.15.3/3a because piconets must be connected to each other through the special parent/child relationship shown in Figure 2.28. The gateway node (the large blue node in the figure) is a normal node in the parent piconet and a PNC in the child piconet. The

INTEL-1010
U.S. Patent 9,265,043

child piconet operates on the same channel as the parent, and it is synchronized to avoid interference to parent piconet. The child piconet must complete its entire superframe during one GTS of the parent piconet, and this severely degrades the bandwidth of the child piconet. A more common is case in IEEE 802.15.3/3a is when piconets are co-located with each other, like the orange and red piconets in the figure. These piconets cannot communicate with each other because they operate on different channels.

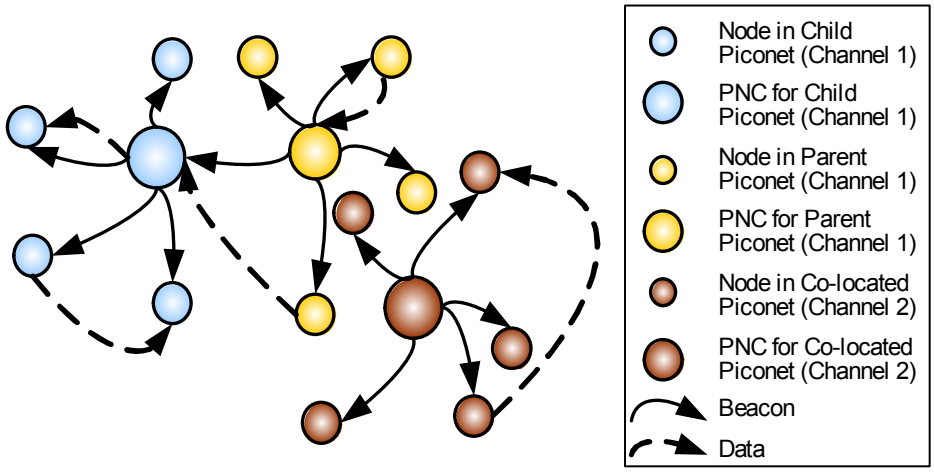

Figure 2.28: Piconet Structure for 802.15.3/3a

2.3.3.2 Code Division

Code division multiple access (CDMA) is generally used in cellular networks where a base station has a multi-user receiver with the capability to simultaneously listen and transmit on each channel. The multi-user receiver allows the base station to translate signals from one user's code to another user's code, but it is complex in hardware. The base station also has the responsibility to assign codes to each user, which requires some handshaking overhead and a control channel. Different code channels, ideally orthogonal to each other, allow nodes to transmit simultaneously. Without the possibility of collisions, nodes avoid the overhead of handshaking and detecting medium activity for I-UWB systems.

INTEL-1010
U.S. Patent 9,265,043

Code division protocols can be modified for distributive medium access, but they incur penalties in hardware and in overhead. Consider an ad hoc network with mobile nodes. The code space is finite and probably much smaller than the number of nodes, which could be thousands or more. To avoid central control, a transmitting node may choose a code at random. Thus, the target node should be listening on all channels simultaneously. This requires every node to adopt a complex multi-user receiver. Further, resistance to near-far effects and multi-user interference increases hardware complexity. Distributed code division protocols incur a penalty in hardware complexity, cost, and power because each node must listen to and decode all code channels concurrently. Nodes could also use a control channel to signal their intent to send data, as in CSMA/CA; but the small control packets add excessive acquisition and synchronization overhead in I-UWB. Hence, most code division MAC protocols for I-UWB are centralized.

In I-UWB, the channel may be divided into code spaces via time hopping codes [34]-[54], direct sequence codes [57]-[62], or frequency hopping codes [21],[65]-[69].

By far, the most popular form of code division for I-UWB is via time-hopping. The time-hopping code is most often combined with PPM modulation, so the user k transmits the signal

$$s^{(k)}(t) = \sum_{i=-\infty}^{\infty} A_p \left(t - iT_f - c_i^{(k)} T_c - \delta d_{\left\lfloor \frac{i}{N_c} \right\rfloor}(t) \right) \quad (2.26)$$

with time-hopping code $c_i^{(k)}$ and fundamental hopping granularity T_c. Figure 2.29 shows a visual representation of time hopping for a length-3 short code, which could support up to eight users (sub-optimally). Note that short codes repeat every symbol such that $c_i = c_{i+Ns}$, and long codes repeat over a longer period. In the figure, User 1 transmits a data '1' and User 2 transmits a data '0', which are spread over the respective time-hopping codes. The time hopping code determines the slot number and

INTEL-1010
U.S. Patent 9,265,043

the data determines the pulse position within that slot. Note that pulses from two different users may interfere with each other in the same slot (as in the second chip), but spreading multiple data chips over a code mitigates such multi-user interference.

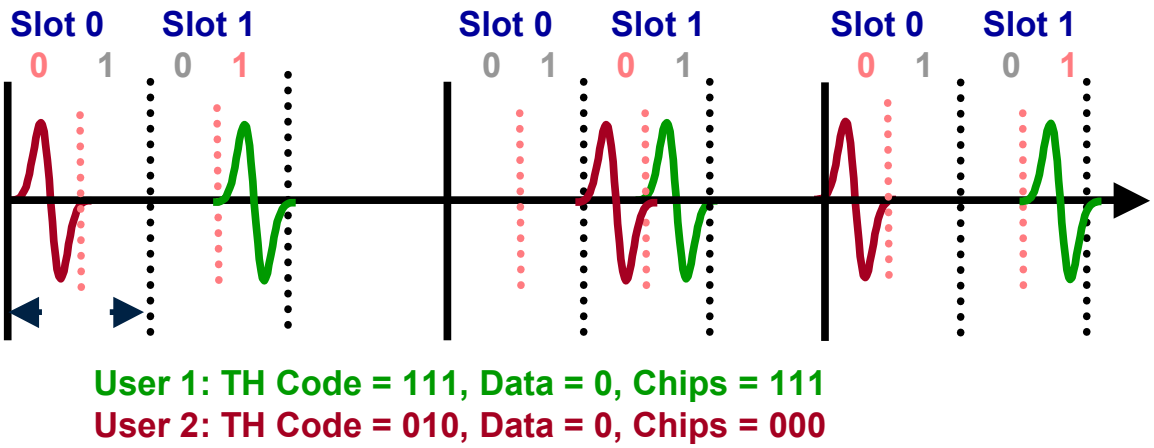

Figure 2.29: Time Hopping

Direct sequence UWB (DS-UWB) is similar to well-known narrowband direct sequence spread spectrum (DS/SS) techniques, but UWB communication systems spread the signal in time as opposed to frequency. Figure 2.30 shows a baseband DS-UWB waveform. A node transmits a continuous train of data with the amplitudes of the chips modulated by the spreading code. Multiple access is provided by assigning different users different spreading codes. The DS-UWB waveform for user k with spreading code $c_j^{(k)}$ for the jth pulse in a length N_c code is represented as

$$s^k(t) = \sum_{i=-\infty}^{\infty} \sum_{j=1}^{N_c} A_p\left(t - iT_f - jT_p\right)\left(c_j^{(k)}\right) d_i(t) \quad (2.27) \quad .$$

A DS-UWB waveform may also be modulated onto a carrier frequency, as is in the DS-UWB proposal for IEEE 802.15.3a [20],[21]. In this case, the chip rate F_{chip} and center frequency f_c of each piconet are harmonically related as $f_c = 3F_{chip}$. The offset chip rates reduce the correlation between data streams and also help to identify piconets. The data rate R_d for DS-UWB is represented as

INTEL-1010
U.S. Patent 9,265,043

$$R_d = \frac{1}{NT_f} \quad (2.28)$$

where:

T_f is the pulse repetition time (inverse of the PRF) [seconds]

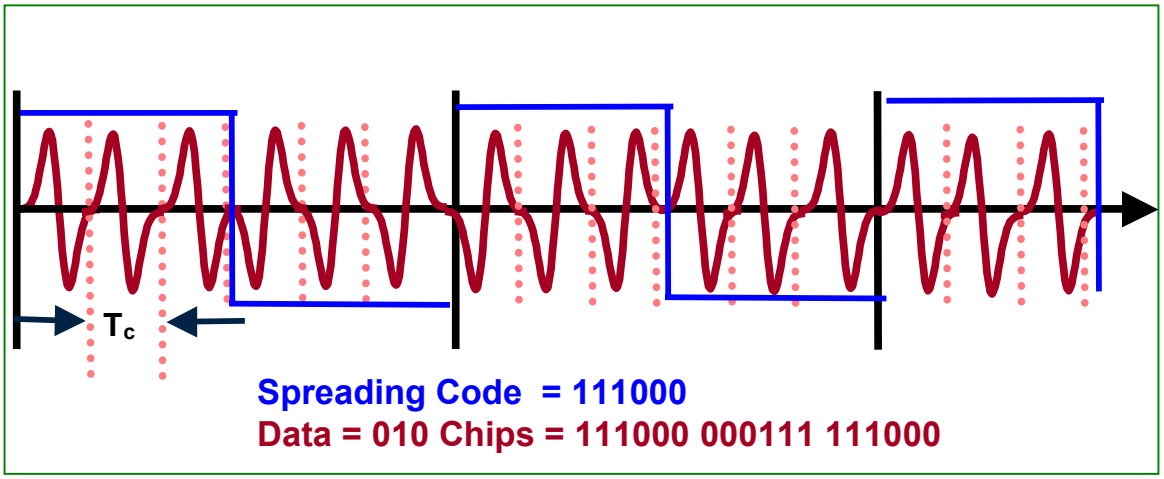

Figure 2.30: Direct Sequence Spreading for UWB

Finally, frequency hopping codes also provide multiple channels, as in the MB-OFDM proposal for IEEE 802.15.3a [28],[29]. An MB-OFDM waveform with N tones and symbol duration of $T_s = NT_b$ is written as

$$s(t) = d\sum_{i=1}^{N} d_i(t) e^{j2\pi\left(\frac{iT}{T_s} + f_c(t)T\right)} \quad (2.29) \quad .$$

The symbol steam $d_i(t)$ modulates the ith tone, and $f_c(t)$ gives the carrier frequency of the current band. In Figure 2.31, a 3-band MB-OFDM system supports simultaneously operating piconets by assigning the length-6 time-frequency codes (TFC) {1, 2, 3, 1, 2, 3} across three different frequency bands.

INTEL-1010
U.S. Patent 9,265,043

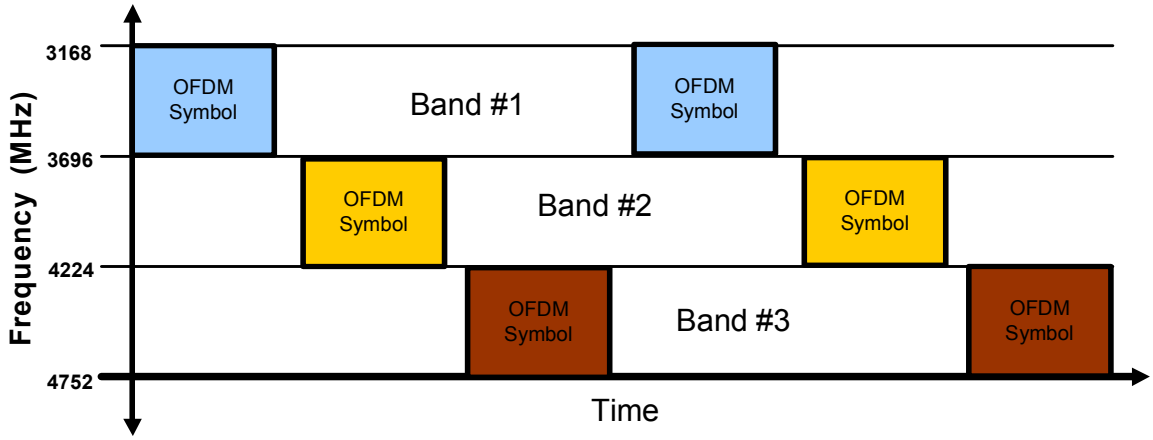

Figure 2.31: MB-OFDM Frequency Hopping

Whether through time hopping, DS-UWB or frequency hopping, centralized CDMA works well for cellular networks with centralized control. Assigning codes requires some handshaking overhead and a control channel (which may be time duplexed with the data channel). Further, the data rate of each flow is fixed by the spreading factor, which is determined *a priori*, based upon the expected level of interference. Therefore, the worst-case scenario, which is unknown in an ad hoc network, restricts the data rate of each node. Code division systems inherently suffer from multiple access interference, and the harsh multipath environment of I-UWB complicates this effect. Distributed versions of code division protocols are not suitable for I-UWB because they require expensive multi-user receivers. Due to the hardware complexity and overhead, centralized CDMA MAC protocols are not suitable for large, low cost, ad hoc networks.

Some recent work examines more distributed approaches to time-hopping MAC protocols in more depth. The code channel may be determined by the address of either the receiver [191], or the sender [192]. To overcome multi-user interference, time-hopping alone is ineffective for close interferers, so other techniques such as additional coding or ignoring corrupted chips are required [191]. To handle simultaneous transmissions to the same node, the protocols require the overhead of control packets to establish a link. Further, the above protocols assume a topology that places every node within range of each other. In a multihop network topology, each node transmits to just

INTEL-1010
U.S. Patent 9,265,043

enough neighbors to ensure a connected network, so there is no need to coordinate a large set of code channels. Thus, ad hoc and sensor networks should not rely on code channels.

In summary, current I-UWB MAC protocols target small WPANs and cellular networks, but they are not suitable for large ad hoc and sensor networks. The centralized approaches of TDMA and code division are good strategies for a small network with heavy traffic and strict Quality of Service (QoS) requirements. However, in larger ad hoc and sensor networks, the central coordination increases complexity and overhead, and it also leads to a central point of failure. Instead, large ad hoc and sensor networks should take a simpler, distributed approach to medium access.

2.4 Applying I-UWB to Ad Hoc and Sensor Networks

Current ad hoc and sensor networks use narrowband radios and MAC protocols tailored to narrowband radios [70],[77]-[80],[97],[98]. However, little effort has been dedicated to the application of either I-UWB radios or their apposite MAC protocols to large-scale ad hoc and sensor networks. An I-UWB radio can provide such benefits as precision ranging, high data rate, robust operation, flexible link distance, and low radiated power. Further, the unique signaling may result in a novel MAC protocol.

Note that (i) MAC protocols for large ad and sensor networks are distributed protocols and (ii) the current MAC protocols for I-UWB are all centralized protocols for smaller networks. This leads to the goals of designing MAC protocols to enable I-UWB radios for ad hoc and sensor networks. The next chapter of this work addresses the unique signaling challenges of I-UWB required to enable a distributed MAC protocol. Distributed protocols are based on CCA functionality, so the chapter studies methods to perform CCA with I-UWB signaling. Subsequent chapters attempt to leverage the unique signaling of I-UWB for a novel MAC protocol not attainable with narrowband radios. Handshaking packets degrade performance in both sensor networks and in I-UWB radios, so the proposed MAC protocols are further constrained to eliminate or mitigate the handshaking overhead of RTS and CTS packets.

INTEL-1010
U.S. Patent 9,265,043

The duality between narrowband systems and I-UWB forms a basic guide for solving the above design challenges in I-UWB. As shown in Figure 2.32, an I-UWB signal can be considered the dual of a traditional narrowband signal. For a narrowband signal, the time domain representation has constant power over a long time period, whereas the frequency domain representation concentrates all the power in a narrow spectral band. These assumptions are inherent in the design of existing narrowband radios and MAC protocols (e.g., carrier sense is taken for granted in narrowband systems). For an I-UWB signal in the frequency domain, the power spectral density is spread over a large spectrum, whereas the time domain representation contains power only during a narrow time window. Thus, novel MAC protocols may result from new assumptions.

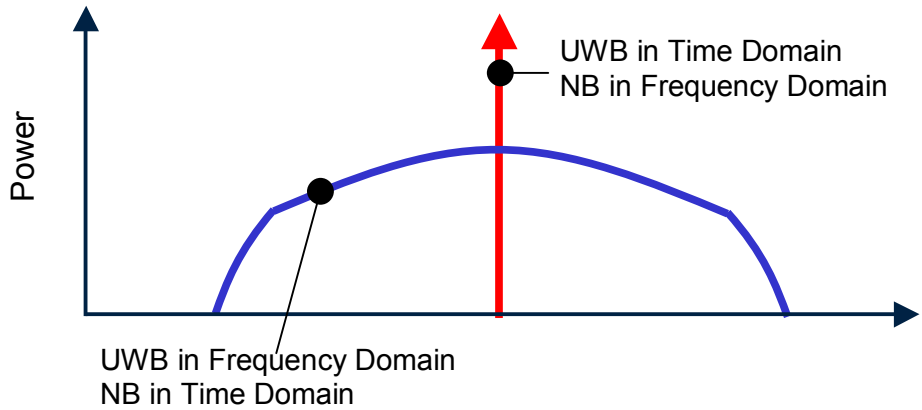

Figure 2.32: Duality of I-UWB and Narrowband Signals

Table 2.6 shows some existing areas in which I-UWB takes advantage of the duality. Table 2.7 shows the areas in which we intend to exploit the duality of I-UWB to develop a MAC for I-UWB in ad hoc and sensor networks.

INTEL-1010
U.S. Patent 9,265,043

Table 2.6: Existing Dual Techniques in Narrowband and I-UWB

NB Technique	*UWB Technique*	*References*
Frequency hopping	Time hopping	[34]-[54]
Direct Sequence Spread Spectrum	DS-UWB	[57]-[62]
FSK	PPM	[107],[108]
Time domain receiver	Frequency domain receiver	[100],[101]

Table 2.7: Proposed Dual Techniques Narrowband and I-UWB

NB Technique	*UWB Technique*	*Chapter*
Carrier Sense	Pulse Sense	3
Frequency Duplexing	Time Duplexing	4, 5
Frequency Agility to Mitigate Interference	Time Agility to Mitigate Interference	6

INTEL-1010
U.S. Patent 9,265,043

Chapter 3: Pulse Sense: A Method to Quickly, Reliably, and Efficiently Detect Medium Activity in I-UWB

Ad hoc and sensor networks must manage a large number of inexpensive, low power nodes. UWB is an attractive technology for such networks due to its high data rate, low radiated power, and accurate ranging capability. For ad hoc and sensor networks, I-UWB has several advantages over other forms of UWB due to its robustness to multipath fading and simple, low power hardware. Existing MAC protocols for I-UWB systems are centralized, so they are unsuitable for sensor and ad hoc networks. In large ad hoc networks, the central coordination increases complexity and overhead, and it also leads to a central point of failure. Large ad hoc and sensor networks with narrowband radios implement distributed MACs, which generally realize random access and require CCA, or the ability to detect a busy medium.

The narrow pulses and low radiated power of I-UWB present difficulties in CCA, which is fundamental to random, distributed MAC protocols. Narrowband systems provide CCA by detecting the energy from a carrier, but I-UWB has no carrier. Currently there is no reliable, quick, and efficient method for CCA in I-UWB networks. This chapter proposes a method for CCA in I-UWB networks. The method is called *pulse sense* because it detects a busy medium in the presence of I-UWB traffic just as carrier sense detects signals in a certain frequency band. Pulse sense enables a distributed, random access MAC for I-UWB, and in turn, enables ad hoc networks to realize the benefits of I-UWB radios.

The key idea is to examine the spectral power components of the received signal, which are always present, to avoid searching for narrow I-UWB pulses in the time domain. Simulations show that the proposed pulse sense circuit detects the presence of I-UWB pulses in a short time period in various channel conditions, and it is moderate in circuit complexity.

This chapter is organized as follows. Section 3.1 reviews existing methods for CCA in I-UWB. Section 3.2 presents the proposed pulse sense architecture, and

INTEL-1010
U.S. Patent 9,265,043

Section 3.3 discusses the operation. Section 3.4 presents simulation results, and Section 3.5 summarizes the chapter.

3.1 Existing Methods for CCA in I-UWB

As compared to a receiver circuit, a CCA circuit should cost much less in terms of hardware and dissipate much less power. Further, a CCA circuit should detect activity reliably in a short amount of time. Otherwise, the receiver could be used for the purpose of CCA. If the power is low as compared to the receiver, a CCA circuit will save significant power because a node usually listens for activity far more often than it receives data.

Existing methods of detecting I-UWB traffic do not meet the above goals. The methods include peak detection, matched filtering, sliding correlation, and interleaved periodic correlation processing (IPCP) [162]. Table 3.1 lists the disadvantages of these methods in performing CCA in I-UWB. Most of these methods are designed for the purpose of signal acquisition or reception, so they perform poorly for the purpose of CCA.

Table 3.1: Existing CCA Methods in I-UWB

Method	Comment
Peak Detector	Susceptible to false alarms from narrowband signals and noise spikes.
Analog Matched Filter	Complex; not adaptable to changing channel conditions and distorted signals.
Digital Matched Filter	Complex ADC; large number of taps; long training period.
Sliding Correlation	Requires a long time – several hundred to a thousand symbols; requires a template; multipaths, ISI, and frequency selective fading degrade performance.
Parallel Correlation	High circuit complexity; requires a template; multipaths, ISI, and frequency selective fading degrade performance
Integrated Periodic Correlation Processing	More useful for a radar signal; sharp correlation peak; ISI, co-channel interference, modulation, and timing jitter degrade performance.

INTEL-1010
U.S. Patent 9,265,043

A peak detector is a simple method, and it holds the peak value of the signals received within a designated time period [163]. In narrowband systems, a peak detector follows the front-end circuitry, which filters out-of-band interference [164]. However, an I-UWB receiver operates over a wide bandwidth, so a peak detector is incapable of separating an I-UWB signal from a (probably much stronger) narrowband signal [165]. This is a problem since UWB is meant to coexist with narrowband devices. Furthermore, noise spikes and narrowband signals cause false alarms. Several I-UWB receivers employ a peak detector for reception, but the peak detector operates after synchronization and conditioning of the received signal [166],[167].

A matched filter seems like an ideal method to detect an impulse signal, as it does not require synchronization to detect the signal energy [94]. In fact, several UWB receiver designs are based on matched filters [168]-[176]. However an I-UWB signal presents some severe challenges for matched filter design. An analog matched filter is not adaptable to dynamic channel conditions and pulse shapes, and it is complex in hardware design. To sample the received signal, a digital matched filter requires a fast ADC with wide dynamic range, which dissipates a large amount of power. The digital matched filter requires a long training period to adapt to the current unknown channel conditions. Further, a digital matched filter requires a large number of taps to handle the dense multipath environment of I-UWB. Although suitable for reception, the complexity and inflexibility of a matched filter makes it unsuitable for the purpose of CCA.

Correlation with a sliding window can also be used to detect low duty cycle I-UWB pulses [94],[177]. In existing I-UWB systems, correlation is used to detect and synchronize the receiver to an incoming transmission [178]-[185]. Correlation may consider either a serial or a parallel search for signal detection. In terms of hardware complexity, a serial correlation provides the simplest circuit for detection. However, serial correlation results in a long sensing time (possibly in excess of 1000 symbols) for I-UWB pulses, so it is unsuitable for CCA purposes.

A sampling bridge circuit operates similarly to a serial correlation. The architecture is used in sampling oscilloscopes, and it can also be used to detect I-UWB pulses. As shown in Figure 3.1, the receiver takes individual samples at random,

INTEL-1010
U.S. Patent 9,265,043

interleaved intervals at a low rate (much lower than the required Nyquist rate). It then combines the multiple samples into a single picture. The sampling bridge circuit requires a large number of pulses to reconstruct a single I-UWB pulse, so it is not practical for CCA.

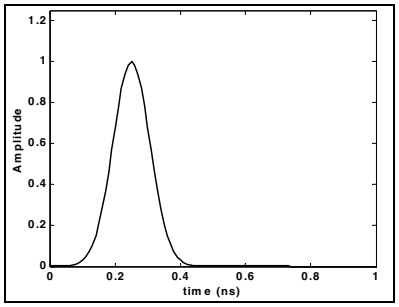

(a) Shape of pulse

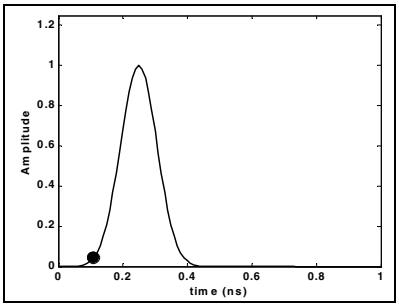

(b) First Sample

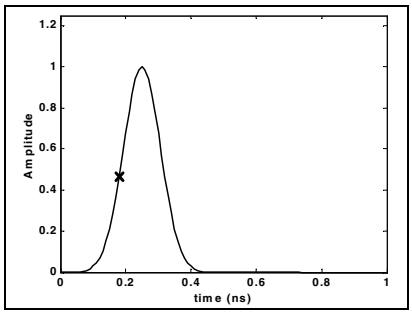

(c) Second Sample

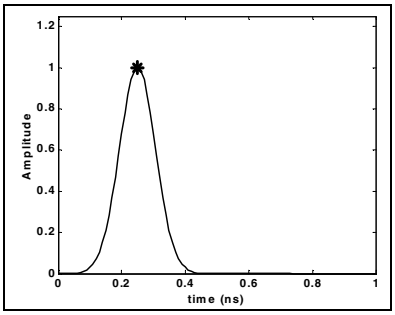

(d) Third Sample

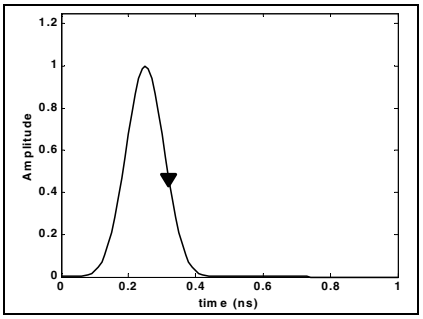

(e) Fourth Sample

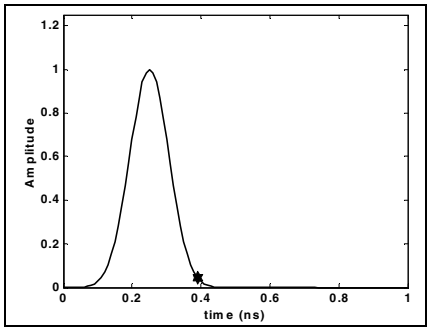

(f) Fifth Sample

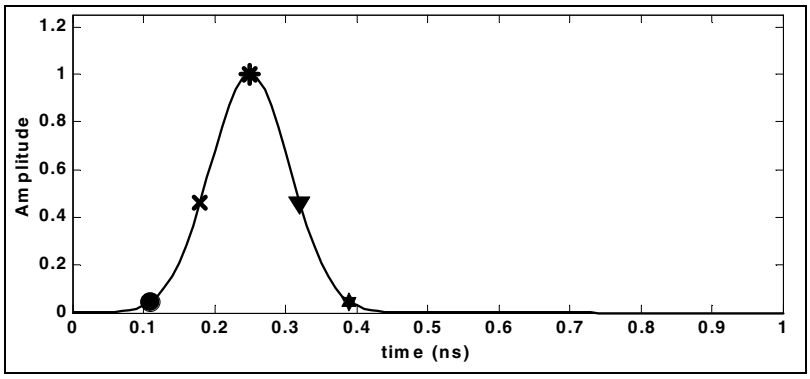

(g) Reconstructed Pulse

Figure 3.1: Operation of a Sampling Bridge Circuit. [161]

INTEL-1010
U.S. Patent 9,265,043

An Integration and Averaging receiver is another implementation that is similar to a sliding correlation [140],[188]. The receiver compresses samples from N high-rate pulses into a single pulse. For a sliding correlator implementation, the time compression is related to the slide factor k [161]:

$$k = \frac{T_{f_{TX}}}{T_{f_{TX}} - T_{f_{RX}}} \tag{3.1}$$

$$T_{d_{OUT}} = kT_{d_{IN}} \tag{3.2}$$

where:

$T_{f_{TX}}$	is the pulse repetition time for the transmitted pulses [seconds]
$T_{f_{RX}}$	is the pulse repetition time for the receiver pulse generator [seconds]
k	is the slide factor
$T_{d_{OUT}}$	is the time duration of the pulse output from the sliding correlator [seconds]
$T_{d_{IN}}$	is the time duration of the pulse input to the sliding correlator [seconds]

Several methods exist to speed up the search process. A parallel correlation improves acquisition speed but at the cost of high circuit complexity, so it is not suitable for CCA. Non-linear searches also improve detection time, but the improvement is still quite inadequate for the purpose of CCA. A random search improves search times marginally [186]. A hierarchical sliding correlation with successively finer time steps [187] also improves search time. For example, consider an I-UWB pulse train with pulse rate of 10 MHz. The receiver produces template pulse trains at rates of 10.01 MHz, 10.006 MHz, and 10.00 MHz. First, the coarse acquisition process performs a sliding correlation with the receiver operating at 10.01 MHz. After detecting a sufficient amount of energy, the receiver then operates at 10.006 MHz for fine synchronization. The receiver then operates at 10.0 MHz. Although faster, the process may encounter more false alarms due to the coarse time step, and it may also increase the standard deviation of search times.

INTEL-1010
U.S. Patent 9,265,043

A Template Match Detection receiver is similar in implementation to parallel correlation. As shown in Figure 3.2, the receiver correlates the received signal with multiple stored waveform templates offset in time with respect to each other. The receiver adds significant hardware complexity for each additional correlation.

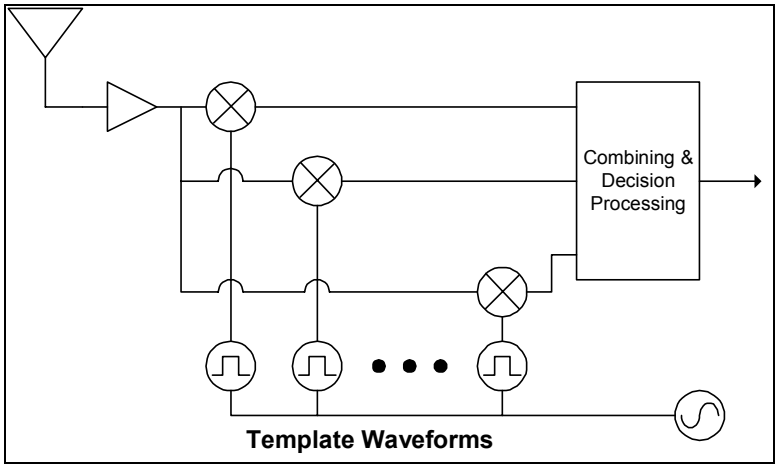

Figure 3.2: A Basic Block Diagram of a Template Match Detection UWB Receiver [161]

An interleaved periodic correlation processing (IPCP) pulse detection system is especially useful for harvesting the combined energy of all multipaths. The IPCP operates by correlating the received signal with samples of itself delayed by one pulse repetition interval (PRI) as in Figure 3.3 [162]. IPCP is mostly useful for detecting homogenous radar signals in the absence of inter symbol interference (ISI), co-channel interference, and modulation, which all produce differences between successive symbols. These differences cause the received signal to be less correlated with a delayed version of itself, which degrades the performance. Additionally, timing jitter causes further degradation due to the long integration period and sharp correlation peak.

INTEL-1010
U.S. Patent 9,265,043

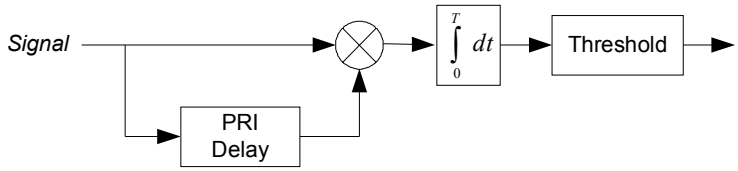

Figure 3.3: IPCP Detection of UWB Impulses.

Pulse sense is designed to be robust to the weaknesses of the above systems. It meets the goals of low power dissipation, simple circuitry, reliable detection, and short detection time. Pulse sense enables I-UWB systems to adopt a distributed MAC protocol for use in ad hoc and sensor networks.

3.2 Architecture

The key idea of pulse sense is to examine the power spectral components of an I-UWB pulse train, instead of searching for a narrow pulse in a large time window. For an I-UWB signal, the frequency domain representation spreads the power spectral density over a large spectrum, whereas the time domain representation contains power only during a narrow time window. Current methods of detecting I-UWB activity rely on searching for the narrow pulse in the time domain, so they are impractical for the purpose of CCA. Pulse sense examines the spectral components – which are always present – of the received signal to avoid the problems associated with searching for a signal in the time domain.

There are many possible implementations of a circuit to perform frequency domain CCA for I-UWB pulses. This section reviews one method, which is much simpler in hardware complexity as compared to a full receiver. Figure 3.4 shows the proposed implementation integrated with the receiver in Figure 2.20. With this receiver, the pulse block may share an LNA, antenna, and filters to simplify front-end design.

INTEL-1010
U.S. Patent 9,265,043

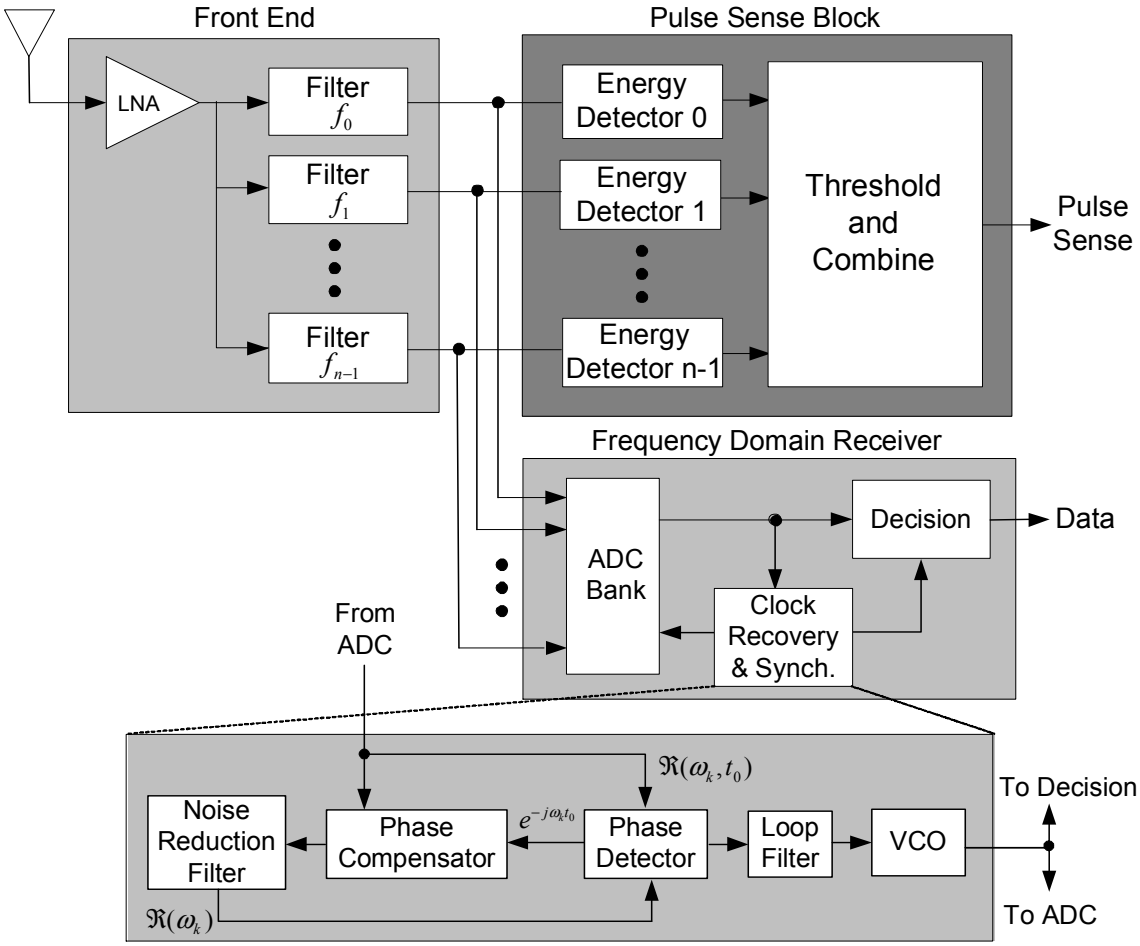

Figure 3.4: UWB Receiver with a Pulse Sense Block

The antenna receives I-UWB signals and passes them to a wideband low-noise amplifier (LNA) that operates over the bandwidth of the I-UWB signal. The amplified signal is fed to a filter bank of typical resonator filters. As shown in Figure 3.5, a filter realizes the second order transfer function $1/(s^2+(k\omega_b)^2)$, and it captures an in-band spectral component of the received signal at frequency f_i, where $f_i = kF_0$ for an integer k and observation period T_p, such that $F_0=1/T_p$.

INTEL-1010
U.S. Patent 9,265,043

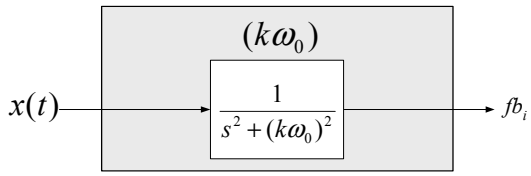

Figure 3.5: Resonator Filter Structure

As shown in Figure 3.6, pulse sense captures spectral coefficients, so it does not require the flat-top bandpass filters used in many I-UWB receivers. Therefore, the associated receiver does not incur an aliasing problem. The flat-top filters are often used to reduce the required sampling speed of an analog-to-digital converter (ADC) in a receiver [189],[190]. Note that pulse sense itself does not require ADC processing, so aliasing is not an issue in the pulse sense circuit.

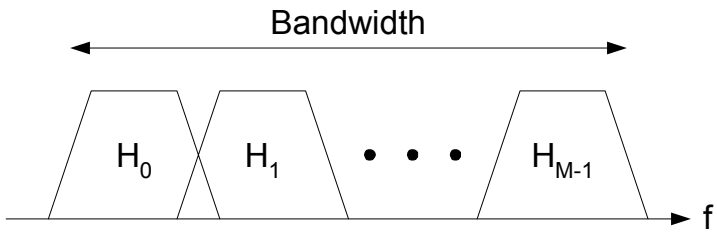

(a) Flat top filters

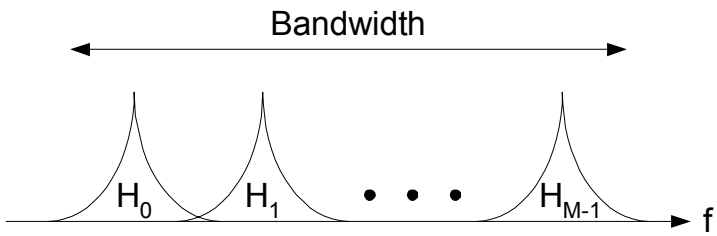

(b) Resonator filters

Figure 3.6: Characteristics of Bandpass Filters for (a) Existing Method and (b) Our Method

INTEL-1010
U.S. Patent 9,265,043

Pulse sense further constrains the locations of the filter banks to multiples of the PRF. The top line in Figure 3.7 shows the spectrum of one I-UWB pulse, and the spectral lines represent the spectrum of a train of those pulses. The spectral lines of the pulse train are maximum for integer multiples of the PRF (the slight deviation from exact multiples is due to the FDFT). The amplitude of the spectral lines relative to the average power increases with decreasing PRF. When the power spectral components are multiples of the PRF, the filter banks capture larger spectral power components to induce larger oscillations. Therefore, $f_i = kF_0$ for an integer k, and also $f_i = nPRF$ for an integer n.

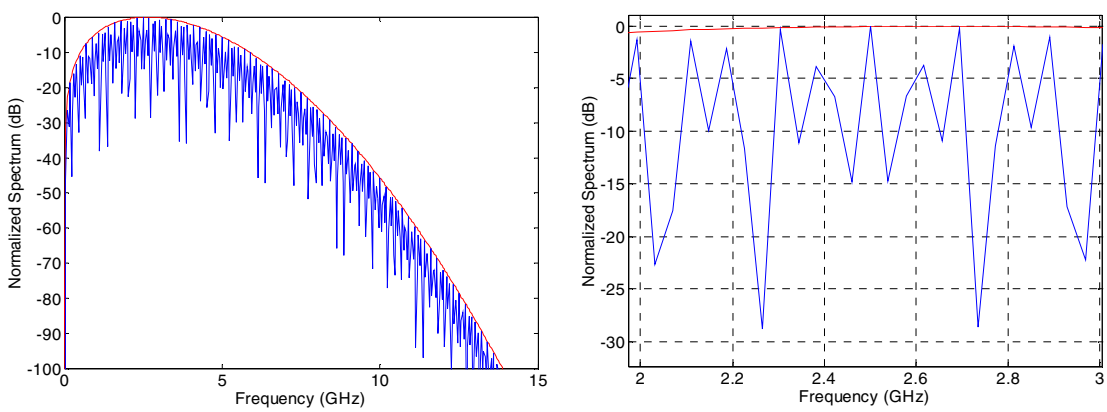

Figure 3.7: Frequency Spectra of Pulse and Pulse Train

After the filters capture the power spectral components of the received signal, the circuit performs CCA with three additional operations: energy detection, threshold detection, and combination. The energy detector detects the presence of the I-UWB spectral energy components. The combiner ensures that several frequency bands are active in a correlated manner to avoid false alarms from narrowband interference. The level of threshold detector sets the probability of detection P_d and the probability of false alarm P_{fa}. The interaction of these blocks is described below.

The energy detectors of the pulse sense block detect the spectral power components captured by the filters. When there is pulse activity at the PRF, the filters oscillate. Figure 3.8 (a) shows a maximum likelihood detector for a signal of unknown

INTEL-1010
U.S. Patent 9,265,043

phase at frequency f_i. The fb_i signal is from a filter bank, and the sine and cosine terms are the basis functions. The remaining blocks compute and combine the energy at frequency f_i. Because a maximum likelihood detector is relatively complex requiring mixers and oscillators, it may not be power efficient. An alternative circuit is an envelope detector followed by an integrator as shown in Figure 3.8 (b).

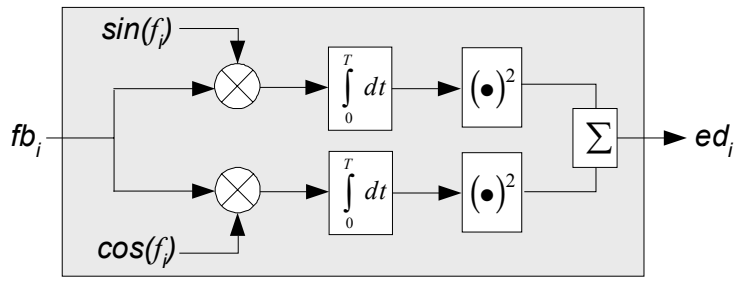

(a) Maximum Likelihood Detector

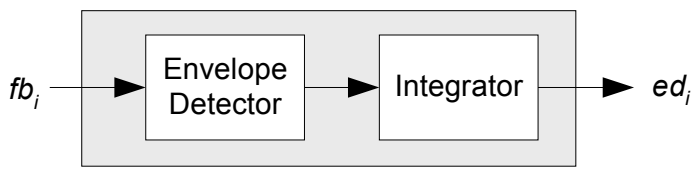

(b) Envelope Detector

Figure 3.8: Energy Detectors

Each energy detector reports the presence or absence of spectral power component at a frequency f_i. These spectral power components now need to be combined with the purpose of detecting the presence of an I-UWB signal while rejecting false alarms from narrowband signals. To this end, the circuit ensures that the majority of spectral components match the low power footprint of an I-UWB signal. The implementation considers two possible methods of combining the spectral power components. The first option performs threshold detection on the output of each energy detector and combines the outputs of the threshold detectors. This is analogous to a hard decision, so it is termed a *hard combination*. The second option combines the outputs of the energy detectors and then performs threshold detection on the sum. This is analogous to a soft decision, so it is termed a *soft combination*.

INTEL-1010
U.S. Patent 9,265,043

Figure 3.9 (a) shows the hard combination scheme. The filter outputs are applied to threshold detectors, which generate binary values. If the sum of binary values exceeds a threshold value X, then a pulse is detected. This operation is robust to a strong narrowband interferer, as high energy in one frequency band will not exceed the threshold value X. Because the threshold detectors produce binary values, the sum and comparator blocks may be implemented efficiently with digital circuits.

Figure 3.9 (b) shows the soft combination scheme. The outputs of the energy detectors pass through limiters, so that a strong narrowband interferer does not dictate the final decision. The analog limiter outputs are summed, and then the sum is compared to a threshold. The soft combination is resilient to frequency selective fading, as the soft decision gives more weight to strong spectral components. Soft combination requires only one threshold detector, but the limiter and the adder circuits are analog to avoid ADC's at the detector input.

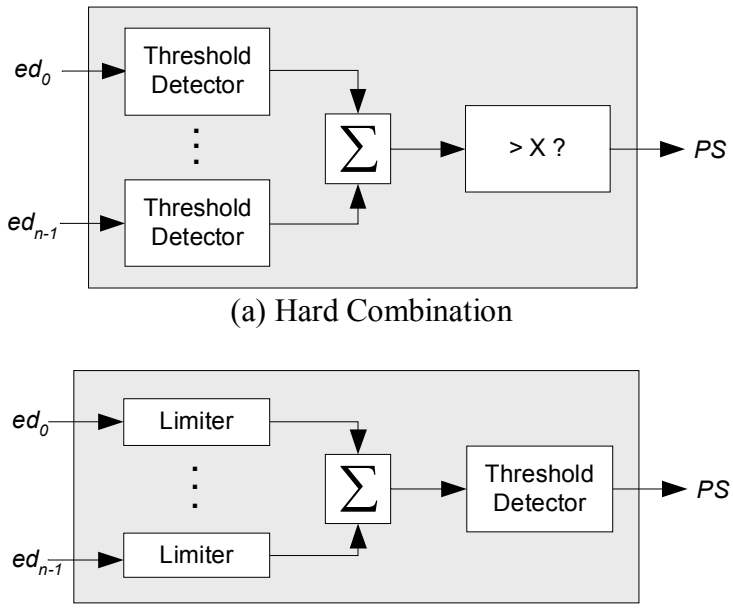

(a) Hard Combination

(b) Soft Combination

Figure 3.9: Combination and Threshold Block

INTEL-1010
U.S. Patent 9,265,043

3.3 Design Considerations

A CCA circuit should have a short sensing period (e.g., the IEEE 802.15.4 MAC specifies an eight symbol maximum) and report a high detection probability P_d and low false alarm probability P_{fa}. The time limit is necessary to prevent the pulse sense block from reporting stale, useless information, as well as to reduce the power dissipation. Design considerations for the sensing period are described next.

The main consideration of the LC tank circuit is the RC time constant, which determines the resonant energy loss over time. The RC constant of the filter can be derived from the quality factor Q of the filter circuit. An implementation of the circuit is discussed in [193]. Although an infinite Q is desirable for both the inductor and the capacitor in an LC tank circuit, finite Q is inevitable in an integrated circuit. Since integrated capacitors generally provide a much higher quality factor compared to integrated inductors, our implementation concentrates on the inductor implementation. We measure a Q of up to 14 in TSMC 0.18 μm CMOS technology, and this limits the performance of the LC tank circuit.

A high quality factor in an inductor means a small resistor in series with the inductor, which can be interpreted as a large parallel resistance in an equivalent parallel RLC model. Figure 3.10 shows the equivalent parallel circuit, where C the nominal capacitor value, Ls is nominal inductor value, R_s is the resistance of the inductor, L_p is the equivalent parallel inductance of L_s, and R_s is the equivalent parallel resistance of R_p. In Figure 3.10, the series and parallel values of R are related as follows.

$$R_p = R_s\left(Q^2 + 1\right) \quad (3.3)$$

$$L_p = L_s\left(\frac{Q^2 + 1}{Q^2}\right) \quad (3.4)$$

From (3.3), a high Q value results in a large series resistance value and thus a large RC time constant. Note that the RC time constant drops with the square of the quality factor. From (3.4), the parallel inductance does not significantly differ from the series inductance.

INTEL-1010
U.S. Patent 9,265,043

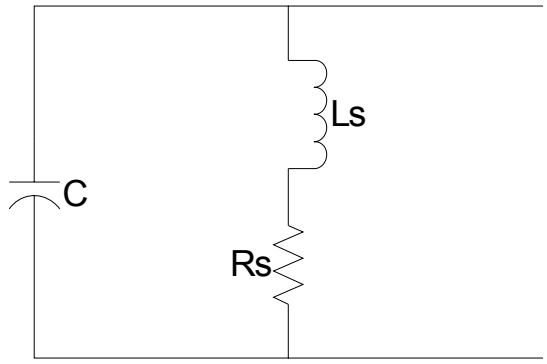

(a) Original Circuit Showing Resistance of Inductor

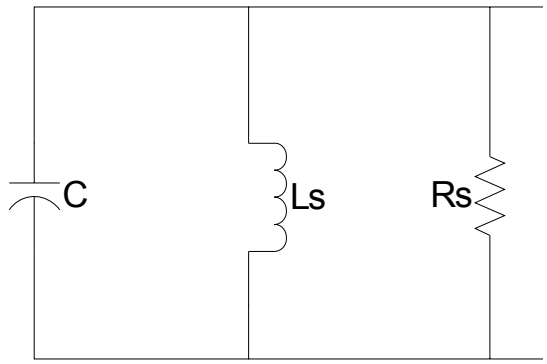

(b) Equivalent Parallel Resistance

Figure 3.10: Equivalent Series Resistance of LC Tank Circuit

Therefore, a high Q provides a long RC time constant, which results in low energy loss over time. In contrast, a low Q provides a short RC time constant and attenuates the oscillation energy. Note that the circuit will achieve its maximum amplitude quickly and independently of the RC time constant, because the circuit implementation stores initial energy in the inductors. Figure 3.11 shows the impulse response of the circuit implementation [193]. The figure illustrates the fast rise time compared to the fall time, which is determined by the RC time constant.

INTEL-1010
U.S. Patent 9,265,043

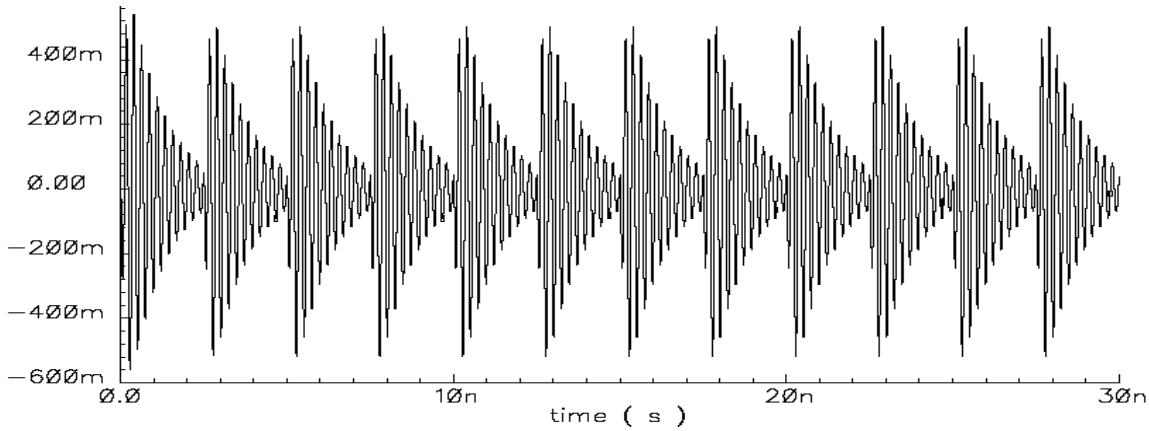

Figure 3.11: Impulse Response of a Filter Circuit

The circuit can accommodate shorter and longer RC constants depending on the achievable Q of the circuit. Higher Q results in a longer RC time constant, but if the technology does not allow for higher Q, we can also design the circuit with a lower RC constant. We have measured a Q of up to 14 in our TSMC 0.13 μm library, which is sufficient to provide a long RC time constant at practical PRI values. Next, we explain two designs targeted for short or long RC time constants (measured relative to the PRI), depending on the achievable Q of the circuit.

We first describe the design procedure for a short RC time constant, defined as $\tau <$ PRI. Note that time is measured relative to the pulse repetition interval (PRI), and practical values of the PRI range from a few nanoseconds to a few microseconds [100]. Figure 3.12 shows the response of filters with a short time constant. The top graph shows the incoming pulse train, and the remaining graphs underneath show the response of resonator filters as the center frequency f_0 increases. Note that all filters have the same RC constant, because the inductor value sets f_0 while the RC value remains constant. Figure 3.12 shows that an integrator should integrate the energy from one pulse over one full PRI with a short time constant. This is because the pulse sense circuit is unsynchronized, and integrating over one full PRI guarantees that the circuit captures the major portion of the oscillation energy. One advantages of a short time constant is that successive pulses cannot interfere with each other destructively because the energy from a pulse is dissipated by the time the next pulse arrives.

INTEL-1010
U.S. Patent 9,265,043

Another advantage of a short time constant is that output of the filters may be used as an aid to synchronization. The filter response has a sharp rise time and the energy from the previous pulse has mostly dissipated, so a clock signal can be extracted from the output of a filter.

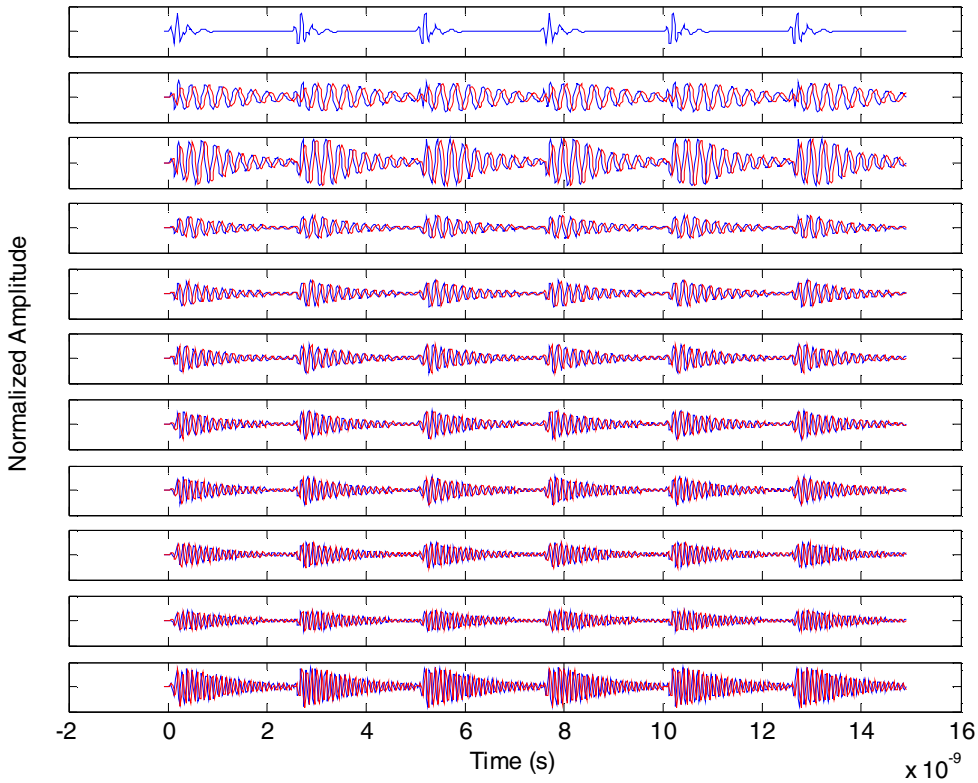

Figure 3.12: Filter Responses with Short (τ < PRI) RC Time Constants

Next, we describe an implementation with a long RC constant, defined as τ > PRI. Note that the following considerations are only necessary if the achievable Q of the implementation technology allows a sufficiently long RC constant as compared to the PRI. Figure 3.13 shows a design challenge that emerges with a longer RC time constant. In the figure, the top graph shows the incoming pulse train, and the remaining graphs below show the oscillations of the filters with successively increasing f_0. Note the pulse polarity changes between the first and second pulses, between the second and third pulses, and between the fifth and sixth pulses. The challenge is that successive pulses with opposite polarity may trigger oscillations 180 degrees out of phase with

INTEL-1010
U.S. Patent 9,265,043

each other. The challenge is limited to pulses with opposite polarity because the center frequency of each filter is harmonically related to the PRI. These oscillations will combine destructively with one another to reduce the captured energy.

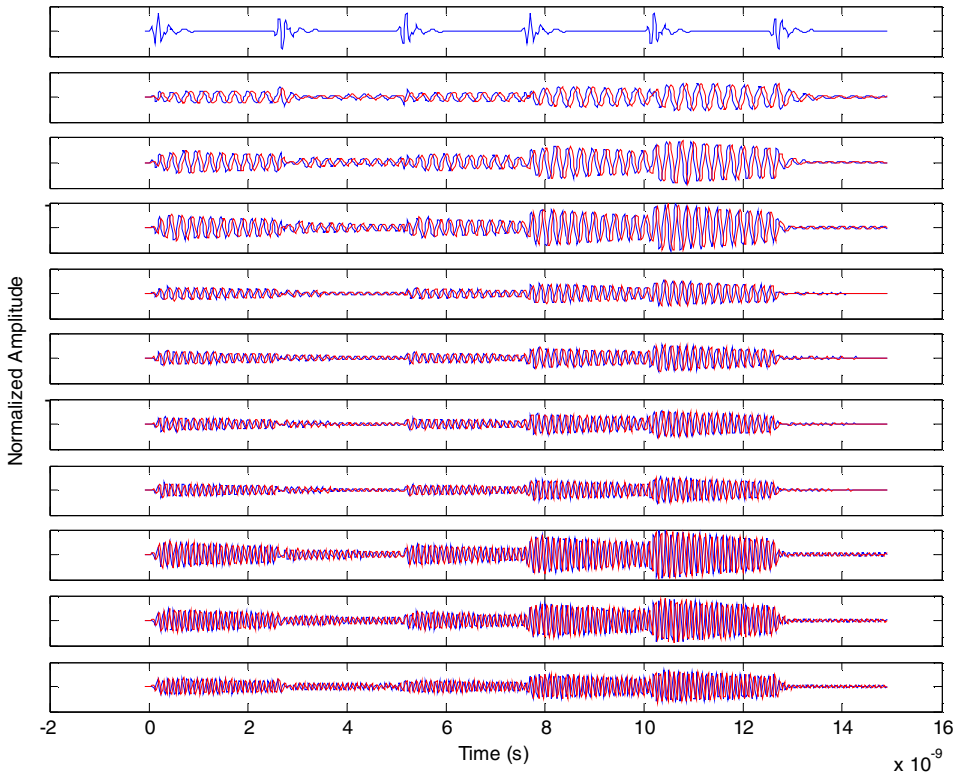

Figure 3.13: Filter Responses with Long (τ > PRI) RC Time Constants

Fortunately, there are several solutions to prevent the destructive combination issue in Figure 3.13. The first solution is to use a modulation scheme other than BPSK. Good candidates include PPM or OOK. In the case of OOK, successive pulses will either be in phase with each other or a successive pulse will be non-existent. In the frequency domain, μ_i in (2.11) is non-zero for OOK and this guarantees the presence of discrete spectral components. To ensure detection, the preamble could include a successive string of identical pulses. In the case of PPM, the time difference between pulse positions can be adjusted such that every pulse creates in-phase oscillation regardless of the pulse position in which it arrives. The condition for this constrains δ in (2.8) such that

INTEL-1010
U.S. Patent 9,265,043

$$\delta = n \cdot \frac{1}{f_i} \quad (3.5) \quad ,$$

where δ is the time difference between pulse positions, n is an integer, and f_1 is the center frequency of the filter with the lowest center frequency. Also, note that (2.17) guarantees the existence of spectral lines at multiples of the PRF.

The second solution, which is targeted for BPSK modulation, adds a squaring circuit at the inputs of the resonator filters. Figure 3.14 shows the new pulse sense circuit with the squaring circuit. Note that the squaring circuit can be bypassed for normal operation. When the pulse train passes through the squaring circuit, successive pulses in BPSK will arrive with the same polarity and the oscillations will be in phase. Figure 3.15 shows that the oscillations increase in amplitude as successive pulses arrive. The amplitude increases until the circuit reaches its steady state value. The squaring circuit prevents the destructive combination of oscillations as seen in Figure 3.13. Further, note that the oscillations last well into successive PRIs, which is different from the case in Figure 3.12 with a short RC time constant. After the circuit reaches a steady state, the oscillations are approximately the same amplitude during the entire PRI. This suggests that a circuit with a long RC constant need not integrate for a full PRI, Further, integration over the full PRI should result in better performance as compared a short RC time constant.

INTEL-1010
U.S. Patent 9,265,043

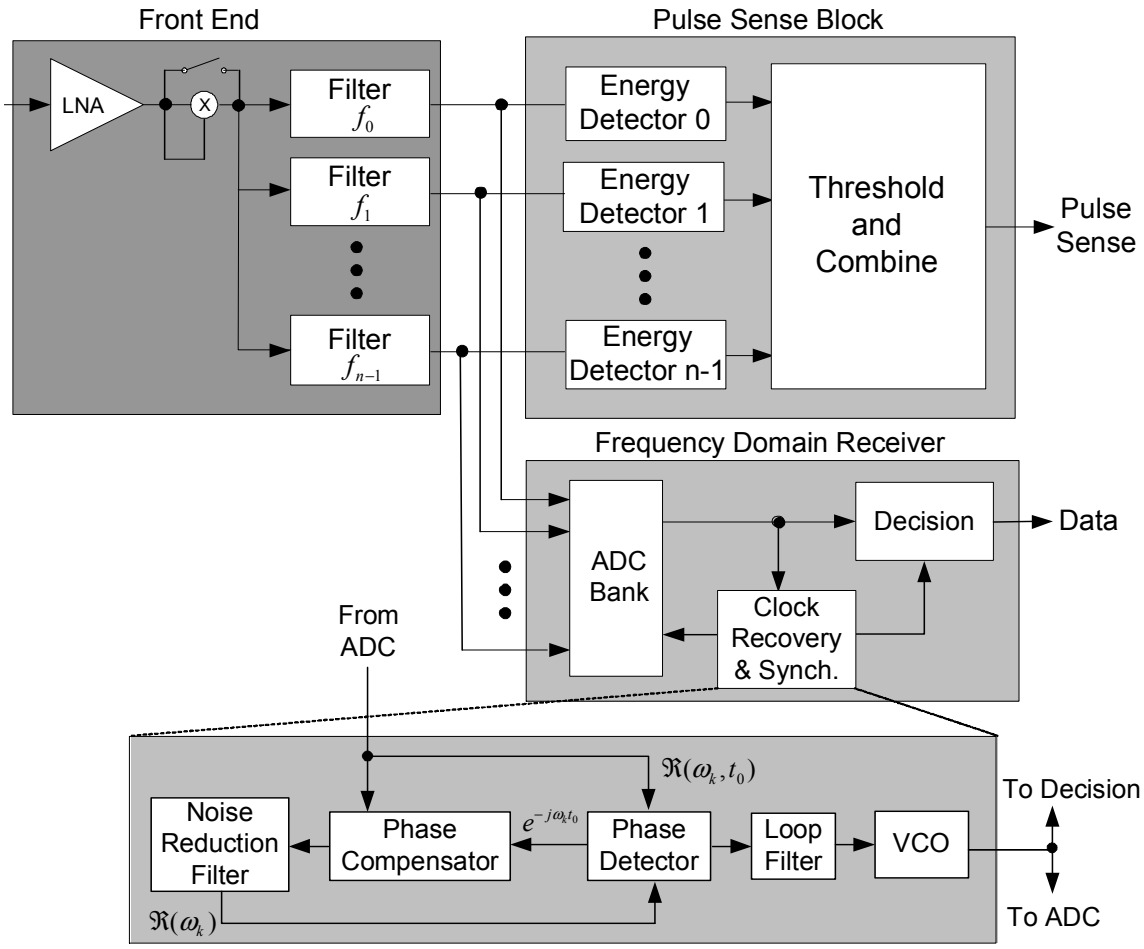

Figure 3.14: Pulse Sense Block with Squaring Circuit at LNA Inputs

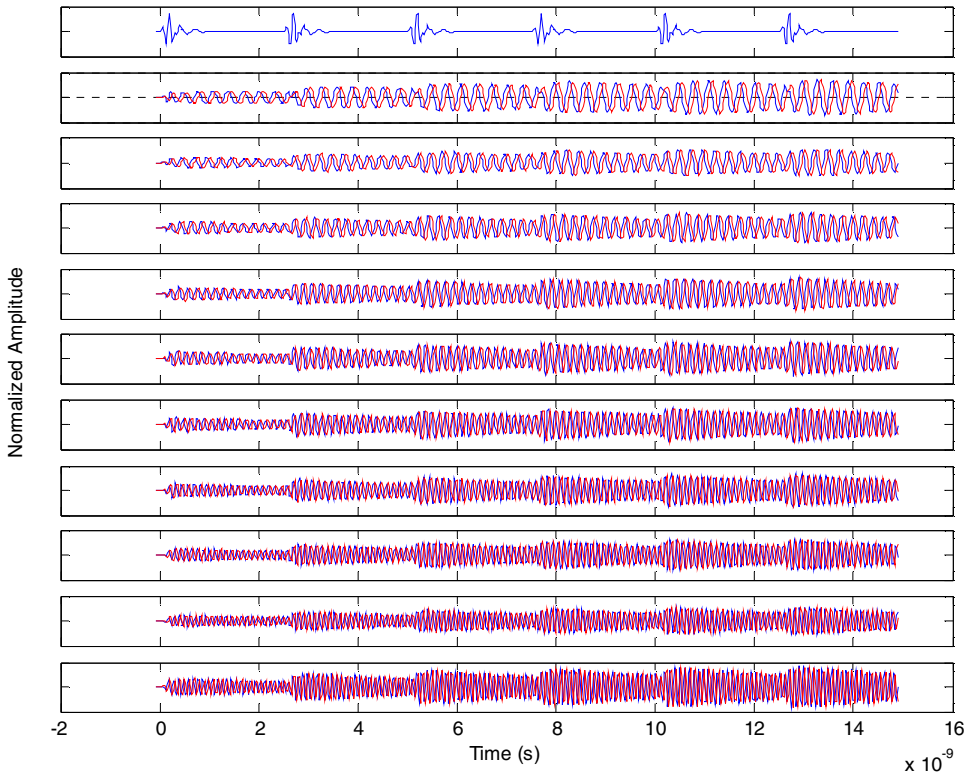

Figure 3.15: Filter Responses with Long (τ > PRI) RC Time Constants and a Squaring Circuit

Next, the energy detectors in Figure 3.8 require a suitable time period for integration. The integration should be at least $1/f_0$ to capture the energy of at least one full oscillation in each filter. The time period $1/f_0$ is well within the period of one PRI because the maximum $1/f_0$ as mandated by FCC regulations is 0.32 ns (1 / 3.1 GHz), and an extremely fast PRI would be 1 ns (1 / 1 GHz). Longer periods of integration harvest more signal energy but also more noise. Further, a longer time period also increases power dissipation, so the integration period should result in acceptable compromise between receiver characteristics and power dissipation.

Finally, the pulse sense circuit may decide that a signal is present or not present with a probability distribution of $p_r(x)$. In addition, the signal may be actually be present or not present with a probability distribution of $p_s(y)$. Thus the pulse sense circuit makes a decision with joint probability distribution for $x \in$ [**present**, **not present**].

INTEL-1010
U.S. Patent 9,265,043

$$P\left(p_r(x)\middle|p_s(y)\right)=\frac{P\left(p_r(x),p_s(y)\right)}{p_s(y)} \quad (3.6)$$

Of particular interest is the case that the circuit decides a signal is present when, in fact, a signal is not present, and this called the probability of false alarm P_{fa}.

$$P_{fa}=P\left(p_r(x=\text{present})\middle|p_s(y=\text{not present})\right)=\frac{P\left(p_r(x),p_s(y)\right)}{p_s(y)} \quad (3.7)$$

The probability distribution $p_s(y)$ is unknown *a priori*, and the circuit makes a decision based only a fixed threshold level. Thus a false alarm occurs due to noise energy only. For a given threshold, the false alarm probability P_{fa} is constant

Likewise, detection occurs when the pulse sense circuit reports a signal when there is signal energy present. For a given threshold and signal power, the probability of detection P_d is constant.

$$P_d=P\left(p_r(x=\text{present})\middle|p_s(y=\text{present})\right)=\frac{P\left(p_r(x),p_s(y)\right)}{p_s(y)} \quad (3.8)$$

The number of "looks" refers to the number of times that the circuit performs the combination and threshold operations. Note that these operations take place at discrete points in time, unlike the continuous time operations of the filter bank and the energy detector. Taking more than one look will increase P_d and decrease P_{fa} at the expense of some additional operating time and power dissipation. Assuming each look is independent, the binomial distribution describes the probability that N occurrences of either a false alarm or a detection occurs within M looks.

$$P(N\text{ False Alarms})=\binom{M}{N}P_{fa}{}^{N}\left(1-P_{fa}\right)^{M-N} \quad (3.9)$$

INTEL-1010
U.S. Patent 9,265,043

$$P(N \text{ Detections}) = \binom{M}{N} P_d^{\,N} (1 - P_d)^{M-N} \qquad (3.10)$$

We make the following decision rule: a signal is present if it is detected at least N times within M looks. With this decision rule, the cumulative probability distributions are

$$P_{fa}^{cum} = \sum_{i=N}^{M} P(i \text{ False Alarms}) \quad (3.11) \quad \text{and}$$

$$P_d^{cum} = \sum_{i=N}^{M} P(i \text{ Detections}) \qquad (3.12) \quad .$$

Considering a practical number of looks to be $M = 3$, 5, or 7, we require that

$$N = \left\lceil \frac{M}{2} \right\rceil \quad (3.13)$$

for a signal detection. Figure 3.16 shows P_{cum} versus p for probabilities ranging from 0 to 1 for [M=3, N=2], [M=5, N=3], and [M=7, N=4]. The x-axis represents the probability of detection or false alarm that a circuit achieves with one look. The y-axis shows the corresponding cumulative probability from (3.11) and (3.12)over multiple looks. Thus, the straight line p=p designates the probability for one look.

INTEL-1010
U.S. Patent 9,265,043

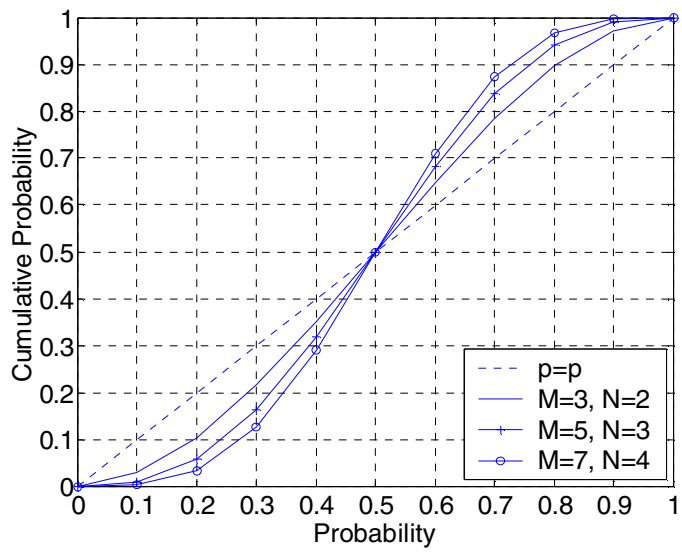

Figure 3.16: Cumulative Probability Distribution

For a useful system, we expect $P_d > 0.5$ and $P_{fa} < 0.5$, otherwise the system performance is worse than guessing. Figure 3.16 shows that for $P_d > 0.5$ and $P_{fa} < 0.5$, the cumulative decision always increases P_d and decreases P_{fa} because the curves intersect the line p=p at p=0.5. Smaller values of N move the intersection to the left and larger values of N move it to the right. Also note that greater M results in better performance, but increases sensing time and power.

A designer may determine specific trade offs among P_d, P_{fa}, sensing time, and power dissipation for a given application. For either hard or soft combination, the threshold detection level sets the probability of detection P_d and the probability of false alarm P_{fa}.

3.4 Results

In general, a CCA circuit should report a low false alarm rate P_{fa}, and a high probability of detection P_d. The total time of operation, after which the circuit outputs a decision, should be a few symbols (e.g. eight symbols in IEEE 802.15.4). These three factors are dependant upon one another. A designer may determine trade offs among

INTEL-1010
U.S. Patent 9,265,043

P_d, P_{fa}, sensing time, and power dissipation for a given application to meet such criteria as latency or power per successful transmission.

The CCA circuit in Figure 3.4 was modeled in Matlab to simulate its performance. In the implementation, there are seven filter banks with center frequencies f_0 = 4 GHz, f_1= 5 GHz, f_2= 6 GHz, …, f_6 = 10 GHz. The pulse repetition interval (PRI) is 5 ns to result in a pulse rate of 200 MHz, and a rate ½ forward error correcting code results in a 100 Mbps data rate with binary phase shift keying (BPSK) modulation. We considered two channel models separated into line-of-sight (CM1) and extreme non-LOS (CM4) conditions [109]. Note that the 5 ns PRI can incur significant inter-symbol interference (ISI) because the RMS delay spread can be up to 25 ns for the NLOS channel model. We vary the E_b/N_0 from 12 dB to 20 dB, which corresponds to transmitter-receiver distances from 10 m to 4 m for an 11 dB noise figure at the antenna terminal. The receiver can demodulate the coded data with a bit error rate (BER) of approximately 2×10^{-4} at the worst-case E_b/N_0 of 12 dB in the NLOS channel. All simulations and analysis use a short time constant, because it performs worse than a longer time constant and we would like to show the practicality of the circuit in the worst case.

Table 3.2 summarizes the link budget we used to obtain the SNR values for each distance. We choose 5 ns as the fastest PRI required in an ad or sensor network, and a longer PRI, *PRI',* would improve the link budget by 10 $\log_{10}$(*PRI'* / 5 ns).

INTEL-1010
U.S. Patent 9,265,043

Table 3.2: Link Budget

Parameter	Value
Pulse Rate	200 MHz
Avg. Tx Power (P_t)	-2.5 dBm
Center Frequency (F_c)	5.7 GHz
Path loss at 1 m (L_1)	47.6 dB
Additional Path loss at 4 m (L_4)	12.0 dB
Additional Path loss at 8 m (L_6)	18.0 dB
Additional Path loss at 10 m (L_{10})	20.0 dB
Rx Antenna Gain (G_r)	0.0 dBi
Tx Antenna Gain (G_t)	0.0 dBi
Rx Power @ 4 m ($P_{r4} = P_t+G_t+G_r-L_1-L_4$)	-62.1 dBm
Rx Power @ 6 m ($P_{r4} = P_t+G_t+G_r-L_1-L_6$)	-65.7 dBm
Rx Power @ 10 m ($P_{r10}= P_t+G_t+G_r-L_1-L_{10}$)	-70.1 dBm
Avg. Noise Power per Pulse (N)	-94.0 dBm
Rx Noise Figure @ Antenna Terminal (N_f)	8 dB
Avg. Antenna Noise Power per Pulse (P_n)	-83 dBm
SNR @ 4 m	**20.9 dB**
SNR @ 6 m	**14.9 dB**
SNR @ 10 m	**12.9 dB**

We first derive theoretical bounds for the performance of the above system in Additive White Gaussian Noise (AWGN) described by

$$p(v) = \frac{1}{\sqrt{2\pi\sigma^2}} e^{\frac{-v^2}{2\sigma^2}} \quad (3.14) \quad ,$$

where $p(v)$ is the probability distribution function of the noise voltage with variance σ^2. When passed through a narrowband filter (bandwidth << center frequency) such as the ones in Figure 3.5, the noise output takes the form of a Rayleigh distribution function [199].

$$p(R) = \frac{R}{\sigma^2} e^{-\frac{R^r}{2\sigma^2}} \quad (3.15)$$

For a threshold voltage V_T, the probability that the noise exceeds the threshold is

INTEL-1010
U.S. Patent 9,265,043

$$p(N > V_T) = \int_{V_T}^{\infty} \frac{R}{\sigma^2} e^{-\frac{R^r}{2\sigma^2}} dR = e^{\left(-\frac{V_t^2}{2\sigma^2}\right)} \quad (3.16) \quad .$$

When the filters resonate with a sine wave of amplitude A, the output of the filters has a probability density function that includes both the noise and the sine wave.

$$p_s(R) = \frac{R}{\sigma^2} e^{-\frac{R^r + A^2}{2\sigma^2}} I_0\left(\frac{RA}{\sigma^2}\right) \quad (3.17)$$

The function I_0 is a modified Bessel function of zero order. Because of the resistance and capacitance of the filters, the output signal takes some time to reach it maximum value as each pulse arrives. After each pulse, the output will decay according to the RC constant. In the architecture shown in Figure 3.4, the filters have equal RC constants because the center frequency is determined by an inductor. Some time after the beginning of a pulse train, the system will reach a steady state response (i.e., the filter output attains the same $V_{max} = A$ after the arrival of every pulse) with respect to the filters. At the steady state, the effective average amplitude of the signal is as follows.

$$A_{eff} = \frac{\int_0^{T_p} A\left(1 - e^{-t/RC}\right) + \int_{T_p}^{PRI} Ae^{-t/RC}}{PRI} \quad (3.18)$$

Thus, from (3.17) and (3.18), the probability of detecting a signal is

$$p_s(S + N > V_T) = \int_{V_T}^{\infty} \frac{R}{\sigma^2} e^{-\frac{R^r + A_{eff}^2}{2\sigma^2}} I_0\left(\frac{RA_{eff}}{\sigma^2}\right) dR \quad (3.19)$$

Figure 3.17, Figure 3.18, and Figure 3.19 demonstrate the proof-of-concept for pulse sense. In the figures, the energy detector takes one look at the filter bank outputs and integrates for a half-bit period of 1 PRI or, equivalently, $20/f_0$. The combination

INTEL-1010
U.S. Patent 9,265,043

scheme is soft combination. Figure 3.17 shows the analytical performance of (3.16) and (3.19) as numerically evaluated in Matlab. Figure 3.18 shows the simulated performance in AWGN, and Figure 3.19 shows the simulated performance under the multipath conditions of CM1 (LOS) and CM4 (extreme NLOS).

Note that the addition of the channel model does not significantly degrade performance from the AWGN case. This is because the circuit considers the total spectral energy in the channel, so spreading the total energy over the multipaths does not significantly affect performance. This is a considerable advantage in the harsh multipath environment of I-UWB. Pulse sense performs slightly better in CM1 than CM4, and this is because CM4 may contain multipaths with a large gain as compared to the first path. These multipaths contribute to spectral power at frequencies other than f_i, so there is some loss in the spectral energy at each f_i.

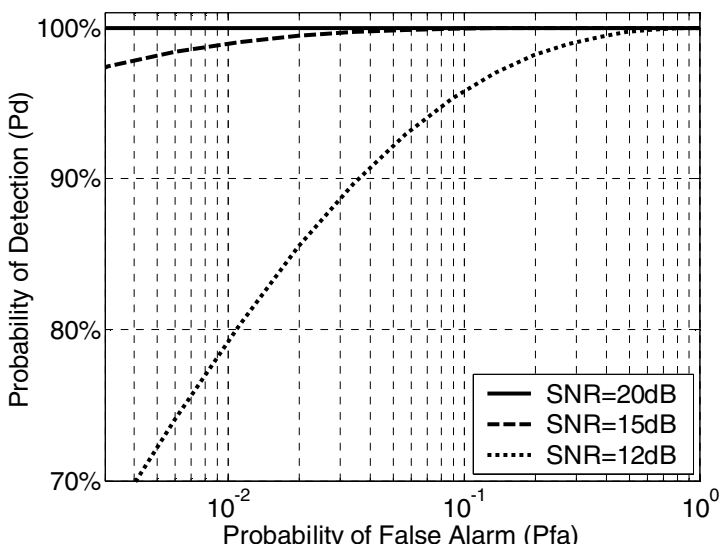

Figure 3.17: Analytical P_d versus P_{fa} for AWGN

INTEL-1010
U.S. Patent 9,265,043

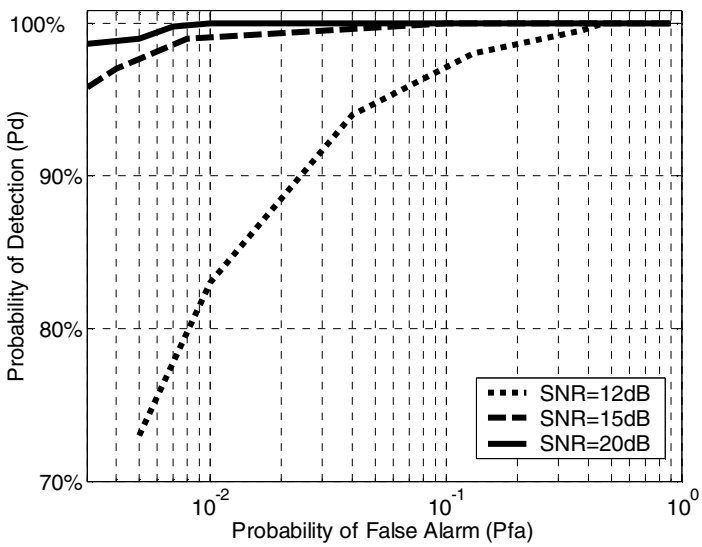

Figure 3.18: Simulated P_d versus P_{fa} AWGN

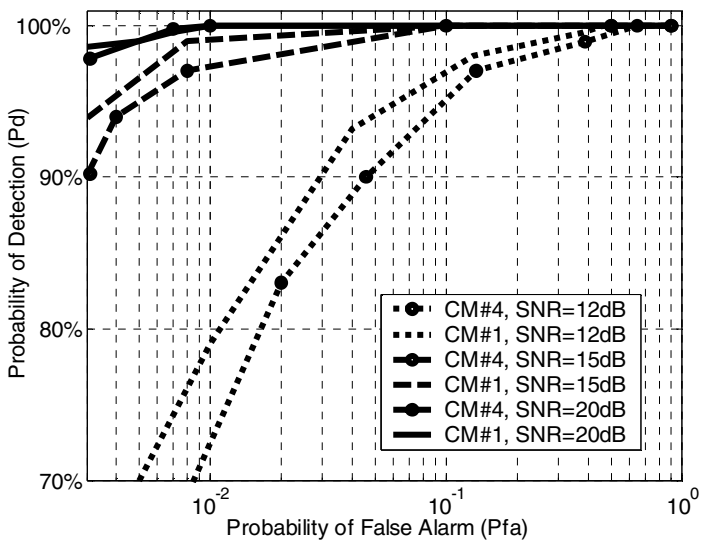

Figure 3.19: P_d versus P_{fa} for CM1 and CM4

With one look and an integration time of one PRI, the circuit is practical in all channel conditions for distances less than 6 m (E_b/N_0 = 15 dB). For greater distances, the pulse sense circuit can lengthen its sensing time to significantly improve performance. Figure 3.20 shows that detection probability P_d and false alarm probability P_{fa} can be improved with additional sensing time. Figure 3.20 considers the worst-case channel model of CM4 and SNR of 12 dB. The sensing time may be

INTEL-1010
U.S. Patent 9,265,043

lengthened via the integration time or the number of looks. As the listening time extends from 1·PRI to 2·PRI for one look, performance does not significantly improve. This is because of the long baseline integration time (as compared to $1/f_0$), and this suggests that the listening time can be reduced to save power. Then, for a listening time of 1·PRI, the number of looks extends to 3, 5, and 7; the decision is based on the result of the majority of looks (e.g. 4 out of 7 looks) as in (3.13). Increasing the number of looks improves performance much more significantly than increasing the already long integration time. Figure 3.20 shows that the proposed circuit can detect medium activity with near 100% P_d and extremely low P_{fa} within 7 symbols.

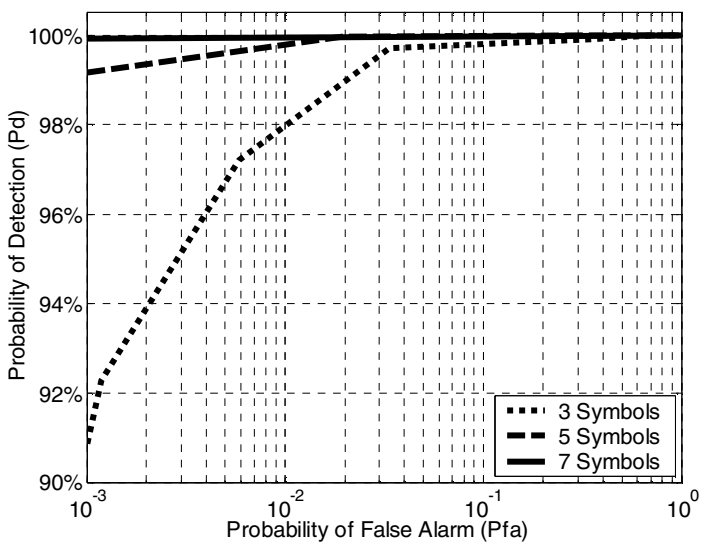

Figure 3.20: P_d versus P_{fa} with Additional Sensing Time, CM4, SNR = 12 dB

Next, Figure 3.21 presents the ability of the hard combination and soft combination schemes to reject a strong narrowband interferer. We choose a tone interferer because it should have more of an effect on a resonator filter than a modulated signal. Further, because the bandwidth of any narrowband interferer is much less than the UWB bandwidth, a narrowband interferer may be modeled as tone. The interferer takes the form of the generic in-band tone interferer of the IEEE 802.15.3a task group [207]

INTEL-1010
U.S. Patent 9,265,043

$$I(t) = \sqrt{2P_I}\cos(\omega_0 t + \theta) \quad (3.20) \quad ,$$

where P_I is the average received power, $\omega_0=2\pi f_0$ is the carrier frequency, and θ is a random phase of the carrier uniformly distributed in $[0,2\pi]$. The interferer is placed in the 5.1 GHz ISM band to activate filter f_1. Further, the IEEE 802.15.3a task group specifies that the tone should have a minimum power such that $P_I - P_d > 3$ dB, where P_d is 6 dB above the receiver sensitivity level. Thus, for the link budget in Table 3.2, the interferer power should be at least -77 dBm. For a greater safety margin, we set the interferer's power level such that the I-UWB signal to narrowband interference ratio is –10 dB. This corresponds to [207], which models a UMTS in-band interferer as a tone 10 dB above the received signal power.

In Figure 3.21, the multipath channel model is the LOS CM1 and the SNR is 15 dB. The hard decision block requires 4 of the 7 spectral components to be present, and the threshold levels are ideal for each P_{fa}. The soft decision block also considers ideal threshold levels, and the limiters have a maximum output of 1.8 dB above the average UWB signal level. For both soft and hard combinations, the presence of a narrowband signal does not cause significantly more false alarms.

The hard combination method performs best when the P_{fa} is relatively high, whereas the soft combination method performs best when the P_{fa} is relatively low. The crossover point is around $P_{fa} = 5\times10^{-3}$. Therefore, for low power applications, the hard combination method is preferable to maximize P_d and avoid retransmissions

The reason that hard combination performs best for high P_{fa} is that the threshold value is low, so the narrowband signal may add up to 1.8 dB of energy into the soft combination block, depending on the threshold value. This energy alone may be enough to trigger false alarms and has the effect of moving the curves in Figure 3.19 to the right. However, for the hard combination, the narrowband energy does not add any extra energy to the hard combination block because the block receives binary input values.

At low P_{fa} the threshold value is high, so the narrowband signal cannot add as much energy to the soft combination block. Thus, soft combination yields a better decision. However, at low P_{fa}, the hard combination block continues to weight all inputs – including the interferer – equally, so it does not perform as well as the soft combination block.

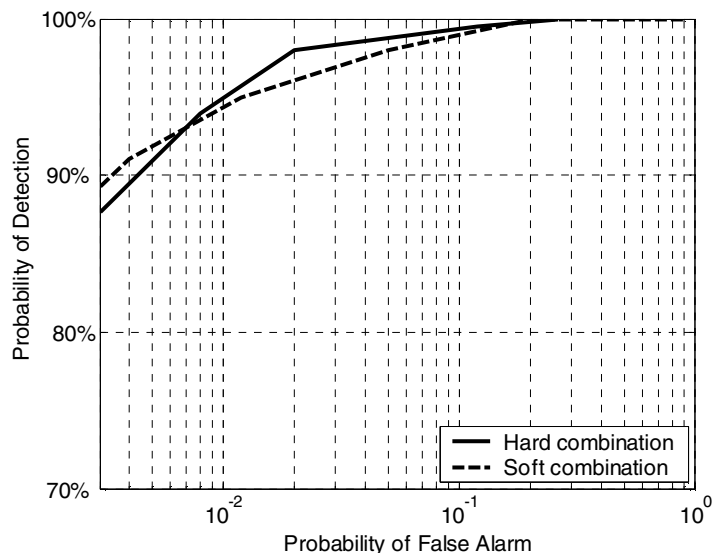

Figure 3.21: P_d versus P_{fa} with Strong Narrowband Interferer, CM1, SNR = 15dB

Next, we separately consider the effects of timing jitter and multiple transmissions in the channel. Both simulations consider a 10 m link distance (12 dB E_b/N_0) in CM1, use soft combination, take one look, and integrate over 1 PRI. The distribution of the jitter ε is

$$p_\varepsilon(x) = \begin{cases} 1/(2\Delta), & -\Delta < x < \Delta \\ 0, & \text{otherwise} \end{cases} \quad (3.21) \quad ,$$

where $\Delta = 3 * RMS_{avg.}$ A value of 5 ps for the RMS average jitter is consistent with current technology of timing chips [4]. In Figure 3.22, the performance with jitter shows no visible difference from the performance without jitter in Figure 3.19. This is because the filters capture approximately the same amount of energy as for the case

INTEL-1010
U.S. Patent 9,265,043

with no jitter. Next, we simulate the performance in the presence of multiple transmissions. The pulse sense circuit sees two transmissions, and one transmission is delayed by a half-PRI with respect to the other. The performance is similar to that in Figure 3.19 at 15 dB E_b/N_0, because the energy in the channel is doubled.

The next set of simulations provides some insight into the performance of pulse sense at different distances, PRIs, and modulation schemes. As the PRI decreases, the energy of each pulse can increase while the pulse train maintains the same average power for the pulse train. This allows systems to increase either the E_b/N_0 or the range by decreasing the PRI. The simulations use soft combination, integrate over 1 PRI, and operate in CM4. Figure 3.23 shows the results of extending the PRI to 20 ns. This increases the E_b/N_0 by a factor of $10 \log_{10}(20 \text{ ns} / 5 \text{ ns}) = 6$ dB, so the resulting E_b/N_0 is 18 dB at 10 m. Note that performance for this longer PRI improves as compared to Figure 3.19, which has the same average power. Note also that performance does not improve as if the E_b/N_0 had been increased by 6 dB for the 5 ns PRI. This is because the filters use the same RC time constant as the 5 ns PRI, so it is important to optimize (in this case lengthen) the RC time constant for operation at different PRIs. Reducing the pulse rate improves the performance of pulse sense or allows pulse sense to operate at extended ranges.

We then change the modulation scheme to binary PPM with orthogonal pulse positions offset by 1 ns. From (2.17), this should create spectral lines at multiples of 1 GHz (1 / 1 ns) to improve performance. The simulation conditions are the same as above. Figure 3.23 shows that the performance of binary PPM closely matches that of BPSK. This is because performance depends more heavily on total energy than on modulation scheme.

INTEL-1010
U.S. Patent 9,265,043

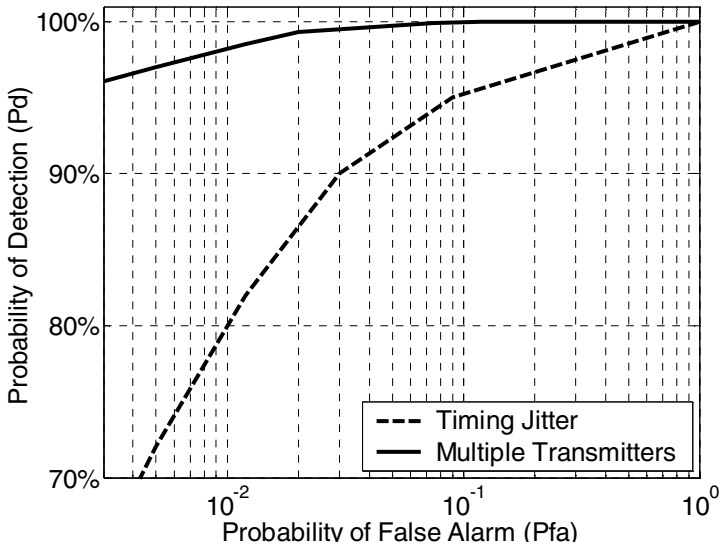

Figure 3.22: P_d versus P_{fa} with Jitter and Multiple Transmissions, CM1, E_b/N_0 = 12 dB

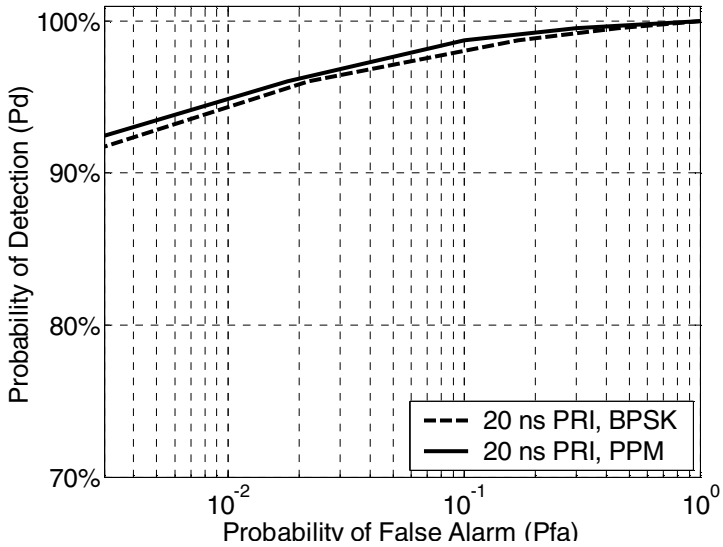

Figure 3.23: P_d versus P_{fa} for longer PRI, CM4. Also with PPM modulation

Finally, we simulate the pulse sense circuit with various RC time constants, and the parameters are extracted from Spice simulations [193]. Figure 3.24 compares the performance of the circuit implementation to the analytical performance from (3.16) and (3.19) and also the system-level simulations in AWGN. The energy detector takes one look at the filter banks and integrates for 1 PRI. The combination scheme is soft combination. Figure 3.24 shows a short RC time constant for consistent comparison

INTEL-1010
U.S. Patent 9,265,043

with the above simulations. The implementation performs as well as the system-level simulations, and both simulations match the expected performance from analysis. We also show the performance with the addition of channel model CM1 to show that the channel model does not significantly deteriorate performance. This is because the pulse sense circuit is essentially an energy detector, and the channel model disperses energy but does not cause any loss of energy.

Figure 3.25 also shows the performance of the system with an RC time constant twice as long as in Figure 3.24 and a squaring circuit. The implementation matches expectations, and the performance improves as compared to a shorter RC time constant at the expense of some additional hardware.

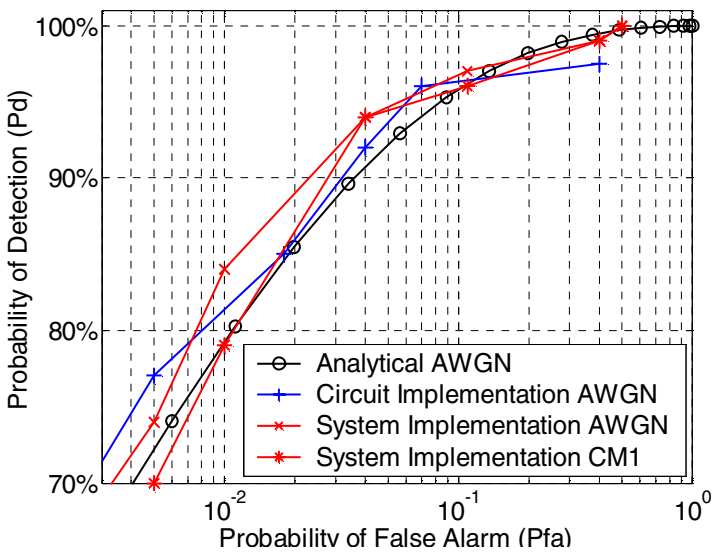

Figure 3.24: Performance Comparison of Circuit-Level Implementation, Analytical Expression, and System-Level Implementation for Short Time Constant.

INTEL-1010
U.S. Patent 9,265,043

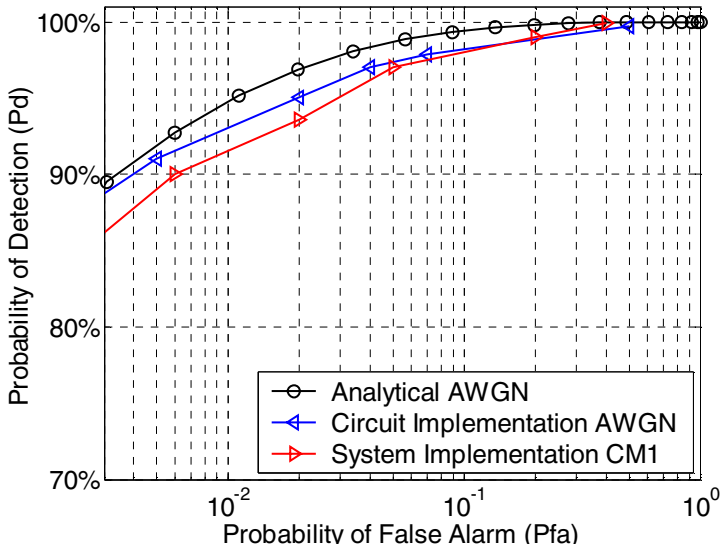

Figure 3.25: Performance Comparison of Circuit-Level Implementation, Analytical Expression, and System-Level Implementation for Long Time Constant.

3.5 Chapter Summary

Impulse-based ultra wideband (I-UWB) is an attractive radio technology for large ad hoc and sensor networks due to its robustness to harmful multipath effects, sub-centimeter ranging ability, simple hardware, and low radiated power.

Current MAC protocols for I-UWB target small WPANs and cellular networks. The centralized approach is a good strategy for a small network with heavy traffic and strict QoS requirements. However, in large ad hoc and sensor networks, the central coordination increases complexity and overhead, and it also leads to a central point of failure. Therefore, large ad hoc and sensor networks usually implement distributed MAC protocols.

This chapter investigates pulse sense as a method to implement a distributed MAC protocol for I-UWB radios. Distributed MAC protocols for ad hoc and sensor networks generally realize random access and require a method of CCA. The low duty cycle, low power, spectral lines, and harsh channel conditions of I-UWB present difficulties in CCA. Existing methods of CCA are either inaccurate or require a prohibitive amount of time or hardware complexity to search for a narrow, low-power

INTEL-1010
U.S. Patent 9,265,043

pulse within a large time window. We propose pulse sense to overcome the challenges of quickly, reliably, and efficiently sensing medium activity in an I-UWB network. The key idea of pulse sense is to examine the spectral power components of the received signal, which are always present, to avoid searching for narrow I-UWB pulses in the time domain.

The proposed pulse sense circuit meets the design goals for CCA, and simulations and analysis of our proposed architecture show that it is practical. It detects medium activity within a short time because the filters start oscillation within the first few pulses of a transmission and the energy detectors reach their maximum values well within one PRI. The detection time is shorter than existing methods by orders of magnitude, and it does not require synchronization.

The circuit considers the total spectral energy in the channel, so the in-band multipath components, which repeat at the PRF, do not significantly affect performance. For the same reason, the proposed method is insensitive to timing jitter, inter-symbol interference (ISI), in-band interference, varying channel conditions, and nonlinear distortion of pulses. If channel conditions change or the pulse shape is distorted, it does not have to dynamically adapt to the change. Further, narrowband interferers do not significantly degrade performance, so the system can coexist with narrowband systems.

The proposed implementation is much less complex than a receiver, and it does not require any sampling of the signal. Because there is no stored template signal, the circuit does not have to dynamically adapt to changing channel conditions and distortions of the pulse shape. Even in a CMOS implementation, the circuit can achieve a quality factor Q for sufficient performance over a range of PRIs. Designers may customize the performance depending required range, SNR, power dissipation, and pulse rate.

Chapter 4: Multi-channel I-UWB MAC

The previous chapter presented a method to enable a distributed MAC protocol for I-UWB ad hoc and sensor networks. This chapter explores a unique benefit that I-UWB signaling may add to a distributed MAC protocol.

In Section 2.3.3, the centralized MAC protocols for I-UWB subdivide the channel into time slots or code channels, so they are also called multichannel protocols. Each sub-channel's data rate is W/N, where W is the full channel data rate and N is the spreading rate or the number of time slots. Although multichannel protocols reduce the link data rate, they increase network throughput at high offered load [81]. This is because the (ideally) orthogonal channels reduce collisions from hidden terminals and concurrently transmitting terminals. At low offered load, the reduced sub-channel bandwidth increases delay. These centralized MAC protocols mainly target smaller networks, and they become complex and inefficient for large networks. The central coordination also leads to a central point of failure. Further, the complex multichannel receiver and/or central timing control conflict with the simple, decentralized design goals of ad hoc and sensor networks.

This chapter proposes a distributed multichannel MAC protocol for I-UWB ad hoc and sensor networks. The proposed I-UWB MAC is based on the ALOHA and CSMA MAC protocols in narrowband systems. The multichannel protocol based on ALOHA is referred to simply as multichannel ALOHA. The proposed multichannel MAC based on CSMA relies on pulse sense instead of carrier sense, so it is called pulse sense multiple access (PSMA).

The low duty cycle of I-UWB allows multichannel implementations of PSMA and ALOHA without centralized control and without modifications to a basic, single-channel I-UWB receiver. Even with the multipath delay spread, I-UWB signals contain a large amount of "dead time" between pulses at moderate pulse rates. The dead time allows several concurrent transmissions to be time-interleaved without incurring the delay penalty of other multichannel protocols.

INTEL-1010
U.S. Patent 9,265,043

This chapter also proposes a multi-user I-UWB receiver to receive multiple time-interleaved transmissions concurrently, and it further improves performance with moderate hardware complexity.

The chapter is organized as follows. Section 4.1 examines multichannel MAC protocols, and Section 4.2 explains the proposed multichannel protocol for I-UWB. Section 4.3 details the architecture for the multi-user transceiver. Section 4.4 develops Physical Layer design considerations, and Section 4.5 presents network simulation results. Section 4.6 concludes the chapter.

4.1 Multichannel MACs

In wireless networks, corrupt packets result from collisions, interference, fading, and noise. Collisions may result from many conditions, including nodes transmitting close together in time and hidden terminals. Protocols such as FAMA implement a virtual carrier sense using a request-to-send/clear-to-send (RTS/CTS) exchange [71] to reduce collisions and mitigate the hidden terminal problem. However RTS and CTS packets are still vulnerable to collisions and hidden terminal problems. Further, the long acquisition time of I-UWB makes an RTS/CTS exchange undesirable. One possible solution is a multichannel MAC, which reduces collisions and hidden terminal effects. Compared to a single channel MAC, the multichannel MAC increases throughput and reduces delays without the overhead of RTS/CTS packets.

A multichannel MAC divides a channel of bandwidth W into N channels of bandwidth W/N. Dividing the channel decreases the probability of collisions because it decreases the normalized propagation delay [81]. The normalized propagation delay is defined as the propagation time over the transmission time. The normalized propagation delay is decreased by a factor of N, so each channel is busy for a longer proportion of time. Because a node may select from a greater number of channels, there is a smaller probability of collisions. However, each sub-channel has a reduced data rate to incur a delay penalty at low offered load.

Note that the centralized MAC protocols in Chapter 2 subdivide the channel into time slots or code channels, so these protocols are multichannel protocols. In these

INTEL-1010
U.S. Patent 9,265,043

traditional multichannel networks, a base station assigns a sub-channel to each node. In ad hoc networks, a base station introduces a central point of failure. Alternatively, each node could assume the capabilities of a base station (e.g. multi-user receiver), but this would make the cost of deploying a large network prohibitive.

It is also possible to assign sub-channels distributively. For example, each node may transmit (or receive) on a code channel determined by a pseudo-noise (PN) sequence seeded by the node address [191],[192]. When the channel is divided according to codes, the medium access is considered non-exclusive since the transmissions may occur in the same frequency band at the same time. Non-exclusive MAC protocols incur multiple access interference because they do not result in perfectly orthogonal channels. Further, there is no near-far power control, so close-by nodes significantly interfere with a long-distance reception. This problem may be overcome with adaptable coding or through ignoring corrupted chips [192]. These non-exclusive protocols also must prevent two nodes from simultaneously transmitting to the same receiver because multiple user receivers are expensive. This problem may be overcome with the re-introduction of handshaking packets that establish an exclusive link [191],[192].

When the channel is divided by frequency bands or time slots, the medium access is exclusive because the channels are orthogonal. Multi-channel protocols may also assign time slots or frequency bands distributively. However, both are also problematic for ad hoc and sensor networks. Multiple frequency bands require a complex front end because each frequency band requires its own RF block. Coordinating multiple time slots requires centralized timing control, which leads to control overhead and a central point of failure.

4.2 Proposed Multichannel Protocols

Due to problems with traditional multichannel protocols in I-UWB ad hoc and sensor networks, this chapter proposes a method to exploit the low duty cycle of I-UWB to allow concurrent transmissions. Even with the multipath delay spread, I-UWB

INTEL-1010
U.S. Patent 9,265,043

contains a large amount of dead time between pulses at moderate pulse rates. This dead time is used to time-interleave additional sub-channels. Under the proposed multichannel protocols, an I-UWB network maintains the full data rate for each sub-channel, so the network increases throughput without increasing delay. Further, for multichannel operation, a PSMA or ALOHA MAC requires neither centralized control nor modification to a single channel I-UWB receiver. Finally, multichannel ALOHA and PSMA maintain a random, distributed MAC approach.

In multichannel PSMA, nodes may transmit any time they sense an idle channel. If a node senses any activity, it waits until the after medium is free to retransmit after a random period. A source node also waits for a random period of time to retransmit if it does not receive an acknowledgement. In the proposed implementation, the random period is bounded by a binary exponential, in which a node chooses a number between $[1,2^n]$, where n is the number of times the node has sensed a busy channel. The operation of ALOHA is similar, but it does not check for an idle channel before transmitting.

The proposed multichannel protocols provide multiple, time-interleaved channels by allowing concurrent transmissions of non-overlapping pulse trains. During an initial reception, the receiver may synchronize with (for a multi-user receiver) or ignore (for a single-user receiver) other concurrent, non-overlapping transmissions. For example, in Figure 4.1, two nodes sense an idle channel at time T_0, so they simultaneously start transmitting at time T_1 to the same receiver. The receiver detects an incoming transmission through pulse sense. Transmitter2 is closer, so its first pulse arrives at T_2, while Transmitter1's first pulse arrives at T_3. After some time, a single synchronization circuit detects the arrival time of the two pulse trains within each PRI. If the receiver is a multi-user receiver, two clock recovery circuits track Transmitter2's pulse train starting at T_4 and Transmitter1's pulse train starting at T_5. The receiver time-shares a single demodulator to decode the incoming signals. If the transmissions were to target different nodes, the receiver would track and decode only the transmission addressed to itself. If the receiver is a single-user receiver, the receiver would track only Transmitter2's pulse train and ignore Transmitter1's pulse train because Transmitter2's pulse train precedes Transmitter1's.

INTEL-1010
U.S. Patent 9,265,043

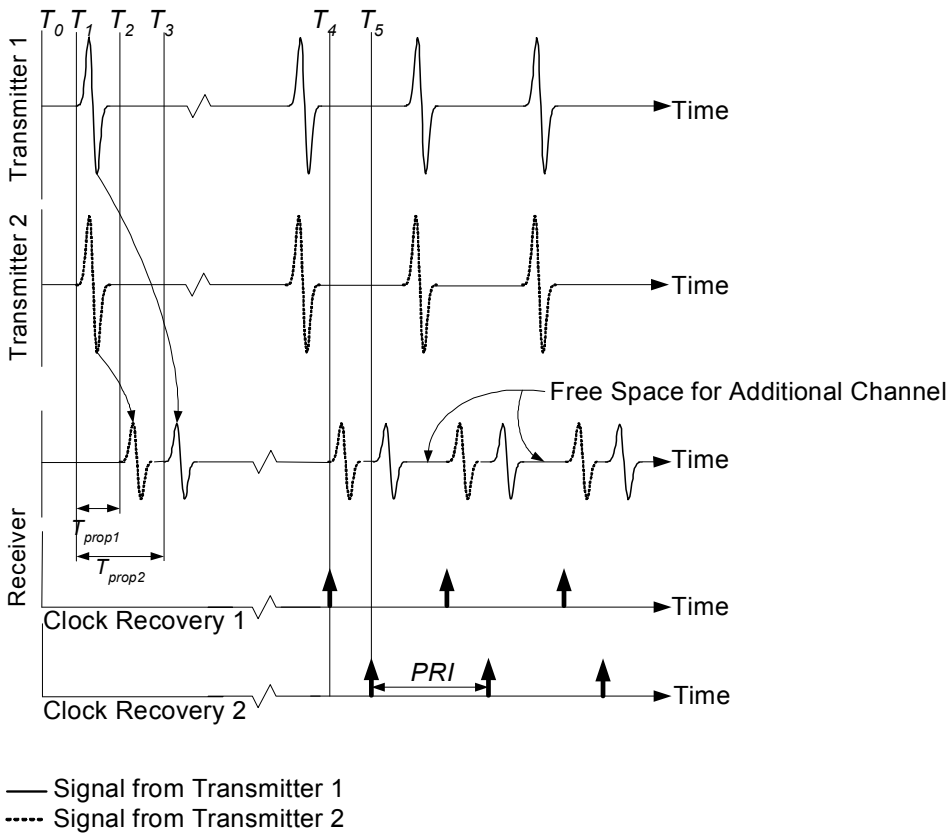

Figure 4.1: Multichannel MAC operation.

At low pulse repetition intervals (PRIs), it is probable that two concurrent transmissions (possibly from a hidden node or two simultaneously starting transmissions) do not overlap in time at a receiver. The probability of overlap increases if more than two nodes transmit concurrently, but it also becomes increasingly less probable that additional (more than two) nodes within the vicinity of any given receiver transmit concurrently. To illustrate this phenomenon, we consider an example network that realizes multichannel ALOHA, and nodes transmit with a Poisson distribution. The mean packet rate is G packets per Packet Time (Packet Time = Packet Size / Data Rate), and the probability P_T of X nodes transmitting during a Packet Time is

INTEL-1010
U.S. Patent 9,265,043

$$P(X \text{ nodes transmit}) = P_T = \frac{G^X e^{-G}}{X!} \quad (4.1) \quad .$$

In Figure 4.2, the dashed line shows P_T for an offered load with a mean of G = 1.0 packets per packet time. The figure shows that the probability of more than two nodes transmitting decreases rapidly for $X \geq 2$. In multichannel ALOHA, if more than two nodes transmit simultaneously, a collision occurs only if the pulses (including multipaths) overlap within a PRI. We assume a version of the protocol that allows up to D non-overlapping pulse positions per PRI, so there may be maximum of D simultaneous transmissions that do not share any slots. For X nodes transmitting, the probability P_S that none of the X nodes share a slot is

$$P(\text{no nodes share a slot}) = P_S = \left(\frac{D-1}{D}\right)\left(\frac{D-2}{D}\right)\left(\frac{D-3}{D}\right)\cdots\left(\frac{D-X}{D}\right) \quad (4.2) \quad .$$

In terms of factorials, (4.2) becomes

$$P_S = \frac{D!}{\left((D-X)!D^X\right)} \quad (4.3) \quad ,$$

so the probability that two or more nodes share a slot is

$$P(\text{at least two nodes share a slot}) = 1 - P_S = 1 - \frac{D!}{\left((D-X)!D^X\right)} \quad (4.4) \quad .$$

Figure 4.2 shows that (4.4) is low when the number of transmitting nodes X is small, and it gradually approaches 100% as X increases to D. The graph considers a total of D

INTEL-1010
U.S. Patent 9,265,043

= 40 slots because a long multipath delay spread is 25 ns [109], a 1 Mpps pulse rate has a PRI of 1000 ns, and 1000 / 25 = 40.

Because the number of nodes transmitting is independent of the time arrival within a PRI (the time of arrival depends on the time of the transmission and link distance), (4.2) and (4.4) are independent. Therefore, the probability of collision P_C for X simultaneous transmissions with D available slots is

$$P(\text{collision}) = P_C = P_T(1-P_S) = \frac{G^X e^{-G}}{X!}\left(1-\frac{D!}{\left((D-X)!\,D^X\right)}\right) = \frac{G^X e^{-G}}{X!} - \frac{D!\,G^X e^{-G}}{\left((D-X)!\,X!\,D^X\right)} \quad (4.5) \quad .$$

Thus from (4.5), even as X grows larger with respect to D, the actual probability of a collision becomes exponentially smaller. The Poisson distribution P_T approaches zero as X increases, and the probability of sharing a slot (1 - P_S) must be bounded by $0 \leq (1 - P_S) \leq 1$. Therefore, the overall probability of collision is bounded by the Poisson distribution, which is small for small X and approaches zero for large X. The probability of collision from (4.5) is also plotted in Figure 4.2 for G=1.0. The multiple channels are huge benefit compared to a traditional single channel protocol in which the probability of collision is 100% if two or more nodes transmit simultaneously.

Figure 4.3 shows the probability of collision for different values of the mean offered load G. Note that the probability of a collision remains low even when G is greater than the number of packets per packet time, i.e. the protocol can offer a throughput *higher* than the data rate!

INTEL-1010
U.S. Patent 9,265,043

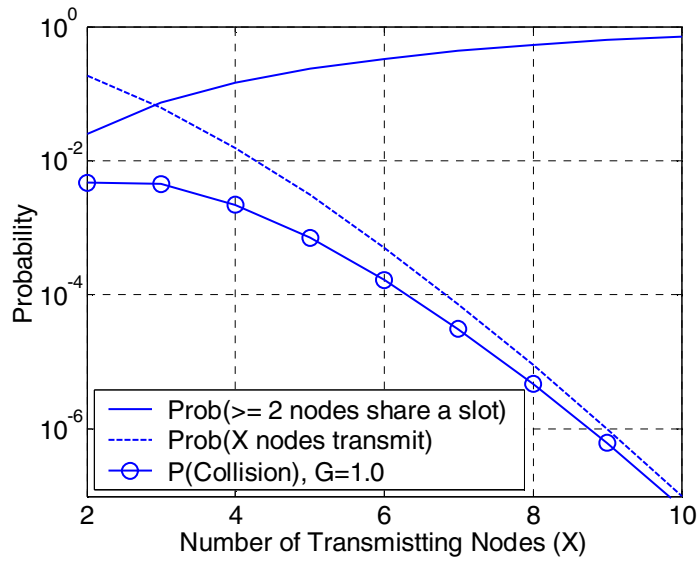

Figure 4.2: Probability of at Least X Nodes Transmitting Simultaneously Compared to the Probability of any of the Pulses Overlapping

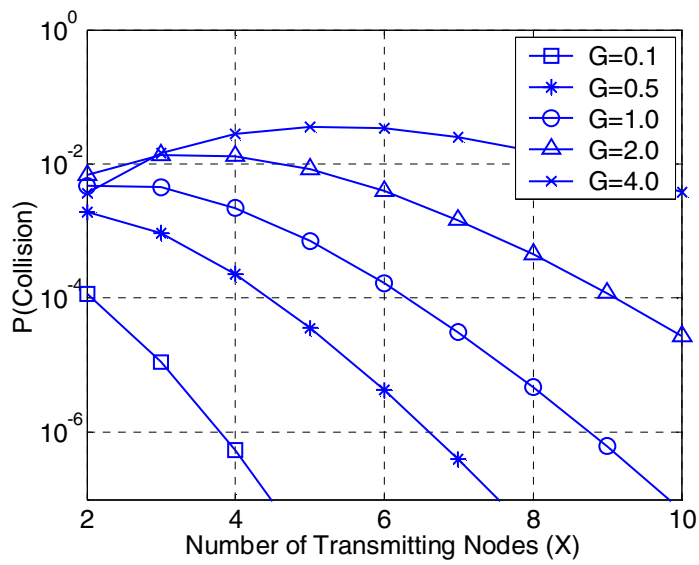

Figure 4.3: Overall Probability of Collision for Different Offered Loads.

Thus, from Figure 4.2 and Figure 4.3, one function of the multichannel ALOHA protocol is to mitigate the reduction in throughput caused by collisions. The multichannel PSMA protocol should result in even fewer collisions because nodes refrain from transmitting if the channel is busy. In multichannel PSMA, the multiple channels prevent collisions from hidden terminals. For example, with G = 2.0, the

INTEL-1010
U.S. Patent 9,265,043

proposed multichannel system has a 95% chance of a successful transmission, whereas a single channel protocol has only a 4% chance of success. Thus, the protocol performs a similar function as RTS and CTS packets, but without the acquisition overhead.

4.3 Multi-user Receiver Architecture

Multi-user receivers, which can receive on several sub-channels concurrently, improve performance for multichannel MACs [81]. However, traditional multi-user receivers are not suitable for ad hoc and sensor networks. In TDMA, the receiver is inherently multi-user but requires centralized control. A multi-user DS-UWB receiver requires separate correlators for each channel, and a multi-user FDMA receiver requires a separate front-end for each channel.

This section proposes a multi-user I-UWB receiver, which is capable of receiving multiple time-interleaved transmissions concurrently. The multi-user receiver further improves performance with moderate hardware complexity. The multi-user receiver is based on the I-UWB receiver architecture in Section 2.1.3 and the pulse sense circuit in Chapter 3 [100],[101],[103],[104]. Under the proposed multichannel PSMA and ALOHA protocols, I-UWB can implement a multi-user receiver with moderate hardware complexity and no central control. The multi-user receiver in

Figure 4.4 only requires an additional clock recovery circuit for each channel. The receiver may sleep until the pulse sense block detects an incoming packet. Then, the receiver starts the synchronization process. During synchronization, the receiver may detect more than one incoming transmission. If this is the case, it assigns an available clock recovery circuit to each non-overlapping incoming transmission. After synchronization, the synchronization circuit continues to look for non-overlapping transmissions from hidden terminals. Because the incoming transmissions do not overlap, all channels share a single front end and decision block, which are time-shared among the incoming transmissions.

INTEL-1010
U.S. Patent 9,265,043

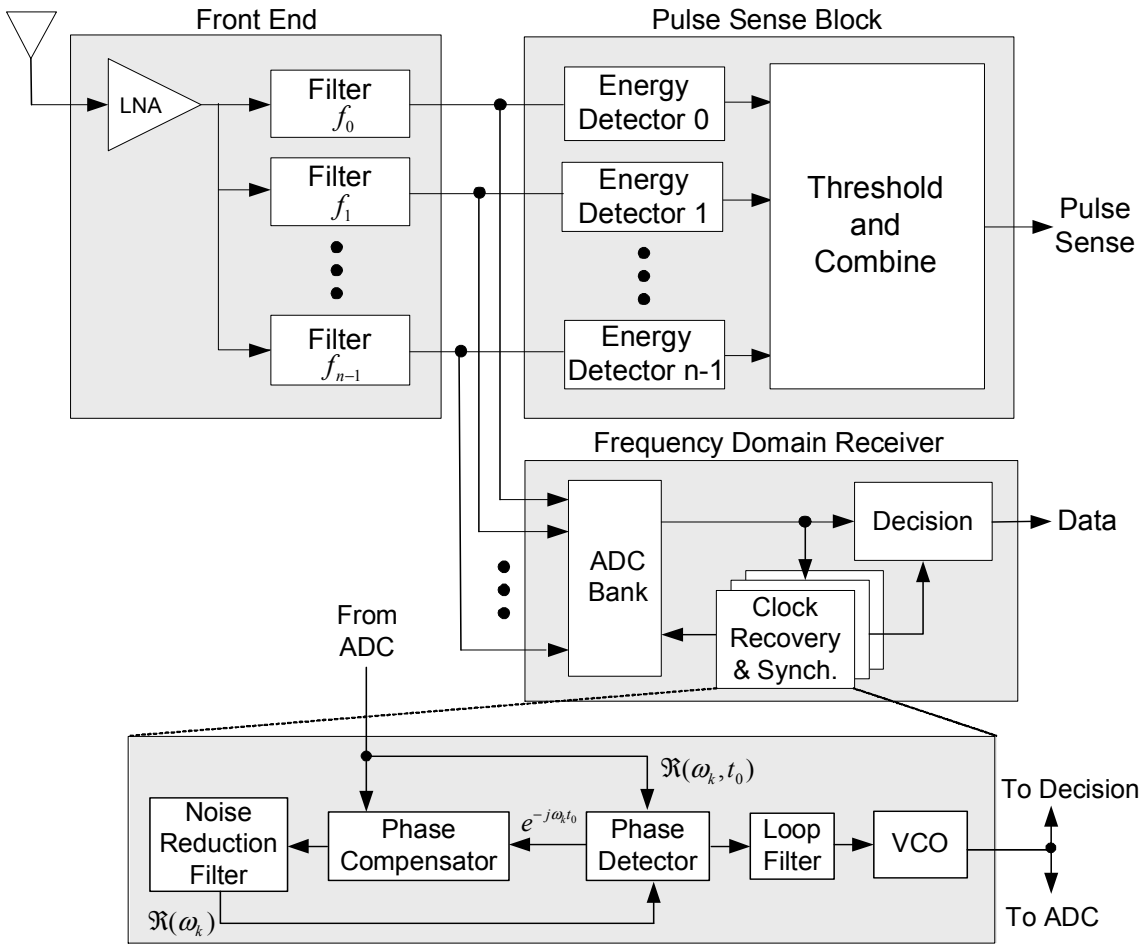

Figure 4.4: I-UWB Receiver with Multiuser Timing Recovery.

4.4 Design Considerations

This section develops design considerations for a multichannel PSMA MAC. When two interleaved pulse trains appear close in time to each other, they begin to interfere with each other due to the multipath spread. As the transmission become closer to each other in time, the interference becomes worse. The receiver must separate the intended signal from its received signal *R(t)*, which is described as

INTEL-1010
U.S. Patent 9,265,043

$$R(t)=\sum_{i\in I} s_i(t-t_i)*h_i(t)+\sum_{j\in J} s_j(t-t_j)*h_j(t)+\sum_{k\in K} s_k(t-t_k)*h_k(t)+n(t) \qquad (4.6) \quad ,$$

where

- ***I*** the set of all transmissions that collide with another transmission
- ***J*** the set of all transmissions do not collide but interfere with another transmission
- ***K*** the set of all transmissions that do not interfere or collide with any other transmission
- $s_i(t)$ a data signal that collides with another data signal
- $s_j(t)$ a data signal that does not collide but interferes with another data signal
- $s_k(t)$ a data signal that does not collide or interfere with any other data signal
- t_i, time offset of arrival within a PRI of signal from node i. $\forall\, i\in \boldsymbol{I}$, $\exists\, n\in \boldsymbol{I}$ s.t. $|t_j - t_n| \le 1 / F_0$ for $i \neq n$ and receiver time window $1 / F_0$
- t_j time offset of arrival within a PRI of signal from node j. $\forall\, j\in \boldsymbol{J}$, $\exists\, n\in \boldsymbol{J}$ s.t. $|t_j - t_n| \le D$ for $j \neq n$. Also, $\forall\, j,n\in \boldsymbol{J}$, $1/F_0 < |t_j - t_n|$ for $j \neq n$, where D is the multipath delay spread
- t_k time offset of arrival within a PRI of signal from node k. $\forall\, k,n\in \boldsymbol{K}$, $D < |t_k - t_n|$ for $k \neq n$
- $h_i(t)$ channel response from node i to the receiver
- $h_j(t)$ channel response from node j to the receiver
- $h_k(t)$ channel response from node k to the receiver
- $n(t)$ the noise at the receiver

Further, the receiver has a template signal for each transmission of interest, and it performs a correlation with result

$$C_n = \int R(t)\cdot T_n(t)\, dt \qquad (4.7) \quad .$$

As implied by (4.6), the received signal can be broken into three separate components plus noise. First consider the case with all transmissions $s\in \boldsymbol{I}$. With the receiver architecture in Figure 4.4, the receiver cannot differentiate between signals that arrive within one time window ($1 / F_0$) of each other. If two signals arrive within a time window, then the receiver drops both of the transmissions.

Next consider the case with all transmissions $s\in \boldsymbol{K}$. No part of the signal s_k overlaps with any other transmission s_l, $l \neq k$, so the correlation result will follow that of normal correlations receiver in AWGN.

INTEL-1010
U.S. Patent 9,265,043

Finally, consider the case with all transmissions $s \in \boldsymbol{J}$. In this case, the first signal arrives at least one time window earlier than the second signal, but the second signal arrives within the multipath delay spread of the first signal. In this case, some multipaths from the first signal interfere with the second signal. The interference becomes more severe as the inter-arrival time shortens from the multipath delay spread D to the time window $1 / F_0$. Because we have applied a constraint to leave the receiver architecture unchanged, the receiver can equalize the ISI within a transmission (for PRIs less than D), but not the interference from the additional transmissions.

Agilent's Advanced Design System (ADS) simulates the physical layer to help characterize the noise added to transmissions in groups ***I***, ***J,*** and ***K***. The simulations use BPSK modulation and the Cassioli channel model. The received signal is 6 dB over the minimum sensitivity level. Because interfering nodes may be at various distances relative to a transmission, the simulations consider interference over a 20 dB range of signal to interference (S/I) levels from -10 dB to + 10 dB. The range corresponds to a 10 meter radius. Although the S/I level of +10 dB places the average interference power below the sensitivity level, the instantaneous power of the interfering signal still affects the transmission.

Starting in group ***I***, the interfering signal arrives within one time window, or 3 ns, of the signal of interest. In this case, the receiver cannot time share its hardware, so the transmissions are discarded.

Next, Figure 4.5 shows the results of nodes in group ***J***. The figure shows the noise added to the transmission of interest as the interfering transmissions arrive closer to the transmission of interest. The noise increases as the interfering transmission arrives closer in time to the transmission of interest. Further, the noise increases as the interference level increases.

INTEL-1010
U.S. Patent 9,265,043

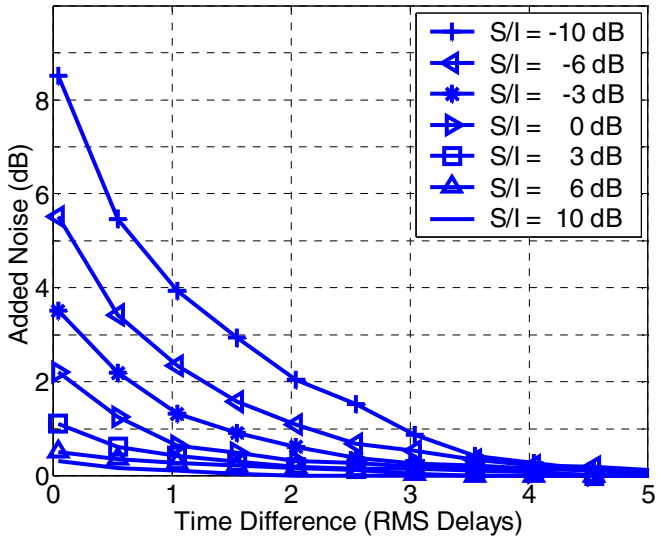

Figure 4.5: Interference from Overlapping Transmissions

For network level simulations, we consider the relative signal strengths and arrival times of signals in group ***J*** to determine if the transmissions can coexist. For a successful transmission, we require that the interfering signal add less than 1 dB of noise. When the signal power is greater than the noise power, no pair of signals in group ***J*** interferes with each other. For signal power less than or equal to the noise, the interfering signal should arrive from 1 to 3 RMS delays earlier than the signal of interest for a successful transmission. Otherwise, the second-arriving packet will be corrupted.

Finally, no multipath signals overlap the transmission of interest in group ***K***. From Figure 4.5, there is no added interference for any S/I level beyond 5 RMS delays. Therefore a transmission is in group ***K*** if it arrives later than 5 RMS delays beyond the signal of interest.

INTEL-1010
U.S. Patent 9,265,043

4.5 Network Level Results

Network level simulations in the popular ns-2 simulator evaluate the performance of the multichannel MAC protocols and the multi-user I-UWB receiver. We characterize the network level performance in terms of throughput, delay, and energy efficiency. The throughput is defined as sum of the rates (bps) of traffic the Physical Layer offers to the MAC Layer of each destination node. The delay is defined as the average time a successful packet spends between the source MAC Layer and destination MAC Layer. The energy efficiency is defined as the energy expended for a successful transmission divided by the total energy expended for all transmitted and received packets, including dropped packets and collisions. The energy includes all energy dissipated in the Physical Layer. Note that, unlike narrowband systems, the baseband processing energy of I-UWB systems is comparable to the transmission energy. These quantities are plotted against the offered load, which is defined as the sum of the rates (bps) of traffic that the Network Layer offers to the Link Layer over all nodes.

The I-UWB Physical Layer, channel model, and multichannel PSMA protocol are implemented as custom blocks in ns-2. When receiving multiple transmissions, the receiver characteristics are determined by Figure 4.5. Table 4.1 describes the simulation environment.

Table 4.1: Simulation Environment

Topology	Grid of 225 stationary nodes. Maximum of 12 neighbors.
Packet Format	4095 byte packets with format from [21]. The header is approximately 900 bits.
Traffic	Poisson traffic with a random source and a random destination.
Pulse Rate	1 Mpps - 100 Mpps. 1 bit per pulse.
Channel Model	CM4 channel model with 25 ns RMS delay spread [109]. Channel may vary between packets but not during a packet.
Receiver	No equalization. Receiver behaves according results in Sections II and III

INTEL-1010
U.S. Patent 9,265,043

First, the simulations evaluate the throughput of the multichannel ALOHA and PSMA MAC protocols as the number of users in a multi-user receiver increases. Figure 4.6 varies the number of users M from $M = 1$ to $M = 16$ for a 1 Mpps pulse rate. Two transmissions overlap if they occur within the delays specified in Figure 4.5. The 1000 ns PRI is much longer than an RMS delay, so there is a low probability that two simultaneous transmissions overlap.

In all cases, multichannel PSMA achieves a higher throughput than multichannel ALOHA. Additionally, multichannel PSMA is more stable at higher offered load. As a multi-user receiver supports more users, performance improves for both protocols, but it reaches a limit around $M = 4$ for PSMA and $M = 8$ for ALOHA. This is because it is highly improbable that a node under PSMA receives more than four simultaneous transmissions. In ALOHA, nodes do not check for a busy the medium before transmitting. Thus, ALOHA reaches a limit at $M = 8$ because it is unlikely that a node has more than eight neighbors. Eight neighbors ensure a fully connected network topology, and the remaining nodes in the vicinity can sleep to save energy [2].

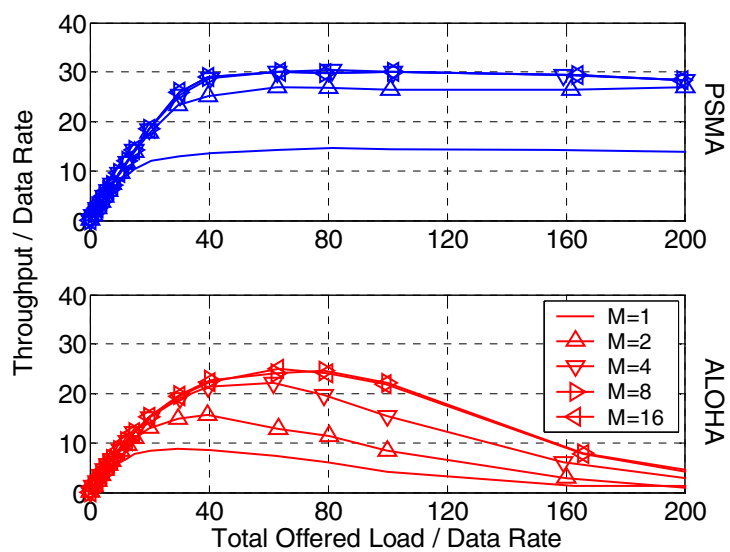

Figure 4.6: Normalized Throughput for Multi-user Receivers in Multichannel PSMA and ALOHA

INTEL-1010
U.S. Patent 9,265,043

Figure 4.7 shows that the benefits of multichannel PSMA and ALOHA diminish as the pulse rate increases. For a clearer comparison, the simulations assume that the hardware scales in proportion to the pulse rate. For example, at 100 Mpps, the switching times and inter-frame times are all 100 times faster than at 1 Mpps. However, the multipath delay spread remains the same, so overlap is more probable. For multichannel PSMA, the throughput starts to decrease rapidly at around 8 Mpps and reaches a floor at 16 Mpps. Beyond the throughput floor, multichannel PSMA operates similarly to a single channel narrowband system where simultaneous transmissions always overlap. The ALOHA network transitions more gradually, but it also reaches a floor around 16 Mpps.

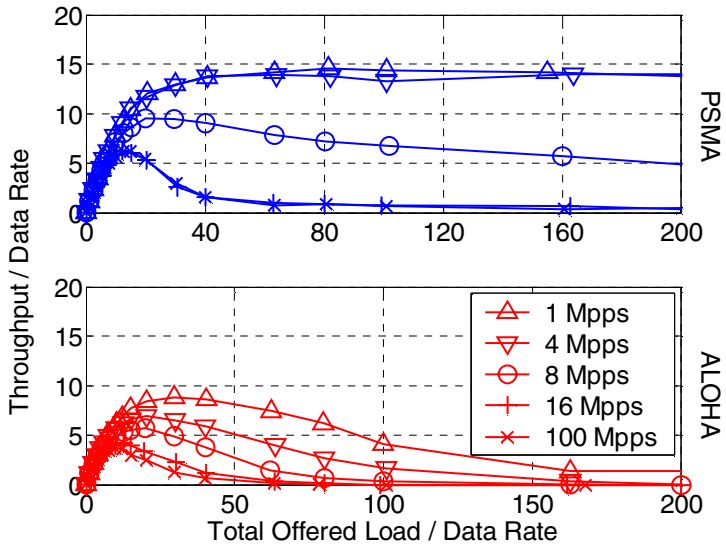

Figure 4.7: Normalized Throughput for Different PRIs in Multichannel PSMA and ALOHA

Next, the simulations evaluate the energy efficiency for multichannel PSMA and ALOHA. Figure 4.8 varies the number of users M from $M = 1$ to $M = 16$ for 1 Mpps. For all M, PSMA achieves greater energy efficiency than ALOHA. Additionally, PSMA is stable at higher offered loads, whereas the energy efficiency for

INTEL-1010
U.S. Patent 9,265,043

ALOHA approaches 0% as the offered load increases for all M. Again, performance reaches a limit around $M = 4$ for PSMA and $M = 8$ for ALOHA.

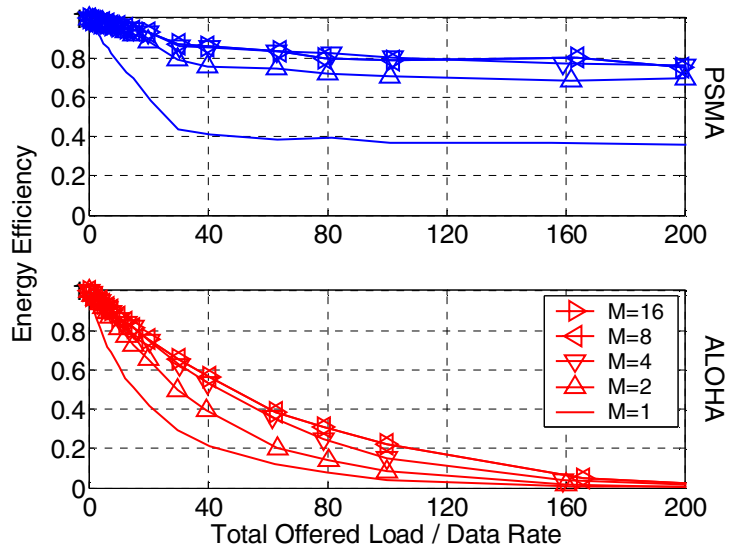

Figure 4.8: Energy Efficiency for PSMA and ALOHA with Multi-user Receivers

Figure 4.9 shows that energy efficiency decreases for multichannel PSMA and ALOHA as the PRI decreases. As the PRI decreases, the reduced number of time slots cause more collisions. For multichannel PSMA, the energy efficiency starts to decrease rapidly at around 8 Mpps and reaches a floor at 16 Mpps. The ALOHA network transitions more gradually with pulse rate, but it also reaches a floor in energy efficiency around 16 Mpps.

INTEL-1010
U.S. Patent 9,265,043

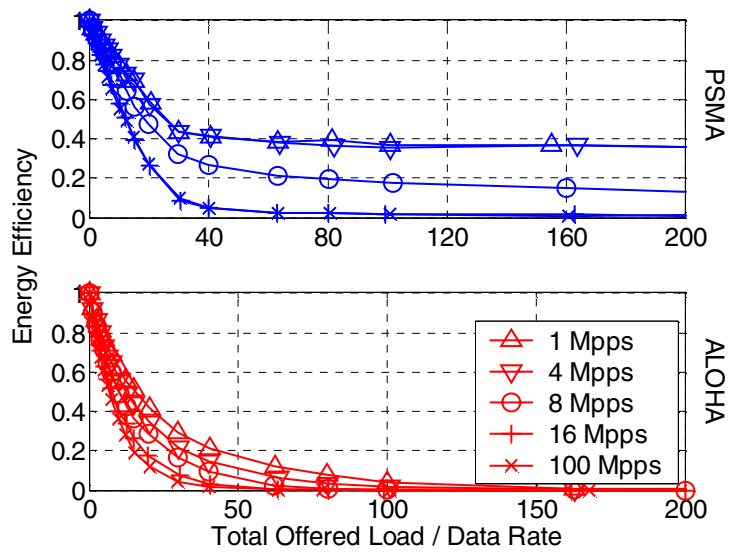

Figure 4.9: Energy Efficiency for PSMA and ALOHA at Different PRIs

Disregarding propagation time, the average packet transmission delay D is [81]

$$D = (G/S - 1) \times (N + \delta) + N \quad (4.8) \quad ,$$

where G is the offered load, S is the throughput at G, N is the reduction in link bandwidth, δ is the average retransmission delay computed from the simulations, and $N + \delta$ is the normalized average delay between successive retransmissions. Figure 4.10 compares the delay of a 1 Mpps PSMA system to a hypothetical 1 Mpps TDMA system that can achieve the same throughput at each M. The PSMA delay is plotted with solid lines and the TDMA delay with dotted lines.

Note that the TDMA MAC incurs longer delay for low offered load (i.e. when G/S is close to 1) as compared to the PSMA MAC. This is because each channel's bandwidth degrades by a factor of $1/N$, so it takes N times longer to transmit a packet on an empty channel. For the proposed PSMA MAC, N is always one because each successful transmission uses the full bandwidth.

INTEL-1010
U.S. Patent 9,265,043

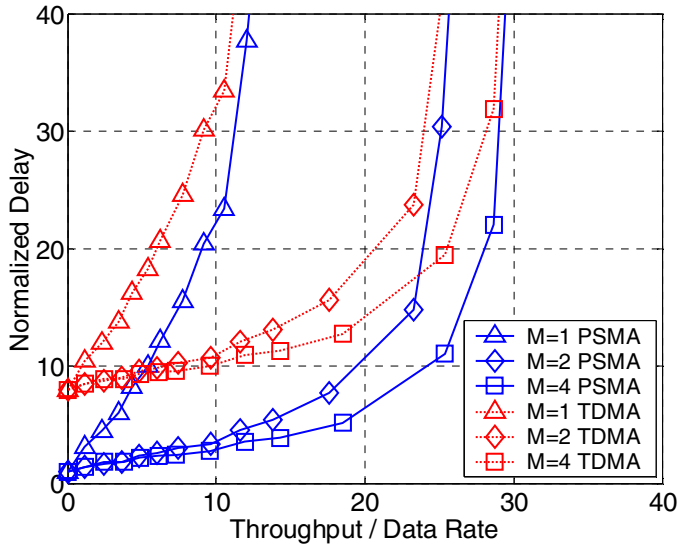

Figure 4.10: Normalized Delay for PSMA and TDMA.

4.6 Chapter Summary

Distributed protocols require some method of mitigating collisions to improve performance. However, the long synchronization time of I-UWB adds significant overhead to protocols such as CSMA/CA that use handshaking packets to avoid collisions. Therefore, this chapter investigates distributed MAC protocols custom tailored to both I-UWB and to ad hoc and sensor networks. We propose two multichannel MAC protocols for I-UWB: multichannel PSMA and multichannel ALOHA. The proposed protocols permit distributed, random access for large ad hoc and sensor networks.

At low pulse rates, the low duty cycle of I-UWB reduces the probability of collisions similarly to a multichannel MAC. In contrast to previous multichannel MAC protocols and to handshaking MAC protocols, the proposed MAC protocols improve performance without reducing link bandwidth, increasing delay, adding hardware complexity, or adding overhead.

INTEL-1010
U.S. Patent 9,265,043

In I-UWB, the probability of a collision depends on the PRI and the channel. Hence, it is important to treat I-UWB differently than narrowband systems, where simultaneous transmissions always result in collisions. We simulate the noise that concurrent transmissions add to a transmission of interest, and we find that several transmissions can coexist with no added noise if they arrive later than 5 RMS multipath spread delays beyond the transmission of interest. Transmissions that arrive closer in time to the transmission of interest may also allow concurrent transmissions, depending on the link distance and the exact time of arrival.

We find that the multichannel PSMA protocols outperforms multichannel ALOHA in terms of energy efficiency and throughput. A multi-user I-UWB receiver improves throughput and energy efficiency for both protocols with moderate additional hardware, but the number of supported users and the network traffic profile limits the improvement. The topology simulated in this chapter reaches at limit at $M = 4$ users for multichannel PSMA and $M = 8$ users for multichannel ALOHA. In addition, collisions become more likely in I-UWB for both protocols as the pulse rate increases, and I-UWB behaves more like a single channel narrowband system at high pulse rates.

INTEL-1010
U.S. Patent 9,265,043

Chapter 5: Busy Signal MAC for I-UWB

The medium access control (MAC) protocol and the radio play a crucial role in determining the energy dissipation and cost of ad hoc and sensor networks [70]. The radio dictates the energy efficiency and hardware complexity of the physical layer, and the MAC protocol implements the collision avoidance strategy. Collisions and corrupt packets waste energy when packets must be retransmitted. Collisions result from hidden terminals and correlated bursts of traffic. Harsh channel conditions, such as the inside of a ship's metal hull, also corrupt packets.

In narrowband systems, nodes rely on collision detection or collision avoidance to reduce the energy wasted on collisions. However, collision detection normally requires the hardware expense of a full-duplex transceiver operating in a two different frequency bands. Due to the tight constraints on cost and power, ad hoc and sensor nodes usually adopt a single transceiver approach. A single transceiver cannot assess the status of existing transmissions, so protocols such as CSMA/CA prevent collisions with handshaking packets. Collision avoidance requires only a single transceiver, but the handshaking packets add excessive overhead in I-UWB.

In the previous chapter, multichannel MAC protocols for I-UWB, improve throughput in ad hoc and sensor networks. However, the protocols treat the energy cost of collisions as a secondary concern. Nodes must a re-transmit an entire packet after a collision, and nodes do not know about the collision until transmitting the entire corrupted packet and receiving a negative acknowledgement.

This chapter proposes an I-UWB radio interface with a single transceiver and a companion MAC protocol that avoids both collisions and handshaking overhead. The MAC protocol, busy signal multiple access (BSMA), provides the immediate feedback of CSMA/CD or BTMA, but it avoids wasting energy on corrupt packets [82]. The unique signaling of I-UWB enables a MAC protocol with performance similar to full-duplex protocols like BTMA, but with only a single transceiver and a single band.

The proposed single transceiver leverages the inherently low duty cycle of an I-UWB pulse train to detect collisions and corrupted packets through transmission of a

INTEL-1010
U.S. Patent 9,265,043

busy signal. The busy signal eliminates handshaking packets such as request-to-send (RTS), clear-to-send (CTS), and acknowledgment (ACK), which add significant overhead from the long acquisition time of I-UWB [159]. Further, because I-UWB systems dissipate far less power transmitting than receiving, the transmission of a busy signal has insignificant impact on the power dissipated in a transaction [95]. The proposed BSMA MAC protocol permits random, distributed medium access with no central point of failure, so it is appropriate for any large ad hoc and sensor network.

This chapter is organized as follows. Section 5.1 describes methods of duplexing for traditional narrowband systems and for I-UWB. Section 5.2 explains the proposed system architecture, and Section 5.3 explains the BSMA MAC protocol. Section 5.4 establishes the design goals, and Section 5.6 presents simulation results.

5.1 Methods of Duplexing

To implement a busy signal MAC protocol, a transceiver must be capable of full duplex operation [194]. Narrowband radios implement full duplex operation with frequency division duplexing (FDD), which requires two transceivers in different frequency bands. Because this is expensive, narrowband systems usually implement half duplex operation with time domain duplexing (TDD), which requires handshaking overhead as in CSMA/CA. The proposed I-UWB duplexing requires only a single transceiver, and it achieves the performance of full duplex through a fine-grained half duplex. This is possible because an I-UWB signal is not continuously transmitted like a narrowband signal. The proposed I-UWB radio exploits the idle time between pulses to assess the state of its transmission.

Figure 5.1 compares TDD, FDD, and fine-grained half duplex with I-UWB. The TDD system in Figure 5.1 (a) cannot simultaneously transmit and receive, so it incurs penalties in latency and data rate. The TDD system also adds a small delay from the propagation time and from the turnaround time, or the time to switch from transmit mode to receive mode. This small delay is insignificant compared to the packet transmission time.

INTEL-1010
U.S. Patent 9,265,043

The FDD system in Figure 5.1 (b) can transmit and receive simultaneously. However, FDD requires an additional frequency band for the feedback channel, so it is inefficient in hardware complexity, power dissipation, and spectral usage. Further, it is difficult to obtain sufficient separation to prevent the two bands from interfering with each other.

The I-UWB system in Figure 5.1 (c) achieves full duplex operation without the latency or speed penalty of the TDD system and without the additional frequency band of the FDD system. An I-UWB system performs the following operations for the fine-grained half duplex. Starting in the receive mode, it receives a single pulse. Then, it switches from receive mode to transmit mode and transmits a pulse. After transmitting, it switches back to receive mode, and it is ready to receive the next pulse. The fine-grained half duplex of I-UWB switches between modes on a symbol level, whereas half duplex narrowband systems switch between modes at a packet level.

INTEL-1010
U.S. Patent 9,265,043

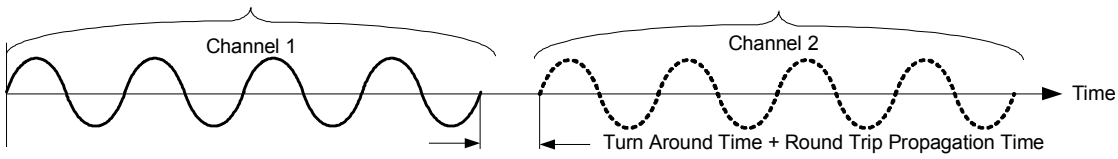

(a) Time Division Duplex

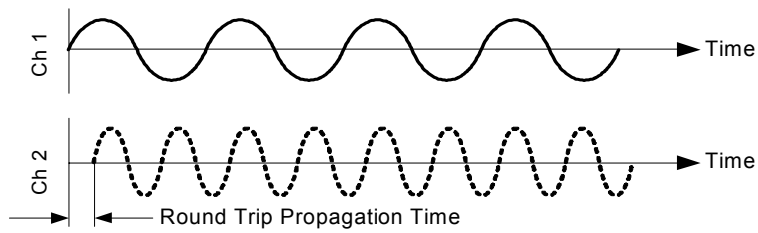

(b) Frequency Division Duplex

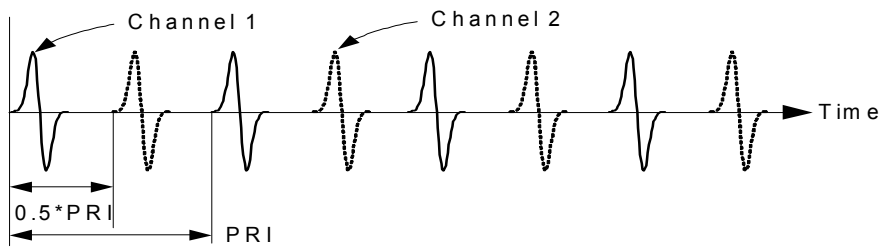

(c) Fine-Grained Time Division Half Duplex with I-UWB

Figure 5.1: Types of Duplexing

At the MAC level, the fine-grained half duplex appears to be full duplex. Ignoring the propagation time, the amount of duplexing D for a system can be measured as

$$D = N_{TxRx} / 2 * N_{Tx} \qquad (5.1) \quad ,$$

where

N_{Tx} – the total number of bits a transceiver can transmit at full speed over T_{packet}

N_{TxRx} – the total number of bits a transceiver can both transmit and receive over T_{packet}

INTEL-1010
U.S. Patent 9,265,043

Thus from (5.1), TDD has $D = 0.5$, FDD has $D \approx 1$, and fine grained half-duplex with I-UWB has $D \approx 1$. Assuming binary antipodal modulation with no spreading or coding, an I-UWB system with BPSK will then have the following parameters for a packet with N_{packet} bits.

$$N_{Tx} = N_{packet} \tag{5.2}$$

$$N_{TxRx} = (N_{packet} - 1) + N_{packet} = 2*N_{packet} - 1 \tag{5.3}$$

$$D_{I\text{-}UWB} = (2*N_{packet} - 1) / (2*N_{packet}) \approx 1,\ N_{packet} >> 1 \tag{5.4}$$

Typical values of N_{packet} are around several thousand bytes, so the I-UWB system performs practically as well as an FDD system. However, as seen in the next section, the I-UWB system is less complex in hardware than the narrowband FDD system.

The amount of duplexing also measures the energy wasted by a packet error. Note that packet errors may result from collisions, fading, or bit errors. For a half duplex system, the source node has no way of detecting a packet error until after the complete packet is sent. The loss ratio due to a collision is as follows.

$$LR = 1 - \left[2D - 1 - \left(\frac{2t_{prop} + t_{detect}}{t_{packet}} \right) \right] \tag{5.5}$$

where

t_{prop} (propagation time) = *Link Distance* / c

t_{detect} (detection time) = N_{detect} / *Rate*

t_{packet} (packet time) = N_{packet} / *Rate*

c = speed of light

N_{detect} = number of bits to detect an error

N_{packet} = number of bits in a packet

Rate = physical layer data rate

INTEL-1010
U.S. Patent 9,265,043

From (5.5), half duplex protocols have a high loss ratio that exceeds 100% due to the overhead to detect packet loss. The half duplex operation prevents the destination node from notifying the source node until the packet is completely sent. The energy required per transmission increases by the loss ratio multiplied by the probability of a packet loss. From (5.1) and (5.5), the high loss ratio of a half duplex system makes it especially unattractive in harsh channel conditions.

However, for full duplex and fine grained half duplex in I-UWB, the loss ratio is quite low because it depends mostly on the propagation time and the time to detect the loss. For example, consider a network where every node has a range of 10 m and a data rate of 1 Mbps. Then the maximum round trip propagation time is around 65 ns, the detection time is 7 μs, and a typical packet time is around 9 ms to result in a loss ratio of less than 1%.

In summary, I-UWB can operate similarly to full duplex, which is necessary for a busy signal MAC, without the overhead in hardware or throughput required of narrowband systems.

5.2 System Architecture

Narrowband radios implement full duplex operation with two transceivers in two different frequency bands. The proposed system requires a single transceiver because it leverages the fine-grained half duplex capability of I-UWB to interleave a busy signal with the data signal. The proposed I-UWB system saves hardware complexity and power dissipation because it requires only a single transceiver that operates in a single band. Figure 5.2 compares FDD architectures to the proposed fine-grained half duplex I-UWB architecture.

Figure 5.2 (a) shows a system architecture for narrowband FDD full duplex radios in ad hoc networks. Nodes cannot simultaneously receive and transmit in a single frequency band because this requires too large of a dynamic range. The transmitted signal energy is many orders of magnitude greater than the received signal, so any received signal would be lost. Further, an ad hoc network has no base station to

INTEL-1010
U.S. Patent 9,265,043

translate between frequency bands for inter-node communication. Therefore, each node must be able to receive and transmit in either band, depending if it is a source node or a destination node. The dual operation requires two transceivers and circulators for the two different frequency bands. The additional hardware results in a radio that consumes more than twice the power and incurs more than twice the cost of a single transceiver. The feedback channel also degrades spectral efficiency.

Figure 5.2 (b) shows a slightly more efficient method of achieving full duplex by inserting frequency nulls into the transmitted data signal [82]-[84]. The busy tone occupies a frequency null. Because the null frequencies are orthogonal to the transmitted signal, they create minimal interference. While the source node transmits data, it listens for the busy tone signal in the null bands of the transmitted signal. Conversely, the destination node receives data while transmitting a busy tone in the null bands of its matched filter. The system structure does not require two full transceivers for the data and the busy signal. However, non-linear effects of the channel and RF hardware will result in imperfect separation of the signals. In addition, the system still must separate the two channels with an echo canceller and circulator, and it requires transmit and receive hardware for each channel. The source node transceiver requires a full transmitter but only a tone detector; likewise the destination node transceiver requires a full receiver but only a tone generator. Further, a matched filter is necessary, and the echo canceller must also be trained. The feedback signal also interferes with clock recovery and uses a significant portion of bandwidth (the signal must be within 6 dB of the data signal, so assuming equal power it occupies at least 20% of the signal bandwidth with perfect isolation) to be detected reliably. In summary, the proposed architecture in [82]-[84] is slightly more efficient than full duplex, but the extra hardware cost is still significant, and performance can be improved.

Figure 5.2 (c) shows the proposed architecture for I-UWB with fine-grained half duplex. The low duty cycle allows a single transceiver to access a feedback channel in the same frequency band as the transmitted data. Because the data signal and the busy signal are in the same band, they share the same RF circuitry. The switching time between transmit and receive modes determines the minimum pulse repetition

INTEL-1010
U.S. Patent 9,265,043

interval. Instead of using a typical T/R switch, the system switches the disable inputs to the PA and the LNA. This scheme improves the switching time to 250 ps and avoids the additional insertion noise of a T/R switch [103],[104]. It also provides the necessary isolation in time, and there is very little leakage into the PA and LNA when they are disabled. The fine-grained half duplex I-UWB transceiver significantly reduces circuit cost and increases spectral efficiency as compared to a narrowband FDD transceiver.

INTEL-1010
U.S. Patent 9,265,043

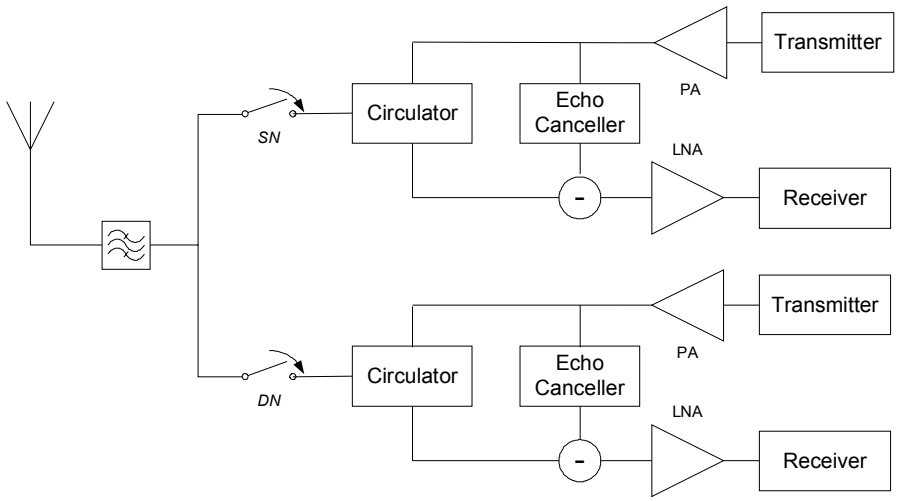

(a) Frequency Division Full Duplex

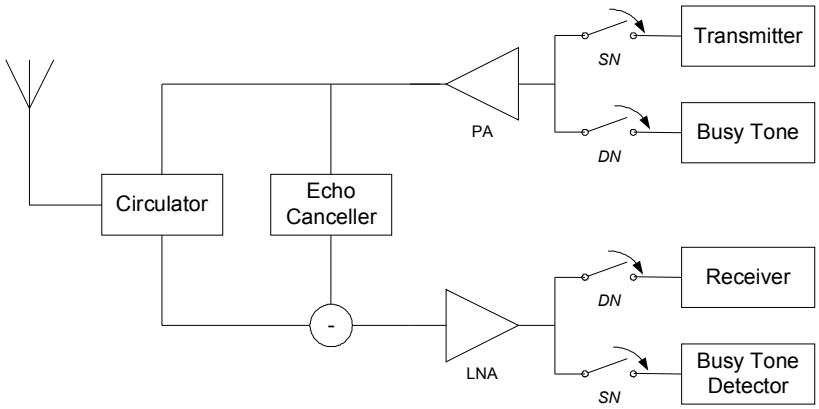

(b) Improved Frequency Division Duplex

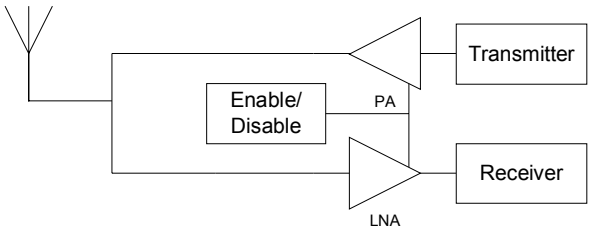

(c) Fine-Grained Time Domain Half Duplex with I-UWB

Figure 5.2: Full Duplex System Architectures for Ad Hoc Radios

INTEL-1010
U.S. Patent 9,265,043

5.3 Busy Signal Protocol

To manage collisions, MAC protocols for ad hoc and sensor networks normally time-multiplex handshaking packets with data packets as in CSMA/CA. For I-UWB, the overhead of the handshaking packets is significant [81]. A more efficient approach in terms of channel utilization is to provide feedback *during* data transmission. The proposed BSMA MAC protocol provides feedback through a busy signal with fine grained I-UWB half duplex operation. Figure 5.3 compares the overhead of CSMA/CA with that of BSMA. In Figure 5.3 (a), the longer acquisition time of UWB adds significant overhead to each of three handshaking packets. In Figure 5.3 (b), there is only one feedback signal, and it immediately informs the source node of a collision and also prevents collisions from hidden terminals. Thus, it performs the function of RTS, CTS and ACK packets without the acquisition overhead. Compared to CSMA/CA, BSMA reduces control traffic overhead, increases throughput, and more efficiently manages collisions.

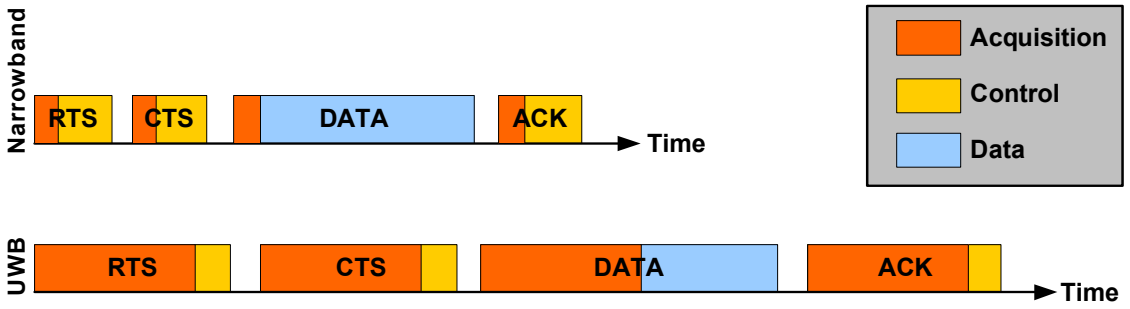

(a) CSMA/CA

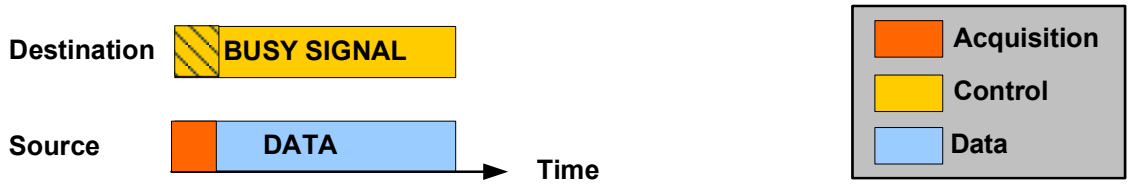

(b) BSMA

Figure 5.3: Handshaking Overhead in CSMA/CA and BSMA

INTEL-1010
U.S. Patent 9,265,043

A busy signal provides three services.

(1) It prevents nodes within range of the destination node from initiating a transmission.
(2) It informs the source node of a successful transmission.
(3) It requests the source node to terminate transmission of a corrupted packet.

The busy signal prevents hidden terminals without control packets such as RTS and CTS, so the protocol does not incur synchronization overhead or require inter-frame spacing between control transmissions. This increases throughput as compared to a handshaking protocol. In addition to providing collision avoidance, the busy signal also serves as a real-time acknowledgment. The busy signal immediately alerts the source node to a dropped packet or a collision, so the source node does not waste energy transmitting a corrupted packet.

The destination node asserts a busy signal throughout a successful transmission. The absence of this busy signal immediately informs the transmitter of a corrupted packet. The source node need only detect the presence or absence of a busy signal. It does not need to acquire and demodulate data from control packets as in handshaking protocols. In this sense, the protocol is similar to CSMA/CD.

We now review some varieties of BSMA supported by the system architecture in Figure 5.2 (c). The BSMA protocols all permit random, distributed medium access with no central point of failure, so they are appropriate for any large ad hoc and sensor network. The following varieties of BSMA leverage the low transmit power of I-UWB by transmitting the busy signal for the duration of the transaction, while the source node only periodically checks for a busy signal. As before, a node always checks for medium activity with pulse sense before transmitting. If a node detects a busy signal or a busy medium, it defers until after the current transmission. Collisions result in binary exponentially increasing backoff delays.

In basic BSMA, any node that detects a transmission emits a busy signal to prevent nodes within $2R$ range (where R is the transmit range of a node) of the source

INTEL-1010
U.S. Patent 9,265,043

node from transmitting. This eliminates hidden nodes but increases the number of exposed nodes [86].

In receiver initiated BSMA (RI-BSMA), the destination node emits a busy signal after it decodes its address. Therefore, the busy signal only prevents nodes within radius R of the destination from transmitting, resulting in no exposed nodes [85]. However, this results in a long vulnerable period before the address is decoded. A node (N_H) hidden from the source node (N_S) could start a transmission that interferes with the destination node (N_D) while N_D acquires the signal. The long acquisition time results in more possible collisions than basic BSMA. However, RI-BSMA provides more accurate information about corrupted packets because the destination node is the only node that can faithfully report this information.

A hybrid of RI-BSMA and BSMA combines the best features of both protocols [82]. During the preamble, all nodes within radius $2R$ of the source node emit a busy signal. After the destination node decodes its address, the other nodes terminate their busy signals, and only the destination node emits a busy signal. This allows exposed nodes to transmit as in RI-BSMA, but without the long vulnerable period. The protocol eliminates hidden nodes, improves spatial multiplexing, and also provides immediate feedback for corrupted packets.

5.4 Design Considerations

This section develops two important design goals to support a busy signal.

(1) The busy signal should not degrade data reception at the destination node.
(2) The busy signal should be easily detectable.

Self-interference complicates the above design goals. After the destination node transmits a busy signal, the multipath channel causes a long ring down time, and some of the reflected busy signal multipaths could interfere with data reception. Likewise, the source node may encounter self-interference from its data transmission while it

INTEL-1010
U.S. Patent 9,265,043

searches for a busy signal. Further, when multiple receivers emit a busy signal, the aggregate signal may interfere with data reception at the destination node and busy signal detection at the source node.

The phenomenon of *overlap* may also degrade performance [194]. Figure 5.4 illustrates the occurrence of overlap as link distance changes. At Time 1, the source node transmits a pulse, which arrives one propagation time, T_{prop}, later at the destination node at Time 2. At Time 3, the destination node sends a busy signal pulse exactly $0.5 \cdot PRI$ after the arrival of the first data pulse. Finally, at Time 4, the source node receives the busy signal pulse from the destination node.

In Figure 5.4 (a), the destination node is distance $d = c \cdot PRI$ meters (e.g., for a PRI of 100 ns, this distance is 30 meters) from the source node, so the round trip propagation time is $2 \cdot PRI$. Therefore, a busy signal pulse arrives exactly $2.5 \cdot PRI$ after the corresponding data pulse. In Figure 5.4 (b), the busy signal pulse overlaps the data transmission. The destination node is distance $d = 0.75 \cdot c \cdot PRI$ meters from the source node; the round trip propagation time is $1.5 \cdot PRI$; and the busy signal pulse arrives exactly $2 \cdot PRI$ after the corresponding data pulse. Because the source node is transmitting at the time, it loses some energy from the busy signal. Note that Figure 5.4 shows only the first multipath of a received pulse. In real-world situations, a receiver could detect a significant portion of the multipath energy.

INTEL-1010
U.S. Patent 9,265,043

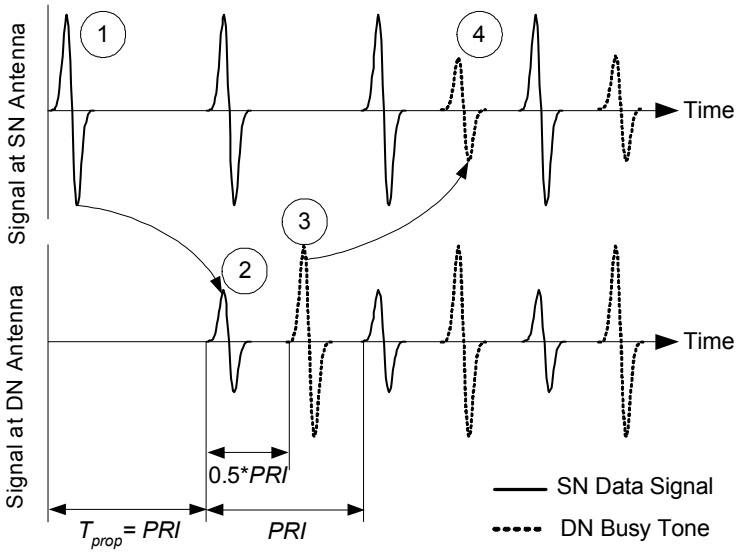

(a) Distance = *c***PRI*

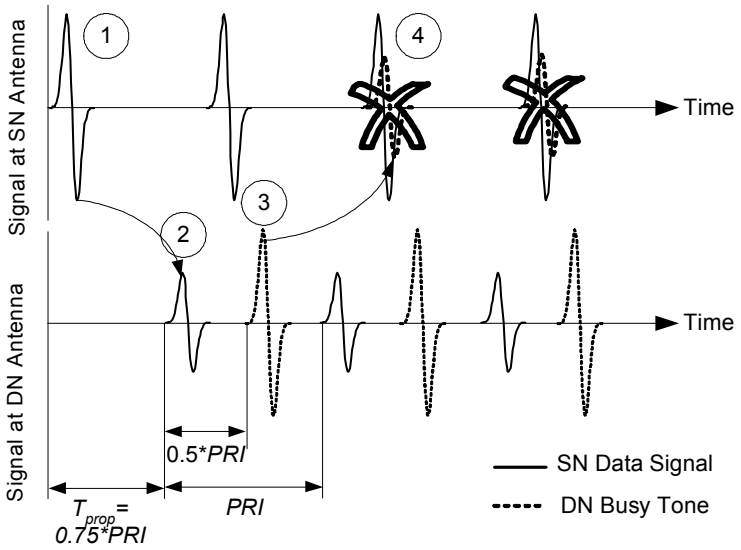

(b) Distance = 0.75**c***PRI*

Figure 5.4: Overlap Effect

Depending on the flight time, a busy signal pulse may overlap a data pulse at either the source node or the destination node. For clarity, we now assume the overlap occurs at the source node, and the destination node is free to transmit the busy signal so as to avoid overlap. Thus, depending on the link distance, a portion of the busy signal (including multipaths) may arrive while the source node transmits a data pulse.

INTEL-1010
U.S. Patent 9,265,043

In an AWGN channel without multipath effects, the occurrence of overlap is constrained to a certain range of link distances. AWGN analysis is useful to predict the efficacy of busy signal strategies, and simulations incorporate the full channel effects. In AWGN, the range of distances (d) where overlap occurs depends on the pulse width (T_p), the switching time (T_s), and the PRI. Overlap occurs if either

$$PRI - 0.5 \cdot T_p - T_s < (2 \cdot d / c + 0.5 \cdot PRI) \bmod PRI \quad (5.6) \quad \text{or}$$

$$(2 \cdot d / c + 0.5 \cdot PRI) \bmod PRI < 0.5 \cdot T_p + T_s \quad (5.7) \quad .$$

In a multipath channel, (5.6) and (5.7) change as follows for a multipath channel spread of T_c.

$$PRI - 0.5 \cdot T_p - T_s - T_c < (2 \cdot d / c + 0.5 \cdot PRI) \bmod PRI \quad (5.8)$$

$$(2 \cdot d / c + 0.5 \cdot PRI) \bmod PRI < 0.5 \cdot T_p + T_s + T_c \quad (5.9)$$

Although the multipath channel increases the probability of overlap, it also decreases the amount of energy lost through overlap. This is because a transmitter is active only for the pulse width and not the full multipath delay spread. Thus, the multipath channel actually helps the source node detect a busy signal. A receiver captures a proportion of energy $E_r(t)$ equal to energy contained in the set of multipaths R, that do not overlap with transmission, divided by the total energy contained in all multipaths.

$$E_r(t) = \frac{\sum_{i \in R} \beta_i}{\sum_{i=1}^{N_p} \beta_i} \quad (5.10)$$

The proportion of non-overlapping multipath energy can be significant, and usually ranges from 50% - 90% depending upon channel conditions. The next two

INTEL-1010
U.S. Patent 9,265,043

sections present design goals from the perspectives of the source node and the destination node, considering sources of interference.

5.4.1 Source Node

The goal of transceiver design from the source node perspective is to detect a busy signal while rejecting noise, other data transmissions, and its own self-interference from the received signal $R_{SN}(t)$.

$$R_{SN}(t) = x_{\hat{i}}(t) * \left[\sum_j b_j(t - t_{j,SN}) * h_{j,SN}(t) + \sum_k s_k(t - t_{k,SN}) * h_{k,SN}(t) + n(t) \right] + x_i(t) * s_{SN}(t - t_d) \quad (5.11)$$

where

$b_j(t)$ busy signal from node j, including destination node, $j \neq$ source node, $j \neq$ k

$h_{j,SN}(t)$ channel response node j to the source node

$x_i(t)$ impulse response of the switch in state $i \in$ (Rx, Tx) including ringing

$s_{SN}(t)$ data signal from the source node

t_d delay to the switch

$t_{j,SN}$ propagation delay from node j to the source node

$t_{k,SN}$ propagation delay from node k to the source node

$s_k(t)$ data transmission from node k, including source node, $k \neq$ destination node, $k \neq j$

$h_{k,SN}(t)$ channel response from node k to the source node

$n(t)$ the noise at the destination node receiver

The source may perform a sliding correlation with result

$$C_m = \int R_{SN}(t) \cdot b(t - t_m)\, dt \quad (5.12) \quad ,$$

INTEL-1010
U.S. Patent 9,265,043

where $t_m \in [0, PRI+T_p]$, and it is changing uniformly each PRI by $(PRI+T_p) / k$, with k the number of sliding correlations. To optimally detect a busy signal in noise, conditions (5.13), (5.14), and (5.15) should be true.

$$\int x_i(t) * s_{SN}(t - t_d) \cdot b(t - t_m)\, dt = 0 \qquad (5.13)$$

$$\int \left[x_{\hat{i}}(t) * \sum_k s_k(t) * h_{k,SN}(t) \right] \cdot b(t - t_m)\, dt = 0 \qquad (5.14)$$

$$\int x_{\hat{i}}(t) * \sum_j b_j(t) * h_{j,SN}(t) \cdot b(t - t_m)\, dt = C_{\max} \qquad (5.15)$$

Condition (5.13) is satisfied if either: (i) the data transmission does not overlap in time with the receiver operation or (ii) the switch can perfectly separate the transmitted pulse from the receiver chain. Because I-UWB signals are not continuous, they can satisfy condition (5.13) with one transceiver if they do not overlap in time the receiver operation. This is not possible in a narrowband system, which requires separation (likely through full duplex operation) of the received busy signal from the transmitted data pulses. Condition (5.14) requires data from other transmitters and multipaths from the source node data arrive at a different time than the busy signal at the source node. Because this is difficult to control, the busy signal should be separated from the data signal. This can be achieved with an orthogonal pulse shape or through spreading techniques such as direct sequence UWB (DS-UWB). Condition (5.15) means that the transceiver should capture as much busy signal energy as possible. Further, in the case of multiple busy signals, the multiple busy signals should not combine destructively with each other.

5.4.2 Destination Node

The goal of transceiver design from the destination node perspective is to demodulate the data signal, while rejecting noise, other busy signal transmissions, and self-interference from the received signal $R_{DN}(t)$.

INTEL-1010
U.S. Patent 9,265,043

$$R_{DN}(t) = x_{\hat{i}}(t) * \left[s_{SN}(t - t_{SN,DN}) * h_{SN,DN}(t) + \sum_j b_j(t - t_{j,DN}) * h_{j,DN}(t) + n(t) \right] + x_i(t) * b_{DN}(t - t_d) \quad (5.16)$$

where

$b_j(t)$	busy signal from node j, including destination node, $j \neq$ source node, within range of destination node
$b_{DN}(t)$	busy signal from the destination node
$h_{j,DN}(t)$	channel response from node j to the destination node
$x_i(t)$	impulse response of the switch in state $i \in$ (Rx, Tx) including ringing
$s_{SN}(t)$	data signal from the source node
t_d	delay to the switch
$t_{SN,DN}$	propagation delay from the source node to the destination node
$t_{j,DN}$	propagation delay from node j to the destination node
$h_{SN,DN}(t)$	channel response from the source node to the destination node
$n(t)$	the noise at the destination node receiver

Assuming coherent detection, the destination node performs the following correlation on the received signal, where s_n is the nth basis function of the signal set.

$$C_n = \int R_{DN}(t) \cdot s_n(t)\, dt \quad (5.17)$$

To optimally detect the data in noise, conditions (5.18), (5.19), and (5.20) should be true.

$$\int x_i(t) * b_{DN}(t - t_d) \cdot s_n(t)\, dt = 0 \quad (5.18)$$

$$\int \left[x_{\hat{i}}(t) * \sum_j b_j(t) * h_{j,DN}(t) \right] \cdot s_n(t)\, dt = 0 \quad (5.19)$$

$$\int x_{\hat{i}}(t) * s_{SN}(t) * h_{SN,DN}(t) \cdot s_n(t)\, dt = C_{\max} \quad (5.20)$$

INTEL-1010
U.S. Patent 9,265,043

To satisfy condition (5.18), the destination node's busy signal should not interfere with reception of the data signal. The low duty cycle of I-UWB satisfies this condition by allowing separation of the signals in time. Condition (5.19) requires the busy signal pulses from other nodes to not interfere with reception, so busy signal pulses should be separated from data pulses as for the source node. Condition (5.20) means that the transceiver should capture as much of the received data signal energy as accurately as possible.

Finally, a node that is neither the source nor the destination must accurately detect a busy signal. This situation is similar to that of a source node detecting a busy signal without overlap.

5.5 Design Approach

This section compares the performance of the following methods to meet the criteria in Section 5.4.

1) Use different PRIs for the data signal and the busy signal. If $PRI_{data\ signal}$ is $n*PRI_{busy\ signal}$, for an integer n, then the source node can detect either n or n-1 busy signal pulses, each having an energy of $1/n$ of the data signal. Alternately, if $PRI_{busy\ signal}$ is slightly less than the $PRI_{data\ signal}$, then the pulses will only overlap at some small beat frequency [194].
2) Use different waveforms for the data signal and the busy signal, e.g. DS-UWB and I-UWB. Also, orthogonal pulse shapes can differentiate the busy signal from the data, e.g. a Gaussian monopulse and the first derivative of a Gaussian monopulse are orthogonal. The transmitter can generate both of these pulses with no modifications.
3) Rely on multipath effects to detect the busy signal. The multipath spread of an I-UWB signal can be quite significant compared to the pulse length. The source receiver is disabled during transmission, but energy from busy signal multipaths arrives for a period much longer than the data pulse width.

INTEL-1010
U.S. Patent 9,265,043

4) Estimate and equalize the channel. A destination node can estimate and subtract its own busy signal reflections and the busy signal of other nodes from the received data. A source node can also estimate the reflections from its own data, but this is slightly more complicated in hardware due to the modulation. In either case, the hardware complexity is much simpler than equalization of unknown data.
5) Use a PRI at least twice the maximum propagation time (R_{max}/c) plus twice the multipath delay spread ($D_{multipath}$). After receiving a data pulse, the destination node waits for a period of time equal to the multipath delay spread before transmitting a busy signal pulse. Likewise, after detecting a busy signal pulse, the source node waits for a multipath delay spread before transmitting data. If the PRI is such that $PRI \geq 2 \cdot (R_{max}/c + D_{multipath})$, then the system avoids interference. For example, a range R_{max} of 10 m and multipath delay spread $D_{multipath}$ of 200 ns results in a minimum PRI of 466 ns. The maximum pulse rate becomes 2.14 Mpps.

To show the feasibility of the proposed I-UWB transceiver for a busy signal protocol, we compare the above methods from the perspective of a source node and the perspective of a destination node. For simulation, the network topology is random with multihop connections. Each node has an average of about six neighbors with a maximum link distance of 10 m. The channel model is based on the Cassioli channel model for indoor UWB propagation [110], and it considers statistical variations in small scale and large scale fading and shadowing. Each transaction results in a different, random instance of the channel model and the topology. The average of 100 simulations results in each data point. The source node performance is measured by the probability of false alarm (P_{FA}) versus the probability of detecting the busy signal (P_D). The destination node performance is measured by the noise that the busy signal adds to the received data signal. Table 5.1 describes the signals used in simulation.

INTEL-1010
U.S. Patent 9,265,043

Table 5.1: Signals Used in the Simulations

Name	Description
Data	The data signal. BPSK modulation. Uncoded.
1 Pulse	A busy signal with the same PRI and energy as the data signal.
Divided PRI	A busy signal. Each pulse has $1/n^{th}$ the energy and $1/n^{th}$ PRI of a data pulse.
2 Pulses	*Divided PRI* busy signal with n=2.
4 Pulses	*Divided PRI* busy signal with n=4.
Different PRI	A busy signal. Each pulse has the same energy as a data pulse, but the PRI is 99.5% of the data signal PRI to result in a beat frequency of 200/PRI.
DS-UWB	A busy signal with spreading factor = *SF*. Each pulse has 1/*SF* the energy of a data pulse. The chips are transmitted back to back and each bit is separated by the PRI of the data signal.
8 DS-UWB	*DS-UWB* with *SF*=8.
16 DS-UWB	*DS-UWB* with *SF*=16.
32 DS-UWB	*DS-UWB* with *SF*=32.

5.5.1 Source Node Results

To show the accuracy of the proposed system in detecting a busy signal without constraining the PRI (as in Method 5), the probability of detection versus the probability of false alarm is plotted for a data rate of 100 Mbps under various conditions of interference. Assuming an 11 dB noise figure at the receiver, the destination node adjusts the busy signal power so that the strongest received multipath has a maximum SNR of 4 dB. This is the maximum SNR allowed at a 10 m link distance under the FCC limits. In real networks, better performance may be achieved with multiple "looks," lower data rates, and shorter distances. The figures are meant to compare the relative performance of the different methods.

For the ideal case of Method 5, Figure 5.5 (a) shows the performance of the busy signal detection with the line labeled *Clear Channel*, which serves as a reference line in the remaining graphs. The other lines show the performance for a busy signal

INTEL-1010
U.S. Patent 9,265,043

that arrives with 3 dB less power than the data signal reflections. Additionally, there is no overlap in Figure 5.5. This situation also corresponds to that of an idle node.

Figure 5.5 (a) does not include the *Different PRI* busy signal because it is guaranteed to overlap the transmission periodically. The best performing busy signal is the *4 Pulse* because it spreads four pulses evenly over the PRI. In the worst case, only one pulse out of four experiences severe interference. The *2 Pulse* busy signal performs next best, as it also spreads its pulses over the PRI; but now half the pulses may experience severe interference. Next, the *DS-UWB* signals (all spreading factors performed similarly) perform almost as well as the *2 Pulse* and *4 Pulse* signals because the spreading code combats interference from the data signal reflections. However, because the chips are sent consecutively, the data signal interferes with all the chips when it does interfere. Hence, the *DS-UWB* performance is not as good a *2 Pulse* or *4 Pulse*. Finally, the *1 Pulse* busy signal performs the worst because it has no method to combat interference. All busy signals result in little performance degradation as compared to the ideal case because the receiver only needs to detect the presence of a busy signal.

Nonlinear effects from the antenna, channel, and RF circuitry may cause the busy signal and the data signal to lose orthogonality. Figure 5.5 (b) shows that performance degradation is still mild even when the data signal and the busy signal have identical pulse shapes.

Finally, Figure 5.5 (c) shows the simulated the performance of each busy signal when the receiver estimates its self-interference from the data signal and equalizes it. The hardware complexity increases but the performance is indistinguishable from the ideal *Clear Channel* case as shown in Figure 5.5 (c).

INTEL-1010
U.S. Patent 9,265,043

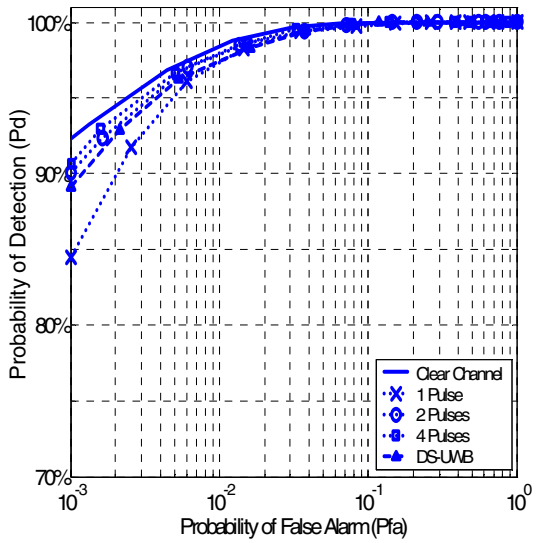

(a) Data Signal Orthogonal to Busy Signal, No Equalization

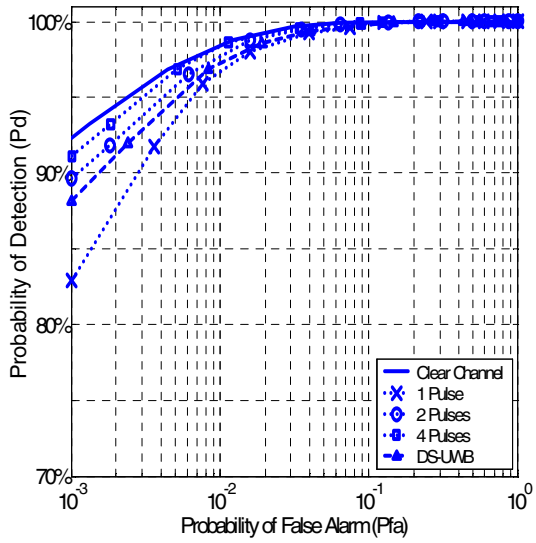

(b) Data Signal Non-Orthogonal to Busy Signal, No Equalization

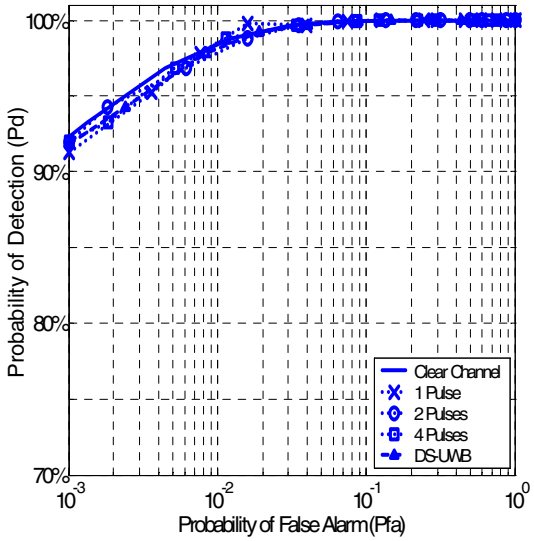

(c) Data Signal Orthogonal to Busy Signal, Equalization

Figure 5.5: P_D versus P_{FA} for Busy Signals with Interference

INTEL-1010
U.S. Patent 9,265,043

Figure 5.6 shows the analytical performance of each busy signal in an AWGN channel. These analytical performance evaluations give a general idea of the performance of each technique in Table 5.1 under the worst case conditions of the busy signal completely overlapping the data transmission. Compared to a multipath channel, the AWGN channel includes factors that both degrade and improve performance. First, the busy signal will have no multipath reflections. Hence, a channel model with multipath reflections should improve performance because not all of the reflections will overlap the transmission. However, the data signal will also lack multipath reflections. Therefore, a channel model with multipath reflections will degrade performance since the reflections act as interference.

In the AWGN channel, the performance depends only upon the busy signal energy that the source node can capture. The destination node transmits signal s_1 for a busy signal and signal s_0 otherwise. The receiver uses the correlation in (5.12) to decide whether the busy signal is present, where the received signal is r and the threshold voltage is V_t. The probability of false alarm and probability of detection are evaluated numerically in Matlab.

$$P_{fa} = P(\mathrm{r} = \mathrm{s}_1 \mid \mathrm{s}_0) = \int_{-\infty}^{V_t} p(\mathrm{r} = \mathrm{s}_1 \mid \mathrm{s}_0) \quad (5.21)$$

$$P_d = P(\mathrm{r} = \mathrm{s}_1 \mid \mathrm{s}_1) = \int_{V_t}^{\infty} p(\mathrm{r} = \mathrm{s}_1 \mid \mathrm{s}_1) \quad (5.22)$$

The *Different PRI* busy signal performs best because it overlaps the data signal transmission only periodically. The next best signal is the *32 DS-UWB* because the source node receiver loses a maximum of 1/32nd of energy due to overlap. The *16 DS-UWB* signal loses a maximum of 1/16th of its energy due to overlap, and so on down to the *2 Pulse* signal, which loses up to half of its energy. The *1 Pulse* signal is undetectable because all of its energy arrives during data transmission. Hence, higher spreading gain improves performance under the conditions of overlap.

INTEL-1010
U.S. Patent 9,265,043

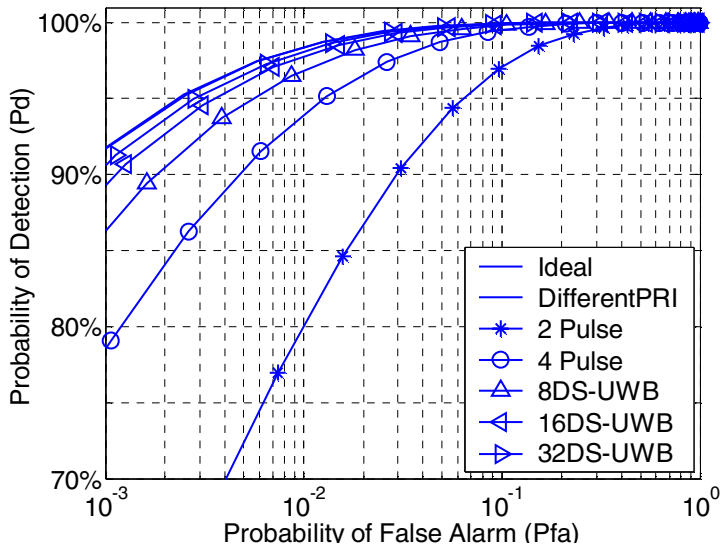

Figure 5.6: Calculated P_D versus P_{FA} Busy Signal with Overlap in AWGN Channel.

Figure 5.7 shows the performance of each busy signal when the strongest multipaths overlap the data signal transmission. The overlap consists of a 1 ns transmission, two 0.25 ns T/R switches, and an additional 0.5 ns of settling time for a total of 2 ns. The busy signal arrives with 3 dB less power than the data signal reflections, and the overlap causes an average loss of about 10% of the total busy signal energy.

Figure 5.7 (a) shows the performance without channel estimation and equalization. The *Different PRI* busy signal performs best in these conditions because it overlaps the data signal transmission only periodically. The next best signal is the *32 DS-UWB* signal because the spreading code is long, and the source node receiver loses a smaller portion of energy due to overlap. The *16 DS-UWB* signal loses twice as much energy as compared to the *32 DS-UWB* signal, and the *8 DS-UWB* signal loses four times as much energy. Hence, higher spreading gain improves performance under the conditions of overlap. The *4 Pulse* busy signal performs similarly to *32 DS-UWB* because it spreads four pulses evenly over the data PRI. The receiver loses energy from only one the pulses due to overlap. The *2 Pulse* busy signal suffers more degradation than the *4 Pulse* case because the overlapped pulse loses twice as much energy. Finally,

INTEL-1010
U.S. Patent 9,265,043

the *1 Pulse* busy signal performs the worst because it has no method to offset the effects of overlap. The *Different PRI*, *Divided PRI* with larger *n,* and the *DS-UWB* with larger *SF* result in mild performance degradation as compared to the ideal *Clear Channel* case. The spreading combats the effects of overlap.

Figure 5.7 (b) displays the performance of each busy signal when the receiver estimates its self-reflected channel and equalizes the interference. As compared to Figure 5.7 (a), the performance improves slightly at the cost of increased hardware complexity and power. The performance gain is limited because the busy signal that overlaps with data transmission is unrecoverable.

INTEL-1010
U.S. Patent 9,265,043

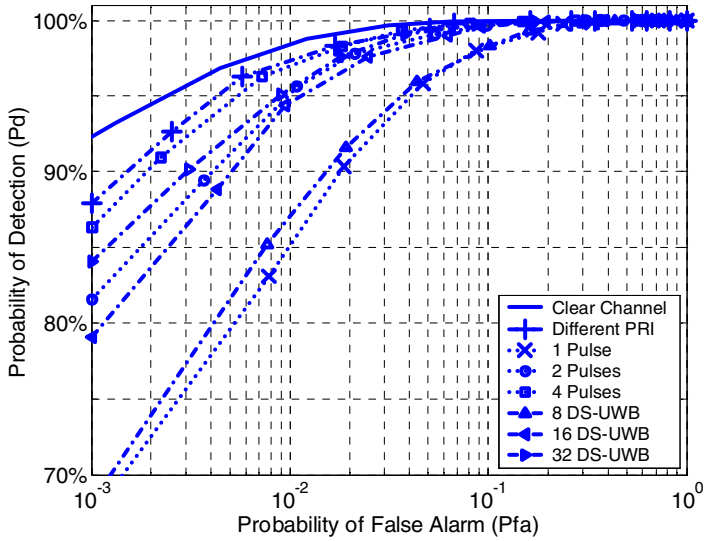

(a) No Equalization

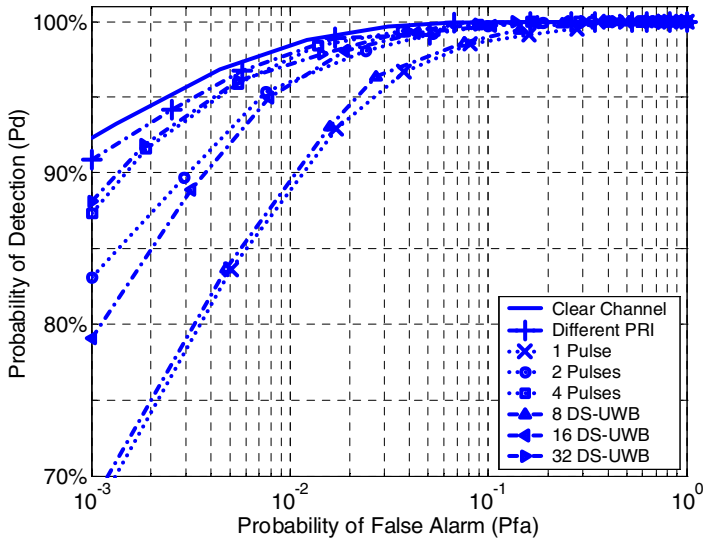

(b) Equalization

Figure 5.7: P_D versus P_{FA} for Orthogonal Busy Signals with Interference and Overlap

Figure 5.8 shows the performance when multiple nodes emit busy signals. Six of the source's neighbors emit the same type of busy signal, and they are uniformly distributed around the source node. The busy signals interfere with each other, and they may combine destructively or constructively. The received busy signal also overlaps

INTEL-1010
U.S. Patent 9,265,043

the data transmission and is corrupted by the data signal multipaths. The total interference results in a busy signal to interference ratio of –7 dB, and the overlap loss averages about 10% of busy signal energy.

The performance of the *Different PRI* busy signal is worse than the single busy signal case because all of the busy signals experience overlap and interference periodically. The *4 Pulse* and *2 Pulse* busy signals improve performance as compared to the single busy signal. Additional energy from one of the other busy signals may experience more favorable channel conditions. The *1 Pulse* busy signal improves performance the most as compared to a single busy signal. The pulses appear in a narrower time window and are less likely to combine destructively. Of the *DS-UWB* signals, the best performing signal is the *32 DS-UWB* busy signal because the spreading code is long, and it combats both overlap and destructive combination. The *Different PRI*, *Divided PRI* with larger *n*, and the *DS-UWB* with larger *SF* all combat the interference from multiple busy signals.

For DS-UWB, the spreading code should be chosen to minimize autocorrelation because since the busy signals may overlap and combine destructively. Figure 5.8 shows simulation results in which an *m*-sequence code is used. Figure 5.8 also shows the performance degradation for *32 DS-UWB* with a random, rather than an *m*-sequence code. Without orthogonal sequences, degradation increases for longer codes, as busy tones are more likely to overlap.

INTEL-1010
U.S. Patent 9,265,043

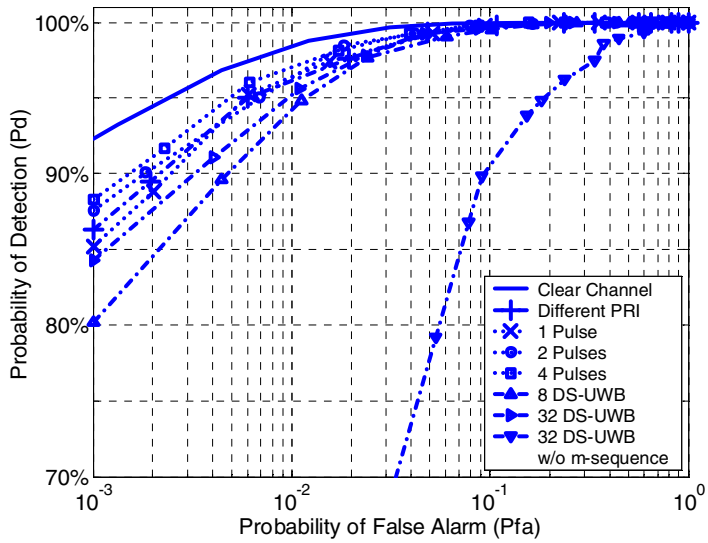

Figure 5.8: P_D versus P_{FA} for Multiple Busy Signals

5.5.2 Destination Node Results

This section presents simulation results for the busy signals in Table 5.1 to determine their impact on data reception as the PRI decreases. Each simulation considers three representative topologies that result in SINRs of 3 dB, 0 dB, and -3 dB as the link distance changes in relation to the distance the reflection travels. The results report the noise that each busy signal adds to data reception, and the effect on BER will depend on various factors including link distance, receiver type, and coding. For reference, in the worst case 10 m link distance, 1 dB of noise increases the BER from 2×10^{-4} to 8×10^{-4}, and 0.5 dB of noise increases the BER to 3×10^{-4}.

Figure 5.9 shows the noise that each busy signal adds to the data signal for the three topologies. The *Different PRI* busy signal performs the worst because its pulses are guaranteed to periodically occur close in time to the beginning of a receive cycle. The *1 Pulse* busy signal results in the least additional noise because it transmits all busy signal energy immediately after a receive cycle (recall the destination node is free to transmit so as to minimize interference from overlap and interference to itself), thus

INTEL-1010
U.S. Patent 9,265,043

allowing the most ring down time before the next receive cycle. The *2 Pulse* busy signal performs slightly worse than the *1 Pulse* case for short PRI because the reduced power of the second pulse does not offset the fact that it appears closer to the beginning of the next receive cycle. Finally *8 DS-UWB* performs similarly to *1 Pulse* because it is also transmitted immediately following a receive cycle. All busy signals add noise to the received signal at short PRIs, so a designer may need to adjust the PRI to meet link budget constraints.

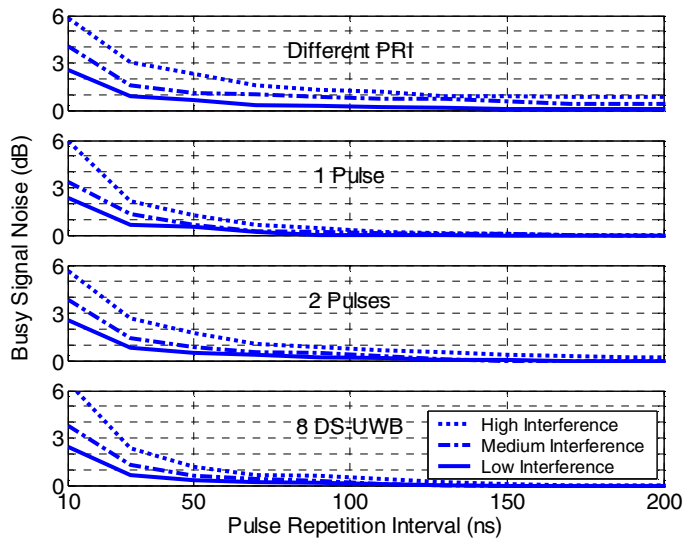

Figure 5.9: Busy Signal Noise for Different Levels of Interference

Figure 5.10 shows the effect of increasing the spreading factor for both *Divided PRI* and *DS-UWB*. The *Divided PRI* signal adds noise as the number of pulses *n* increases. Although the signal power decreases with increasing *n*, more busy signal energy occurs near the beginning of the next receive cycle. The *DS-UWB* signal does not incur as much noise penalty as compared to the *1 Pulse* case for any spreading factor. This is because the destination node transmits the chips of the *DS-UWB* busy signal immediately after the receive cycle, so it contributes less interference to the next receive cycle.

INTEL-1010
U.S. Patent 9,265,043

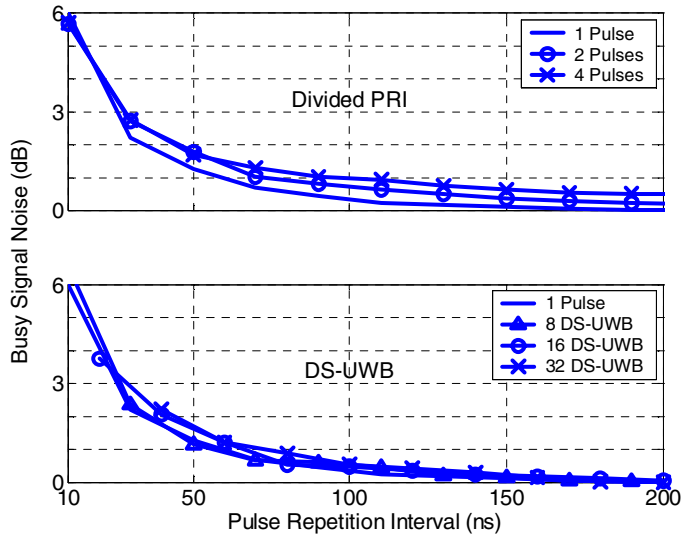

Figure 5.10: Busy Signal Noise for Different Spreading Factors

Because the antenna, channel, and transceiver front-end may introduce non-linear effects into the received signal, the busy signal and data signal pulses may lose orthogonality. Figure 5.11 shows the simulation results for a busy signal pulse shape that is identical to the data pulse shape under the highest level of self-interference. The *Different PRI* busy signal adds from 0.5 dB to 1 dB of noise. The *1 Pulse* busy signal adds noise at shorter PRIs because longer PRIs allow the multipath reflections to ring down. The *2 Pulses* busy signal adds slightly more noise than the *1 Pulse* busy signal due to the closer proximity of the second busy signal pulse to the beginning of the next receive cycle. Finally, the *8 DS-UWB* signal incurs negligible additional interference due to the spreading gain. In all cases, the effects of non-orthogonal signals are moderate, and the total energy in the channel has a greater impact on performance.

INTEL-1010
U.S. Patent 9,265,043

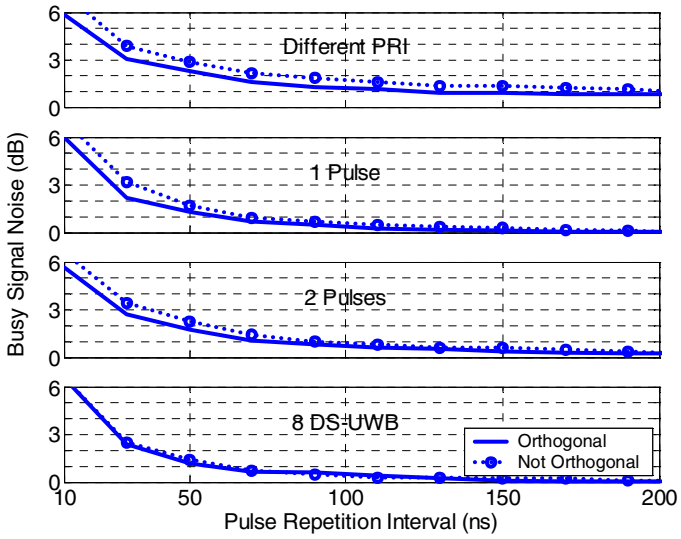

Figure 5.11: Busy Signal Noise for Different Pulse Shapes

Figure 5.12 shows the effects of multiple nodes emitting a busy signal. Six neighbors are situated around the destination node with a uniform, random distribution of distances. The six nodes each emit the same type of busy signal. Each graph compares a single busy signal with low self-interference to multiple busy signals with low self-interference. For all cases, the multiple busy signals add significantly more noise than a single busy signal. This is because the destination node cannot control the time at which it receives the busy signals from other nodes. For the three cases of *Different PRI*, *1 Pulse*, and *2 Pulses*, the loss of orthogonality is more significant than the case with just one node. However, the *DS-UWB* busy signal still performs as well as the orthogonal case.

INTEL-1010
U.S. Patent 9,265,043

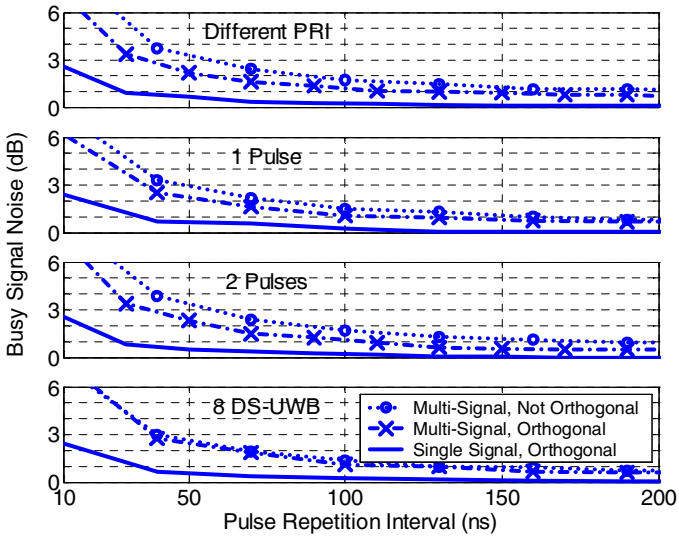

Figure 5.12: Busy Signal Noise for Different Busy Signal Protocols

Finally, for busy signals, the estimation and equalization process is relatively simple because the busy signal is known and it never changes. The simulation uses 8-bit quantization of seven frequency domain samples. Equalization dramatically reduces noise at shorter PRIs but adds small quantization noise at longer PRIs. Figure 5.13 shows that the quantization noise averages about 0.2 dB for both single and multiple busy tones. The channel estimation scheme improves performance at the expense of additional hardware and power.

INTEL-1010
U.S. Patent 9,265,043

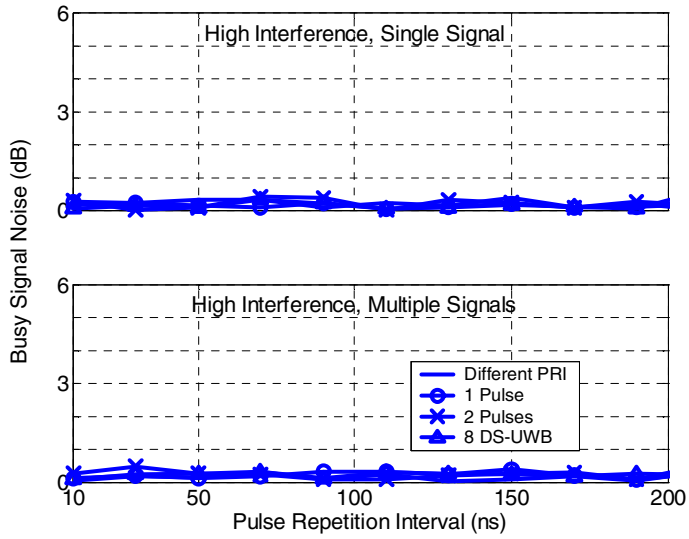

Figure 5.13: Busy Signal Noise with Equalization Scheme

We apply the above results to network level simulations. A data signal is corrupted if the busy signal reflections add enough noise to reduce the link budget below the safety margin. The probability of detecting a busy signal is taken from curves in Section 5.5.1.

5.6 Network Results

We characterize the network level performance through the same metrics as in Chapter 4, throughput, delay, and energy efficiency. To review, the throughput is defined as sum of the rates (bps) of traffic the Physical Layer offers to the MAC Layer of each destination node. The delay is defined as the average time a successful packet spends between the source MAC Layer and destination MAC Layer. The energy efficiency is defined as the energy expended for a successful transmission divided by the total energy expended for all transmitted and received packets, including dropped packets and collisions. The energy includes all energy dissipated in the Physical Layer. Note that, unlike narrowband systems, the baseband processing energy of I-UWB

INTEL-1010
U.S. Patent 9,265,043

systems is comparable to the transmission energy. These quantities are plotted against the offered load, which is defined as the sum of the rates (bps) of traffic that the Network Layer offers to the Link Layer over all nodes.

The I-UWB Physical Layer, channel model, and MAC protocols are implemented as custom blocks in ns-2. Table 5.2 describes the simulation environment.

Table 5.2: Simulation Environment

Topology	Grid of 225 stationary nodes. Maximum of 12 neighbors.
Packet Format	4095 byte packets with format from [21]. The header is approximately 900 bits.
Traffic	Poisson traffic with a random source and a random destination.
Pulse Rate	1 Mpps - 100 Mpps. 1 bit per pulse.
Channel Model	CM4 channel model with 25 ns RMS delay spread [109]. Channel may vary between packets but not during a packet.
Receiver	No equalization. Receiver behaves according results in Chapter 3, Chapter 4, and Section 5.4.

Figure 5.14 compares the throughput of multichannel PSMA, multichannel PSMA with collision avoidance (PSMA/CA), multichannel ALOHA, BSMA, and TDMA at 1 Mpps. The number of users is $M = 1$ except for TDMA, which is inherently $M = 8$. In TDMA, an omniscient central controller perfectly schedules time slots for exclusive channel access and spatial multiplexing. In an actual network, the centralized control and single point of failure would be undesirable, so we implement TDMA as a baseline reference system.

We briefly describe the operation of PSMA/CA below, as it has not been explained previously. Narrowband systems resolve most hidden terminal conditions by implementing CSMA with collision avoidance (CSMA/CA). Like narrowband CSMA, PSMA for I-UWB can also be augmented with collision avoidance in the form of CTS and RTS packets. PSMA/CA takes a more conservative approach than either multichannel PSMA or multichannel ALOHA, and it prevents most hidden terminal collisions. Because I-UWB requires a relatively longer acquisition time than narrowband systems, the RTS and CTS packets add greater overhead than in

INTEL-1010
U.S. Patent 9,265,043

narrowband systems [159]. Therefore, PSMA/CA may not be practical for most systems.

Like multichannel ALOHA and multichannel PSMA, PSMA/CA also allows for a time-interleaved multi-channel approach. However, RTS packets comprise the vast majority of time-interleaved packets because the virtual CCA usually prevents nodes from transmitting during the CTS, data, and ACK packets. The transmission of RTS packets occurs similarly to multichannel PSMA data packets. The source node first performs CCA to determine the status of the medium, and it transmits the RTS packet if the medium is free. Note that two RTS packets can be corrupted by simultaneous transmissions or a hidden terminal condition – the same two conditions that corrupt packets for multichannel PSMA.

If two concurrent RTS packets do not collide, they can still cause corruption of the subsequent CTS, data, or ACK packets because these packets are not synchronized with respect to each other. Different link distances and packet sizes cause further de-synchronization of the subsequent packets. If the RTS packets target the same destination node, then the destination node must choose and respond to a single RTS. If the RTS packets are directed to different destination nodes, then the CTS packets collide if they overlap at either of the source nodes. If the CTS packets do not overlap, the data packets may still overlap at either of the destination nodes. Finally, the ACK packets may also overlap at either of the source nodes. Note the above events are relatively rare because virtual CCA and pulse sense prevent most concurrent transmissions.

In Figure 5.14, the multichannel PSMA system attains the highest throughput. It outperforms TDMA, BSMA, and PSMA/CA because it allows channel interleaving; and it outperforms multichannel ALOHA because it checks for a busy medium before transmitting.

BSMA performs the next best. The random scheduling achieves a throughput almost as high as the centralized TDMA system. The performance of BSMA is due to its collision avoidance properties and its efficient handling of collisions when they do occur.

INTEL-1010
U.S. Patent 9,265,043

Next, PSMA/CA performs worse than BSMA due to the handshaking packets, which add significant acquisition overhead. PSMA/CA performs worse than multichannel PSMA because most transmissions do not have the benefit of channel interleaving. Further, the virtual CCA prevents transmissions that may not result in collisions, so it allows far less spatial multiplexing. However, unlike multichannel ALOHA, PSMA/CA remains stable at high offered loads. Multichannel ALOHA performs similarly to PSMA/CA at low offered loads, but it results in too many collisions at high offered load.

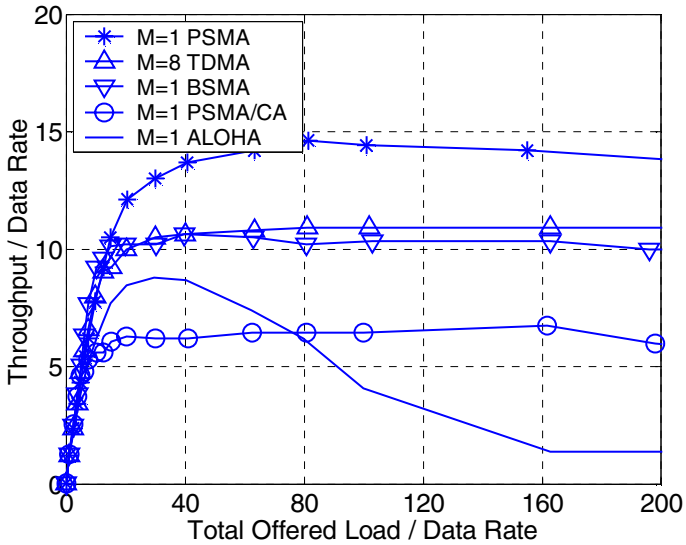

Figure 5.14: Throughput for PSMA, PSMA/CA, ALOHA, BSMA, and TDMA.

Figure 5.15 compares the energy efficiency of multichannel PSMA, PSMA/CA, multichannel ALOHA, BSMA, and TDMA at 1 Mpps. From the perspective of energy efficiency, the protocols rank much differently than from the perspective of throughput.

BSMA is the most energy efficient distributed protocol. It outperforms PSMA/CA because RTS packets are still vulnerable to collisions. RTS packets may directly collide with data packets, and they may also indirectly cause collisions by interfering with control packets and corrupting the virtual carrier sense of affected nodes. BSMA outperforms multichannel ALOHA and multichannel PSMA because neither of them have mechanisms to detect or avoid collisions.

INTEL-1010
U.S. Patent 9,265,043

Multichannel PSMA/CA attains the second highest energy efficiency because the handshaking packets avoid most collisions. The multichannel PSMA system has poor energy efficiency because it has no mechanism to avoid collisions. Multichannel ALOHA performs the worst since it does not check for channel activity before transmitting. At high offered load, the energy efficiency is close to 0% because most transmissions collide with each other. Multichannel ALOHA and multichannel PSMA have a single-user receiver, so some transmissions that arrive uncorrupted may be dropped due to a busy receiver. However, even with multi-user receivers, the energy efficiency is still worse than either PSMA/CA or BSMA.

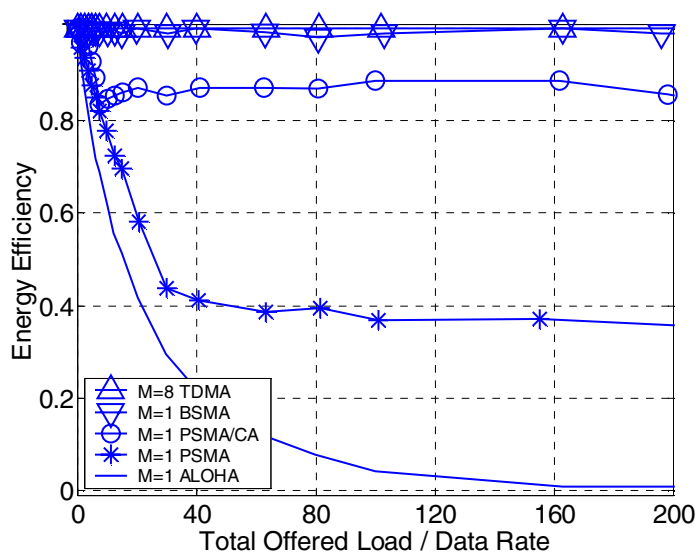

Figure 5.15: Energy efficiency for PSMA, PSMA/CA, ALOHA, BSMA, and TDMA.

5.7 Chapter Summary

For ad hoc and sensor networks, the MAC protocol and the radio play a crucial role in determining both the node cost and the amount of energy spent on a successful transmission. Therefore, this chapter investigates a bust signal MAC protocol, which is specifically tailored to improve energy efficiency in I-UWB ad hoc and sensor networks. Whereas narrowband systems require two transceivers to implement a busy

INTEL-1010
U.S. Patent 9,265,043

signal MAC protocol, the proposed I-UWB system requires only a single transceiver to save cost, power, and circuit complexity. A busy signal MAC provides performance similar to CSMA/CD, which is efficient in throughput, delay, and energy per successful transmission [82]. The busy signal MAC provides superior performance because nodes can assess the status of ongoing transmissions. It also permits random, distributed medium access with no central point of failure, so it is appropriate for any large ad hoc or sensor network.

The single transceiver leverages the inherently low duty cycle of an I-UWB pulse train to detect collisions and corrupted packets through a busy signal. The busy signal avoids the overhead of time-duplexed control packets, as in PSMA/CA. The system finely multiplexes the busy signal channel with the data channel to re-use the same frequency band and radio front end. Further, I-UWB systems dissipate far less power transmitting than receiving, so the busy signal does not significantly increase power.

Simulations show that the busy signal is easily detectable and does not interfere with data reception. At the cost of lower data rate, the simplest and most effective method of implementing the busy signal is to require a PRI that is long enough to avoid any interference. At shorter PRIs, the simulations find that channel equalization at both the source node and the destination node provides comparable performance to the ideal case at the cost of moderate additional hardware. To implement the busy signal without increased hardware complexity, an orthogonal *DS-UWB* signal with a high spreading gain incurs only a slight degradation of BER at the destination node, and it is easily detected at the source node. In addition, the transmitter in Figure 2.19 is capable of transmitting orthogonal pulse shapes to further separate the data signal from the busy signal. Finally, the multipath delay spread actually helps the source node detect busy signals in the event of overlap.

At the network level, we compared the proposed BSMA protocol to three distributed MAC protocols for I-UWB: multichannel ALOHA, multichannel PSMA, and PSMA/CA. Additionally, we compared BSMA to a baseline, centralized TDMA protocol. For an ad hoc network environment, none of the distributed protocols significantly complicates hardware, adds control traffic overhead, or has a central point

INTEL-1010
U.S. Patent 9,265,043

of failure. However, the throughput and energy efficiency characteristics of these protocols are different than their narrowband counterparts because of the unique nature of I-UWB signaling. In terms of energy efficiency, BSMA outperforms all other distributed MAC protocols for I-UWB. Hence, it is a suitable protocol for energy-sensitive sensor networks. In terms of throughput and delay, BSMA performs as well as centralized TDMA.

INTEL-1010
U.S. Patent 9,265,043

Chapter 6: Cross Layer Adaptation

I-UWB is an attractive technology for applications such as ad hoc and sensor networks, and it offers flexibility in many dimensions. If an I-UWB radio adapts various parameters, its performance may also change, and some configurations may be optimal under certain channel conditions. As channel conditions change dynamically, an application may want to optimize a specific performance metric. For example, data rate may be traded to maintain a link in harsh channel conditions [21]. The effects of adapting many Physical Layer parameters unique to I-UWB, such as modulation or pulse shape, are unexplored. Further, these parameters are relatively easy to adapt, and they may affect upper layers. Thus, this chapter proposes an adaptive I-UWB Physical Layer, which is less complex in hardware than a traditional narrowband adaptive system [195], to meet constraints set by ad hoc and sensor network applications.

Depending on the specific application and type of data, a communications system must meet various quality of service (QoS) constraints – e.g., bit error rate (BER), data rate, or energy dissipation – at different times. For example, a sensor network may require a low BER for control data [87], a high data rate for real-time data [88], or minimal energy dissipation for regular updates [89]. Typical communications systems are built to meet these QoS constraints even under the worst channel conditions. However, a communications system operates in the worst conditions infrequently, so it wastes valuable resources as a result. Existing approaches to meet QoS requirements in ad hoc and sensor networks focus on the medium access control (MAC) layer and above, but these optimizations are often application dependant [196],[197]. With a general interface to the Application Layer, an adaptive I-UWB radio can meet such QoS requirements in the Physical Layer for any application.

The adaptive I-UWB system is motivated by the characteristics of m-ary pulse position modulation (PPM), which is a common modulation scheme for I-UWB [198]. With m-ary PPM modulation, a UWB system can easily adapt its pulse repetition interval (PRI) and/or the number of bits per symbol ($\log_2 m$). Digital control circuitry

INTEL-1010
U.S. Patent 9,265,043

can easily provide the discrete delays required by *m*-ary PPM. This chapter defines a PPM modulation scheme as a combination of a PRI and an *m*. Thus, the modulation scheme will affect the data rate and the required E_b/N_0 ratio – where E_b is the bit energy and N_0 is the noise level – to meet a BER target. Channel conditions vary depending on the transmitter-receiver distance and the level of interference, and QoS constraints change depending on the type of data. We explore the effects of adapting the modulation scheme under various channel conditions to meet QoS criteria. The goal is to improve overall BER, energy efficiency, and data rate.

The chapter is organized as follows. Section 6.1 introduces the adaptive resource allocation strategy, and Section 6.2 explains the system architecture that implements the adaptive resource allocation. Section 6.3 describes a specific the PPM modulation scheme that is suitable for an I-UWB adaptive system. Section 6.4 presents simulation results in terms of data rate, energy, and bit error rate. Section 6.5 concludes the chapter.

6.1 Adaptive Resource Allocation

Under the conditions of dynamic traffic, unpredictable signal propagation, and frequent network topology changes, traditional communications systems with fixed resources are inadequate to efficiently meet variable QoS requirements. A non-adaptive system provides resources to meet the worst channel conditions and most demanding QoS requirements at all times, so it wastes resources.

The resource allocation procedure in Figure 6.1 proposes a method to efficiently meet QoS requirements by dynamically configuring an I-UWB radio. The first step in the resource allocation procedure examines the current QoS requirements, the current resources of each node, and the current channel conditions. The second step identifies a suitable system configuration to meet the current requirements, resources, and channel conditions through a cost function. The third step allocates available resources to achieve the desired QoS.

INTEL-1010
U.S. Patent 9,265,043

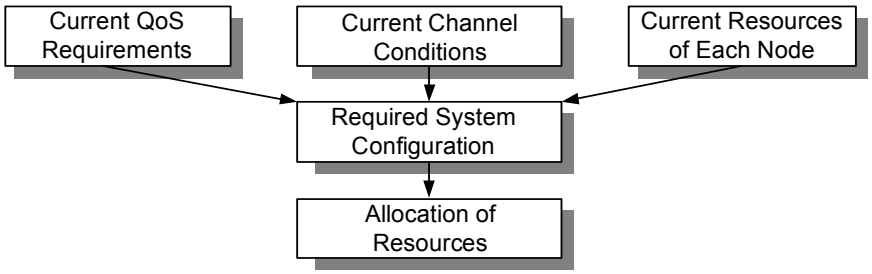

Figure 6.1: Proposed Approach for Resource Allocation

For the first step, the Physical Layer, Application Layer, and MAC Layer share the current QoS requirements, resources, and channel conditions with each other via the *adaptive configuration block* (ACB) in Figure 6.2. In this chapter, the QoS requirements include data rate, BER, and energy dissipation; the channel conditions include link distance and level of interference; and the resources are the possible values of PRI and *m*. Note that QoS requirements, resources, and channel conditions can include many more parameters, and the above parameters are representative for the I-UWB system. This information is short relative to the length of a data packet, and the source node sends the information during the configuration period of a transaction. For a MAC protocol with handshaking such as PSMA/CA, the source node includes this information in a request to send (RTS) message, which are transmitted with a common modulation scheme. In a protocol such as BSMA or multichannel PSMA, the source node includes this information in a header that is sent with a common modulation scheme. For TDMA protocols such as IEEE 802.15.3, the source node sends the information to the piconet coordinator (PNC) while requesting a time slot.

In the second step, the destination node selects the optimal modulation scheme, so the systems must have *a priori* knowledge of the characteristics of each possible configuration. This necessitates characterizing quantitative relationships among the modulation schemes, the data rate, the channel conditions, and the E_b/N_o required to meet a target BER. A cost function then allocates the appropriate resources. System

INTEL-1010
U.S. Patent 9,265,043

characterization and resource allocation are the focuses of this paper, and they are discussed in detail in Section 6.3.

In the third step, systems must allocate resources for the appropriate modulation scheme. The destination node configures its modulation scheme after notifying the source node of the chosen modulation scheme. For PSMA/CA, the source node extracts the suggested modulation scheme from a CTS packet, which is sent with a common modulation scheme. In TDMA, the central coordinator informs the source node of the modulation scheme. The proposed BSMA protocol encodes the modulation scheme onto the busy signal. The multichannel PSMA protocol piggybacks the chosen modulation scheme onto every ACK packet, so that only the first transaction between two nodes is sent with a common modulation scheme.

Note that nodes transmit control packets with a common modulation scheme. However, nodes transmit data with the most efficient modulation scheme that is supported. As channel conditions change, a transmitter and a receiver must determine an appropriate method to reallocate their resources. Periodic updates result in no improvement if no data is sent between updates. Updates prior to every transaction can incur large overhead if the system topology and environmental conditions change slowly with respect to the transaction rate. For simulation, a system changes its configuration only when it has data to send. Each new allocation should exist long enough to offset any overhead from the reallocation algorithm.

INTEL-1010
U.S. Patent 9,265,043

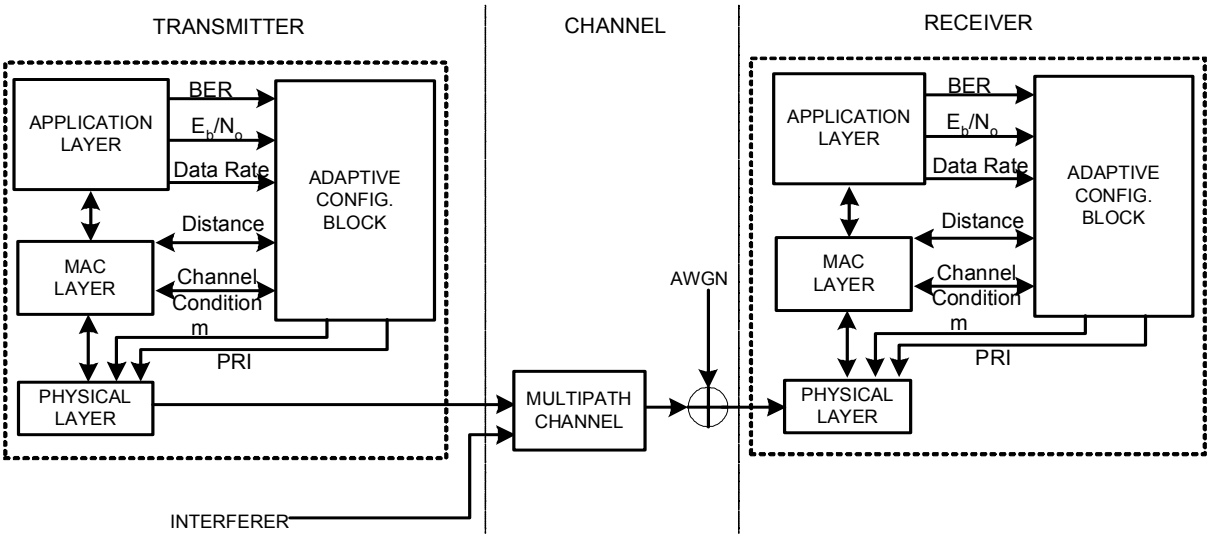

Figure 6.2: Block Diagram of Adaptive I-UWB System

6.2 Adaptive System Architecture

Each adaptive system consists of a Physical Layer (transmitter and receiver), MAC layer, Application Layer, and ACB as shown in Figure 6.2. Other network layers that do not interact with the ACB are omitted from the figure. Note that Figure 6.2 modifies the ISO/OSI network model to include communication between non-adjacent layers. This is a departure from established network design techniques, but it is well suited to the unique characteristics of I-UWB. Although the inter-layer communication complicates the design process, it meets the special demands of ad hoc and sensor networks far better than traditional single-layer techniques [2].

In the Physical Layer, the transmitter is the energy efficient pulse generator of Figure 2.19 [102]. The transmitter modulates an input bit stream into a train of Gaussian monopulses with center frequency of 6.85 GHz and a bandwidth of 7.5 GHz. Energy outside the 3.1 GHz to 10.6 GHz range is attenuated with a bandpass filter to meet the FCC mask. We now briefly review PPM, and a PPM pulse train is described as

INTEL-1010
U.S. Patent 9,265,043

$$s(t)=\sum_{i=-\infty}^{\infty} Ap\left(t-iT_f-\delta d_i(t)\right) \quad (6.1) \quad ,$$

where $d_i(t)$ shifts the pulse in time by some multiple δ, which is larger than the pulse width to assure an orthogonal signal set. Note that for PPM, a single pulse can represent multiple bits or chips. If there are m time slots, then the signal may represent $\log_2 m$ chips or bits. It is possible for δ to be less than the pulse width and still obtain an orthogonal signal set, but this imposes impractical timing requirements on transceivers [107],[108]. The function $p(t)$ is a Gaussian monocycle pulse, A is the amplitude of the pulse, and the parameter T_f is the duration of the PRI or the inverse of the symbol rate. The system uses m different non-overlapping pulse positions. The combination of m and T_f constitute a modulation scheme, which the ACB adjusts based on the environmental conditions and QoS requirements.

Using the energy efficient pulse generator of Figure 2.19 [102] and the receiver in Figure 2.20 [100],[101], PPM is particularly suited to an adaptive system. In the transmitter, the various m-ary modulation schemes and PRI values are easily changed through a programmable delay unit in digital logic. Thus, the generator can generate different m-ary modulation schemes and different PRI values with no architectural modifications.

The performance of a basic correlation receiver is rather poor, because the total energy is spread over the multipaths, and the first multipath contains relatively little energy compared with the total energy. The frequency domain receiver in Figure 2.20 receiver performs much better because it harvests the energy dispersed over the multipaths [100],[101]. Compared to a conventional rake receiver, the proposed energy harvester reduces power dissipation, captures more energy, and requires simpler hardware. Because the receiver collects frequency domain samples, the circuit complexity is independent of the number of multipaths and modulation type. Further, the receiver demodulates PPM data based on the phase of the frequency components, so it will not incur greater implementation complexity for larger values of m. To adjust to different values of T_f, the receiver need only adjust the reference timing of the timing recovery circuit. Finally, the sampling rate, which may be programmable, is based only

INTEL-1010
U.S. Patent 9,265,043

on the PRI, so it is provides efficient implementation of a wide range of modulation schemes.

The channel model includes AWGN, multipath effects, and also sources of co-channel interference. The multipath model is the Cassioli indoor UWB channel model [110], which considers large-scale and small-scale effects. Multipath effects may last up to 300 ns, although, on average, over 92% of energy is dissipated after 100 ns. The channel is slow fading, so changes occur on a packet level.

Note that techniques such as coding and spreading would achieve better performance in a practical system, but they are omitted from the model to focus on the effects of the adaptive modulation scheme.

The MAC layer can be any of PSMA/CA, TDMA, multichannel PSMA, or BSMA. In relation to the adaptive scheme, the function of the MAC protocol is inter-node communication of the current conditions, resources, and, QoS requirements. It communicates these directly to and from the Physical Layer as header information. The MAC is also responsible for tracking such Physical Layer conditions as channel conditions and link distances [56]. The MAC layer provides these parameters to the ACB.

The Application Layer provides pre-defined QoS constraints depending on the specific data type. For example, control data may require the lowest possible BER because it is typically not resilient to errors. An example of control data is a microcode update to patch system operation or to change the function of a node. Real time data may require the highest possible data rate. Consider an intruder detection network, which will sacrifice energy (future operating time) and accept a margin of error in order to track a current threat. Alternatively, when that intruder detection network monitors normal system activity, it would desire to save energy to track a future intruder. In such a situation, the error rate and data rate could be sacrificed to operate with minimal energy dissipation. Still other applications may desire a trade-off that results in a compromise between data rate, BER, and energy dissipation.

The ACB block provides a standard interface for the above blocks to communicate. It gathers the channel, QoS, and resource information. Based on that information, it calculates the cost function and determines the most appropriate

INTEL-1010
U.S. Patent 9,265,043

modulation scheme. The ACB is also responsible for informing other layers of its decision.

6.3 Adaptive Modulation Scheme

The overall strategy for choosing a modulation scheme is motivated by the behavior of PPM in different environmental conditions. This section characterizes some of this behavior.

For an I-UWB system with PPM, several types of interference are possible. Co-channel interference occurs in a network when the target system captures the intended signal while one or more additional I-UWB systems transmit simultaneously. Inter-symbol interference (ISI) is such that a delayed multipath from the previous symbol interferes with the current symbol. In contrast, intra-symbol interference may cause a multipath from a current symbol to provide a higher correlation than the first multipath, which causes misinterpretation of the current symbol. ISI increases as PRI decreases, while the effects of intra-symbol interference and co-channel interference increase as *m* increases [198]. Thus, configurations with high *m* and a short PRI are more susceptible to interference, which eventually limits the performance regardless of the E_b/N_0. In contrast, configurations with low *m* and a long PRI are less susceptible to interference, and therefore the performance is more limited by the E_b/N_0 ratio. Therefore, for low E_b/N_0 ratios, modulation schemes with high *m* are preferable. However, for higher E_b/N_0 ratios, the interference dominates the noise, and modulation schemes with low values of *m* are preferable.

The *local cost function,* β, defines the cost of a transaction.

$$\beta = \frac{(\alpha \cdot BER) \cdot (\beta \cdot E_b / N_0)}{(\chi \cdot Data\ Rate)} \quad (6.2)$$

In the local function, each performance parameter includes a weighting function that shows the relative contribution of BER, energy, and data rate to the overall cost. In

INTEL-1010
U.S. Patent 9,265,043

(6.2), α is the weighting function of the BER, β is the weighting function of the energy, and χ is the weighting function of the data rate. The BER is a function *W* of *m*, *PRI*, E_b/N_0, channel impulse response *h(x)*, and interference *i(x)*. The E_b/N_0 is a function *Y* of the transmitter-receiver distance, the channel impulse response, and the maximum radiated energy allowed by the FCC for a given data rate. The data rate depends only on the PRI and *m*.

$$BER = W\left(E_b/N_0, PRI, m, h(x), i(x)\right) \quad (6.3)$$

$$E_b/N_0 = Y\left(dist, m, PRI, h(x)\right) \quad (6.4)$$

$$Data\,Rate = (\log_2 m)/PRI \quad (6.5)$$

Thus, from (6.2) - (6.5), $\beta(z)$ defines the local cost function, where *z* is a set of environmental and QoS 6-tuples **[E_b/N_0, *m*, *PRI*, *h(x)*, *i(x)*, *dist*]** within ***Z***, the set of all possible 6-tuples.

$$\beta(z) = \frac{\chi}{\alpha\beta} \cdot \frac{PRI \cdot W\left(E_b/N_0, PRI, m, h(x), i(x)\right) \cdot Y\left(dist, m, PRI, h(x)\right)}{\log_2 m} \quad (6.6)$$

When environmental conditions vary over several transactions, the local cost function is described in terms of the *local expected cost function*

$$\overline{\beta} = \sum_{\forall z \in Z} \beta(z) \cdot p(z) \quad (6.7)$$

where *p(z)* is the probability distribution of z $\in$ Z, and *p(z)* is determined from observation. The adaptive system chooses a modulation scheme by optimizing the local expected cost function[2]. A configuration is said to be optimal if it costs less than any other possible configuration for the given environmental and QoS parameters.

[2] Note that there is also a global cost function, which is defined as the sum of all local cost functions in the network. This calculation leads to overall network optimization, but it requires a centralized knowledge of all transactions. The local cost function is a distributed calculation that can be computed locally at each node, so it is more suitable for ad hoc and sensor networks.

INTEL-1010
U.S. Patent 9,265,043

Numerical gradient-based optimization techniques can be used to minimize or maximize the cost function. However, gradient calculations can be costly for implementation, and hence, calculation may consume more resources than it saves. To reduce implementation complexity, the nodes use linear approximations to choose the optimal modulation scheme for the current operating conditions.

Next, the cost function is considered from the perspective of three likely scenarios that ad hoc and sensor nodes may encounter.

6.3.1 Minimum BER

Networks update microcode to provide patches or to change a node's function on the fly. The microcode must be transmitted error free and may traverse several hops, thus increasing the probability of error. Therefore, the nodes involved in the transfer attempt to minimize the cost function by minimizing BER with an appropriate modulation scheme. FCC limitations constrain the radiated power level, and the network sets an acceptable data rate.

Figure 6.3 plots BER versus E_b/N_0 for different *m*-ary PPM modulation schemes for a constant data rate of 25 Mbps and the maximum radiated power allowed by the FCC. The different modulation schemes operate at different PRIs to maintain the data rate. The 2-ary PPM operates at a PRI of 40 ns, 4-ary at 80 ns, 8-ary at 120 ns, 16-ary at 160 ns, and 32-ary at 200 ns.

INTEL-1010
U.S. Patent 9,265,043

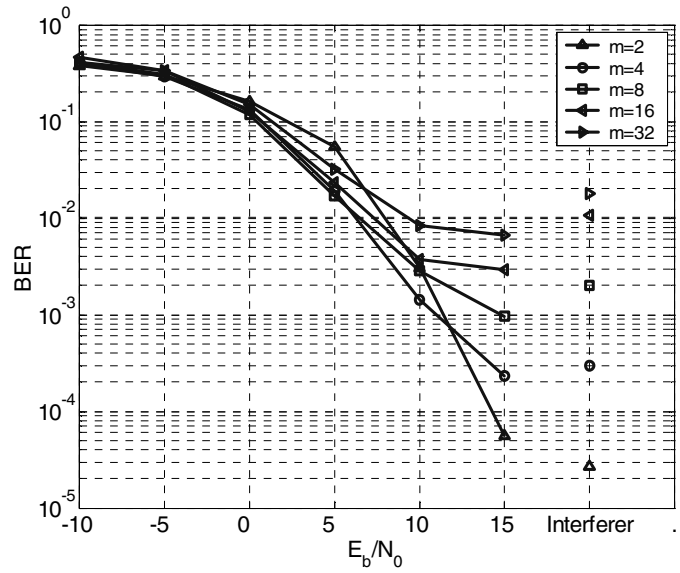

Figure 6.3: BER versus E_b/N_0 at a Data Rate of 25 Mbps

As the hop distance changes, the E_b/N_0 also changes. For all *m*-ary modulation schemes, the BER decreases as E_b/N_0 increases, but the rate of BER decrease depends on the modulation scheme. For the case marked "Interferer," the source of errors is co-channel interference with an S/I ratio of 0 dB. Depending on the received power level and the level of interference, each ACB pair chooses the modulation scheme that minimizes BER. This minimizes the cost function for a microcode update, which prioritizes BER over energy or data rate. From Figure 6.3, the ACB would choose 8-ary PPM for E_b/N_0 = 5 dB, 4-ary PPM for E_b/N_0 = 10 dB or 2-ary PPM for strong interference. Note that different modulation schemes are the best choice for different environmental conditions. A fixed modulation scheme would only be optimal at one distance.

6.3.2 Maximum Data Rate

Next, when an intruder detection network detects activity, throughput has priority over BER and energy. If the network reports video data, some predefined minimum BER results in acceptable video quality. The radiated power will be the

INTEL-1010
U.S. Patent 9,265,043

maximum allowed under FCC limits. Therefore, depending on the channel condition, the ACB chooses a system configuration to maximize data rate for a target BER and given E_b/N_0. For this type of application, maximizing data rate minimizes the cost function.

Figure 6.4 shows the maximum data rate possible at each E_b/N_0 compared to a non-adaptive system operating at a data rate of 25 Mbps. When E_b/N_0 = 5 dB, 8-ary PPM provides the highest data rate of 100 Mbps and meets the target BER. When conditions change to E_b/N_0 = 15 dB, the ACB chooses 4-ary PPM to provide the highest rate of 68 Mbps. A non-adaptive system is forced to maintain a 25 Mbps data rate to meet the minimum BER in all channel conditions.

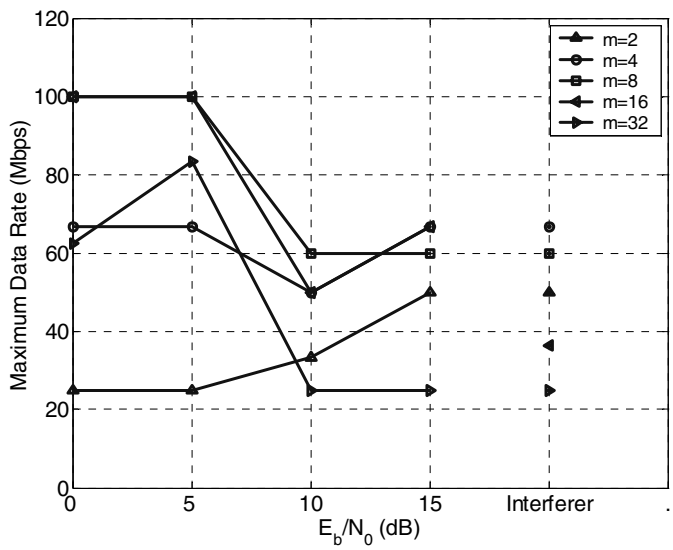

Figure 6.4: Maximum Data Rate versus E_b/N_0

6.3.3 Minimum Energy

For energy-constrained ad hoc and sensor networks, minimizing the transmitted energy per bit is of significant interest. During routine operation, such networks often adjust their radiated energy to meet only the minimum QoS requirements. The ACB

INTEL-1010
U.S. Patent 9,265,043

further reduces energy consumption by choosing the modulation scheme that meets the QoS requirements with minimum energy per bit.

Figure 6.5 shows the energy required in each configuration for two different QoS scenarios. First, when the target BER is 5×10^{-3} and the data rate is 33 Mbps (QoS1), the 4-ary PPM scheme requires the minimum E_b to meet the QoS requirements. Likewise, if the QoS requirements change such that the target BER is 2×10^{-2} and the data rate is 80 Mbps (QoS2), then the ACB switches to 16-ary PPM. In general, for low BER and data rates, the ACB chooses lower order *m*-ary PPM schemes. For higher BER and data rates, the ACB chooses higher order *m*-ary PPM schemes.

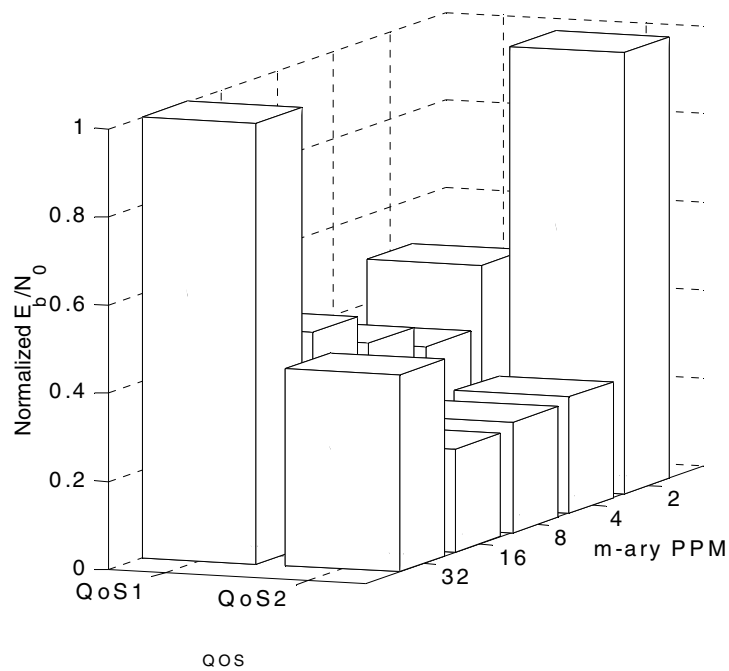

Figure 6.5: Energy per Bit for Various QoS Requirements

For all of the above goals (minimum BER, maximum data rate, and minimum energy), there is no single modulation scheme that performs best in all environmental conditions. Further, a node may change its goal changes, for example, from minimum BER to minimum energy in the event it is sensor node that just completed transmitting a microcode update. In this case, no single modulation scheme performs best for different QoS goals.

INTEL-1010
U.S. Patent 9,265,043

6.4 Simulation Results

The adaptive I-UWB system in Figure 6.2 is modeled in ADS (Advanced Design System) and compared to a non-adaptive I-UWB system for varying channel conditions and QoS goals. The simulations consider five different values of *m,* which are 2, 4, 8, 16, and 32 with a PRI that ranges from 10 to 210 ns.

The first case is a microcode transaction that requires the minimum BER, has a fixed data rate, and radiates the maximum allowed E_b. The distances of each transaction determine the E_b/N_0 such that it varies from 0 dB to 15 dB in integer steps, and the distribution is shown in (6.8).

$$p(E_b/N_0) = \begin{cases} 0.0625, & 0dB \le E_b/N_0 \le 15dB \\ 0, & else \end{cases} \quad (6.8)$$

Also, an interferer randomly interferes with the received signal, and it causes the S/I ratio to be 0 dB 10% of the time. The channel impulse response is a random instance of the Cassioli model for each transaction, and the ACB considers *m* and *PRI* values that result in the minimum BER without regard without unacceptably high energy dissipation or unacceptably low data rate.

Table 6.1 and Figure 6.6 compare the costs of five non-adaptive systems to the costs of an adaptive system for a data rate of 50 Mbps and a data rate of 5 Mbps. The costs are given in (6.7), and the non-adaptive systems cannot change *m* or *PRI* to reduce the cost. The last column shows the decrease in BER of the adaptive system compared to that of the worst performing non-adaptive system. The adaptive system always performs better than the best performing non-adaptive system at a given data rate, and it can approximately halve BER (or cost) as compared to 2-ary PPM. The adaptive system performs even better if the data rate changes dynamically. This is because the adaptive system chooses the configuration with minimum BER, whereas the non-adaptive system always meets the BER for the worst case.

INTEL-1010
U.S. Patent 9,265,043

Table 6.1: BER of Non-adaptive versus Adaptive System

Data Rate (Mbps)	Non-Adaptive System BER					Adaptive System BER	Percentage Decrease in BER
	m=2	**m=4**	**m=8**	**m=16**	**m=32**		
50	0.0474	0.0310	0.0303	0.0289	0.0355	0.0263	44.7%
25	0.0418	0.0239	0.0233	0.0252	0.0322	0.0212	49.3%

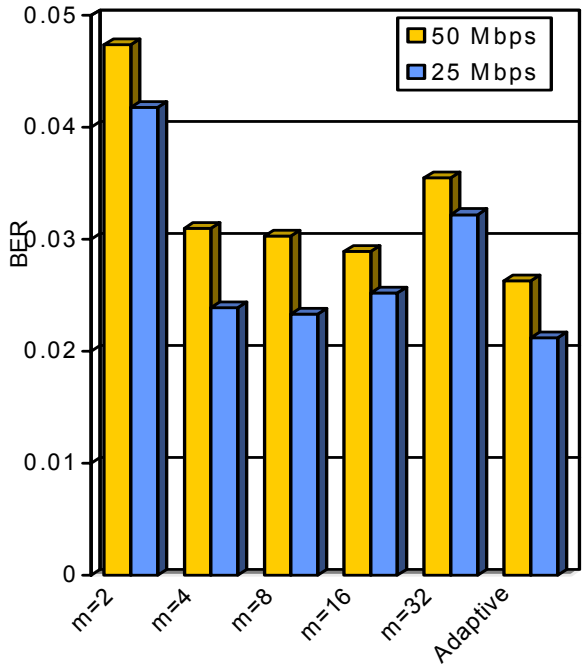

Figure 6.6: BER of Adaptive versus Non-Adaptive System

Next, the adaptive system maximizes the data rate for a target BER in various channel conditions. The environmental and QoS parameters are the same as above, but now the adaptive system increases the data rate by choosing an appropriate system configuration. Any non-adaptive system must operate at the fixed data rate of 25 Mbps to meet the target BER even in the best channel conditions. Table 6.2 and Figure 6.7 compare simulation results of the adaptive UWB system and the non-adaptive UWB system. In every case, the adaptive system provides a faster data rate than a non-

INTEL-1010
U.S. Patent 9,265,043

adaptive scheme. The data rate (or cost) can be improved by up to 260 % for the data rate of 25 Mbps. Generally, the improvement in data rate is larger at lower data rates because the ACB can choose from a larger range of PRI values, whereas at higher data rates, the ACB chooses from a much smaller range of PRI values. This results from the fact the *m*-ary PPM require *m* different non-overlapping pulse positions within a PRI, and hence lengthens the minimum PRI. For example, 32-ary PPM with 1 ns pulse width cannot choose a 10 ns PRI, because it is constrained to choose a PRI greater than 32 ns.

Table 6.2: Data Rate of Non-adaptive versus Adaptive System

Non-Adaptive System Data Rate	Adaptive System Data Rate	Percentage Increase in Data Rate
50 Mbps	84.1 Mbps	68.2%
25 Mbps	90.4 Mbps	261%

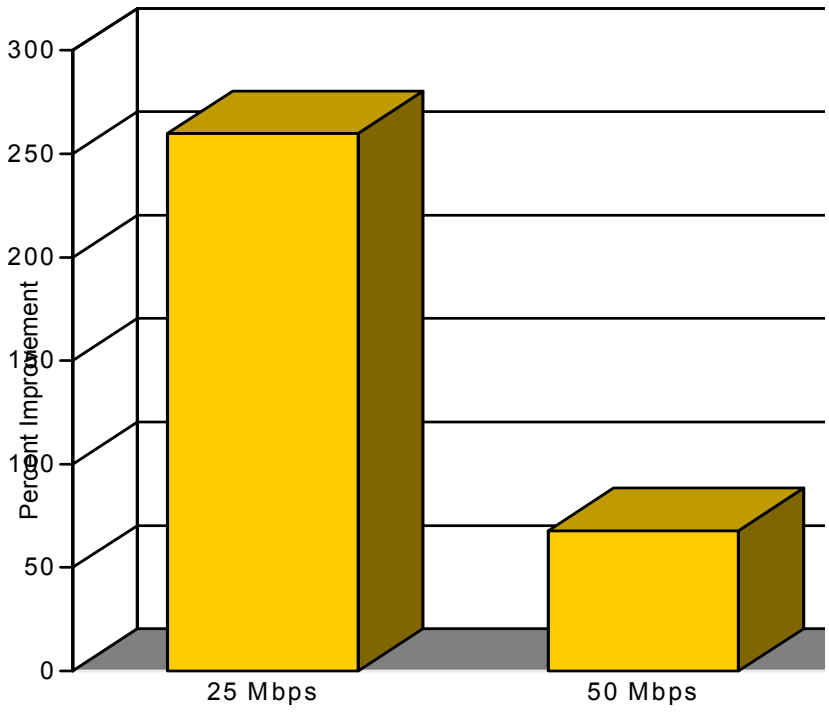

Figure 6.7: Data Rate Maximization of Adaptive versus Non-Adaptive System

INTEL-1010
U.S. Patent 9,265,043

Third, the adaptive system minimizes the radiated energy over various QoS constraints. The first QoS constraint requires a BER of 5×10^{-3} and a data rate of 33 Mbps, and this represents the case of distributing microcode over several hops. The second case requires a BER of 2×10^{-2} and a data rate of 80 Mbps, and this represents the case of video data. Table 6.3 and Figure 6.8 show the normalized radiated energy per bit for the two QoS goals. The last column shows the energy saved in adaptive system as compared to the non adaptive system. Again, the adaptive scheme performs best, and it consumes just 40% of the energy of a non-adaptive system with *m*=2.

Table 6.3: Normalized Energy Efficiency of Non-Adaptive versus Adaptive System

Non-Adaptive System					Adaptive System	Energy Savings
m=2	**m=4**	**m=8**	**m=16**	**m=32**		
1.00	0.415	0.443	0.477	0.964	0.395	61.5%

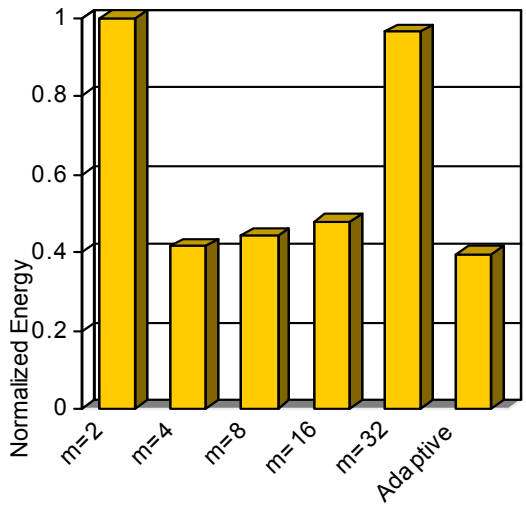

Figure 6.8: Energy of Adaptive versus Non-Adaptive System

For the above three scenarios, the adaptive system always performs best, and different fixed systems performed second best depending on the QoS goal. For

INTEL-1010
U.S. Patent 9,265,043

example, the fixed system with m=16 achieved the second best BER when BER is the goal, and the fixed system with m=4 achieved the best energy efficiency when energy efficiency is goal. Thus, the adaptive system should be especially suitable for systems that have changing QoS goals. For example, a sensor network may wish to minimize energy dissipation during normal operation, minimize BER for control data, and maximize data rate when it detects an event.

We now compare the performance of the adaptive system to the non-adaptive systems as all three of the QoS goals change. The following results consider that the goals of minimum BER, minimum energy, and maximum data rate all occur with equal probability. Further, the network designer weights each performance parameter such that $\alpha = \beta = \chi = 1$. Note that designers are free to change the weighting function to result in optimal performance for specific applications. The results in Figure 6.9 and Table 6.4 are normalized and obtained from the cost function of (6.7). The adaptive system performs much better each of the non-adaptive systems. This is in contrast to the previous results that concentrate on just one QoS parameter. In the previous results, one non-adaptive system may have similar performance to the adaptive system. When the QoS goals change, none of the non-adaptive systems has performance that comes close to that of the adaptive system.

Table 6.4: Normalized Cost of Non-Adaptive versus Adaptive System

Non-Adaptive System					Adaptive System	Cost Savings
m=2	**m=4**	**m=8**	**m=16**	**m=32**		
1.00	0.677	0.681	0.695	0.907	0.436	56.4%

INTEL-1010
U.S. Patent 9,265,043

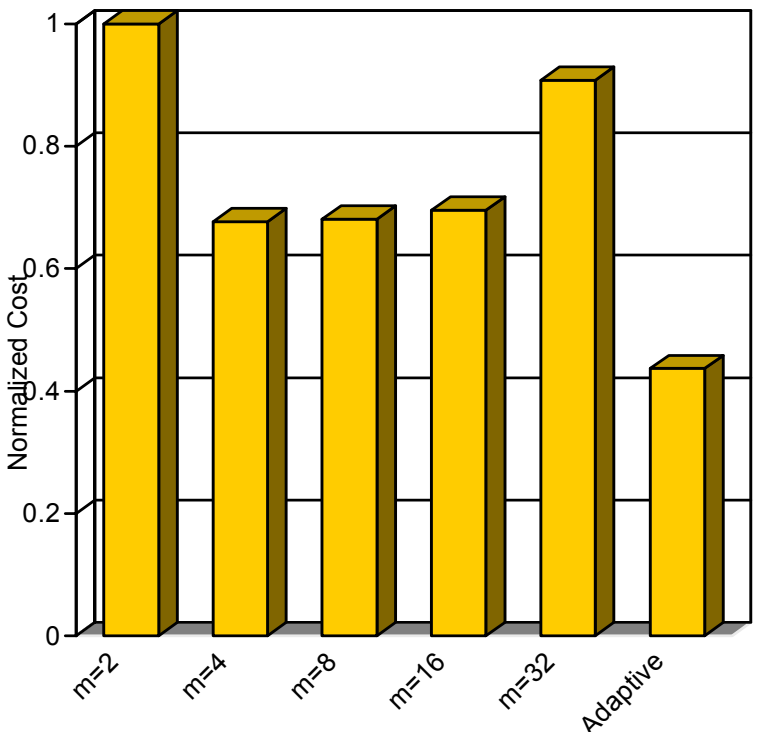

Figure 6.9: Cost of Adaptive versus Non-Adaptive System

6.5 Chapter Summary

This chapter proposes an I-UWB system that adapts its resources to efficiently meet QoS requirements in dynamic channel conditions. The system is particularly suitable for applications such as ad hoc and sensor networks, which have demanding QoS requirements that change for various types of data. The ACB block works across the Application, MAC and Physical Layers, which is a departure from established network design techniques. Although this complicates the design process, it meets the special demands of ad hoc and sensor networks. The ACB configures the I-UWB radio based on the current environmental conditions, resources, and QoS requirements. Because the worst environmental conditions occur infrequently, the adaptive system conserves resources that are typically wasted in a non-adaptive system.

INTEL-1010
U.S. Patent 9,265,043

The adaptive I-UWB system is motivated by the characteristics of *m*-ary PPM in various environmental conditions. In general, for low values of E_b/N_o, the noise dominates the interference, and therefore, efficient modulation schemes with high *m* are preferable. However, for larger values of E_b/N_o, the interference dominates the noise and modulation schemes with low values of *m* are preferable. The choice of the modulation scheme is based on optimizing a cost function that is defined in terms of E_b/N_0, BER, and data rate. An optimal solution to the cost function is prohibitively costly, so it is necessary to use linear approximations to efficiently configure the system.

Simulations of the adaptive system show that it improves performance significantly as compared to a conventional, non-adaptive system under variable environmental and QoS requirements. The adaptive system improves BER by 50%, data rate by 260%, or energy by 60% without sacrificing performance of any other parameter. The adaptive always outperforms the non-adaptive systems for a single, static QoS goal. When the QoS goals change dynamically, the adaptive system performs significantly better than for a static QoS goal.

The adaptive I-UWB system improves performance for ad hoc and sensor networks by supplementing the MAC protocols in the previous chapters to improve BER, energy efficiency, or data rate. Further, the adaptive system does not increase the hardware cost or complexity of the I-UWB transceiver architecture in Chapter 2, because it requires changes only to the digital control logic.

INTEL-1010
U.S. Patent 9,265,043

Chapter 7: Conclusion

Ad hoc and sensor networks enable exciting new applications from home networking to structural integrity monitoring. Nodes rely on limited energy resources, and the useful lifetime of the network depends on each node's ability to conserve energy. Because these networks may contain several thousand nodes or more, low node cost is essential to contain the overall network cost. I-UWB is an attractive radio technology for such networks due to its robustness to multipath fading, sub-centimeter ranging ability, and low-cost, low-power hardware.

Current MAC protocols for I-UWB target small WPANs and cellular networks. The centralized approach is a good strategy for a small network with heavy traffic and strict QoS requirements. In large ad hoc and sensor networks, the central coordination increases complexity and overhead, and it also leads to a central point of failure. Therefore, large ad hoc and sensor networks implement distributed MAC protocols. Because there are currently no distributed MAC protocols for I-UWB, large ad hoc and sensor networks have thus far been unable to realize the benefits of I-UWB.

This dissertation investigates distributed MAC protocols custom tailored to both I-UWB and to ad hoc and sensor networks.

First, Chapter 2 examines the effect of the unique signaling of I-UWB on ad hoc and sensor networks. Distributed MAC protocols for ad hoc and sensor networks generally realize random access and require a method to detect medium activity. The low duty cycle and low power of I-UWB present difficulties in implementing a distributed MAC protocol because there is no good method to detect medium activity. Nodes are unsynchronized with each other, so it becomes a significant challenge to search for a narrow, low-power pulse within a large time window. Existing methods are either inaccurate or require a prohibitive amount of time or hardware complexity. The channel spreads the signal power over multiple paths to further complicate detection of I-UWB activity. In the frequency domain, the pulse train causes spectral lines, which restrict the average power and cause even further difficulty in detecting activity.

INTEL-1010
U.S. Patent 9,265,043

Distributed protocols also require some method of mitigating collisions. The long synchronization time of I-UWB adds significant overhead to protocols such as CSMA/CA that use handshaking packets to avoid collisions.

Next, Chapter 3 proposes a method to overcome the challenges of applying I-UWB to ad hoc and sensor networks. The method to detect I-UWB activity is termed pulse sense, as it is analogous to carrier sense in narrowband systems. The key idea of pulse sense is to examine the spectral lines of the received signal, which are always present, to avoid searching for narrow I-UWB pulses in the time domain. The circuit considers the total spectral energy in the channel, so it is insensitive to multipath interference, timing jitter, inter-symbol interference (ISI), co-channel interference, varying channel conditions, and nonlinear distortion of pulses. Further, narrowband interferers do not significantly degrade performance, so the system can coexist with narrowband systems. The signaling of I-UWB allows a system to trade data rate for link distance, and the circuit performs consistently as the PRI and link distances change. The proposed implementation is much less complex than a receiver, and it does not require any sampling or synchronous operation. In fact, the circuit may be used as an aid to synchronization. Because there is no stored template signal, the circuit does not have to dynamically adapt to changing channel conditions and distortions of the pulse shape. Pulse sense enables distributed, random medium access for I-UWB, and in turn, offers the advantages of I-UWB to ad hoc and sensor networks.

Chapter 4, Chapter 5, and Chapter 6 each provide a method to exploit the unique signaling of I-UWB to benefit ad hoc and sensor networks. Chapter 4 builds upon our pulse sensing method to create distributed multichannel MAC protocols for I-UWB. The multichannel PSMA and ALOHA protocols do not require centralized control, handshaking overhead, or modifications to a basic, single-channel I-UWB receiver. The low duty cycle of I-UWB allows several concurrent transmissions to be time-interleaved, so the probability of a collision depends on the PRI and the channel. Hence, it is important to treat I-UWB differently than narrowband systems, where simultaneous transmissions always result in collisions. At low pulse rates, the low duty cycle of I-UWB reduces the probability of collisions similarly to a traditional multichannel MAC. In contrast to traditional multichannel MACs and handshaking

INTEL-1010
U.S. Patent 9,265,043

schemes, the multichannel PSMA MAC improves throughput without reducing link bandwidth, increasing delay, adding hardware complexity, or adding overhead. A multi-user I-UWB receiver, which can receive several time-interleaved transmissions concurrently, further improves throughput with moderate hardware complexity.

Chapter 5 also builds upon pulse sense and suggests using the unique signaling of I-UWB for a busy signal MAC. A busy signal MAC provides superior performance to current wireless MAC protocols, because a node can assess the status of ongoing transmissions. Further, the busy signal avoids the overhead of handshaking and time-duplexed control packets. Whereas narrowband systems require two transceivers to implement a busy tone MAC, the proposed I-UWB system requires only a single transceiver to save cost, power, and circuit complexity. The system finely multiplexes the busy signal channel with the data channel to re-use the same frequency band and radio front end. At the MAC level, the fine-grained half-duplex operation appears as full duplex operation. Because I-UWB systems dissipate far less power transmitting than receiving, the transmission of a busy signal has insignificant impact on the power dissipated in a transaction. The proposed busy signal MAC permits random, distributed medium access with no central point of failure, so it is appropriate for any large ad hoc or sensor network. Simulations show that the busy signal is easily detectable and does not interfere with data reception. At the network level, the BSMA protocol performs better than a collision avoidance MAC protocol in terms of throughput, and as well as a centralized TDMA protocol in terms of energy efficiency.

Next, Chapter 6 introduces a cross-level optimization scheme that adapts the I-UWB radio to meet various application level QoS constraints as channel conditions change. The adaptive I-UWB system is motivated by the characteristics of m-ary PPM, which may easily adapt the PRI and m to operate most efficiently in various channel conditions. An adaptive configuration block chooses the modulation scheme based on a cost function. The block, which communicates across network layers, represents a departure from the traditional compartmentalized network design model. Because the worst environmental conditions occur infrequently, the adaptive system conserves resources that are typically wasted in a non-adaptive system. The system design is particularly suitable for applications such as ad hoc and sensor networks, which have

INTEL-1010
U.S. Patent 9,265,043

demanding QoS requirements that change during the lifetime of the system. Simulations of the adaptive system show that it improves performance significantly as compared to a conventional non-adaptive system under variable environmental and QoS requirements.

In summary, the unique signaling of I-UWB presents challenges to implementing a distributed MAC protocol. Pulse sense overcomes the challenge of detecting I-UWB medium activity. We propose novel MAC protocols for I-UWB that improve performance and cost over traditional MAC protocols without handshaking overhead. Cross layer optimization further improves performance for any protocol. The protocols and the optimization scheme are custom tailored to meet the requirements of both I-UWB and ad hoc and sensor networks. Thus, they significantly outperform more general approaches.

INTEL-1010
U.S. Patent 9,265,043

References

[1] I.F. Akyildiz, S. Weilian, Y. Sankarasubramaniam, and E. Cayirci, "A survey on sensor networks" *IEEE Communications Magazine*, vol.40, no. 8, pp. 102-114, Aug. 2002.

[2] A. J. Goldsmith and S. B. Wicker, "Design Challenges for Energy-Constrained Ad Hoc Wireless Networks," *IEEE Wireless Communications Magazine*, pp. 8-27, August 2002.

[3] M. Perkins, N. Correal, and B. O'Dea, "Emergent wireless sensor network limitations: a plea for advancement in core technologies," *Proceedings of IEEE International Conference on Sensors*, Vol.2, pp.1505-1509, 2002.

[4] D. Kelley, S. Reinhardt, R. Stanley, M. Einhorn, "PulsON second generation timing chip: enabling UWB through precise timing", *Digest of Papers 2002 IEEE Conference on Ultra Wideband Systems and Technology*, pp. 117-121, May 2002.

[5] S. Verdu, "Spectral efficiency in the wideband regime," IEEE Transactions on Information Theory, vol. 48, no. 6, pp. 1319-1343, 2002.

[6] L. W. Fullerton, "Reopening the electromagnetic spectrum with ultrawideband radio for aerospace" *IEEE Aerospace Conference Proceedings*, Vol. 11, pp. 201-210, Mar. 2000.

[7] R. J. Fontana, "Ultra Wideband Technology - The Wave of the Future?" Keynote Address, *International Telemetry Conference,* San Diego, CA, Oct. 2000.

[8] R. J. Fontana, A. Ameti, E. Richley, L. Beard, and D. Guy "Recent advances in ultra wideband communications systems" *Digest of Papers IEEE Conference on Ultra Wideband Systems and Technologies,* pp. 129-133, May 2002.

[9] R. Fontana, E. Richley, and J. Barney, "Ultra wideband technology for aircraft wireless intercommunications systems (AWICS) design" *Proc. IEEE Conference on Ultra Wideband Systems and Technologies*, Reston, VA, Nov. 2003.

INTEL-1010
U.S. Patent 9,265,043

[10] R. J. Fontana and S. J. Gunderson, "Ultra-wideband precision asset location system" *Digest of Papers IEEE Conference on Ultra Wideband Systems and Technologies*, pp. 147-150, May 2002.

[11] A. Ameti, R. Fontana, E. Knight, and E. Richley, "Commericalization of an ultra wideband precision asset location system," *Proc. 2003 IEEE Conference on Ultra Wideband Systems and Technologies Conference Proceedings*, Reston, VA, Nov. 2003.

[12] R. J. Fontana, E. A. Richley, A. J. Marzullo, L. C. Beard, and R. W. T. Mulloy, "An ultra wideband radar for micro air vehicle applications" *Digest of Papers IEEE Conference on Ultra Wideband Systems and Technologies*, pp. 187-191, May 2002.

[13] R. Fleming and C. Kushner, Principal Investigators, "Low-Power, Miniature, Distributed Position Location and Communication Devices Using Ultra-Wideband, Nonsinusoidal Communication Technology," Semi-Annual Technical Report, ARPA Contract J-FBI-94-058, Jul. 1995. Available: http://www.aetherwire.com/PI_Report_95/awl_pi95.pdf.

[14] R. Fleming, C. Kushner, G. Roberts, and U. Nandiwada, "Rapid acquisition for ultra-wideband localizers," *Digest of Papers IEEE Conference on Ultra Wideband Systems and Technologies*, pp. 245 – 249, May 2002.

[15] T. W. Barrett, "History of Ultrawideband (UWB) radar and communications: Pioneers and innovators," *Proceedings of Progress in Electromagnetics Symposium (PIERS) 2000*, Cambridge, MA, July 2000.

[16] T. W. Barrett, "History of ultrawideband communications and radar: Part 1, UWB communications," *Microwave Journal*, pp. 22-56, January 2001.

[17] T. W. Barrett, "History of Ultra Wideband Communications and Radar: Part 2, UWB Radar and Sensors," *Microwave Journal*, pp. 22-46, February 2001.

[18] T. E. McEwan, *Ultra-wideband radar motion sensor*, US Patent 5,361,070, issued November 1, 1994.

[19] E. C. Kisenwether, "Ultra wideband (UWB) impulse signal detection and processing issues," *IEEE Tactical Communications Conference*, Ft. Wayne, IN, April 1992, Vol. 1, pp 87-93.

INTEL-1010
U.S. Patent 9,265,043

[20] R. Fisher, R. Kohno, H. Ogawa, H. Zhang, M. Mc Laughlin, and M. Welborn,, "DS-UWB Proposal Update", doc.: IEEE 802.15-04/140r3, May, 2004. Available: ftp:// ftp.802wirelessworld.com/15/04/15-04-0140-00-003a-merger2-proposal-ds-uwb-presentation. pdf

[21] R. Fisher, R. Kohno, H. Ogawa, H. Zhang, M. Mc Laughlin, and M. Welborn, "DS-UWB Physical Layer Submission to 802.15 Task group 3a," doc.: IEEE 802.15-04/137r0, March, 2004. Available: ftp://ftp.802wirelessworld.com/15/04/15-04-0137-00-003a-merger2-proposal-ds-uwb-update.pdf

[22] R. Kohno, H. Zhang, and H. Nagasaka, "Ultra Wideband impulse radio using free-verse pulse waveform shaping , Soft-Spectrum adaptation, and local sine template receiving," IEEE 802.15-03/097, rev. 1, Mar., 2003.

[23] C. Mitchell and R. Kohno, "High data rate transmissions using orthogonal modified Hermite pulses in UWB communications," 10th International Conference on Telecommunications, vol. 2, pp. 1278 – 1283, March 2003.

[24] R. W. Chang, "Orthogonal Frequency Division Multiplexing," U.S. Patent 3,488,445, filed 1966, issued Jan. 6, 1970.

[25] S. B. Weinstein and P. M. Ebert, "Data Transmission by Frequency--Division Multiplexing Using the Discrete Fourier Transform," *IEEE Tansactions on Communication Technology*, Vol. COM--19, No.5, pp.628--634, Oct. 1971.

[26] L. C. Cimini Jr., "Analysis and Simulation of a Digital Mobile Channel Using Orthogonal Frequency Division Multiplexing", *IEEE Transactions on Communication*, Vol. 33, No. 7, pp. 665-675, July 1985

[27] MBOA, "Frequency Division Multiplexing," *IEEE Transactions on Communications*, Vol. COM--33, No.7, pp.665--675, July 1985.

[28] Anuj Batra, et al., "Multi-band OFDM Physical Layer Proposal Update," IEEE 802.15-04/0220r3, May 2004. Available: ftp://ftp.802wirelessworld.com/15/04/15-04-0220-03-003a-multi-band-ofdm-physical-layer-proposal-update.ppt

[29] Anuj Batra, et al., "Multi-band OFDM Physical Layer Proposal for IEEE 802.15 Task group 3a," IEEE 802.15-03/268r3, March 2004. Available: http://www.ieee802.org/15/pub/2003/Jul03/03268r2P802-15_TG3a-Multi-band-CFP-Document.pdf

[30] M. Nakagawa, H. Zhang, and H. Sato, "Ubiquitous homelinks based on IEEE 1394 and ultra wideband solutions," *IEEE Communications Magazine*, vol. 41 issue 4, pp. 74-82, April 2003.

[31] D.G. Leeper, "A Long-Term View of Short-Range Wireless," IEEE Computer, pp. 39-44, June 2001.

[32] S. Basagni, I. Chlamatac, V. R. Syrotiuk, & B. A. Woodward, "A Distance routing effect algorithm for mobility (DREAM)", *Proc. of Mobicom'98*, Dallas, TX, pp. 76-84, Oct. 1998.

[33] J. Liu, P. Cheung, L. Guibas, and F. Zhao, "A Dual-Space Approach to Tracking and Sensor Management in Wireless Sensor Networks," *Proc. of the 1st ACM international workshop on Wireless Sensor Networks and Applications (WSNA)*, pp 131-139, Sep. 2002.

[34] M. Welborn, T. Miller, J. Lynch, and J. McCorkle, "Multi-user perspectives in UWB communications networks," *Digest of Papers 2002 IEEE Conference on Ultra Wideband Systems and Technologies*, pp. 271-275, May 2002.

[35] L. DeNardis and M.-G. Di Bennedetto, "Medium access control for UWB communication systems: review and trends," *IEEE Journal of Communications and Networks*, vol. 5, no. 4, pp. 386 – 393, Dec 2003

[36] M.-G. Di Bennedetto and B. R. Vojcic, "Ultra wide band communications: a tutorial," *IEEE Journal of Communications and Networks*, vol. 5, no. 4, pp. 290-302, Dec. 2003.

[37] J.L. Richards, M.D. Roberts, M.H. Pendergrass, and L.W. Fullerton, "Method and apparatus for positioning pulses over time by applying time-hopping codes having pre-defined characteristics," U.S. Patent 6 671 310, Dec. 30, 2003.

[38] F. Cuomo, C. Martello, A. Baiocchi, and F. Capriotti, "Radio resource sharing for ad hoc networking with UWB," *IEEE Journal on Selected Areas in Communications*, vol. 20, issue 9, pp 1722-1732, Dec. 2002.

[39] J. Gronkvist, A. Hansson, and J. Nilsson, "A comparison of access methods for multi-hop ad hoc radio networks," *IEEE 51st Vehicular Technology Conference Proceedings*, vol. 2, pp. 1435-1439, May 2000.

INTEL-1010
U.S. Patent 9,265,043

[40] R. Scholtz, "Multiple access with time hopping impulse modulation," *Conference Record of the IEEE Military Communications Conference*, vol. 2 pp. 447-450, Oct 1993.

[41] S. S. Kolenchery, J. K. Townsend, and J. A. Freebersyser, "A novel impulse radio network for tactical military wireless communications," *Proc. IEEE Military Communications Conference*, vol. 1, pp. 59-65, Oct. 1998.

[42] W. Zhiqiang, Z. Fang, and C.R. Nassar, "Ultra wideband time hopping systems: performance and throughput enhancement via frequency domain processing," *Conference Record of the Thirty-Sixth Asilomar Conference on Signals, Systems and Computers*, vol. 1, pp. 722-727, Nov. 2002.

[43] Y. Guangrong, G. Yue, G. Lijia, and L. Shaoqian, "Performance of UWB time-hopping spread-spectrum impulse radio in multipath environments," *The 57th IEEE Semiannual Vehicular Technology Conference*, vol. 3 pp. 1644-1648, Apr. 2003.

[44] M. Hamalainen, R. Tesi, J. Iinatti, and V. Hovinen, "On the performance comparison of different UWB data modulation schemes in AWGN channel in the presence of jamming," *IEEE RAWCON 2002*, pp. 83-86, Aug. 2002.

[45] D.C. Laney, G.M. Maggio, F. Lehmann, and L. Larson, "Multiple access for UWB impulse radio with pseudochaotic time hopping," *IEEE Journal on Selected Areas in Communications*, vol. 20, no. 9, pp/ 1692-1700, Dec. 2002.

[46] C. Muller, S. Zeisberg, H. Seidel, and A. Finger, "Spreading properties of time hopping codes in ultra wideband systems," *IEEE Seventh International Symposium on Spread Spectrum Techniques and Applications*, vol. 1, pp. 64-67, 2002.

[47] I. Bergel, E. Fishler, and H. Messer, " Narrowband interference suppression in time-hopping impulse-radio systems," *Digest of Papers 2002 IEEE Conference on Ultra Wideband Systems and Technologies*, pp. 303-307, May 2002.

[48] V.S. Somayazulu, "Multiple access performance in UWB systems using time hopping vs. direct sequence spreading," *IEEE Wireless Communications and Networking Conference, 2002,* vol. 2, pp. 522-525, Mar. 2002.

INTEL-1010
U.S. Patent 9,265,043

[49] H. Bo and N.C. Beaulieu, "Exact bit error rate analysis of TH-PPM UWB systems in the presence of multiple-access interference," *IEEE Communications Letters*, vol. 7, no. 12, pp. 572-574, Dec. 2003.

[50] W.D. Wu, C.H. Wang, and C.C Chao, "Effects of hopping codes in TH-SS UWB signals," *IEEE 58th Vehicular Technology Conference*, vol. 2, pp. 1308-1312, Oct. 2003.

[51] G. Durisi and S. Benedetto, "Performance evaluation and comparison of different modulation schemes for UWB multiaccess systems," *IEEE International Conference on Communications, 2003*, vol. 3 , pp. 2187-2191, May 2003.

[52] J. Zhang, R.A. Kennedy, and T.D. Abhayapala, "New results on the capacity of M-ary PPM ultra-wideband systems," *IEEE International Conference on Communications, 2003*, vol. 4, pp. 2867-2871, May 2003.

[53] D.J. Clabaugh, M.A. Temple, and R.A. Raines, and C.M. Canadeo, "UWB multiple access performance using time hopped pulse position modulation with biorthogonal signaling," *Proceedings 2003 IEEE Conference on Ultra Wideband Systems and Technologies*, pp. 330-333, Nov. 16-19.

[54] M.Z. Win and R.A. Scholtz, "Ultra-wide bandwidth time-hopping spread-spectrum impulse radio for wireless multiple-access communications," *IEEE Transactions on Communications*, vol. 48, no. 4, pp. 679-689, Apr. 2000.

[55] J. P. K. Gilb, *Wireless Multimedia: A Guide to the IEEE 802.15.3 Standard,* The Institute of Electrical and Electronics Engineers, Inc., ISBN 0738136689, Apr. 2004.

[56] The Institute of Electrical and Electronics Engineers, Inc., *802.15.3 Draft Standard for Telecommunications and Information Exchange Between Systems - LAN/MAN Specific Requirements - Part 15: Wireless Medium Access Control (MAC) and Physical Layer (PHY) Specifications for High Rate Wireless Personal Area Networks*, Draft P802.15.3/D17, Feb. 2003.

[57] N. Boubaker and K.B. Letaief, "Ultra wideband DSSS for multiple access communications using antipodal signaling," *IEEE International Conference on Communications, 2003*. vol. 3, pp. 2197-2201, May 2003.

INTEL-1010
U.S. Patent 9,265,043

[58] J.R. Foerster, "The performance of a direct-sequence spread ultrawideband system in the presence of multipath, narrowband interference, and multiuser interference," *Digest of Papers 2002 IEEE Conference on Ultra Wideband Systems and Technologies*, pp. 97-91, May 2002.

[59] W. Siriwongpairat, M. Olfat, and K.J Ray Liu, "On the performance evaluation of TH and DS UWB MIMO systems," *IEEE Wireless Communications and Networking Conference, 2004*, vol. 3, pp. 1800-1805, Mar. 2004.

[60] L. Qinghua and L.A. Rusch, "Multiuser detection for DS-CDMA UWB in the home environment," *IEEE Journal on Selected Areas in Communications*, vol. 20, no. 9, pp. 1701-1711, Dec. 2002.

[61] P. Runkle, J. McCorkle, T. Miller, and M. Welbor, "DS-CDMA: the modulation technology of choice for UWB communications," *Proceeedings 2003 IEEE Conference on Ultra Wideband Systems and Technologies*, pp. 364-368, Nov. 2003.

[62] W. Horie and Y. Sanada, "Novel CSMA scheme for DS-UWB ad-hoc network with cariable spreading factor," *Proc. Joint IWUWBS and UWBST Conference*, May 2004.

[63] J.F. Larrick, Jr. and R.J. Fontana, "Ultra wideband data transmission system and method," U.S. Patent 6 690 741, Feb. 10, 2004.

[64] J.F. Larrick, Jr. and R.J. Fontana, "Waveform adaptive ultra-wideband transmitter," U.S. Patent 6 026 125, Feb. 15, 2000.

[65] E. Saberinia and A.H. Tewfik, "Multi-user UWB-OFDM communications," 2003 IEEE Pacific Rim Conference on Communications, Computers and signal Processing, vol. 1, pp. 127-120, Aug. 2003.

[66] G.R. Aiello and G.D. Rogerson, "Ultra-wideband wireless systems," *IEEE Microwave Magazine*, vol. 4, no. 2, pp. 36-47, Jun. 2003.

[67] Z. Shiwei, L. Huaping, and S. Mo, "Performance of a multi-band ultra-wideband system over indoor wireless channels," *First IEEE Consumer Communications and Networking Conference*, 2004. pp. 700-702, Jan. 2004.

[68] D. Gerakoulis and P. Salmi, "An interference suppressing OFDM system for ultra wide bandwidth radio channels," *Digest of Papers 2002 IEEE Conference on Ultra Wideband Systems and Technologies*, pp. 259-264, May 2002.

[69] J. Balakrishnan, A. Batra, and A. Dabak, "A multi-band OFDM system for UWB communication," *Proceedings 2003 IEEE Conference on Ultra Wideband Systems and Technologies*, Nov. 2003.

[70] A. Woo and D. E. Culler, "A transmission control scheme for media access in sensor networks," *Proceedings of the Seventh Annual International Conference on Mobile Computing and Networking*, p.221-235, July 2001.

[71] C. L. Fullmer and J. J. Garcia-Luna-Aceves, "Floor acquisition multiple access (FAMA) for packet radio networks," *Proc. SIGCOMM'95*, vol. 25, no. 4, pp. 262-273, 1995.

[72] A. Chandra, V. Gummalla, and J. O. Limb, "Wireless medium access control protocols," *IEEE Communications Surveys and Tutorials*, vol. 3, no. 2, pp. 2-15, Second Quarter 2002.

[73] P. Karn, "MACA – A new channel access method for packet radio," ARRL/CRRL Amateur Radio 9th Computer Networking Conf., 1990.

[74] V. Bhargavan et al., "MACAW: a wireless media access protocol for wireless LANs," Proc. ACM SIGCOMM '94, vol. 24, no. 4, 1994, pp. 212-225.

[75] C. L. Fullmer and J. J. Garcia-Luna-Aceves, "Solutions to hidden terminal problems in wireless networks," *Proc. ACM SIGCOMM '97*, vol. 27, no. 4, 1997, pp 39-49.

[76] B. Crow, et al., "Performance of IEEE 802.11 wireless local area networks," SPIE, vol. 2917, pp. 480-91.

[77] The Institute of Electrical and Electronics Engineers, Inc., IEEE Std 802.11 - Wireless LAN Medium Access Control (MAC) and Physical Layer (PHY) Specifications, 1999 edition.

[78] The Institute of Electrical and Electronics Engineers, Inc., 802.15.4 Standard for Telecommunications and Information Exchange Between Systems – LAN/MAN Specific Requirements - Part 15.4: Wireless Medium Access

INTEL-1010
U.S. Patent 9,265,043

Control (MAC) and Physical Layer (PHY) Specifications for Low-rate Wireless Personal Area Networks (LR-WPANs), IEEE Std 802.15.4-2003, 2003.

[79] Macro Motes of Smart Dust Project available at http://www-bsac.eecs.berkeley.edu/archive/users/hollar-seth/macro_motes/macromotes.html.

[80] Y. Wei, J. Heidemann, and D. Estrin, "An energy-efficient MAC protocol for wireless sensor networks," Proceedings of INFOCOM 2002. Twenty-First Annual Joint Conference of the IEEE Computer and Communications Societies. pp. 1567-1576, vol. 3, June 2002.

[81] A. Nasipuri, J. Zhuang, S. Das, "A multichannel CSMA MAC protocol for multihop wireless networks," *Proc. IEEE WCNC*, vol. 3, pp. 1402-1406, Sep. 1999.

[82] A.C.V. Gummalla and J.O. Limb, "Design of an access mechanism for a high speed distributed wireless LAN," *IEEE Journal on Selected Areas in Communications*, vol. 18, no. 9, pp. 1740-1750, Sep. 2000.

[83] A.C.V. Gummalla and J.O. Limb, "Wireless collision detect (WCD): multiple access with receiver initiated feedback and carrier detect signal," *2000 IEEE International Conference on Communications*, vol. 1, pp. 397-401, Jun. 18-22 2000.

[84] A.C.V. Gummalla and J.O. Limb, "Receiver architecture for high-speed wireless LAN protocols," *Fall 1999 Vehicular Technology Conference*, vol. 2, pp. 1207-1211, Sep. 1999.

[85] C. Wu and V. Li, "Receiver-initiated busy-tone multiple access in packet radio networks," *Proceedings of the ACM Workshop on Frontiers in Computer Communications Technology,* p.336-342, August 11-13, 1987, Stowe, Vermont, United States.

[86] F. Tobagi and L. Kleinrock, "Packet switching in radio channels: part II--the hidden terminal problem in carrier sense multiple-access and the busy-tone solution," *IEEE Transactions on Communications*, vol. 23, no. 12, pp. 1417-1433, Dec 1975.

INTEL-1010
U.S. Patent 9,265,043

[87] C.-Y. Wan, A. T. Campbell, and L. Krishnamurthy, "PSFQ: a reliable transport protocol for wireless sensor networks," *Proceedings of the 1st ACM International Workshop on Wireless Sensor Networks and Applications* (WSNA 2002), pp. 1-11, Sep. 2002.

[88] Chenyang Lu, B.M. Blum, T.F. Abdelzaher, J.A. Stankovic, Tian He, "RAP: a real-time communication architecture for large-scale wireless sensor networks", Real-Time and Embedded Technology and Applications Symposium Proceedings, pp. 55 – 66, Sept 2002

[89] R. Min, et. al, "Energy-centric enabling technologies for wireless sensor networks," *IEEE Wireless Communications,* vol. 9, no. 4, pp. 28-39, Aug. 2002.

[90] A.S. Tanenbaum, Computer Networks, Prentice Hall, Englewood Cliffs, New Jersey, 1989.

[91] U.S. Federal Communications Commission, FCC Revision of part 15 of the commission's rules regarding ultra-wideband transmission systems: First report and order. Technical report, Feb. 2002.

[92] U.S. Federal Communications Commission, *Part 15 – Radio frequency Devices,* Dec. 8, 2003, Available: http://www.fcc.gov/oet/info/rules/part15/part15_12_8_03.pdf .

[93] I.I. Immoreev, D.V. Fedotov, "Ultra Wideband Radar System: advantages and Disadvantages" *Digest of Papers 2002 IEEE Conference on Ultra Wideband Systems and Technologies*, pp. 201-206, May 2002.

[94] V.S. Somayazulu, J.R. Foerster, and S. Roy, "Design challenges for very high data rate UWB systems," Conference Record of the Thirty-Sixth Asilomar Conference on Signals, Systems and Computers, Vol.1, pp. 717- 721, 2002.

[95] M. Welborn, B. Shvodian Ultra-Wideband Technology for Wireless Personal Area Networks- The IEEE 802.15.3/3a Standards UWBST Tutorial, UWBST 2003 Conference, Nov. 17, 2003.

[96] P. Rouzet, "PULSERS Presentation to IEEE 802.15.4," IEEE P802.15 Working Group for Wireless Personal Area Networks Publications, doc.: IEEE 802.15-03/044r0, January 2003, Available: http://grouper.ieee.org/groups/802/15/pub/

INTEL-1010
U.S. Patent 9,265,043

2003/Jan03/03044r0P802-15_TG4-PULSERS_IEEE_802.15.4_PULSERS-presentation-to-802-15-4.ppt.

[97] M. Leopold, M.B. Dydensborg, and Philippe Bonnet, "Bluetooth and Sensor Networks: A Reality Check," Proceedings of the first ACM International Conference on Embedded Networked Sensor Systems (SenSys), pp. 103-113, November 2003.

[98] O. Kasten and M. Lamgheinreich, "First Experiences with Bluetooth in the Smart-ITS distributed Sensor Network," In Workshop on Ubiquitous Computing and Communications, PACT, 2001.

[99] A. Rajeswaran, V. S. Somayazulu, and J. R. Foerster, "Rake performance for a pulse based UWB system in a realistic UWB indoor channel," *IEEE International Conference on Communications*, May 2003, Vol. 4, pp. 2879-2883.

[100] H. Lee and D. Ha, "A frequency domain approach for all-digital CMOS ultra wideband receivers," *Proc. 2003 IEEE UWBST Conf.*, pp. 86-90, Nov. 2003.

[101] H.J. Lee, D.S. Ha, and Hyung-Soo Lee, "Toward Digital UWB Radios: Part II – A System Design to Increase Data Throughput for a Frequency Domain UWB Receiver," to appear in *Proceedings of the 2004 Joint UWBST Conference and IWUWB Symposium*, May 2004.

[102] K. Marsden, H.-J. Lee, D.S. Ha, and H.-S. Lee, "Low Power CMOS Re-programmable Pulse Generator for UWB Systems," *IEEE Conference on Ultra Wideband Systems and Technologies*, pp. 443-337, November 2003.

[103] H. J. Lee and D. S. Ha, "A systematic approach to CMOS low noise amplifier design for ultra wideband applications," *Proceedings ISCAS*, to be published May. 2005.

[104] S. Jose, H. J. Lee, and D. S. Ha, "A low power CMOS power amplifier for ultra wideband (UWB) applications," *Proceedings ISCAS*, to be published May 2005.

[105] Time Domain Corporation. "Comments of Time Domain Corporation before the Federal Communications Commission in the Matter of Revision of Part C of

INTEL-1010
U.S. Patent 9,265,043

the FCC's Rules Regarding Ultra-Wideband Transmission Systems," Docket 98-153, Dec 1998.

[106] X. Chen and S. Kiaei, "Monocycle shapes for ultra wideband system" *Proceedings of the 2002 IEEE International Symposium on Circuits and Systems (ISCAS 2002)*, vol.1, pp.I597-I600, 2002.

[107] L. Zhao and A.M. Haimovich, "Capacity of m-ary PPM ultra wideband communications over AWGN channels," *IEEE Vehicular Technology Conference*, vol. 2, pp1191-1195, Oct. 2001.

[108] W.M. Lovelace and J.K. M. Townsend, "The effects of timing jitter and tracking on the performance of impulse radio," *IEEE Journal on Selected Areas in Communications*, vol. 20, no. 6, pp. 1646-1651, Dec. 2002.

[109] J. Foerster, "Channel Modeling Subcommittee Report (Final)," Technical Report P802.15-02/368r5-SG3a, IEEE 802.15 Working Group for Wireless Personal Area Networks (WPANs), December 2000. http://grouper.ieee.org/groups/802/15/pub/2002/Nov02/02490r0P802-15_SG3a-Channel-Modeling-Subcommittee-Report-Final.zip.

[110] D. Cassioli, M.Z. Win, and A.F. Molisch, "The ultra-wide bandwidth indoor channel: from statistical model to simulations," IEEE Journal on Selected Areas in Communications, Vol. 20, No. 6, pp. 1247-1257, Aug. 2002.

[111] L. W. Fullerton, *Spread Spectrum Radio Transmission System*, United States Patent 4,641,317, February 3, 1987.

[112] H. Kim, D. Park, and Y. Joo, "Design of CMOS Scholtz's Monocycle Pulse Generator," *UWBST2003, IEEE Conference on UWB Systems and Technologies*, Reston, Virginia, November 16 - 19, 2003.

[113] S. Lee, "Design and Analysis of Ultra-Wide Bandwidth Impulse Radio Receiver," Ph.D. Dissertation, EE Department, University of Southern California, August 2002.

[114] K. W. Robbins United States Patent 3,662,316, Short Base-Band Pulse Receiver, May 9, 1972.

INTEL-1010
U.S. Patent 9,265,043

[115] P. Withington, R. Reinhardt, and R. Stanley, "Preliminary Results of an Ultra-Wideband (Impulse) Scanning Receiver," IEEE MILCOM, vol.2, pp. 1186-1190, Atlantic City, NJ, November 1999.

[116] R. T. Hoctor and H. W. Tomlinson, "An Overview of Delay-Hopped, Transmitted-Reference RF Communications," G.E. Research and Development Center, Technical Information Series, pp. 1-29, January 2002.

[117] J. D. Taylor, *Introduction to Ultra-Wideband Radar Systems*, CRC Press, Inc., 1995.

[118] W. C. Chung and D. S. Ha, "An accurate ultra wideband (UWB) ranging for precision asset location," *Proc. 2003 IEEE Conference on Ultra Wideband Systems and Technologies Conference*, pp. 389-393, Nov. 2003.

[119] I. Gresham, A. Jenkins, R. Egri, C. Eswarappa, F. Kolak, R. Wohlert, J. Bennett, and J.-P. Lanteri, "Ultra wide band 24GHz automotive radar front-end" *IEEE MTT-S International Microwave Symposium Digest*, Vol. 1, pp. 369-372, Jun. 2003.

[120] Y.-J. Park, K. - H. Kim, S.-B. Cheo, D.-W. Yoo, D.-G. Youn, and Y.-K. Jeong, "Development of a UWB GPR system for detecting small objects buried under ground," *Proc. IEEE Conference on Ultra Wideband Systems and Technologies*, pp. 384-388, Nov. 2003.

[121] B. Scheers, M. Piette, and A. Vander Vorst, "The detection of AP mines using UWB GPR," *Proc. of the Second International Conference on the Detection of Abandoned Land Mines*, IEE conf. publ. no. 458, pp. 50-54, Oct. 1998.

[122] E. M. Staderini, "UWB radars in medicine", *IEEE Aerospace and Electronic Systems Magazine*, Vol. 17, No. 1, pp. 13-18, Jan. 2002.

[123] E. J. Bond, X. Li; S. C. Hagness, and B. D. Van Veen, "Microwave imaging via space-time beamforming for early detection of breast cancer," *IEEE Transactions on Antennas and Propagation*, Vol. 51 , No. 8 , pp. 1690-1705, Aug. 2003.

[124] M. Akahane, B. Huang, S. Sugaya, K. Takamura, "CE requirements for alternative PHY CFA," IEEE P802.15 Working Group for Wireless Personal Area Networks Publications, doc.: IEEE 802.15-02/043r0, Jan. 2002, Available:

INTEL-1010
U.S. Patent 9,265,043

http://grouper.ieee.org/groups/802/15/pub/2002/Jan02/02043r0P802-15_SG3a-CE-Requirements-for-Alternative-PHY-CFA.ppt.

[125] P. Gandolfo, "XtremeSpectrum – SG3a CFA Response," IEEE P802.15 Working Group for Wireless Personal Area Networks Publications, doc.: IEEE 802.15-02/031r0, Jan. 2002, Available: http://grouper.ieee.org/groups/802/15/pub/2002/Jan02/02031r0P802-15_SGAP3-CFAReaponseAltPHY.ppt.

[126] C. Brabenac, "Intel SG3a CFA Response – Wireless Peripherals," IEEE P802.15 Working Group for Wireless Personal Area Networks Publications, doc.: IEEE 802.15-02/139r0, Mar. 2002, Available: http://grouper.ieee.org/groups/802/15/pub/2002/Mar02/02139r0P802-15_SG3a-Intel-CFA-Response-Wireless-Peripherals.ppt.

[127] Intel Corporation, "Wireless USB The First High-Speed Personal Wireless Interconnect," White Paper, 2004, Available: http://www.intel.com/technology/ultrawideband/downloads/wirelessUSB.pdf.

[128] K. Siwiac, "SG3a Application Summary," IEEE P802.15 Working Group for Wireless Personal Area Networks Publications, doc.: IEEE 802.15-02/149r0, Mar. 2002, Available: http://grouper.ieee.org/groups/802/15/pub/2002/Mar02/02149r0P802-15_SG3a-Application-Summary.doc.

[129] R. Aeillo, J. Ellis, and L. Taylor, "Application Opportunities for High Rate WPANs," IEEE P802.15 Working Group for Wireless Personal Area Networks Publications, doc.: IEEE 802.15-02/143r0, Mar. 2002, Available: http://grouper.ieee.org/groups/802/15/pub/2002/Mar02/02143r0P802-15-SG3a-Application-Opportunities-GA.ppt.

[130] J. Ellis and L. Taylor, "IEEE P802.15.4SG4a call for applications," IEEE P802.15 Working Group for Wireless Personal Area Networks Publications Doc.: IEEE 802.15-03/330r1, Aug. 2003. Available: ftp://ftp.802wirelessworld.com/15/03/15-03-0330-01-004a-sg4a-call-applications.doc

[131] J. Ellis and L. Taylor, "802.15.4IGa informal call for application response," IEEE P802.15 Working Group for Wireless Personal Area Networks Publications Doc.: IEEE 1802.15-03/537r0, Jul. 2003. Available:

INTEL-1010
U.S. Patent 9,265,043

ftp://ftp.802wirelessworld.com/15/03/15-03-0537-00-004a-formal-submission-802-15-4iga-informal-cfa-response-ppt.ppt.

[132] R. Roberts, "Low probability of detection applications," IEEE P802.15 Working Group for Wireless Personal Area Networks Publications Doc.: IEEE 802.15.SG4a-03/430r0, Nov. 2003. Available: ftp://ftp.802wirelessworld.com/15/03/15-03-0430-00-004a-802-15-sg4a-cfa-response-lpd-low-probability-detection.ppt

[133] http://www.ubisense.net/healthcare/index.html

[134] W. Hirt, "Low data rate and/or positioning applications," IEEE P802.15 Working Group for Wireless Personal Area Networks Publications Doc.: IEEE 802.15-03/443r0, Oct. 2003. Available: ftp://ftp.802wirelessworld.com/15/03/15-03-0443-00-004a-sg4a-low-rate-data-and-positioning-applications.ppt

[135] S. Davis, "Communication and navigation for robotic applications," IEEE P802.15 Working Group for Wireless Personal Area Networks Publications Doc.: IEEE 802.15-03/486r0, Nov. 2003. Available: ftp://ftp.802wirelessworld.com15/03/15-03-0486-00-004a-robotic-communication-location.ppt

[136] V. Dhingra, "Water and gas meter reading application," IEEE P802.15 Working Group for Wireless Personal Area Networks Publications Doc.: IEEE 802.15-03/436r0, Nov. 2003. Available: ftp://ftp.802wirelessworld.com/15/03/15-03-0436-00-004a-echelon-sg4a-call-application-response.ppt.

[137] J. Ryckaert, "Wireless body area networks," IEEE P802.15 Working Group for Wireless Personal Area Networks Publications Doc.: IEEE 802.15-03/484r0, Nov. 2003. Available: ftp://ftp.802wirelessworld.com/15/03/15-03-0484-00-004a-sg4a-cfa-response-wireless-body-area-networks.ppt

[138] R. J. Fontana, E. Richley, and J. Barney, "Commercialization of an ultra wideband precision asset location system," *Proc. IEEE Conference on Ultra Wideband Systems and Technologies Conference*, Reston, VA, pp. 369-373, Nov. 2003.

[139] H. Urkowitz, *Signal Theory and Random Processes*, Artech House, 1983.

INTEL-1010
U.S. Patent 9,265,043

[140] T.S. Rappaport, *Wireless Communications: Principles and Practice*, 2nd ed., Upper Saddle River, NJ: Prentice Hall, 2002.

[141] Z. Zhang and A.S. Acampora, "Performance of a modified polling strategy for broadband wireless LANs in a harsh fading environment." Proc. IEEEE GLOBECOM, 1991, pp. 1141-1146.

[142] R.J. Haines and A.H. Aghvami, "Indoor radio environment considerations in selecting a media access control protocol for wideband radio data communications," Proc IEEE ICC 1994, vol. 3, 1994, pp. 1306-1311.

[143] A.S. Acampora and S.V. Krishnamurthy, "A new adaptive MAC layer protocol for wireless ATM networks in harsh fading and interference environments," Proc. ICUPC 1997, vol. 2, Oct. 1997, pp.410-415.

[144] G. Wu, K. Mukumoto, and A. Fukuda, "An intergrated voice and data transmission system with idle signal multiple access – dynamic analysis," IEEE Trans. Comm., vol. E76B, no. 11, Nov. 1993, pp. 1398-1407, 1998.

[145] G. Wu, et al., "An R-ISMA integrated voice/data wireless information system with different packet generation rates," Proc. IEEE ICC 1996, vol. 3, pp 1263-1269.

[146] G. Wu, M. Mukumoto, and A. Fukuda, "Slotted idle signal multiple access with collision detection for two-way centralized wireless communication networks," Proc. IEE ICC, 1993, pp. 995-999.

[147] K.C. Chen and C. H. Lee, "RAP – a novel medium access protocol for wireless data networks," Proc IEEE GLOBECOM, 1993, pp 1713-1717.

[148] J.-J. Lai, Y.-W. Lai, and S.-J. Lee, "A Medium access control for wireless networks," Proc IEEE ICC 1998, vol. 1 pp. 146-150.

[149] H. Chou, C. Lee and K. Chen, "Group randomly addresses polling with reservation for wireless integrated service network," Proc. PIMRC, 1995, pp. 6218-622.

[150] W.C. Chong and D.J. Goodman, "Integrated data and speech transmission using packet reservation multiple access," Proc. IEEE ICC 1993, May 1993, pp. 172-176.

INTEL-1010
U.S. Patent 9,265,043

[151] P. Narasimhan and R.D. Yates, "A new protocol for the integration of voice and data over PRMA," IEEE JSAC, vol. 14, no. 4, Oct. 1995 , pp. 623-631.

[152] J.M. DeVile, "A reservation-based multiple access scheme for future universal mobile telecommunications system," Proc. IEE Conf. Mobile and Personal Comm., Dec 1993, pp. 210-215/

[153] G. Bianchi, et al., "C-PRMA: a centralized packet reservation multiple access for local wireless communications," IEEE Trans. Vehic. Tech., vol. 46, no. 2, May 1997.

[154] M. Aciardi, G. Casalino, and F. Davoli, "Independent stations algorithm for the maximization of one-step throughput in a multiple access channel," IEEE Trans. Comm., Aug. 1998, pp. 795-800.

[155] M.J. Karol, Z. Liu, and K.Y. Eng, An Efficient Demand Assignment Multiple Access Protocol for Wireless Packet ATM Networks, Wireless Networks, ACM Press, Baltzer Science Publishers, vol. 1.3, 1995, pp. 267-279.

[156] J. Mikkonen et al., "The MAGIC WAND – functional overview," IEEE JSAC, vol. 16, no. 6, Aug. 1998, pp. 953-972.

[157] D. Petras, "Performance evaluation of medium access control protocols for mobile broadband systems," Technical Report RACE Project, Jan. 1996.

[158] P. Gorday, J. Martinez, and P. Jamieson, "IEEE 802.15.4 overview," IEEE P802.15 Working Group for Wireless Personal Area Networks Publications Doc.: IEEE 802.15-01-0509r0, Nov. 2001 Available http://grouper.ieee.org/groups/802/15/pub/2001/Nov01/01509r0P802-15_TG4-Overview.ppt.

[159] J. Ding, L. Zhao, S. Medidi, and K. Sivalingam, "MAC Protocols for Ultra-Wide-Band (UWB) Wireless Networks: Impact and Channel Acquisition Time," Proc. SPIE ITCOM02, July 2002.

[160] N. Kumar, "MAC and physical layer design for ultra-wideband communications," Masters Thesis, Virginia Polytechnic Institute and State University, http://scholar.lib.vt.edu/theses/index.html, May 2004.

INTEL-1010
U.S. Patent 9,265,043

[161] C.R. Anderson, A.M. Orndorff, R.M. Buehrer, and J.H. Reed "An introduction and Overview of Ultra Wideband Communications," *MPRG Technical Report*, Virginia Tech, May 2004.

[162] I.I. Immoreev, D.V. Fedotov, "Detection of UWB signals reflected from complex targets," *Digest of Papers 2002 IEEE Conference on Ultra Wideband Systems and Technologies*, pp. 193-196, May 2002.

[163] W. A. Lindgren, "Pulse peak detector," U.S. Patent 3 939 365, Feb. 17, 1976.

[164] R. G. Meyer, "Low-power monolithic RF peak detector analysis," *IEEE Journal of Solid-State Circuits*, vol. 30, no. 1, pp. 65-67, Jan. 1995.

[165] F. Chin, Z. Wanjun, and C.-C. Zhi, "System performance of IEEE 802.15.4 low rate wireless PAN using UWB as alternate-PHY layer," *IEEE Proc. 14th PIMRC 2003*, vol. 1, pp. 487-491, Sep. 2003.

[166] R. J. Fontana, J. F. Larrick, J, and J. E. Cade "UWB dual tunnel diode detector for object detection, measurement, or avoidance," U.S. Patent 6 239 741, May 29, 2001.

[167] R. J. Fontana and J.F. Larrick, Jr. "Ultra wideband receiver with high speed noise and interference tracking threshold," U.S. Patent 5 901 172, May 4, 1999.

[168] J. W. McCorkle and M. Rofheart, "Ultra wide bandwidth spread-spectrum communications system" U.S. Patent 6 700 939, Mar. 2, 2004.

[169] L.W. Fullerton and I.A. Cowie, "Ultrawide-band communication system and method," U.S. Patent 5 960 031, Sep. 28, 1999.

[170] G. Moussally, R. Ziernicki, P. A. Fialer, and F.J. Heinzman, "Three-dimensional underground imaging radar system," U.S. Patent 5 673 050, Sep. 30, 1997.

[171] W.B. Dress, Jr. and S.F. Smith, "Pulse transmission receiver with higher-order time derivative pulse generator," U.S. Patent 6 606 350, Aug. 12, 2003.

[172] P. Van Etten, and M.C. Wicks, "Unambiguous range-doppler processing method and system," U.S. Patent 5 657 022, Aug. 12 1997.

[173] J.W. McCorkle, T.R. Miller, and M. Rofheart, "Carrierless ultra wideband wireless signals for conveying application data," U.S. Patent 6 505 032, Jan. 7, 2003.

[174] B. Juhel, E. Legros, and M. Le Goff, "Algorithms and experimental results in ultra-wideband SAR imaging," *Radar 97* (*Conf. Publ. No. 449*), pp. 673-677, Oct. 1997.

[175] B.M. Sadler and A. Swami, "On the performance of UWB and DS-spread spectrum communication systems," *Digest of Papers 2002 IEEE Conference Ultra Wideband Systems and Technologies*, pp. 289-292, May 2002.

[176] S. Gezici, H. Kobayashi, and H.V. Poor, "A comparative study of pulse combining schemes for impulse radio UWB systems," *IEEE/Sarnoff Symposium on Advances in Wired and Wireless Communication*, pp. 7-10, Apr. 2004.

[177] R. Blazquez, P. Newaskar, and A. Chandrakasan, "Coarse acquisition for ultra wideband digital receivers," *Proc. IEEE ICASSP 2003*, vol. 4, pp. 137-140, Apr. 2003.

[178] L.W. Fullerton and J.L. Richards, "Fast locking mechanism for channelized ultrawide-band communications, " U.S. Patent 5 832 035, Nov. 3, 1998.

[179] L.W. Fullerton, I.A. Cowie, W.D. Welch, Jr, and R.S. Stanley, "System for fast lock and acquisition of ultra-wideband signals," U.S. Patent 6 556 621, Apr. 29, 2003.

[180] R.C. Qiu, "A study of the ultra-wideband wireless propagation channel and optimum UWB receiver design," *IEEE Journal on Selected Areas in Communications*, vol. 20, no. 9, pp. 1628-1637, Dec. 2002.

[181] X. Xiaojian and R.M. Narayanan, "Impact of different correlation receiving techniques on the imaging performance of UWB random noise radar," *Proceedings IGARSS '03*, vol. 7, pp. 4525-4527, Jul. 2003.

[182] T. Zhi and G.B. Giannakis, "BER sensitivity to mistiming in correlation-based UWB receivers, *IEEE GLOBECOM '03*, vol. 1 pp. 441-445, Dec. 2003.

[183] L.W. Fullerton, J.L. Richards, I.A. Cowie, and V.R. Brethour , "Vector modulation system and method for wideband impulse radio communications," U.S. Patent 6 763 057, Jul. 13, 2004.

[184] J.W. McCorkle, "Ultra wideband communication system, method, and device with low noise pulse formation," U.S. Patent 6 735 238, May 11, 2004.

INTEL-1010
U.S. Patent 9,265,043

[185] J. Joe, "PSK transmitter and correlator receiver for UWB communications system," U.S. Patent 6 724 269, Apr. 20 2004.

[186] E.A. Homier and R.A. Scholtz, "Rapid acquisition of ultra-wideband signals in the dense multipath channel," *Digest of Papers 2002 IEEE Conference on Ultra Wideband Systems and Technologies*, 2002, pp. 105-109, May 2002.

[187] H. Bing, X. Hou, X. Yang, T. Yang, and C. Li, "A "two-step" synchronous sliding method of sub-nanosecond pulses for ultra-wideband (UWB) radio," *IEEE International Conference on Communications, Circuits, and Systems and West Sino Expositions*, June 2002, vol. 1, pp. 142-145.

[188] C. R. Anderson, "Design and Implementation of an Ultrabroadband Millimeter-Wavelength Vector Sliding Correlator Channel Sounder and In-Building Measurements at 2.5 & 60 GHz," Masters Thesis, Virginia Polytechnic Institute and State University, http://scholar.lib.vt.edu/theses/index.html, May 2002.

[189] S. R. Velazquez, T. Q. Nguyen, and S. R. Broadstone, "Design of Hybrid Filter Banks for Analog/Digital Conversion," IEEE Transactions on Signal Processing, Vol. 4, pp. 956–967, April 1998.

[190] W. Namgoong, "A Channelized Digital Ultrawideband Receiver," IEEE Transactions on Wireless Communications, Vol. 2, No. 3, pp. 502-510, May 2003.

[191] J.-Y. LeBoudec, R. Marz, B. Radunovic, and J. Widmer, "DCC-MAC: A Decentralized MAC protocol for 802.15.4a-like UWB mobile ad hoc networks based on dynamic channel coding," *Proceedings of First International Conference on Broadband Networks*, Oct. 2004.

[192] M.-G. Di Benedetto, L. De Nardis, M. Junk, G. Giancola, "(UWB)^2: uncoordinated, wireless, baseborn, medium access control for UWB communication networks," to appear in *Mobile Networks and Applications special issue on WLAN Optimization at the MAC and Network Levels,* 2nd quarter 2004.

[193] N.J. August, H.-J. Lee, and D.S. Ha, "Design of a pulse sensor to detect medium activity in ultra wideband networks," Submitted to International Conference on Ultra Wideband (ICU) March 31,2005.

INTEL-1010
U.S. Patent 9,265,043

[194] L.W. Fullerton, "Full duplex ultrawide-band communication system and method," U.S. Patent 5 687 169, Nov. 11, 1997.

[195] S. Nanda, K. Balachandran, and S. Kumar, "Adaptation techniques in wireless packet data services," *IEEE Communications Magazine*, Jan. 2000.

[196] S. Singh and C.S. Raghavendra, "PAMAS – Power aware multi-access protocol with signaling for ad hoc networks," *ACM Sigcomm Computer Communication Review,* Vol. 28, No. 3, pp.5-26, July 1998.

[197] C. K. Toh, "Maximum battery life routing to support ubiquitous mobile computing in wireless ad hoc networks," *IEEE Communications Magazine*, Vol. 39, No. 6, pp. 138-147, June 2001.

[198] N.J. August, W.C. Chung, and D.S. Ha, "Energy efficient methods of increasing data rate for ultra wideband (UWB) communications systems," *IEEE Conference on Ultra Wideband Systems and Technologies (UWBST 2003)*, pp. 280-284, Nov. 2003.

[199] M. I. Skolnik, *Introduction to Radar Systems*, McGraw-Hill Book Company, 1962.

[200] J.R. Reed, editor, *An Introduction to Ultra Wideband Communications*, Prentice Hall, 2005.

[201] A. Saleh and R. Valenzuela, "A Statistical Model for Indoor Multipath Propagation," IEEE JSAC, Vol. SAC-5, No. 2, Feb. 1987, pp. 128-137.

[202] M. Pendergrass, "Empirically Based Statistical Ultra-Wideband Channel Model," IEEE doc.: P802.15-02/240-SG3a. Available: http://grouper.ieee.org/groups/802/15/pub/2002/Jul02/02240r1p802-15_SG3a-Empirically_Based_UWB_Channel_Model.ppt

[203] J. Foerster and Q. Li, "UWB Channel Modeling Contribution from Intel," doc.: IEEE P802.15-02/279-SG3a. Available: http://grouper.ieee.org/groups/802/15/pub/2002/Jul02/02279r0P802-15_SG3a-Channel-Model-Cont-Intel.doc

[204] J. G. Proakis, *Digital Communications*, 4th Edition, McGraw-Hill, New York, NY, 2001.

INTEL-1010
U.S. Patent 9,265,043

[205] M. Z. Win, "Spectral density of random time-hopping spread-spectrum UWB signals with uniform timing jitter," *Proc. IEEE Military Communications Conference Proceedings*, vol. 2, pp. 1196 – 1200, Oct. 1999.

[206] M. Hamalainen, V. Hovinen, R. Tesi,, J.H.J. Iinatti, and M. Latva-aho, "On the UWB system coexistence with GSM900, UMTS/WCDMA, and GPS," *IEEE Journal on Selected Areas in Communications*, vol. 20, no. 9, pp. 1712-1721, Dec. 2002.

[207] J. Ellis, K. Siwiak, and R. Roberts, "P802.15. 3a Alt PHY Selection Criteria," IEEE P802-15_03031r11_TG3a-PHY-Selection-Criteria, May 18, 2003. Available: http://grouper.ieee.org/groups/802/15/pub/2003/May03/03031r11P802-15_TG3a -PHY-Selection-Criteria.doc.

Vita

Nathaniel John August was born in Cumberland, Maryland on May 5 1975. He graduated *summa cum laude* with a Bachelor of Science in Computer Engineering and a minor in Computer Science from Virginia Tech in Blacksburg, Virginia in May 1998.

He also graduated *summa cum laude* with a Master of Science in Electrical Engineering from Virginia Tech in May 2001. D. He worked under Dr. Dong Ha at the Virginia Tech VLSI for Telecommunications (VTVT) Laboratory and studied low power VLSI design and signal processing. During his M.S. degree, he worked as a research assistant for a startup company integrating the H.263 video codec into a modem for third generation (3G) cell phones. His thesis was on the low power design of an ASIC for H.263.

He re-entered the Bradley Department of Electrical and Computer Engineering at Virginia Tech in August 2002 to obtain a Doctorate. He again worked under Dr. Dong Ha at the VTVT Laboratory as a Bradley Fellow and a Cunningham Fellow. His current research interests include low power VLSI design in ultra wideband (UWB) systems for applications such as wireless personal area networks (WPANs), radio frequency identification (RFID), and wireless ad hoc and sensor networks. He plans to graduate in the spring of 2005.

He is first author of over a dozen IEEE journal and conference papers. In addition, he has contributed to several magazine articles and co-authored a textbook on ultra wideband. He has also applied for a patent disclosure relating to his research.

In between degrees, he worked as a validation engineer for Intel Corporation in Portland, OR and Folsom, CA on various projects including pre-silicon validation of gigabit Ethernet adapters and post-silicon validation of PCI chipsets. After receiving his Ph.D. degree, he plans to look for a job in Portland, Oregon.

INTEL-1010
U.S. Patent 9,265,043

APPENDIX K

INTERNET ARCHIVE WEB TEXTS VIDEO AUDIO SOFTWARE IMAGES SIGN UP | LOG IN UPLOAD Search

ABOUT BLOG PROJECTS HELP DONATE CONTACT JOBS VOLUNTEER PEOPLE

DONATE INTERNET ARCHIVE WayBackMachine Explore more than 916 billion web pages saved over time

http://scholar.lib.vt.edu/theses/available/etd-05082005-223850/

Calendar · Collections · Changes · Summary · Site Map · URLs

Saved **35 times** between November 16, 2005 and April 16, 2024.

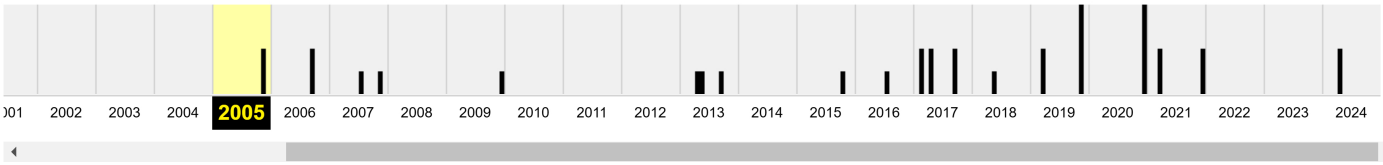

JAN						
						1
2	3	4	5	6	7	8
9	10	11	12	13	14	15
16	17	18	19	20	21	22
23	24	25	26	27	28	29
30	31					

FEB						
		1	2	3	4	5
6	7	8	9	10	11	12
13	14	15	16	17	18	19
20	21	22	23	24	25	26
27	28					

MAR						
		1	2	3	4	5
6	7	8	9	10	11	12
13	14	15	16	17	18	19
20	21	22	23	24	25	26
27	28	29	30	31		

APR						
					1	2
3	4	5	6	7	8	9
10	11	12	13	14	15	16
17	18	19	20	21	22	23
24	25	26	27	28	29	30

MAY						
1	2	3	4	5	6	7
8	9	10	11	12	13	14
15	16	17	18	19	20	21
22	23	24	25	26	27	28
29	30	31				

JUN						
			1	2	3	4
5	6	7	8	9	10	11
12	13	14	15	16	17	18
19	20	21	22	23	24	25
26	27	28	29	30		

JUL						
					1	2
3	4	5	6	7	8	9
10	11	12	13	14	15	16
17	18	19	20	21	22	23
24	25	26	27	28	29	30
31						

AUG						
	1	2	3	4	5	6
7	8	9	10	11	12	13
14	15	16	17	18	19	20
21	22	23	24	25	26	27
28	29	30	31			

SEP						
				1	2	3
4	5	6	7	8	9	10
11	12	13	14	15	16	17
18	19	20	21	22	23	24
25	26	27	28	29	30	

OCT						
						1
2	3	4	5	6	7	8
9	10	11	12	13	14	15
16	17	18	19	20	21	22
23	24	25	26	27	28	29
30	31					

NOV						
		1	2	3	4	5
6	7	8	9	10	11	12
13	14	15	16	17	18	19
20	21	22	23	24	25	26
27	28	29	30			

DEC						
				1	2	3
4	5	6	7	8	9	10
11	12	13	14	15	16	17
18	19	20	21	22	23	24
25	26	27	28	29	30	31

Note

This calendar view maps the number of times **http://scholar.lib.vt.edu/theses/available/etd-05082005-223850/** was crawled by the Wayback Machine, *not* how many times the site was actually updated. More info in the FAQ.

FAQ | Contact Us | Terms of Service (Dec 31, 2014)

The Wayback Machine is an initiative of the Internet Archive, a 501(c)(3) non-profit, building a digital library of Internet sites and other cultural artifacts in digital form. Other projects include Open Library & archive-it.org.

Your use of the Wayback Machine is subject to the Internet Archive's Terms of Use.

https://web.archive.org/web/20051119154406/http://scholar.lib.vt.edu/theses/available/etd-05082005-223850/ December 12, 2024

INTERNET ARCHIVE WayBackMachine http://scholar.lib.vt.edu/theses/available/etd-05082005-223850/ Go OCT NOV 19 SEP
35 captures 2004 2005 2007 About this capture
16 Nov 2005 - 16 Apr 2024

digital library and archives
formerly the scholarly communications project

etd@vt

Title page for ETD etd-05082005-223850

Type of Document	Dissertation
Author	August, Nathaniel John
Author's Email Address	nate_august@yahoo.com
URN	etd-05082005-223850
Title	Medium Access Control in Impulse-Based Ultra Wideband Ad Hoc and Sensor Networks
Degree	PhD
Department	Electrical and Computer Engineering
Advisory Committee	**Advisor Name** — **Title** Dr. Dong Ha — Committee Chair Dr. Jeffrey Reed — Committee Member Dr. Jim Armstrong — Committee Member Dr. Joeseph Tront — Committee Member Dr. Thurman Lockhart — Committee Member
Keywords	• ultra wideband • carrier sense • medium access control • busy signal • ad hoc networks • multi-channel • sensor networks
Date of Defense	2005-05-05
Availability	unrestricted

Abstract

This thesis investigates distributed medium access control (MAC) protocols custom tailored to both impulse-based ultra wideband (I-UWB) radios and to large ad hoc and sensor networks. I-UWB is an attractive radio technology for large ad hoc and sensor networks due to its robustness to multipath fading effects, sub-centimeter ranging ability, and low-cost, low-power hardware. Current medium access control (MAC) protocols for I-UWB target small wireless personal area networks (WPANs) and cellular networks, but they are not suitable for large, multihop ad hoc and sensor networks. Therefore, this paper proposes a new type of MAC protocol that enables ad hoc and sensor networks to realize the benefits of I-UWB radios. First, we propose a method to overcome the challenges of quickly, reliably, and efficiently sensing medium activity in an ultra wideband network. This provides a base MAC protocol similar to carrier sense multiple access (CSMA) in narrowband systems. Next, we propose to exploit the unique signaling of I-UWB to improve performance over the base MAC protocol without the associated overhead of similar improvements in narrowband systems. I-UWB enables a distributed multichannel MAC protocol, which improves throughput. I-UWB also facilitates a busy signal MAC protocol, which reduces wasted energy from corrupt packets. Finally, because the I-UWB Physical Layer and MAC Layer affect the network and application layers, we propose a cross-layer adaptive system that optimizes performance. Physical Layer simulations show that both the base protocol and the improvements are practical for an I-UWB radio. Networks level simulations characterize the performance of the proposed MAC protocols and compare them to existing MAC protocols.

Files

Filename	Size	Approximate Download Time (Hours:Minutes:Seconds)				
		28.8 Modem	56K Modem	ISDN (64 Kb)	ISDN (128 Kb)	Higher-speed Access
Dissertation_NA_final_print.pdf	1.82 Mb	00:08:25	00:04:20	00:03:47	00:01:53	00:00:09

Browse All Available ETDs by (Author | Department)

dla etds image base journals news online class materials special collections
virginia tech home contact dla university libraries

INTEL-1010
U.S. Patent 9,265,043

If you have questions or technical problems, please Contact DLA.